AFCRC-TR-56-200

NWRC LIBRARY

GEOPHYSICAL RESEARCH PAPERS

NO. 46

AD-101943

RESULTS OF NUMERICAL FORECASTING WITH THE BAROTROPIC AND THERMOTROPIC ATMOSPHERIC MODELS

W. LAWRENCE GATES
LEON S. POCINKI
CARL F. JENKINS

AUGUST 1955

GEOPHYSICS RESEARCH DIRECTORATE
AIR FORCE CAMBRIDGE RESEARCH CENTER
BEDFORD MASSACHUSETTS

PREFACE

The research presented in this paper represents the bulk of the work performed on the numerical integration of simple non-linear atmospheric models by the Numerical Prediction Project, a group jointly supported by the Geophysics Research Directorate and the Air Weather Service, during the period from the project's activation in February, 1953 to August, 1954. Members of the project are connected with the Directorate's Atmospheric Analysis Laboratory.

Partly to determine the operational feasibility of the models then available for numerical forecasting purposes and partly to lay the foundation for a systematic research program in numerical prediction, it was decided to examine the performance of the familiar barotropic model and of a simple baroclinic model under a wide variety of synoptic conditions. The month of January, 1953, was selected for this test, comprising a continuous series of 60 cases.

The efforts of the members of the project were then focused on the development of a suitable baroclinic model, the plotting, analysis and tabulation of the required synoptic data, the design and construction of the programs and codes for solution on a high-speed computer, and finally on the analysis and interpretation of the results. The overall organization of this effort was directed by Major P. D. Thompson, who was also responsible for the development of the thermotropic equations tested. The analysis and tabulation of the synoptic charts was supervised by Mr. C. F. Jenkins, while the calculation and summary of the statistical properties of the forecasts was supervised by Dr. L. S. Pocinki. Dr. W. L. Gates assisted Major Thompson in supervision of preparation of the numerical forecasts, and was responsible for the development of the thermotropic code. The code for solution of the barotropic model was written by Major H. A. Zartner. The successful completion of the tests was materially aided by other members of the project during this period, including Mr. L. Berkofsky, Mr. E. J. Aubert, Major J. F. Blackburn, Lt. M. E. Stern, Mr. J. J. Paznokas, Lt. Patricia Hayes, and Sgts. D. Casey and D. Grennan. Special recognition is due Mr. E. A. Bertoni for his preparation of the figures in this report. Mr. W. S. hering and Mr. W. D. Mount of the Atmospheric Analysis Laboratory assisted in verification and synoptic summary of the forecasts.

The details of the theoretical development and a statement of the overall results have been presented in a separate paper.[1] This paper has been prepared to present the detailed analysis of the results of this series of numerical forecasts, in the hope that they may serve as a standard of comparison with other methods of prediction and allow the improvement of such techniques of dynamical prediction through the focusing of further research on their inadequacies. In particular, it is hoped that the statistical and synoptic analyses of the results will permit an evaluation of these techniques by synoptic meteorologists unfamiliar with the theoretical aspects of numerical prediction. To further these purposes the actual 24-hour numerical forecast charts for 1500 G.C.T. of each day of the series are presented in the appendix to this paper.

TABLE OF CONTENTS

TABLE OF CONTENTS (Continued)

LIST OF ILLUSTRATIONS

LIST OF ILLUSTRATIONS (Continued)

LIST OF ILLUSTRATIONS (Continued)

LIST OF ILLUSTRATIONS - (Continued)

LIST OF ILLUSTRATIONS (Continued)

LIST OF ILLUSTRATIONS (Continued)

ABSTRACT

Following a resume of the theory of thermotropic flow, a simple baroclinic model in which the direction of the thermal wind is assumed invariant with height, a discussion of the methods employed for the numerical integration of this model and the barotropic model is presented.

On a finite-difference grid of 414 points covering the United States and immediately surrounding regions, a series of sixty comparative 24-hour forecasts during January, 1953, at the 500 and 1000 mb levels was obtained by relaxation methods. The median correlation coefficients between the forecast and observed 24-hour height changes were 0.80 for both thermotropic and barotropic models at 500 mb and 0.69 for the thermotropic model at 1000 mb. In comparison with a method of pure interpolation, the numerical forecasts are shown to display a positive "skill" toward the center of the forecast region where the influence of the lateral boundaries is smallest. By normalizing the root-mean-square forecast errors to allow for the normal latitudinal variation, the Rocky Mountains are found to exert a marked influence on the forecasts at both 500 and 1000 mbs over the south central United States.

From a synoptic point of view, the numerical forecasts are found to compare favorably with conventional forecasts for the same period, although they appear to introduce a small but systematic tendency to move fully developed disturbances too slowly. This error is felt to stem from the truncation errors of the finite-difference schemes employed.

Recommendations for further research to reduce the several sources of error and to extend the physical basis of the model are made.

RESULTS OF NUMERICAL FORECASTING WITH THE BAROTROPIC AND THERMOTROPIC ATMOSPHERIC MODELS

1. General Introduction

During 1952 a number of workers succeeded in devising several alternative baroclinic models (approximate formulations of the general theory of baroclinic flow) that are workable from the computational standpoint, and which contain some of the ingredients essential to the intensifications of weather disturbances. These models include the two-parameter model of Eliassen,[2] the so-called "2 1/2-dimensional" model of Eady,[3] the equivalent-barotropic model of Thompson,[4] the two-level model of Charney and Phillips,[5] and the two-layer model of Sawyer and Bushby.[6] All are substantially equivalent.

These methods had been applied in a few selected cases of rapid development with very encouraging results; the coefficients of correlation between the observed and predicted behavior of the height of the 500 mb surface averaged around 0.7, and indicated that numerical methods might be successfully applied in situations of strong cyclogenesis. Since these results could be assumed to hold in less extreme weather situations, it was generally agreed that the methods of numerical weather prediction showed promise of producing a significant increase in the accuracy of short-range forecasts. These methods might also be applied on an operational basis.

It must be emphasized, however, that even the simplest of these baroclinic models had been applied only in a few specially selected and rather unusual cases. It therefore appeared reasonable that several methods of numerical prediction, varying as to generality and complexity, should be subjected to extensive comparative tests.

The present series of tests was consequently organized with the following general objectives in view: (1) to establish the over-all accuracy of several existing methods, by applying them to a standard, representative sample of weather situations, and thereby lay the foundation for a continuing program of research in numerical forecasting, and (2) to develop and standardize procedures for producing forecasts on a regular basis from existing or anticipated methods of numerical prediction.

This research program involved the performance of a comparative series of numerical forecasts, based on different methods of prediction but on the same observational data. It was planned to compute 12- and 24-hour forecasts from 60 consecutive sets of initial data spaced 12 hours apart, in the expectation that errors could be more easily isolated and analyzed in a consecutive series than in a series chosen at random from a larger sample. The month selected for study was January 1953, when radiosonde and rawinsonde observations over the United States were quite dense, and when a fairly representative variety of weather conditions prevailed over the continental United States and environs.

After preliminary study, it was decided to compute forecasts from the equations for the barotropic model and for the so-called "thermotropic" model, a vertically-integrated two-parameter model summarized in Section 2. Comparisons between these two parallel series of numerical predictions, the changes actually observed to occur, and the forecasts prepared by conventional methods would, of course, comprise an essential first step toward the objectives of the program. These comparisons from both a statistical and a synoptic viewpoint are presented in Sections 3 and 4, wherein the present technique and theory of numerical prediction is evaluated both as a research tool and as a forecasting technique.

2. The Numerical Integration of the Thermotropic Model

2.1 Resume of the Thermotropic Equations

The derivation of the thermotropic equations for an adiabatic, frictionless atmosphere in hydrostatic and quasi-geostrophic balance has been described in detail by Thompson and Gates,[1] but will be summarized here in order to provide an introduction as well as a background to the detailed discussion of results in subsequent chapters. This so-called thermotropic model is a baroclinic two-parameter model for vertically-integrated flow, of which the basic meteorological assumption is that of an isogonal thermal wind, i.e. the direction of the wind shear does not change with height although the magnitude of the shear may change. In terms of the temperature, T, the thermotropic or two-parameter model may be characterized by the equation,

$$\nabla T = F(p)\,\nabla \bar{T}$$

where ∇ is the isobaric gradient vector, and where $\overline{T} = p_0^{-1}\int_0^{p_0} T\,dp$, with the function F(p) expressing the (magnitude) variation of the thermal wind vector. This characterization of the atmosphere's baroclinity is essentially that embodied in the two-parameter or 2 1/2-dimensional models of Eady, Sawyer and Bushby, and Eliassen; it may also be shown to be the essential basis of the two-layer baroclinic model of Charney and Phillips.

Neglecting the vertical advection of vorticity, by assuming that the relative (geostrophic) vorticity is much less than the Coriolis parameter, and neglecting the terms in the vorticity equation which represent a "twisting" or re-orientation of the vortex tubes, the equations of the thermotropic model may be written:

$$\nabla^2\frac{\partial\bar{\psi}}{\partial t} + J(\bar{\psi},\nabla^2\bar{\psi}) + \beta\frac{\partial\bar{\psi}}{\partial x} + K J(\bar{\phi},\nabla^2\bar{\phi}) + \frac{\lambda\rho}{RT_0} J(\bar{\psi}-\bar{\phi},\xi) = 0, \tag{1}$$

$$(\nabla^2-\mu^2)\frac{\partial\bar{\phi}}{\partial t} + J(\bar{\psi},\nabla^2\bar{\phi}) + J(\bar{\phi},\nabla^2\bar{\psi}) + L J(\bar{\phi},\nabla^2\bar{\phi}) + \beta\frac{\partial\bar{\phi}}{\partial x} - \mu^2 J(\bar{\psi},\bar{\phi}) + \frac{\lambda\rho p_0}{RT_0(\bar{p}F-p_0)} J(\bar{\psi}-\bar{\phi},\xi) = 0. \tag{2}$$

The bar-operator $\bar{(\,)} = p_0^{-1}\int_0^{p_0}(\,)\,dp$, and $\psi = g z/\lambda$ is a stream function for isobaric contour height z; $\phi = RT/\lambda$ is a stream function for temperature, and ξ is the elevation of the terrain. In these equations λ is the Coriolis parameter, R is the gas constant for dry air, T_0 is a representative temperature at the isobaric surface p_0 near the ground, g is the gravitational acceleration, $\beta = \partial\lambda/\partial y$ is the northward rate of change of the Coriolis parameter λ. These equations have been written in the familiar x, y, p coordinate system, with the positive x and y axes directed eastward and northward, respectively. All differentiations indicated by the Jacobian operator $J(a,b) = (\partial a/\partial x)(\partial b/\partial y) - (\partial a/\partial y)(\partial b/\partial x)$ and by the Laplacian

operator $\nabla^2 a = \partial^2 a/\partial x^2 + \partial^2 a/\partial y^2$, are to be carried out with the pressure p held fixed, as are differentiations with respect to the time t .

Equations (1) and (2) are the basic dynamical equations governing the behavior of the thermotropic model. The first three terms of Eq. (1) will be recognized as simply those of the barotropic model representing the local vorticity changes due to the individual conservation of absolute vorticity. The fourth term of Eq. (1) represents the rate of production or destruction of mean vorticity by the advection of "thermal" vorticity by the "thermal" wind, such that absolute vorticity will be increased in a disturbance when the thermal trough is "lagging" behind the contour trough - an easily recognized and well-known synoptic condition. The last term in Eq. (1) represents the mean vorticity generation due to the effects of terrain-enforced vertical motions, such that a vorticity increase or cyclogenesis tends to occur in strong flow on the lee side of elevated terrain. The several terms of Eq. (2) can be similarly interpreted as due to the effects of either thermal or contour vorticity advections or to the effects of terrain-induced vertical motions; the sixth term of Eq. (2), however, represents the effects of mean vertical motions on the changes of thermal vorticity, and thereby explicitly introduces the thermodynamical relation for adiabatic flow into the system.

By introducing the concept of an equivalence level in the middle troposphere, at which the mean wind is equal to the vertically-integrated wind, the equations of the thermotropic model may be written in terms of the height of a selected isobaric surface, say 500 mb., and the height of an isobaric surface near the ground, say 1000 mb. With this identification, Eqs. (1) and (2) become for flow over perfectly flat terrain ($\zeta = 0$):

$$\nabla^2\left(\frac{\partial z}{\partial t}\right) + \frac{g}{\lambda} J(z, \nabla^2 z) + \beta \frac{\partial z}{\partial x} + \frac{g}{\lambda} K J(h, \nabla^2 h) = 0, \qquad (3)$$

$$(\nabla^2 - \mu^2)\frac{\partial h}{\partial t} + \frac{g}{\lambda} J(z, \nabla^2 h) + \frac{g}{\lambda} J(h, \nabla^2 z)$$

$$+ \frac{g}{\lambda} L J(h, \nabla^2 h) + \beta \frac{\partial h}{\partial x} - \frac{g}{\lambda} \mu^2 J(z, h) = 0, \qquad (4)$$

where z is the 500 mb height, and h is the 500-1000 mb thickness. The factor c embodies the effect of the height of the level of equivalence in this model and is given by,

$$c = (2 - \bar{p}/p^*)^{-1} ,$$

where $\bar{p}$ is the mean pressure, $\bar{p} = p_0/2$, and p^* is the pressure at the equivalence level, taken to be 600 mb.

The thermotropic coefficients K and L which appear in Eqs. (1-4) are defined by the theory to be functions of pressure alone, and are given by Thompson and Gates,[1]

$$K = 2\left(\overline{\frac{F}{p}\int_0^p F(p')\,dp'}\right) - 1 , \qquad (6)$$

$$L = \frac{p_0}{(p_0 - \bar{p}\bar{F})}\left[K - 1 - \frac{2}{p_0}\left(\overline{\frac{F}{p}\int_0^p p' F(p')\,dp'} - \bar{p}F\right)\right] , \qquad (7)$$

where $F(p)$ is the thermotropic parameter describing the vertical variation of the wind shear as introduced earlier. The quantity μ^2 is a measure of static stability and is given by,

$$\mu^2 = \frac{2\lambda^2(\bar{p}\bar{F})}{(\bar{p}\bar{F} - p_0)(RT_0 - gh(1+\kappa))} , \qquad (8)$$

with $\kappa = R/c_p$, c_p being the specific heat of air at constant pressure.

The simplified dynamical formulas, Eqs. (3) and (4), are now to be solved by an iterative procedure wherein the system is regarded as linear with the time derivatives of z and h as the dependent variables, and all other terms regarded as known non-homogeneous members of the equations. Starting from the known initial distributions of 500 mb height z and 500-1000 mb thickness h, all terms not involving time derivatives in Eqs. (3) and (4) may be evaluated, a solution carried out to obtain $\partial z/\partial t$ and $\partial h/\partial t$

from the resulting Poisson and Helmholtz equations, respectively, and finally a time-extrapolation made from $\partial z/\partial t$ and $\partial h/\partial t$ to regenerate z and h a short time later than the initial data. This iterative process may then be repeated cyclically until the aggregate of the time extrapolations is equal to the desired period of the forecast.

The actual solutions of Eqs. (3) and (4) were carried out on a rectangular finite-difference grid, and for variables expressed in non-dimensional measure. In the numerical solutions, the selection $p^* = 600$ mb was made, resulting in $c = 0.86$ when $\bar{p} = 500$ mb. The thermotropic coefficients K and L in these equations were assigned the constant values 0.28 and -0.18, respectively,* which were determined by fitting the observed winds over North America to an idealized wind profile for a series of ten cases selected from January, 1953. In the expression for μ^2, as given by Eq. (8), the factors in parentheses were found to be nearly constant for the same series of cases, with μ^2 an average value of $+5.0 \times 10^{-16}$ cm^{-2}, which was accordingly used throughout the series of integrations.

Accounting these modifications, Eqs. (3) and (4) may be written in non-dimensional form, with the omission of primes understood, and for a rectangular grid, as follows:

$$\Delta^2\left(\frac{\partial z}{\partial t}\right)_{ij} = 0.86\, A'_{ij}\, I_{ij}(z, \Delta^2 z) + 0.24\, A'_{ij}\, I_{ij}(h, \Delta^2 h) + A^2_{ij}\, \Delta_x z + A^3_{ij}\, \Delta_y z = Z_{ij}(x, y), \tag{9}$$

$$(\Delta^2 + B'_{ij}/4A'_{ij})\left(\frac{\partial h}{\partial t}\right)_{ij} = -0.86\, A'_{ij}\, I_{ij}(z-h, \Delta^2(z-h)) - 0.86\, A'_{ij}\, I_{ij}(z, \Delta^2 z) - 0.70\, A'_{ij} I_{ij}(h, \Delta^2 h) + A^2_{ij}\, \Delta_x h + A^3_{ij}\, \Delta_y h + 0.86\, B'_{ij}\, I_{ij}(z, h) = H_{ij}(x, y), \tag{10}$$

*For a linear wind profile, such as that embodied in the equivalent-baroclinic model,[4] the values corresponding to the thermotropic coefficients K and L are 1/3 and zero, respectively.

The coefficients A^1_{ij}, A^2_{ij}, A^3_{ij} and B^1_{ij} are point-wise variable and given by,

$$A^1_{ij} = -\frac{gH}{16\lambda m^2 l^2 \Omega} , \tag{11}$$

$$A^2_{ij} = -\frac{\beta m l \cos n\varphi}{\Omega} , \tag{12}$$

$$A^3_{ij} = -\frac{\beta m l \sin n\varphi}{\Omega} , \tag{13}$$

$$B^1_{ij} = -\frac{\mu^2 g H}{\lambda \Omega} . \tag{14}$$

Here H is the reference unit of contour height (such that $z' = zH^{-1}$, where z' is the non-dimensional variable), Ω is the reference unit of non-dimensional frequency, l is the mesh constant of the finite-difference grid, m and n are the mapping or scale factor and the cone constant, respectively, of the projection on which the calculations are performed, and φ is the longitude deviation of a grid point from the meridian about which the grid is symmetrical ($\varphi > 0$ to east). In the present case, $l = 2.2$ cm on the WBAN-1 synoptic chart, a Lambert conic conformal projection whose scale factor is $m = (R/r_E)\cos\theta\, n^{-1}[\tan(\pi/2 - \theta)/2]^n$ where R/r_E is the ratio of the pole-to-equator distance of the map to the earth's radius, θ is the geographical latitude, and $n = 0.7156$ the cone constant. The unit H was taken for convenience to be 100 ft, Ω as $(1\ \text{day})^{-1}$, and the reference unit of length $L = ml$ was taken as the distance between adjacent grid points. Thus, while the "physical" coefficients K, L and μ^2 of the thermotropic equations have been taken as constants in the present solutions, the "geographical" coefficients λ, β and m have been allowed their full x, y variability.

The finite-difference operators used in Eqs. (9) and (10) are given by,

$$\Delta_x ( )_{ij} = ( )_{i+1j} - ( )_{i-1j} \quad ,$$

$$\Delta_y ( )_{ij} = ( )_{ij+1} - ( )_{ij-1} \quad ,$$

$$\Delta^2 ( )_{ij} = ( )_{ij+2} + ( )_{i-2j} + ( )_{ij-2} + ( )_{i+2j} - 4 ( )_{ij} \quad ,$$

and $$I_{ij}(a,b) = \Delta_x a_{ij} \Delta_y b_{ij} - \Delta_y a_{ij} \Delta_x b_{ij} \quad ,$$

where i and j denote measure along the now rectangular x, y axes of the grid, respectively.

In addition to the numerical forecasts for the 500 mb height and 1000 mb height (or 500 - 1000 mb thickness), forecasts of the average vertical motion were made from the first law of thermodynamics for adiabatic flow in the form,

$$\frac{\partial \bar{\Phi}}{\partial t} + J(\bar{\psi}, \bar{\Phi}) + \left(\frac{\Phi_0 - (1+\kappa)\bar{\Phi}}{p_F} \right) \bar{\omega} = 0, \qquad (15)$$

where $\bar{\omega} = \overline{(dp/dt)} \simeq \bar{\rho} g \bar{w}$ with ρ the density and $w = dz/dt$. When written in finite-difference form for the non-dimensional variables z and h , the vertical motion equation may be written,

$$\bar{w} = N \left(\frac{\partial h}{\partial t} - 4 A'_{ij} I_{ij}(z,h) \right) \quad , \qquad (16)$$

where $N = \tau R \bar{\rho}_F (p_F \lambda)^{-1} (\Phi_0 - (1+\kappa)\bar{\Phi})^{-1}$. The coefficient N was found to be approximately constant, and was assigned the average value-11.2 (dimensionless) throughout the calculations.

2.2 Method of Numerical Integration

With selected boundary conditions, the method of solution consisted of the determination of the tendencies $\partial z/\partial t$ and $\partial h/\partial t$ by a relaxation method, followed by an extrapolation over a short time interval to generate new initial data, after which the entire process was repeated

until forecasts of the desired length were obtained. The finite-difference expressions, Eqs. (9) and (10), are to be regarded as applying to the finite-difference grid shown in Fig. 4.1, Section 4. This is a square grid of 18 x 23 points, spaced approximately 2 1/2° latitude apart and covering the continental United States, southern Canada, and the immediately surrounding territory. This grid probably has sufficient resolution to faithfully display the large-scale disturbances, and does not appear to emphasize small irregularities in the analysis of initial conditions. With the presently employed method of determining vorticity, the complete non-homogeneous terms of Eqs. (9) and (10) are determined only on and within the third interior grid points, yielding solutions for $\partial z/\partial t$ and $\partial h/\partial t$ on an interior grid of 12 x 17 points.

The first step in the solution of Eqs. (9) and (10) at each net point consisted of the calculation of a set of residuals given by,

$$R_{ij} = \Delta^2\left(\frac{\delta z}{\delta t}\right)_{ij} - Z_{ij} \quad , \tag{17}$$

$$S_{ij} = \left(\Delta^2 + \frac{B'_{ij}}{4A'_{ij}}\right)\left(\frac{\delta h}{\delta t}\right)_{ij} - H_{ij} \quad , \tag{18}$$

for the z- and h- equations, respectively, where $(\delta z/\delta t)$ and $(\delta h/\delta t)$ are a set of initial solution estimates. For $t=0$, these tendencies were taken as the actually observed 24-hour changes, centered on the initial instant; for later times, $t>0$, they were taken as the most recent solutions, i.e., the solutions for the immediately preceding time stage. The residues generated in this manner were probably somewhat larger for the first step in the iteration process than for the subsequent ones, with a consequent increase in the required amount of initial relaxation.

The relaxation itself proceeded by means of a modified form of the extrapolated Liebmann process,[1] according to which the residues R_{ij} and S_{ij} as computed from

Eqs. (17) and (18) are regarded as a measure of the "error" of the estimated solution, and are "corrected" by an amount depending upon these residues according to the process,

$$\left(\frac{\delta z}{\delta t}\right)_1 = \left(\frac{\delta z}{\delta t}\right)_0 + \alpha R_{ij} \quad , \tag{19}$$

$$\left(\frac{\delta h}{\delta t}\right)_1 = \left(\frac{\delta h}{\delta t}\right)_0 + \alpha S_{ij} \quad , \tag{20}$$

where the subscripts denote successive approximations in the relaxation process. Here α is a coefficient of over-relaxation, defined as,

$$\alpha = \frac{1}{2}(\alpha_F + \alpha_R) \tag{21}$$

where α_F is the over-relaxation coefficient of Frankel,[7] designed to give optimum convergence,

$$\alpha_F = \frac{1}{2}\left[1 + \sin\cos^{-1}\frac{1}{2}\left(\cos\frac{\pi}{p} + \cos\frac{\pi}{q}\right)\right]^{-1} \quad , \tag{22}$$

with $p = i_{max} - 1$, $q = j_{max} - 1$, equal to the number of grid intervals along the x and y axes, respectively. In Eq. (21) α_R is the so-called Richardson relaxation coefficient, a constant and equal to 1/4. For the grid employed in the present solutions, the average of these two coefficients was found to 0.54, and was employed throughout the calculations. Use of this coefficient undoubtedly speeded the convergence of the relaxation relative to the Richardson process, at least during the earlier stages; the use of the full Frankel coefficient α_F was not attempted, although it is possible that this may have speeded the relaxation convergence still more. Charney and Phillips[5] have, in fact, found the use

of such an average over-relaxation coefficient to produce the most satisfactory convergence in the solution of similar equations.

The relaxation cycle, as represented by Eqs. (19) and (20), was repeated in successive row-by-row scans of the grid until the residues everywhere and simultaneously satisfied the condition,

$$|R_{ij}|,\ |S_{ij}| \leq \epsilon ,$$

at which point the approximations $\delta z/\delta t$ and $\delta h/\delta t$ were assumed to be sufficiently close to the actual tendencies. With $\epsilon = 10$ ft day^{-1} representing the maximum disposable residue, an average of six scans of the grid were required to satisfy this convergence condition at each stage of the solution.

Upon completion of the relaxation as described above, the iteration process, or the advance of the solutions in time, was carried out by use of the "centered" extrapolation formula,

$$v^{n+1} = v^{n-1} + 2\Delta t \left(\frac{\partial v}{\partial t}\right)^{n} , \qquad (23)$$

where $n = 1, 2, \ldots$ denotes the iteration stage, Δt the increment of time over which the solutions are to be extrapolated, and $v = z$ or h, the variables of the thermotropic model. Having selected the grid point spacing Δs beforehand to faithfully portray the large-scale disturbances, the time increment Δt was selected as one hour in order to satisfy the Courant-Friedrichs-Lewy criterion of computational stability.[8] For two-parameter or two-layer models of the sort here considered, and for the iteration scheme of Eq.(23), the condition that the solutions not grow exponentially with time is approximately of the form,

$$\frac{\Delta s}{\Delta t} \geq \sqrt{2}\, C_{max} ,$$

where C_{max} is to be interpreted as the maximum particle speed in the flow.[5,8] The selection

of $\Delta t = 1$ hr proved computationally stable for all cases examined. (See, however, footnote, page 18.)

For the first hour's forecasts, Eq. (23) must, of course, be replaced by a "forward" extrapolation formula,

$$v' = v^{\circ} + \Delta t \left(\frac{\partial v}{\partial t} \right)^{\circ} . \qquad (24)$$

The lateral boundary conditions required in the solution of Eqs. (9) and (10) were taken as the observed 24-hour changes centered at the initial instant $t = 0$ in an effort to specify the boundary tendencies during the initial stages of the solution as correctly as possible. This is probably an adequate boundary condition for some research purposes. In operational application, however, a boundary tendency obtained solely from past data, a synoptically-estimated tendency, or a zero tendency will have to be used for this type of solution. To permit the regeneration of initial z and h data on the original 18 x 23 grid, these boundary conditions were specified on the three outermost grid rows, and were held fixed throughout the forecast period of 24 hours.

2 3 The Program for Machine Solution

The finite-difference equations for the thermotropic model were programmed and coded for the IBM Model 701 electronic calculator, a high speed digital computer of the stored program type.* The program itself was divided into several logical blocks or subroutines as follows:

(1) Basic initialization. This portion of the program prepares and positions the initial data input, and sets various program controls and internal tests into readiness.

---

* The basic engineering and performance characteristics of the 701 computer are described and compared with those of similar machines in Proc. I.R.E., Vol. 41, No. 10, Oct. 1953.

(2) Calculation of non-homogeneous terms. This sub-program calculates the several members of $\mathfrak{Z}$ and $\mathfrak{H}$ in Eqs. (9) and (10) using the finite-differences discussed earlier.

(3) Calculation of residues and relaxation. This portion of the program computes the residuals from Eqs. (17) and (18) corresponding to the variables s and h, using the initially-loaded observed changes as a first approximation for t = 0 and the solutions at $t=(n-1)\Delta t$ for $t=n\Delta t$. The relaxation is then performed according to Eqs. (19) and (20), the solution of each equation being completed separately.

(4) Iteration. This subprogram carries out the extrapolations of Eqs. (23) and (24) and thereby represents, from one point of view, the actual numerical "integrations" of the governing equations in time.

(5) Calculation of vertical motion. This portion of the program was utilized only at t = 0, 12, 24 hours, and computes the average vertical velocity according to Eq. (16). These computations at t = 0 are shown in the Appendix.

Each of these subroutines is characterized by: (a) an initial series of orders or machine instructions in which the addresses (data locations in the computer's electrostatic memory) of the pertinent data and constants are "initialized" or set to the beginning of the finite-difference grid; (b) a sequence of instructions by means of which the actual calculations is performed--e.g. addition, multiplication and (c) a series of instructions which "modify" or alter the addresses of the data used in the calculations in order that the computation may proceed to the next grid point. The sequence of steps (b) and (c) is repeated cyclically until the required computation has been performed for each point of the finite-difference grid.

While the approximate character of the results from the machine integration of the thermotropic model could, of course, be anticipated to some extent, it was found necessary to carry out

a careful manual calculation of the instantaneous tendencies $\partial z/\partial t$ and $\partial h/\partial t$ in order to obtain a detailed verification of the correctness of the design and operation of the code. These calculations allowed, furthermore, an examination of the round-off or truncation error allowable in the machine, and made possible a more nearly optimum selection of the constants α and ϵ and a consequent speeding of the relaxation process.

While executing the thermotropic code for a 24-hour forecast at 500 and 1000mb, the machine performs about 500,000 multiplications, approximately half of which are made in the course of the relaxation process, performed each hour for Eqs. (9) and (10). In addition, the machine executes approximately 15,000,000 additional orders in the course of the forecasts. All of the calculations are performed completely in the machine's high-speed electrostatic memory, without the assistance of auxiliary storage units such as magnetic drums or magnetic tapes; for a larger program or when a larger finite-difference grid is involved, the use of these lower-speed storage units will probably be a necessary ingredient of the program. In its present form, the thermotropic program requires approximately 25 minutes for the production of 12-and 24-hour forecasts at 500 and 1000 mb, together with the forecast vertical motions; this time includes about one minute for loading the program into the calculator, and approximately three minutes for the automatic printing of the forecasts. In all, a total of sixty 12-hour forecasts and sixty 24-hour forecasts were prepared at both 500 and 1000 mb from this code, starting with the 1500 G.C.T. synoptic chart for 1 Jan., 1955, and including each 0300 and 1500 G.C.T. chart through 0300 G.C.T. 31 Jan., 1955.

2.4 Integration of the Barotropic Model

As the second model in this series of comparative numerical integrations, the barotropic model representing the behavior of a frictionless adiabatic atmosphere in two-dimensional, non-divergent motion over flat terrain under hydrostatic and quasi-geostrophic balance was examined. This

model may, of course, be recognized as a special case of thermotropic flow. When the 500 mb surface is identified with an equivalence level representing the mean motion of the atmosphere, the governing equation of the barotropic model may be written,

$$\nabla^2\left(\frac{\partial z}{\partial t}\right) + \frac{gc}{\lambda} J(z, \nabla^2 z) + \beta \frac{\partial z}{\partial x} = 0, \qquad (25)$$

where the symbols are as defined earlier. For the barotropic model, the equivalence factor c was taken as unity. Upon the introduction of a scheme of non-dimensional measure and finite-differences as for the thermotropic model, Eq. (25) may be written,

$$\Delta^2\left(\frac{\partial z}{\partial t}\right)_{ij} = A^1_{ij} I_{ij}(z, \Delta^2 z) + A^2_{ij} \Delta_x z + A^3_{ij} \Delta_y z \,. \qquad (26)$$

The solution of Eq. (26) proceeded exactly as in the case of the thermotropic equation for 500 mb flow. After the computation of residues, the relaxation proceeded with the same lateral boundary conditions, over-relaxation coefficient α, maximum disposable residue ϵ, and the same iteration process as for the thermotropic solutions. The code of approximately 600 instructions was written by Major Zartner and requires an average of five minutes for execution on the IBM 701 computer, including the performance of the loading and printing routines. In the barotropic case there is, of course, only a forecast of 500 mb height changes, and no information regarding the 1000 mb changes and associated vertical motion was obtained.

3. The Statistical Summary and Analysis of Forecasts

3.1 Introduction

Upon completion of the integration of the barotropic and thermotropic models for the series of 60 cases, it became a primary concern to establish some measure of the accuracy of the thermotropic and barotropic forecasts, and to compare the results of integrating the thermotropic equations

with those obtained from the barotropic equation. Although meteorologists generally recognize the shortcomings of the linear correlation as a measure of forecasting accuracy it is nevertheless the most commonly employed statistic. It was therefore decided to compute the linear correlation between the forecast and observed height changes for each series of numerical forecasts. Since the correlation is principally sensitive to phase differences the root mean square error was computed in addition to furnish a more amplitude-sensitive measure of accuracy.

It is unfortunate that the correlations obtained here are not directly comparable with those presented by other investigators, since the results depend on the size and location of the forecast region and on the nature of the boundary conditions used for a particular calculation. In fact, the possibility of making such a controlled comparison was a major motivation of the present work in which the solutions of two numerical prediction models, the thermotropic and barotropic, were produced under identical conditions.

While Charney and Phillips[5] have compared correlations for a barotropic model with those for a "2- 1/2 dimensional" model, the barotropic model produced a forecast at the 500 mb level and the 2- 1/2 dimensional model produced forecasts at the 300 and 700 mb levels. The quantities compared were the correlations of the barotropic forecast 500 mb changes with the observed 500 mb changes and the correlations of the 2- 1/2 dimensional model forecast 700 mb changes with the observed 700 mb changes. Charney[9] has more recently presented a comparison of the 500 mb forecasts of a three-level model with 500 mb forecasts of a one-level model and the 700 mb forecasts of a two-level model during a three-day period of intense cyclogenesis. The correlations of forecast 24-hour changes with observed 24-hour changes were high for the three series of forecasts preceding the storm, but only those for the three-level forecasts remained high after the storm developed. Neither of these comparisons were felt to constitute a conclusive

examination of the relative performance of the one-, two-, and three-level models, although they documented for the first time the anticipated superiority of the three-level model in a case of strong baroclinity. There remains to be made, however, systematic model comparisons in a wide variety of synoptic situations.

From the present work we are in a position to compare the performances of the barotropic and thermotropic models in predicting 500 mb height changes over a long series of forecasts, in which both models were integrated under identical conditions.

In the following sections, the several basic statistics (correlations, root-mean-square errors) summarizing the results of the integrations will be presented and briefly described. Further statistical tests conducted will be discussed; finally, an evaluation of the "skill" of the forecasts from a statistical viewpoint will be made.

3.2 Space Statistics

Linear correlations between the forecast and observed height changes and the root mean square errors of the forecast height changes were computed for the 12- and 24-hour 500 mb barotropic and thermotropic forecasts, and the 12- and 24-hour 1000 mb thermotropic forecasts. In addition to the space correlation and space root mean square error for each forecast, a time correlation and time root mean square error at each grid point were computed for each series of forecasts. All of the computations were performed on the IBM type 701 electronic computer.

Figures 3.1 through 3.6 are the space correlations for each series of forecasts plotted as a function of time; Figures 3.7 through 3.12 are the space root mean square errors plotted as a function of time. The most striking feature of the time distribution of the space correlations is to be noted by comparing the results for the barotropic and thermotropic 500 mb predictions (Figures 3.1 through 3.4). For the 12- and 24-hour

predictions the barotropic and thermotropic space correlations are almost identical. In those cases for which the space correlation of the barotropic prediction is low the space correlation of the thermotropic prediction is also low.* Two possible explanations may be offered for this result:

(1) Errors in the prediction may be due to the failure to include some pertinent physical process, in which case it must be concluded that the omission occurs in both models.

(2) There is some overpowering influence, which may not be a physical influence, that causes both models to behave similarly. This may be an effect due to the mathematical formulation of the problem, or due to the use of similar numerical approximations in the solutions of the two models.

---

* One exception to this behavior is to be noted in the 24-hour 500 mb prediction made at 0300Z 17 January. The space correlation is much lower for the barotropic forecast than for the thermotropic forecast; there is a corresponding difference in the space root mean square errors. This difference is due to a very large error in the 24-hour barotropic forecast, which is concentrated in the northeast corner of the forecast area. This error is as yet unexplained, but since it arose in the computations after a successful 12-hour forecast had been made, it is conceivable that the error is a manifestation of some form of computational instability.

The general level of the 24-hour 500 mb space correlations (Figures 3.3 and 3.4) is only slightly lower than the 12-hour 500 mb space correlations (Figures 3.1 and 3.2) except for the forecasts made at 15Z-7 Jan., 15Z-18 Jan., 03Z-19 Jan., 15Z-19 Jan., and 15Z-28 Jan., when the 24-hour correlation is much lower than the 12-hour correlation. This implies that the forecast calculations compound an error in the change pattern. A forecast which starts off badly during the first 12 hours goes further astray during the next 12 hours; a forecast which starts off well during the first 12-hour period will be a good forecast at the end of the 24-hour period. A comparison of the graphs of the space RMSE for the barotropic and thermotropic 500 mb predictions (Figures 3.7 through 3.10) reveals the same striking similarity present in the graphs of the correlation coefficients. The RMSE for the 24-hour forecasts are greater than those for the 12-hour forecasts in all cases. The correspondence between cases for which the RMSE of both the 12- and 24-hour predictions are relatively large may be noted.

The 12-hour 500 mb barotropic and thermotropic space correlation coefficients were examined in some detail. The average correlation coefficient for the barotropic predictions, 0.817, was slightly higher than the value for the thermotropic predictions, 0.812; the difference between these correlations is not statistically significant. The differences between the daily values of the normally distributed Fisher's Z for the barotropic and for the thermotropic predictions were compared to an estimate of the standard error based on a population of 204 (number of grid points) independent pairs. Since the number of independent pairs is considerably less than 204 this procedure leads to an underestimate of the standard error. The daily differences of the Z values exceeded twice the estimated standard error in only three of the 60 cases (5%). Since the standard error was considerably underestimated it must be concluded that the barotropic and thermotropic space correlation coefficients for the 12-hour 500 mb forecasts are not significantly different for any of the 60 predictions.

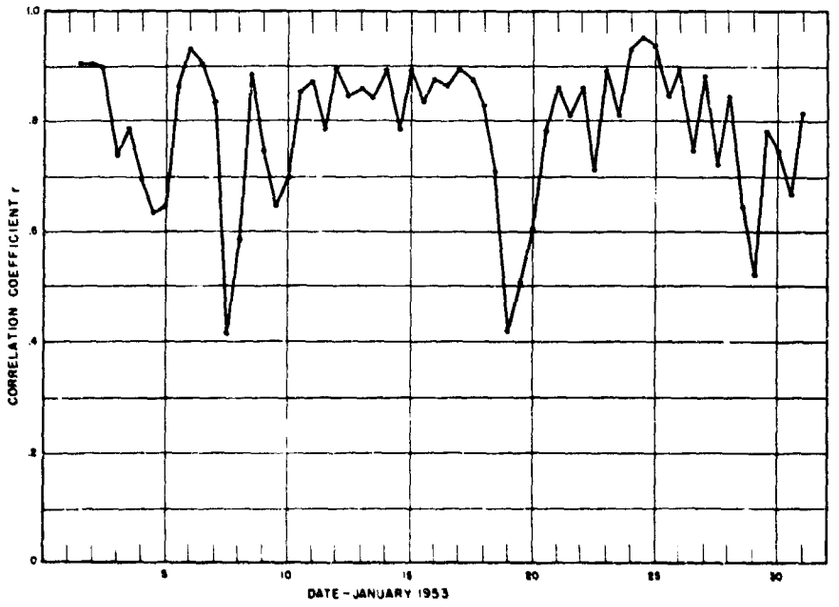
CORRELATION COEFFICIENT r
1.0
.8
.6
.4
.2
0
5
10
15
20
25
30
DATE - JANUARY 1953

Fig. 3.1

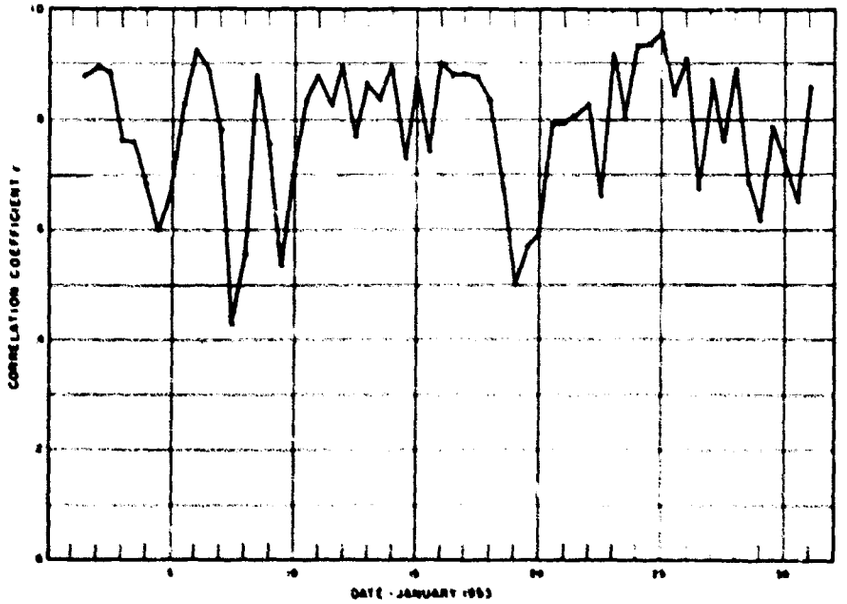
CORRELATION COEFFICIENT r
DATE - JANUARY 1953

Fig. 3.2

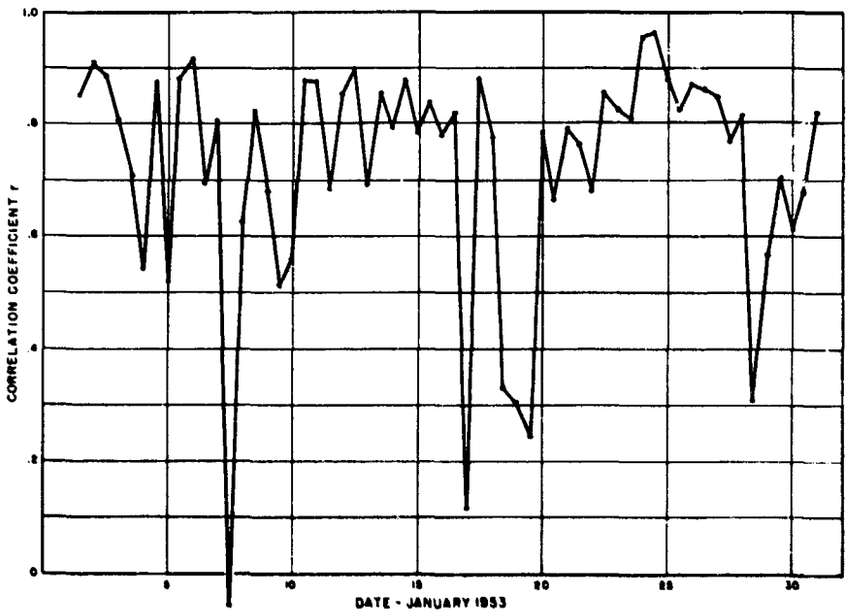
CORRELATION COEFFICIENT r
1.0
.8
.6
.4
.2
0
5
10
15
20
25
30
DATE - JANUARY 1953

Fig. 3.3

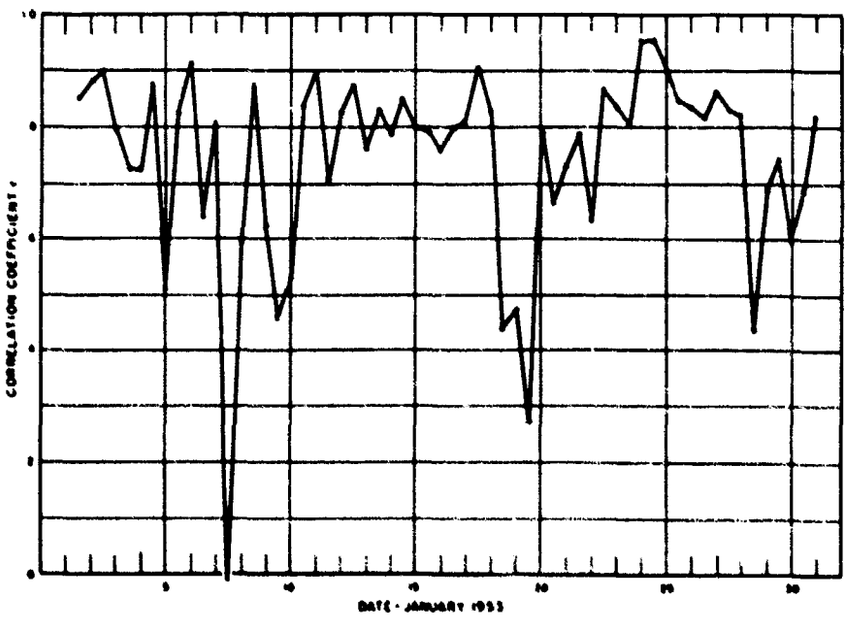
CORRELATION COEFFICIENT r
DATE - JANUARY 1953

Fig. 3.4

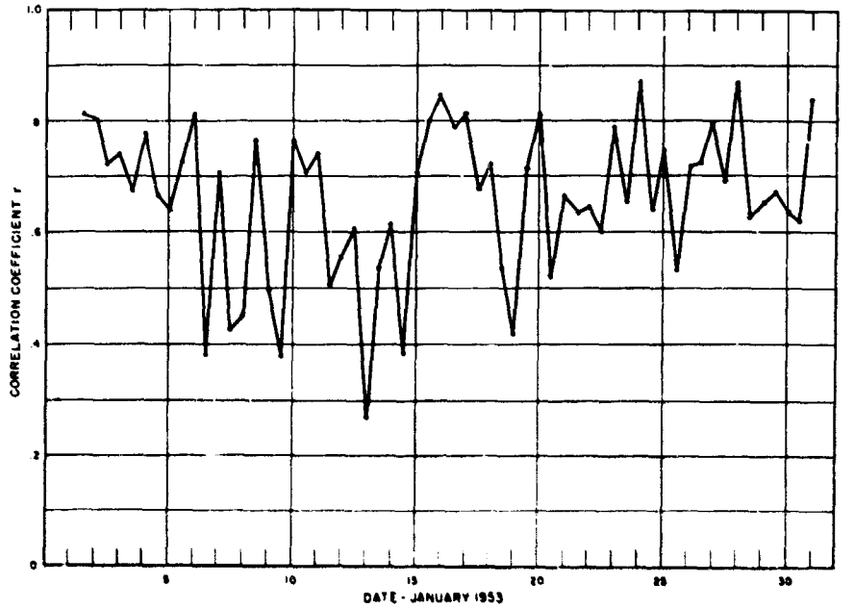
1.0
CORRELATION COEFFICIENT r
0
2
4
6
8
5
10
15
20
25
30
DATE - JANUARY 1953

Fig. 3.5

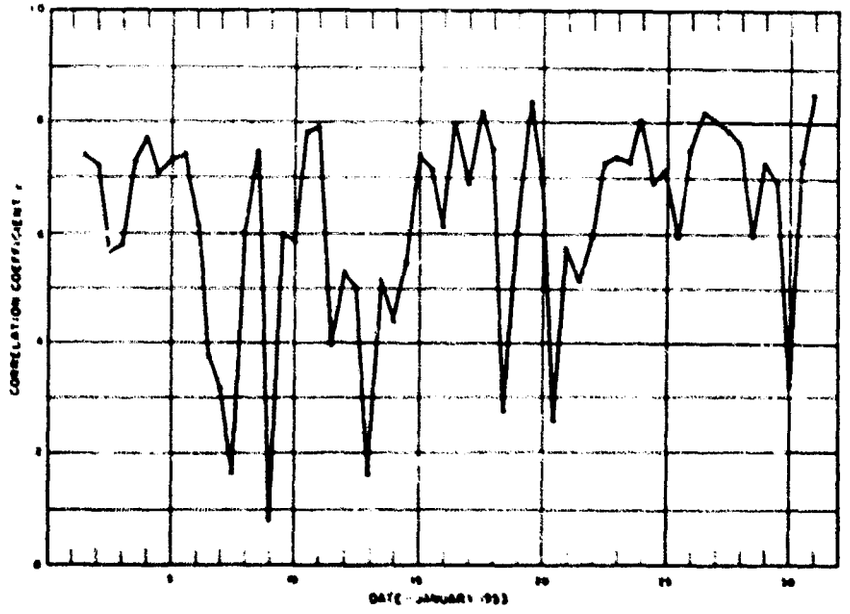
1.0
0
2
4
6
8

Fig. 3.6

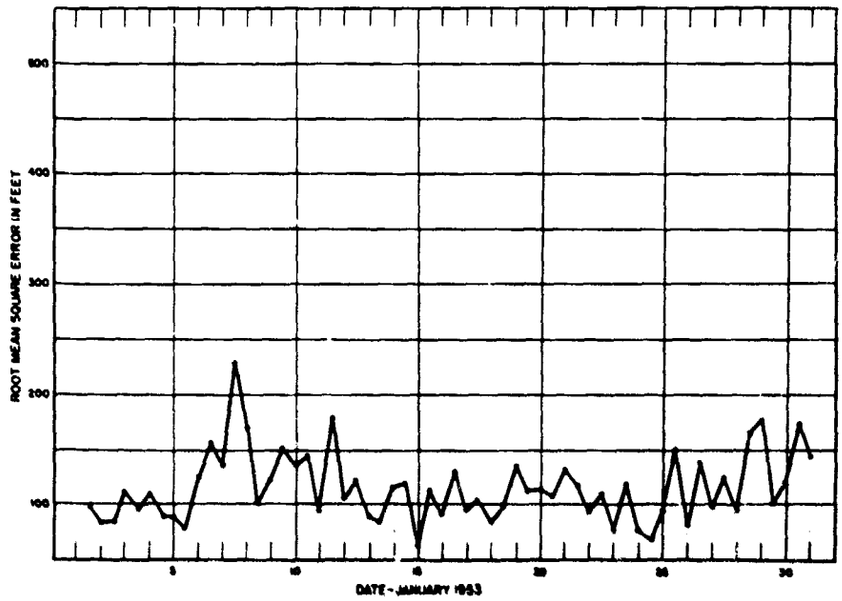
ROOT MEAN SQUARE ERROR IN FEET
DATE - JANUARY 1963

Fig. 3.7

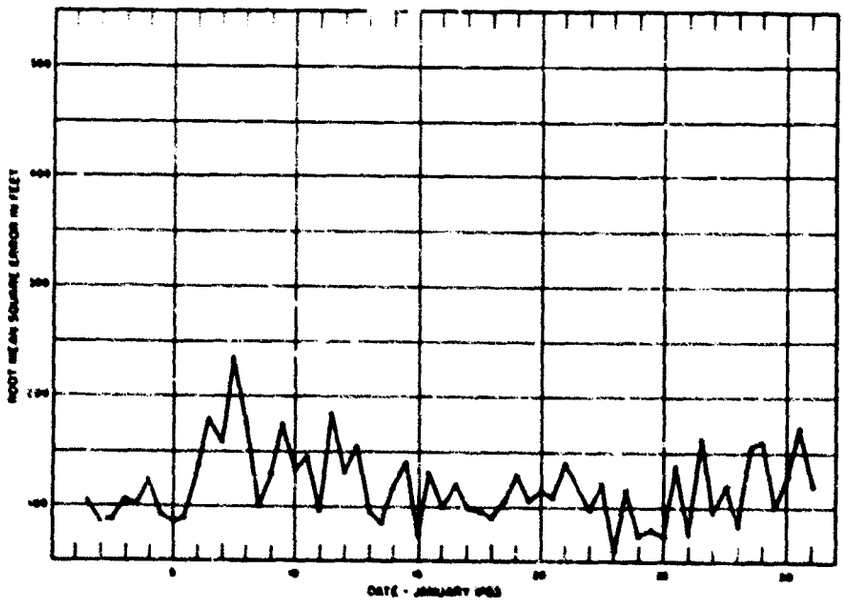
ROOT MEAN SQUARE ERROR IN FEET

Fig. 3.8

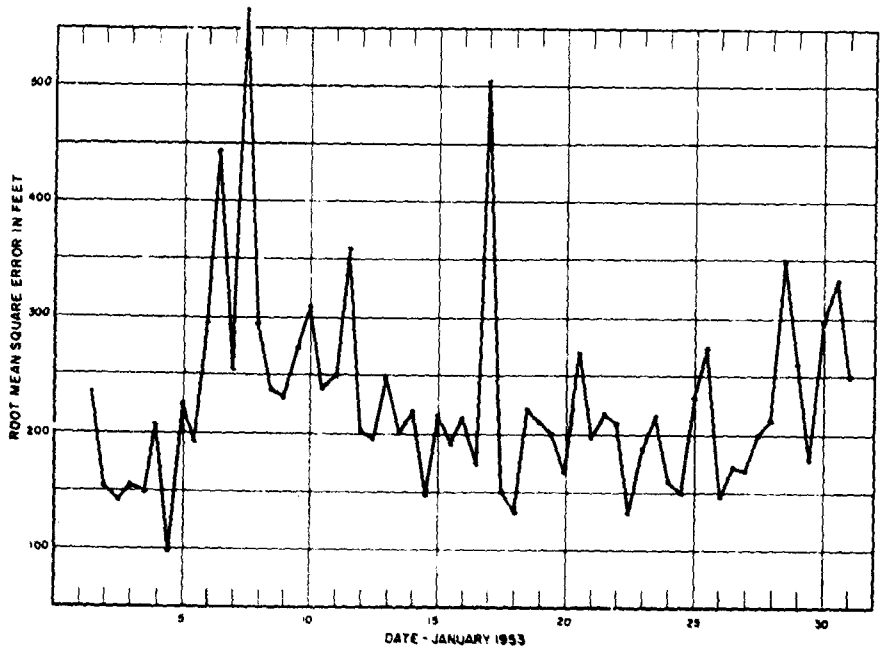

Fig. 3.9

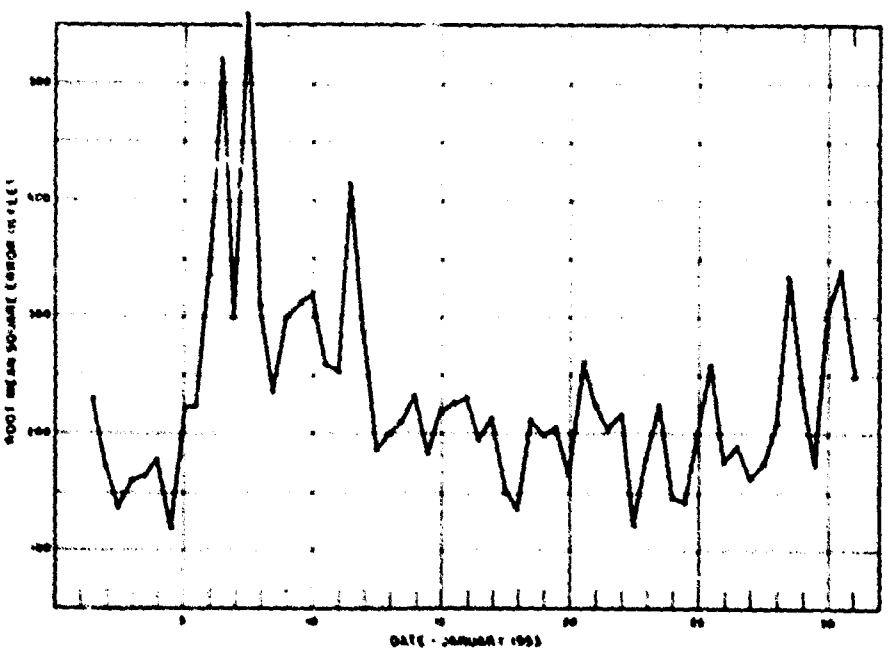

Fig. 3.10

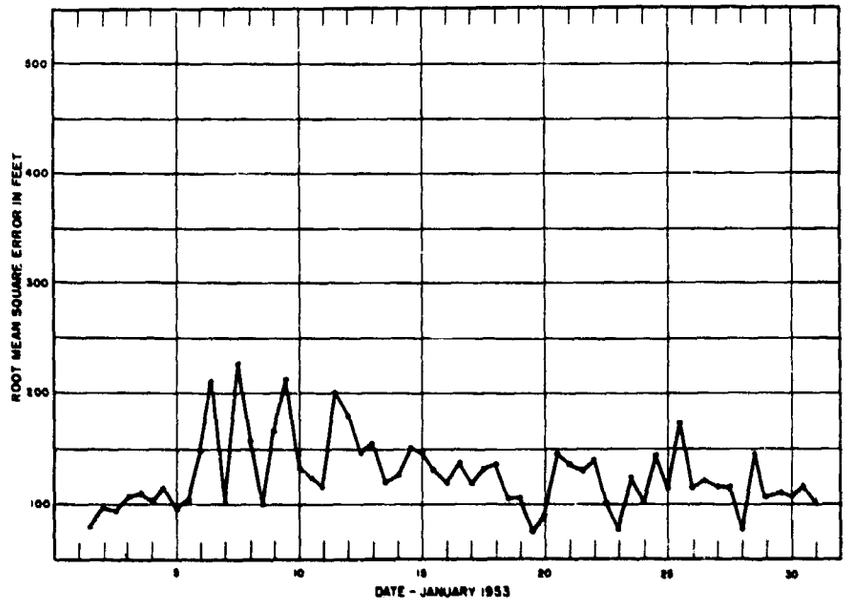

Fig. 3.11

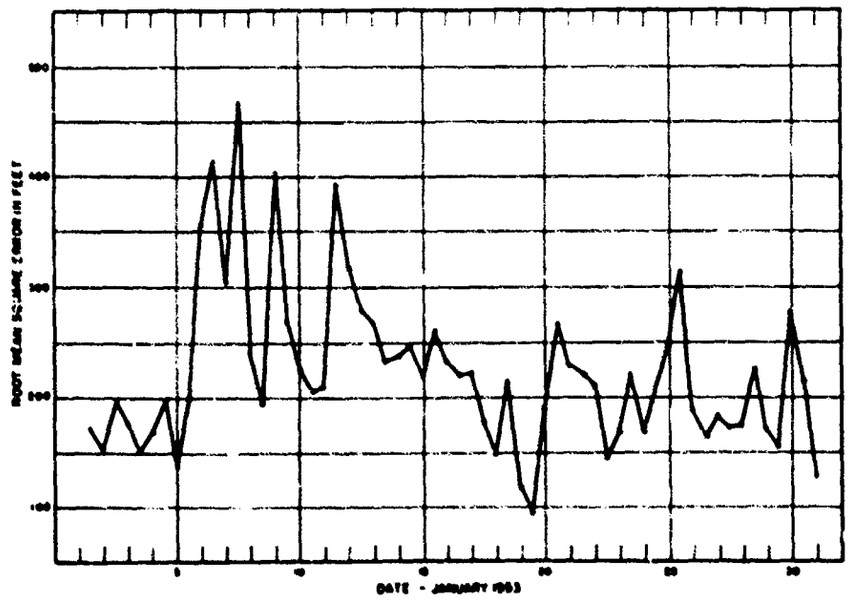

Fig. 3.12

The space correlation coefficients for the 1000 mb thermotropic predictions are generally lower than those for the 500 mb predictions. The general level of the 1000 mb space correlations is about the same for the 12- as for the 24-hour predictions, except that the minimum 24-hour correlations are considerably lower than the minimum 12-hour correlations (Figures 3.5 and 3.6). The correspondence between poor 12-hour predictions and poor 24-hour predictions is not as well marked as for the 500 mb forecasts. The space root mean square errors of the 24-hour 1000 mb predictions are greater than those for the 12-hour predictions for all cases; the increase in error from the 12- to 24-hour forecast is almost linear in time.

The frequency distributions of the space correlation coefficients are presented in Figures 3.13 through 3.18. A comparison of the frequency distributions of the space correlations for the 500 mb thermotropic and barotropic forecasts (Figures 3.13 through 3.16) again illustrates the similarity of the two sets of forecasts. The distributions of the 1000 mb space correlations are flatter than the distributions of the 500 mb space correlations. The median value of the space correlation for each set of forecasts is tabulated in Table 3.1. From each frequency distribution the percentage of forecasts for which the space correlation exceeded 0.7 may be computed. In these cases the forecast method explained approximately 50% or more of the variance of the change pattern. These percentages are also given in Table 1. Considerably more than half of the barotropic and thermotropic 500 mb forecasts exceed the 0.7 correlation level; less than half of the thermotropic 1000 mb forecasts exceeded the 0.7 correlation level.

In concluding our discussion of the space correlations some general observations may be noted. The result that the correlation is higher if the actual height changes are larger (in absolute magnitude) has been observed and reported by Lonnqvist [10] in the case of standard forecast techniques and by the Staff Members, Institute of Meteorology, University of Stockholm [11] in the case of numerical forecasts using the barotropic model.

Table 3.1 -- Space correlations. Median values and percentage of cases for which correlation was greater than 0.7.

Level	Model	Period	Median Value	Percentage Exceeding 0.7
500 mb	Thermotropic	12 Hour	.82	75.0
		24 Hour	.80	73.3
	Barotropic	12 Hour	.83	78.3
		24 Hour	.80	66.6
1000 mb	Thermotropic	12 Hour	.68	46.7
		24 Hour	.69	48.3

Table 3.2 -- Average space root-mean-square errors.

Level	Model	Period	Mean RMSE in Feet
500 mb	Thermo-tropic	12 Hour	118.7
		24 Hour	231.2
	Baro-tropic	12 Hour	115.8
		24 Hour	228.1
1000 mb	Thermo-tropic	12 Hour	126.4
		24 Hour	223.1

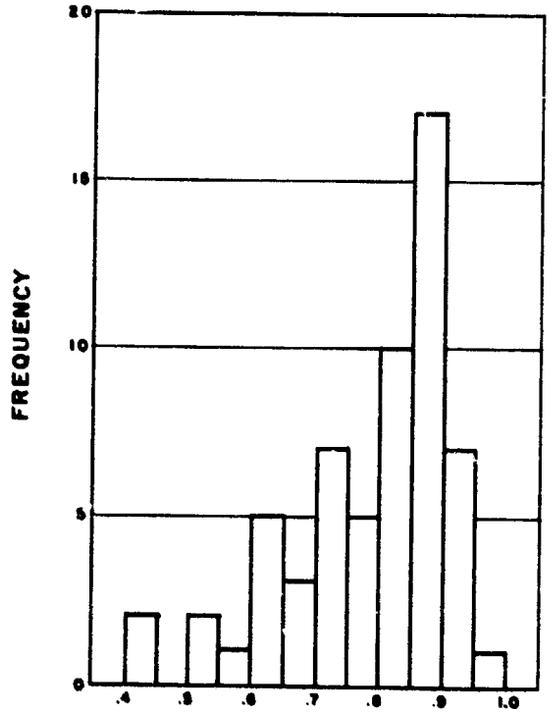

Fig. 3.13

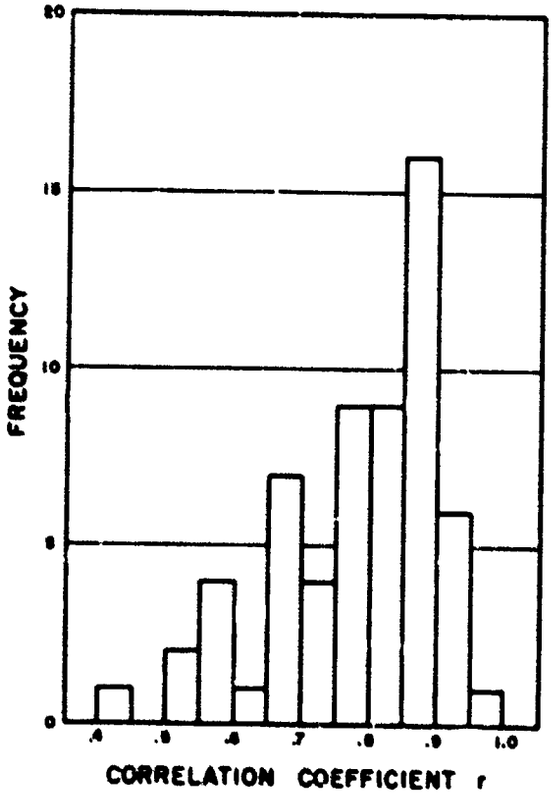

Fig. 3.14

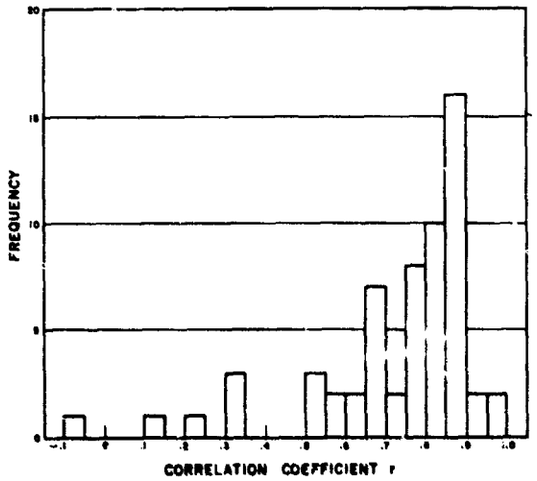

Fig. 3.15

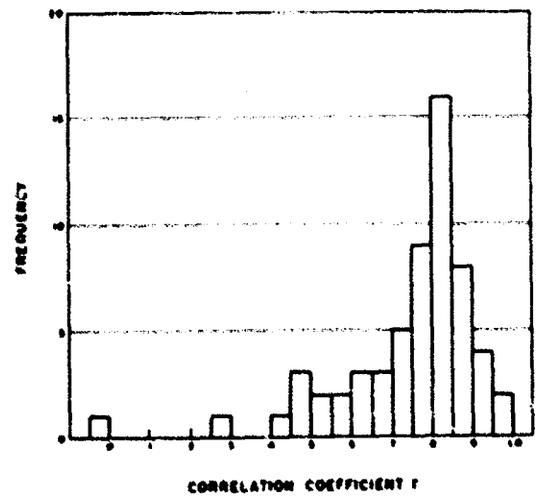

Fig. 3.16

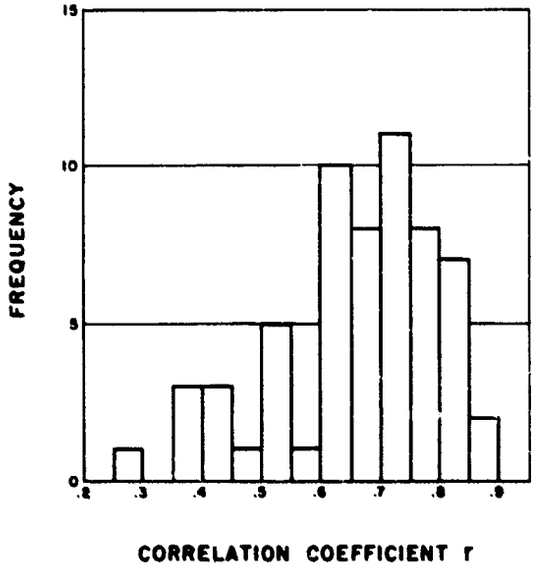

Fig. 3.17

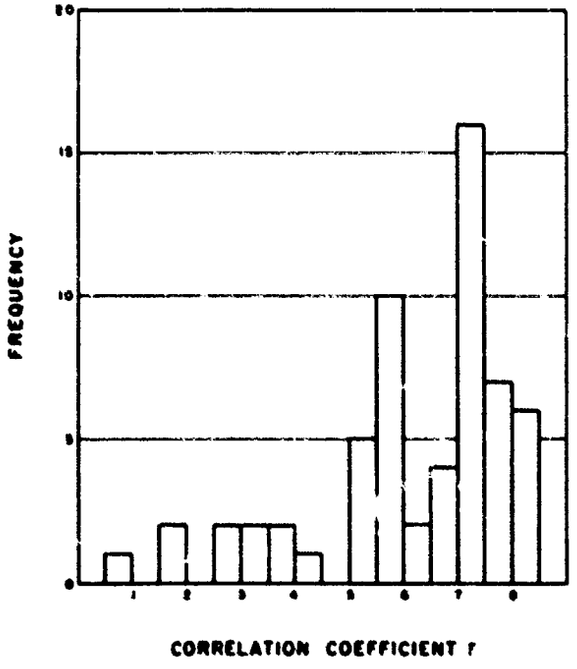

Fig. 3.18

The same general trend has been observed in the present investigation. This is probably a manifestation of the tendency to obtain a high correlation between two populations if each population has a bimodal distribution. If the average absolute value of the height change for a particular case is high, the field is generally one of relatively large rises and falls of contour height, with only a small area of little change. The nature of the linear correlation is such that a higher correlation is to be expected in such cases than in cases for which the height change field is of smaller contrast.

The average space root mean square errors are given in Table 3.2. We again note the similarity between the results of the 500 mb thermotropic and barotropic predictions. The average space root mean square errors for the 12- and 24-hour 1000 mb forecasts are approximately equal to the averages for the corresponding 500 mb forecasts. This means that the 1000 mb predictions are somewhat poorer than the 500 mb predictions since the standard deviation of the observed changes of the height of the 500 mb surface is approximately 30% larger, in the average, than the standard deviation of the 1000 mb changes. This is further indicated by the result that the space correlations for the 1000 mb predicted changes are considerably lower than those for the 500 mb predicted changes. The average RMSE for the 24-hour forecasts is approximately twice the average RMSE for the corresponding 12-hour forecasts. The error in magnitude of the forecast changes is essentially linear in time.

3.3 Time Statistics

The geographical distributions of the time correlation coefficients are presented in Figures 3.19 through 3.24. For each series of forecasts the forecast changes at a grid point, ordered sequentially in time, were correlated with the observed changes, in the same order, at the same grid point; this yields correlation coefficients for all of the grid points as a measure of the geographical variation of the forecast accuracy. There are some features of the geographical pattern common to each forecast series. Each figure has two pronounced maxima, one over the eastern U. S., and the other over the southwestern U. S.

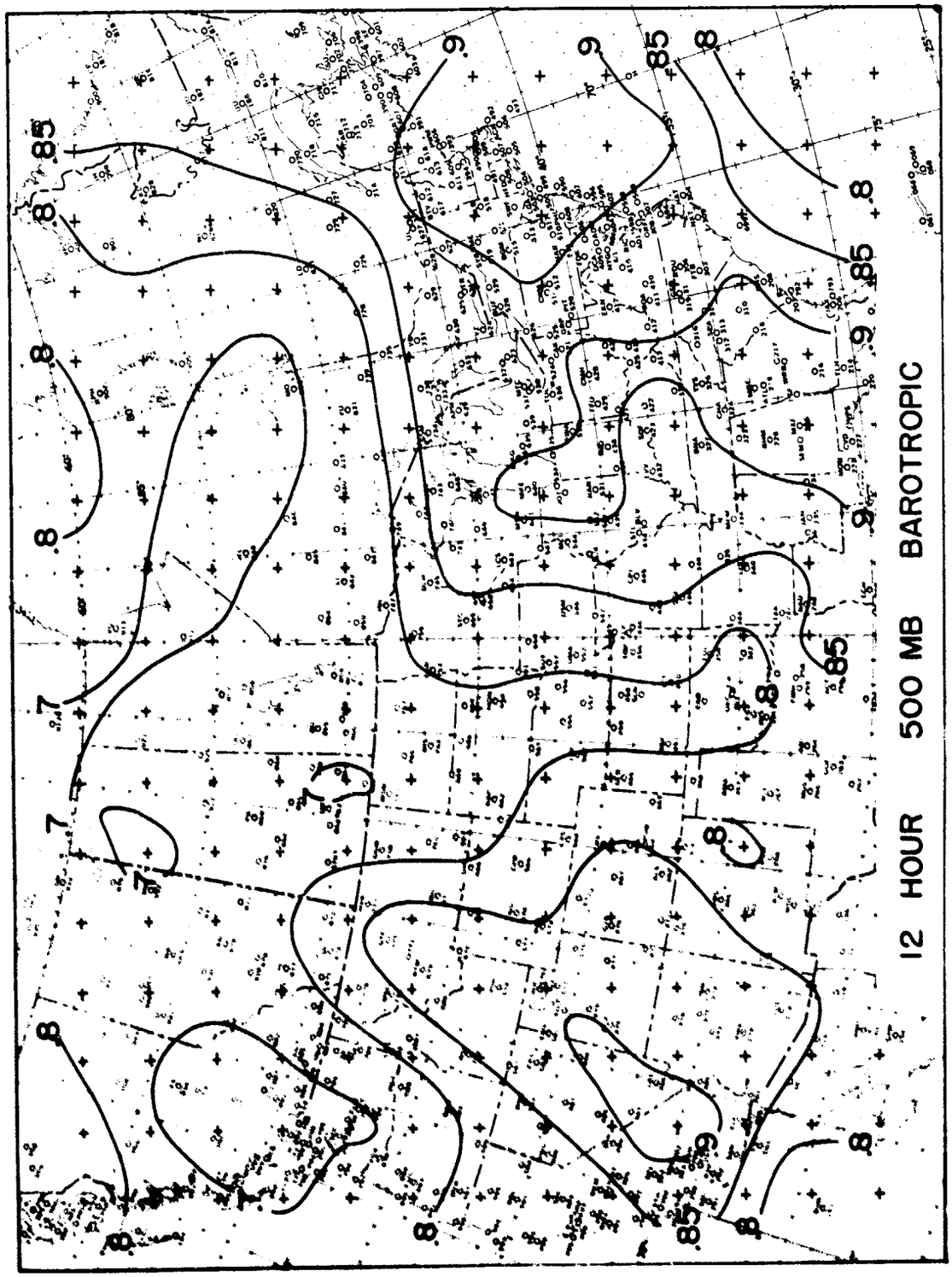

Fig. 3.19

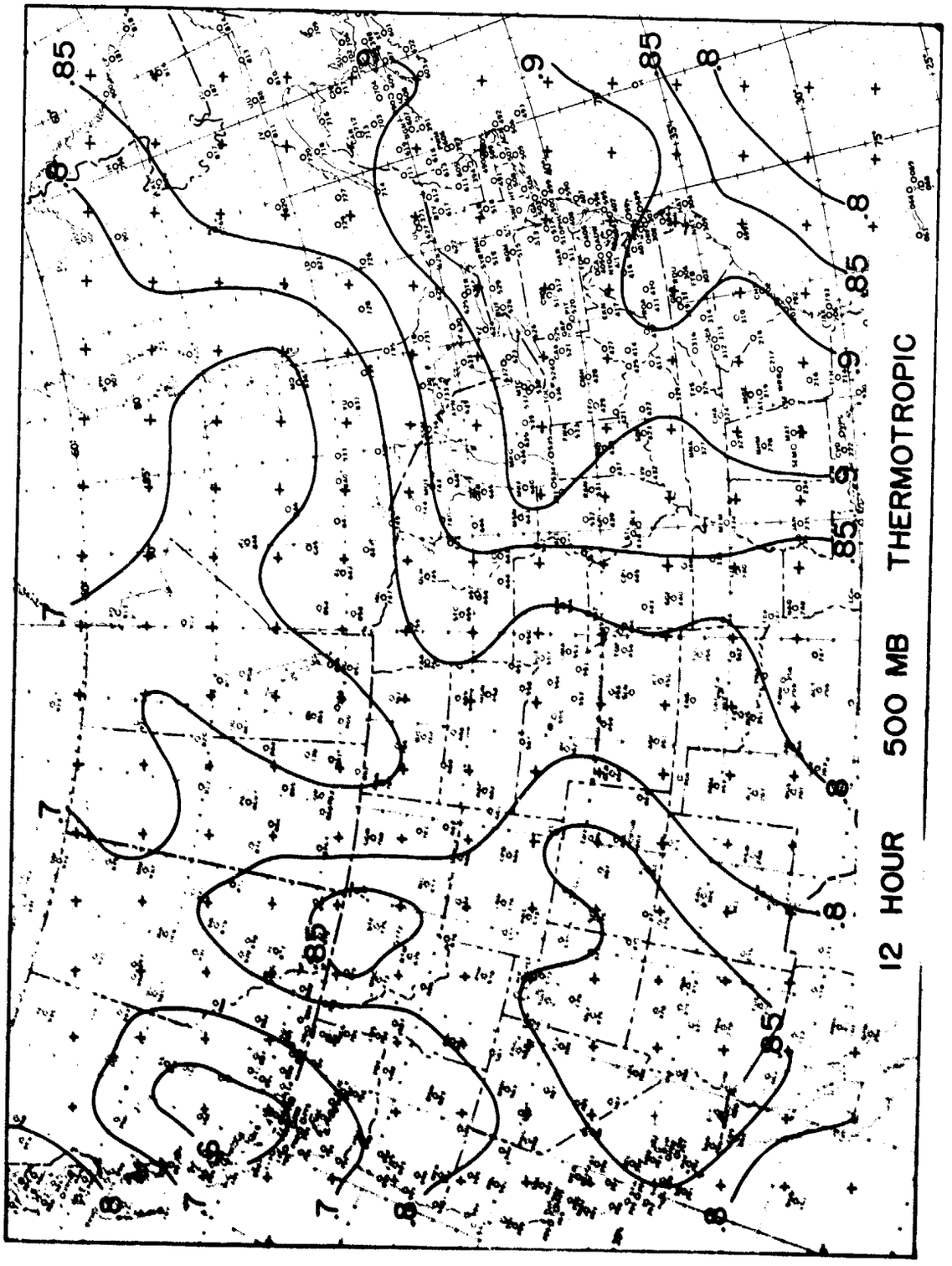

Fig. 3.20

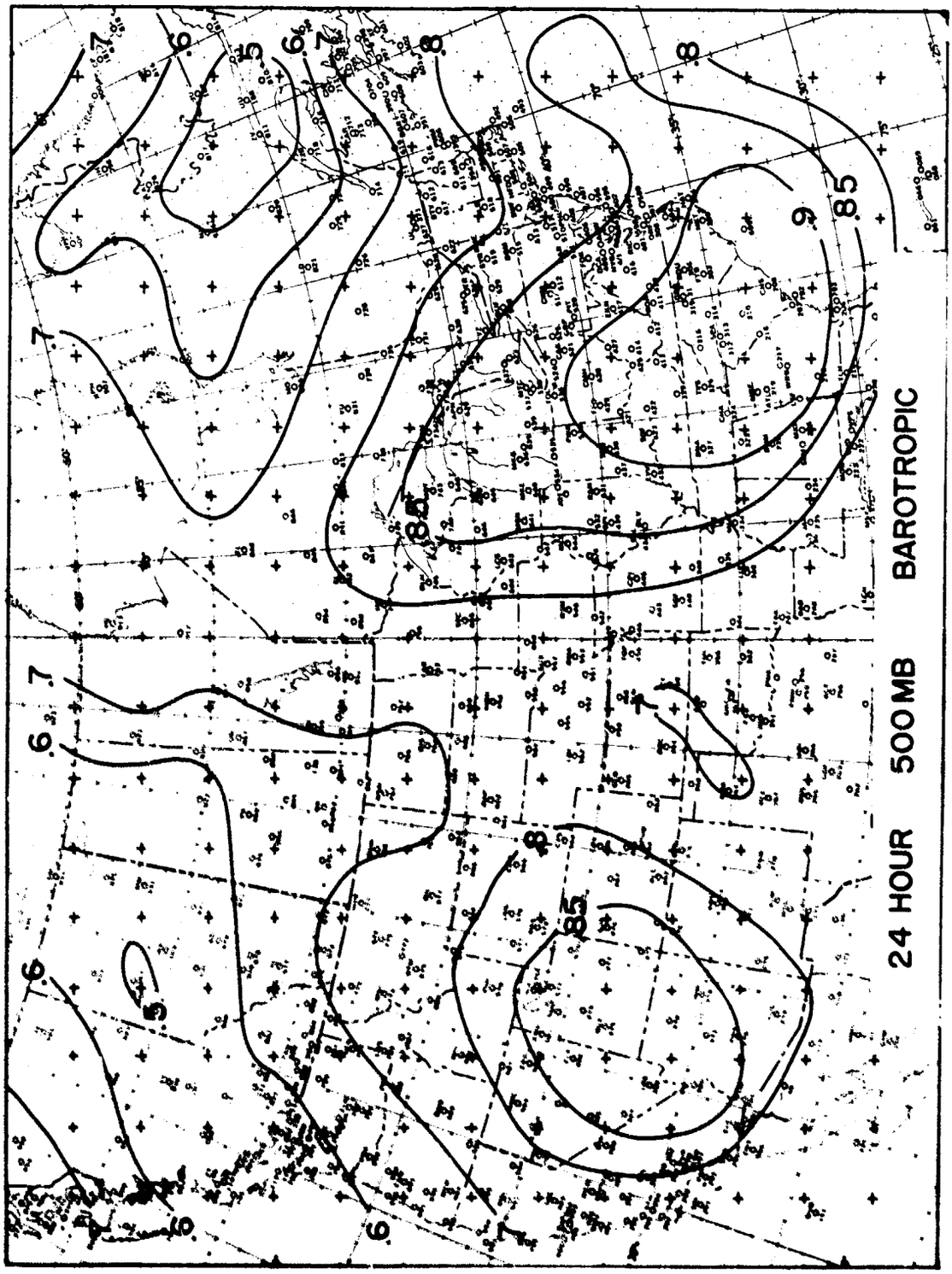

Fig. 3.21

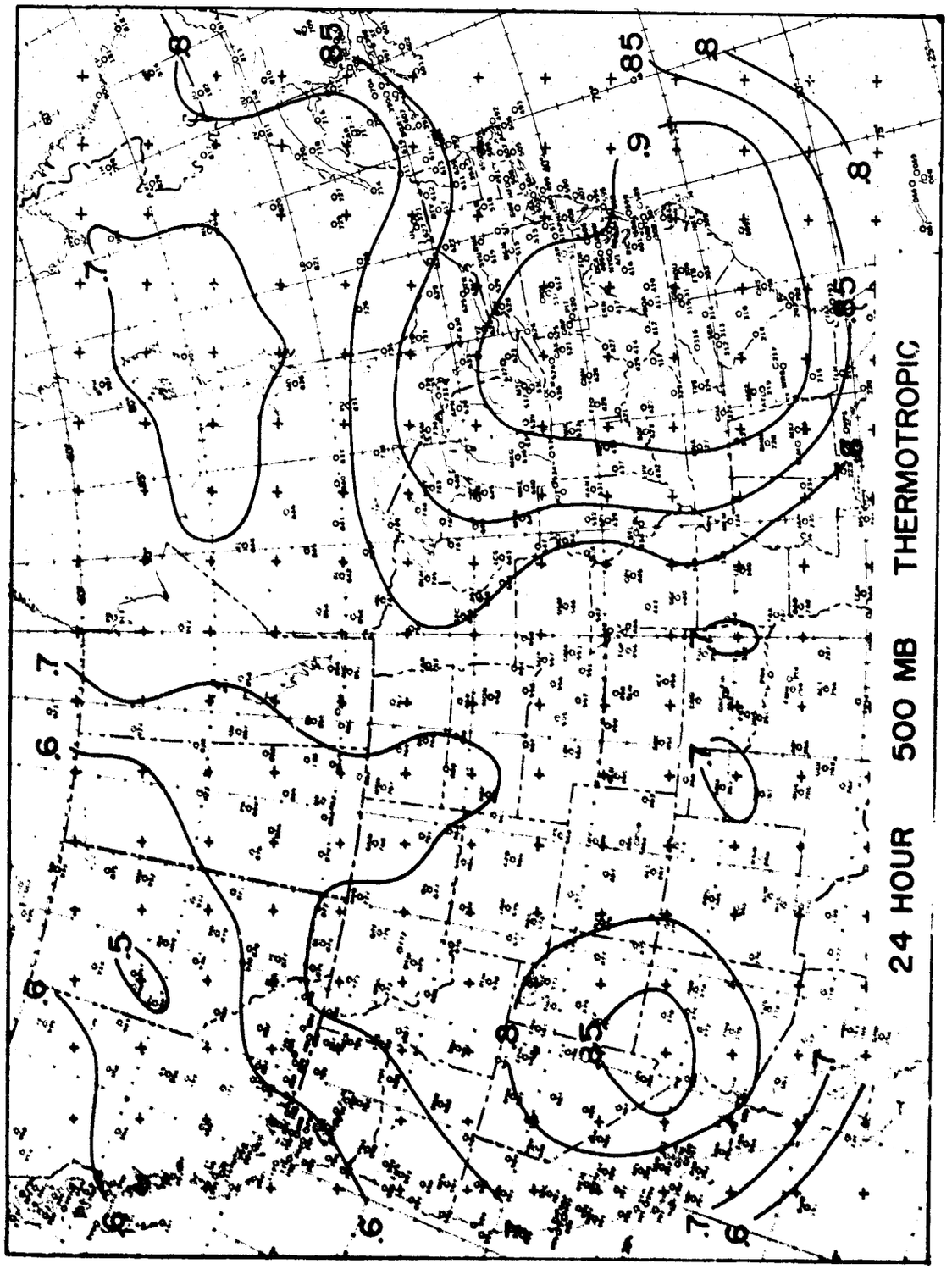

Fig. 3.22

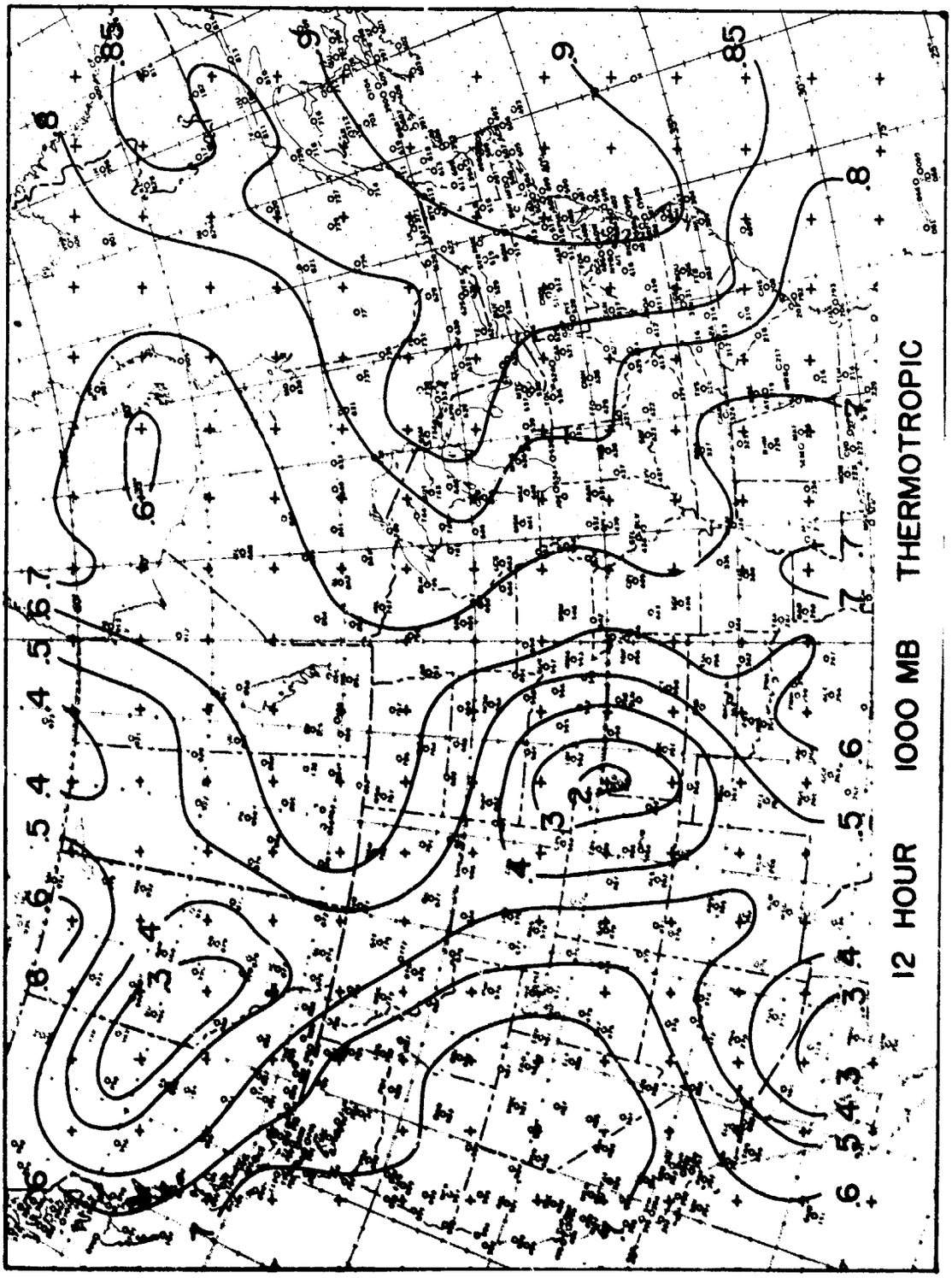

Fig. 3.23

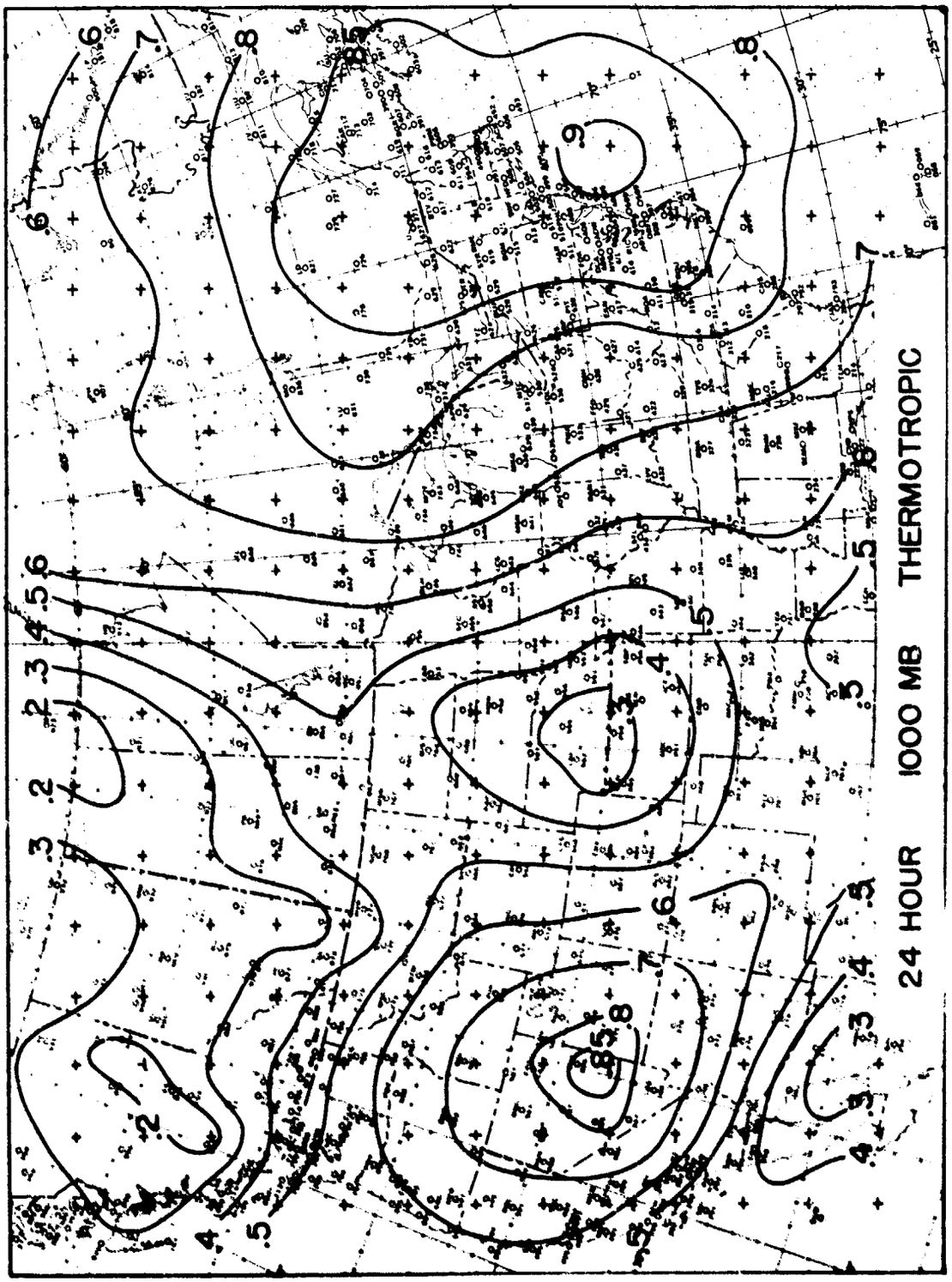

Fig. 3.24

There is a minimum value over the northwestern part of the forecast area which entends southeastward into the central U. S. The distributions of the time correlations for the barotropic and thermotropic 12-hour 500 mb predictions (Figures 3.19 and 3.20) are strikingly similar (as were the time distributions of the space correlations). A comparison of these sets of time correlations indicates that there is no grid point for which the difference between the correlations is statistically significant. The chart of the time correlations for the 24-hour 500 mb barotropic predictions (Figure 3.21) differs from the chart of the time correlations for the 24-hour 500 mb thermotropic predictions in the northeast corner of the forecast area where the barotropic correlations have a minimum. This minimum is caused by one very poor barotropic 24-hour prediction (see footnote, page

A comparison of the charts for the 12-hour 500 mb forecasts and the 24-hour 500 mb forecasts indicates that the area of high correlation in the eastern part of the forecast region is smaller for the 24-hour forecasts than for the 12-hour forecasts. Consider the area with correlation greater than 0.85; its western edge is at approximately the same position for the 12- and 24-hour 500 mb predictions, but its northern extent is diminished. The western area of correlation greater than 0.85 is considerably smaller for the 24-hour 500 mb forecasts than for the 12-hour 500 mb forecasts. The minimum value of the correlation is lower for the 24-hour predictions than for the 12-hour predictions. The area of correlation lower than 0.7 is larger on the charts of the 24-hour 500 mb time correlations than on the charts of the 12-hour 500 mb time correlations. The decrease of the correlation from 12- to 24-hours is especially marked in the northwest portion of the forecast area and in the "trough" east of the Rockies.

The principal features of the pattern of the time correlation coefficients for the 1000 mb thermotropic forecasts (Figures 3.23 and 3.24) are quite similar to the patterns of the 500 mb correlations. The maximum values of the correlation are of the same magnitude as those for the 500 mb predictions, but the minimum values are much lower. The result is that the gradient of correlation for the 1000 mb forecasts is much greater than on the charts for the 500 mb forecasts. The region of low correlation in the northwest, extending southeastward into the region east of the Rockies in the U. S., is much more pronounced.

The general result that the correlation of observed changes with forecast changes is higher for the eastern part of the forecast region than for the western part has also been obtained by Bushby and Hinds[12] for integrations of the Sawyer-Bushby two-parameter baroclinic model. The forecast region in this case covered the North Atlantic Ocean and Western Europe. The result was indicated for both the 500 and 1000 mb forecasts, although only a limited number of forecasts were made. Bushby and Hinds showed that the space correlations were higher if only the eastern portion of the forecast region was used in the verification than if the entire forecast region was used. The Staff Members, Institute of Metecrology, University of Stockholm[4] have presented a chart of the time correlations between observed and computed 500 mb height changes for a somewhat longer series of barotropic forecasts over approximately the same area, and find the same increase of correlation coefficient in the eastern portion of the forecast region. In both of these series of forecasts "operational" assumptions were made concerning the boundary conditions so that only information available at the start of the forecast period was used.

The geographical distributions of the time root-mean-square errors are shown in Figures 3.25 through 3.30. The patterns are partially obscured by a north-south gradient introduced by "climatology." Since the variability of the height of a constant pressure surface increases toward the north of the forecast area, the magnitude of the error in the forecast height change increases toward the north. This effect superimposes a zonal pattern on the root-mean-square error charts. It is still possible to

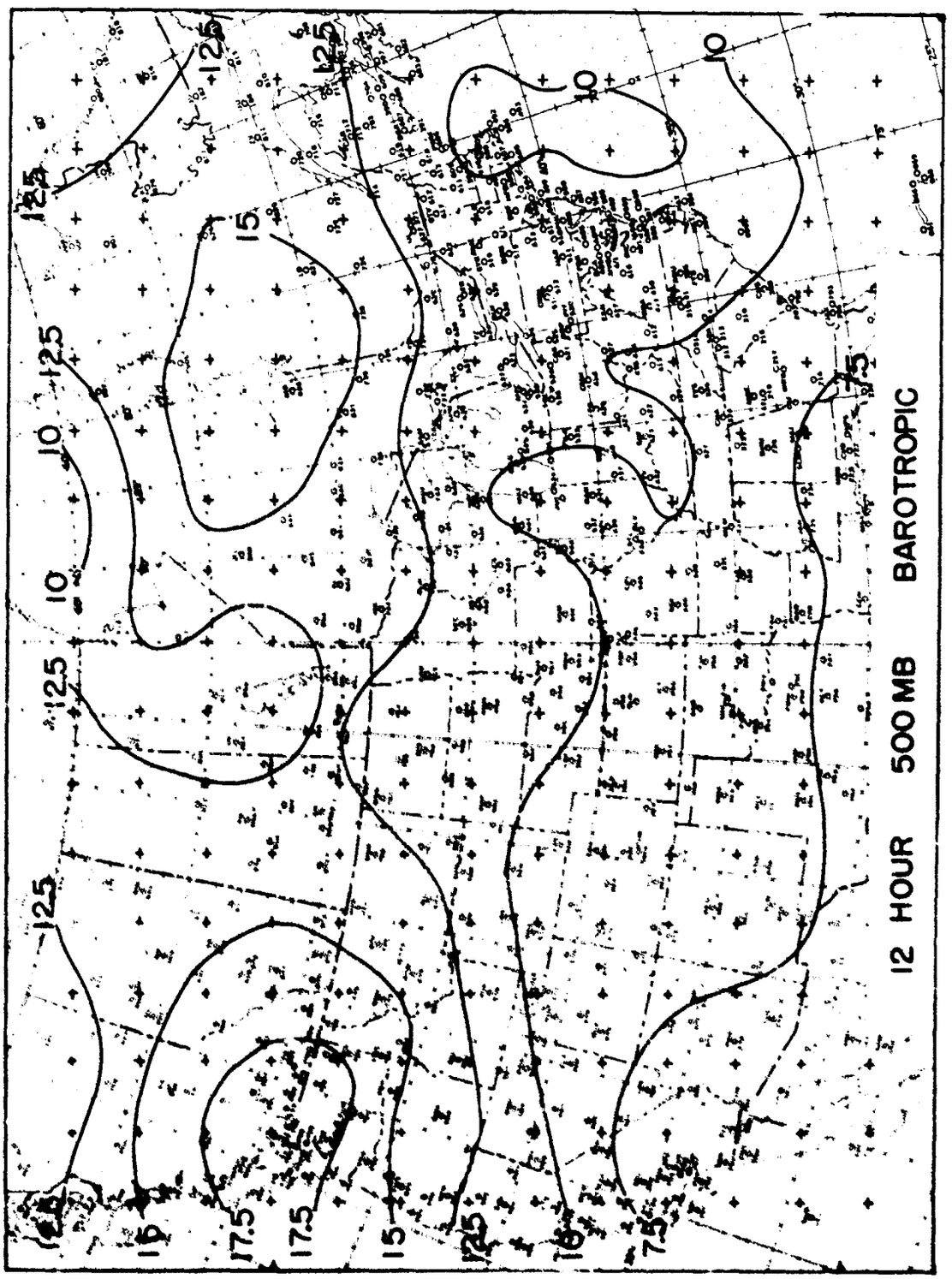

Fig. 3.25

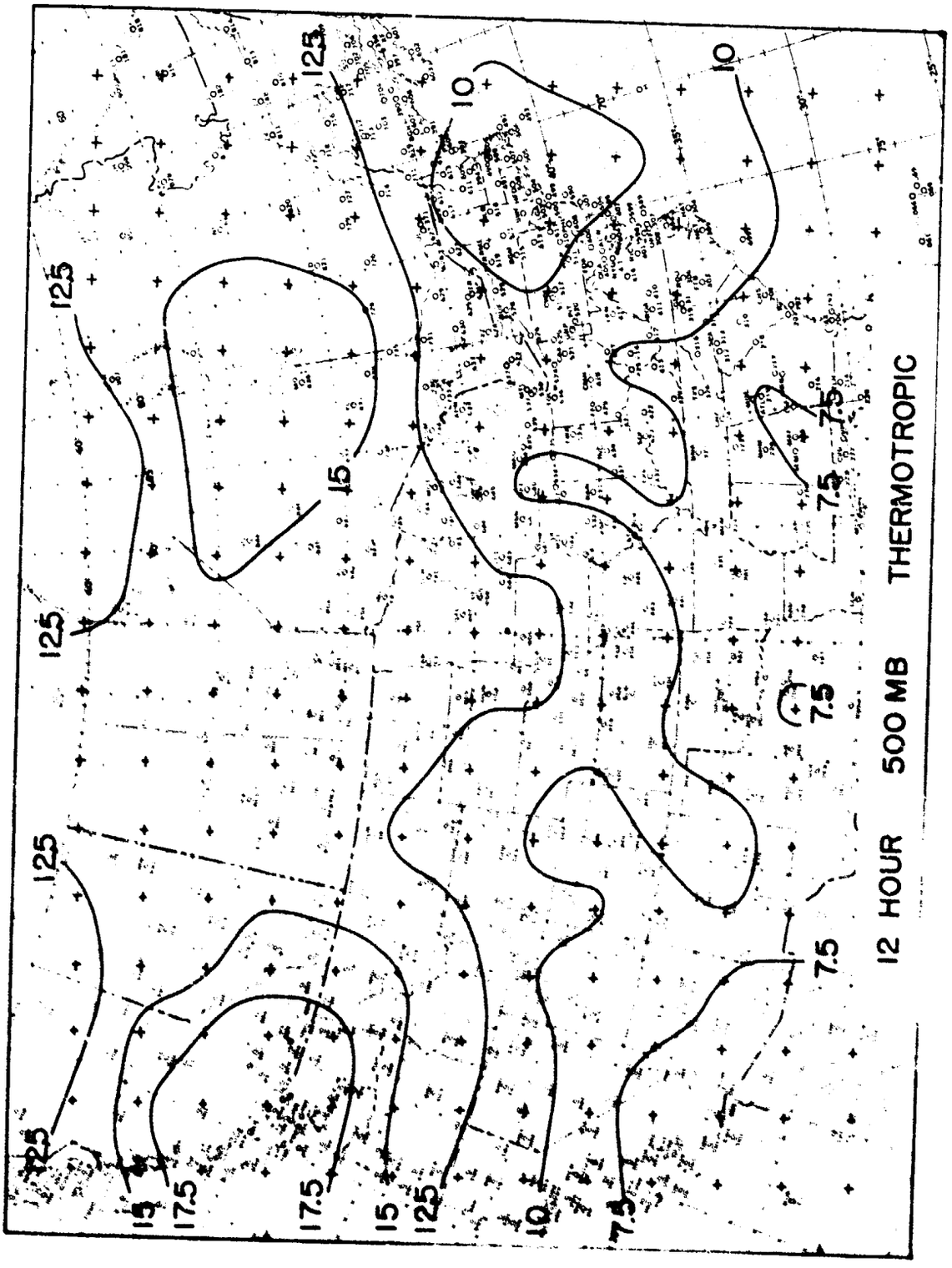

Fig. 3.26

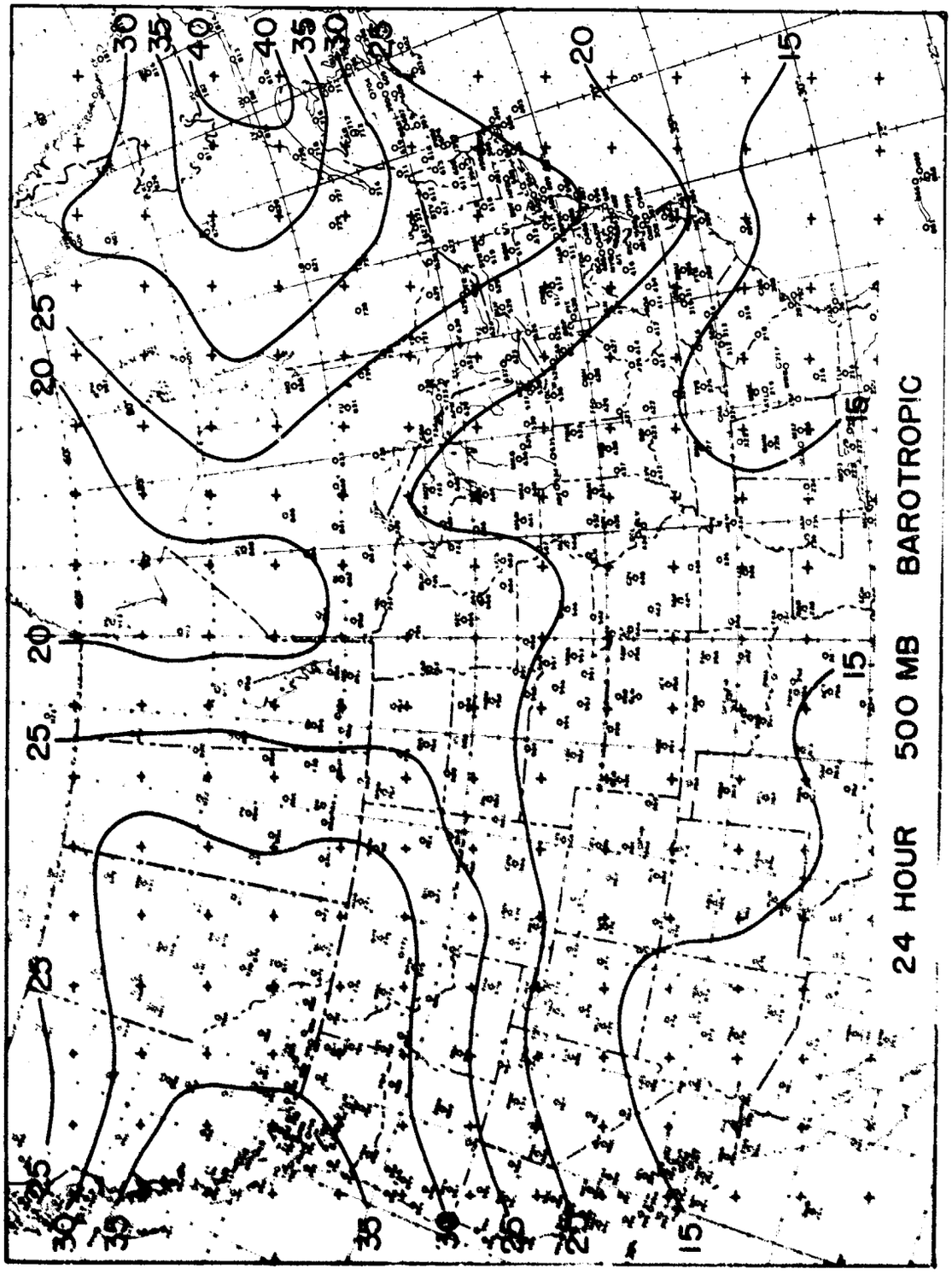

Fig. 3.27

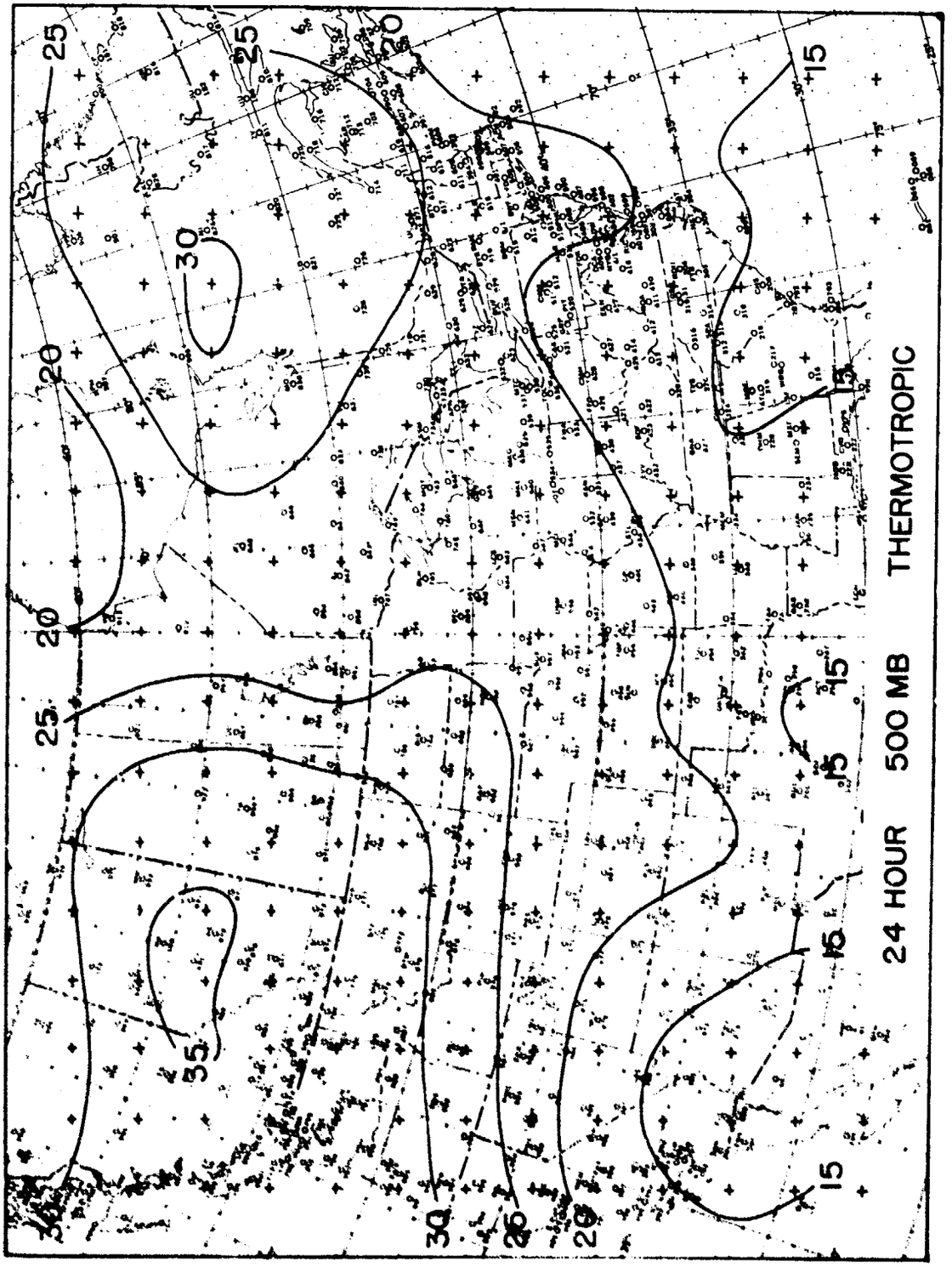

Fig. 3.28

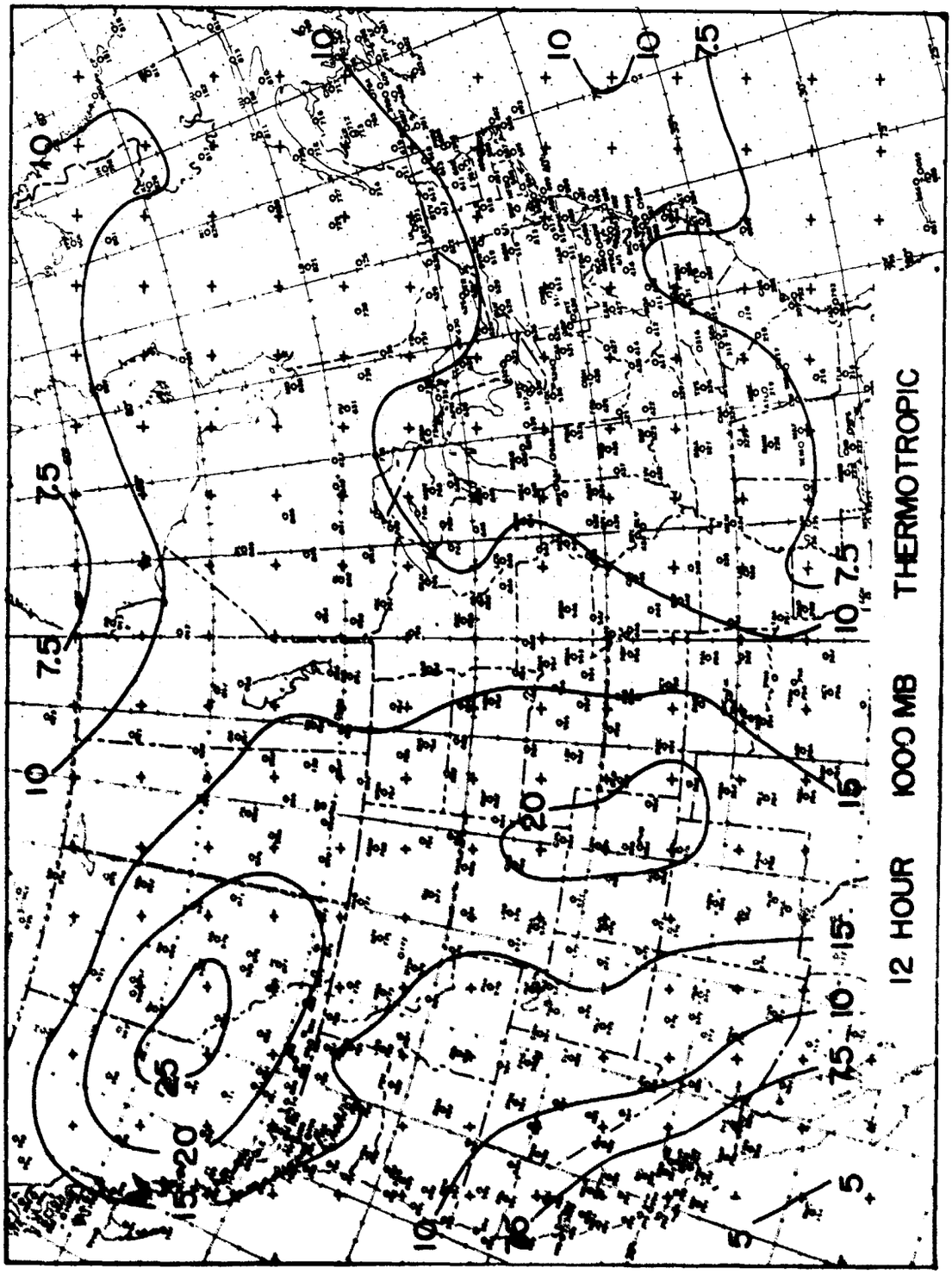

Fig. 3.29

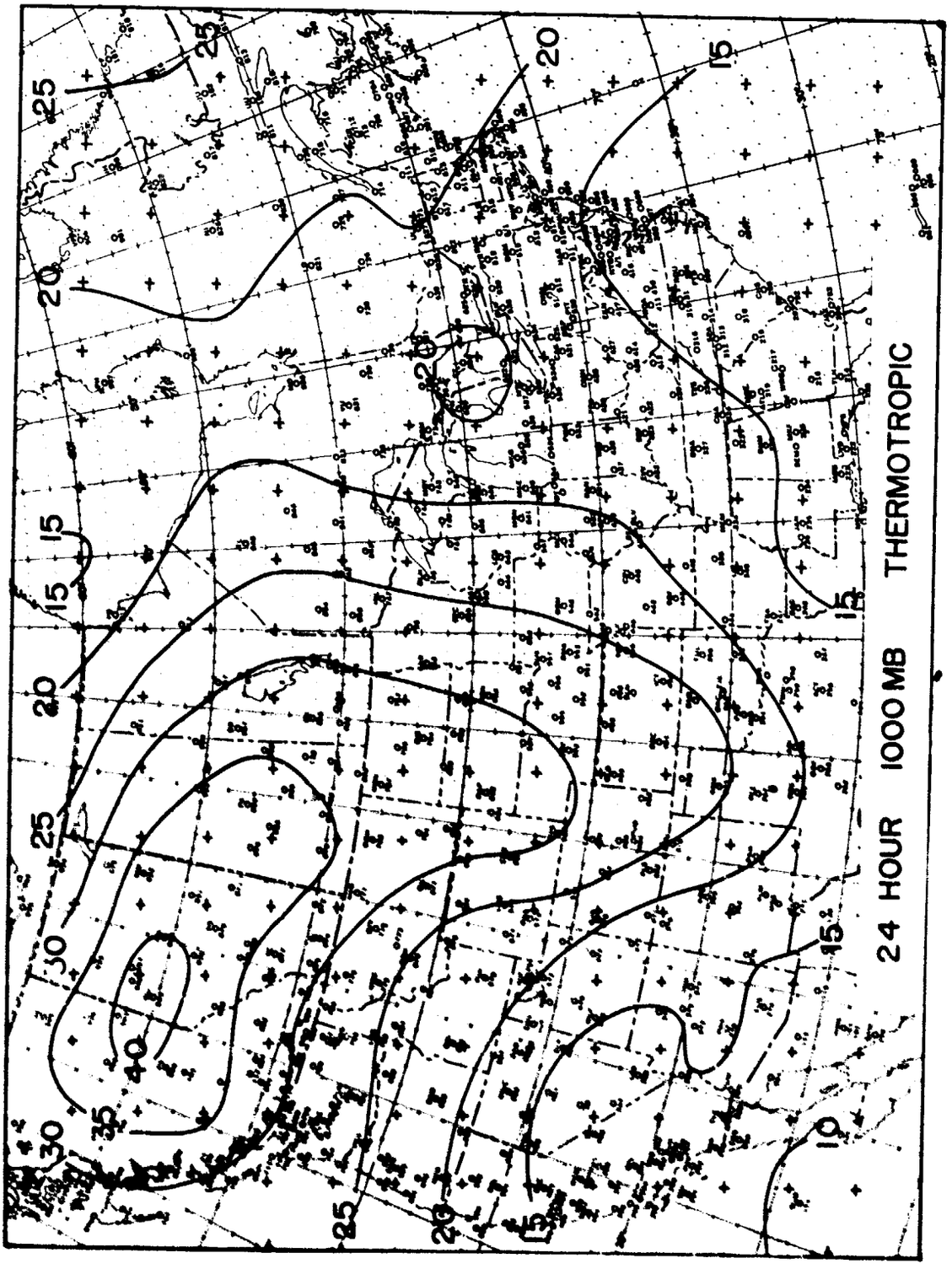

Fig. 3.30

distinguish some features apart from the zonal pattern. The errors along the northeast coast of the U. S. are somewhat smaller than those along the Pacific northwest for the 12-hour 500 mb predictions; the maximum errors in eastern Canada are smaller than the maximum errors in western Canada. A comparison of the charts for the 12- and 24-hour 500 mb predictions shows the same linearity in time of the root-mean-square error that was noted in the space root-mean-square errors.

The space distribution of the time root-mean-square errors of the 24-hour 500 mb thermotropic predictions (Figure 3.28) shows that the error along most of the eastern edge of the forecast area is less than the error along the western edge. The maximum error over eastern Canada is less than the maximum error over western Canada. The geographical distribution of the time root-mean-square errors of the 24-hour 500 mb barotropic predictions shows a pronounced maximum at the northeast corner of the forecast region. These large errors are caused by one very poor barotropic forecast (see footnote, page

The geographical distributions of the time root-mean-square errors of the 1000 mb thermotropic forecasts correspond strongly to the time correlation patterns, expecially in the areas of poor forecast (cf. Figures 3.23 and 3.29, 3.24 and 3.30). The locations of the time root-mean-square error maxima are in the same region as the minima of the time correlations. This region is the principal feature of the 1000 mb time root-mean-square error patterns. Each chart also shows regions of error minima at the southern corners of the forecast area.

3.4 Normalized Time Root-Mean-Square Error

The time root-mean-square errors may be normalized in order to remove the bias toward a purely zonal pattern. It shall first be hypothesized that the standard deviation of the time RMSE in one row of grid points is approximately equal to the standard deviation that would be obtained for each grid point in the row if values of the RMSE were available from many sets of 60 forecasts. It is also assumed that the values of the RMSE are normally distributed. The normalized RMSE shall then be defined by:

$$RMSE_N = \frac{RMSE - \overline{RMSE}}{\sigma\,(RMSE)} \quad ,$$

where $\overline{RMSE}$ is the mean of all values in a row and $\sigma\,(RMSE)$ is the standard deviation of the values in the row. The normalized RMSE is such that values at different latitudes may now be directly compared since the bias in the RMSE due to the increase in magnitude of the observed height changes with increasing latitude has been removed. A point at which the value of $RMSE_N$ is greater than one ($RMSE_N > 1$) is a point for which the forecasts were poor in the sense that the value of the RMSE is greater than the mean RMSE by more than one standard deviation. A difference of this magnitude would occur randomly in less than 33 cases in a hundred. (Under our assumptions this means 33 values out of one hundred values of the RMSE computed for each of 100 sets of 60 forecasts each.) A value of the $RMSE_N$ greater than two is a "poor" value in the sense that a difference of this magnitude would occur randomly in less than five cases in a hundred. Values of the $RMSE_N$ less than -1 and -2 are "good," in the same sense, at the 33% and 5% level, respectively. The normalized time RMSE were computed for the 24-hour thermotropic 500 and 1000 mb forecasts. Values of the normalized RMSE in different geographical regions are directly comparable and it is possible to examine the geographical pattern of the normalized RMSE in some detail. For the purpose of comparing this pattern with the earth's topography in the forecast region a special base map with contour lines drawn to fit values of the terrain elevation averaged over five degree latitude-longtitude areas was prepared.

The patterns of normalized RMSE for the 24-hour thermotropic 1000 and 500 mb forecasts are presented superimposed on the topography chart in Figures 3.31 and 3.32, respectively. The most striking feature is the location of the region of $RMSE_N > 1$ on the chart for 1000 mb (Figure 3.31) in the lee of the Rocky Mountains. In terms of the measure provided by the normalized RMSE the region

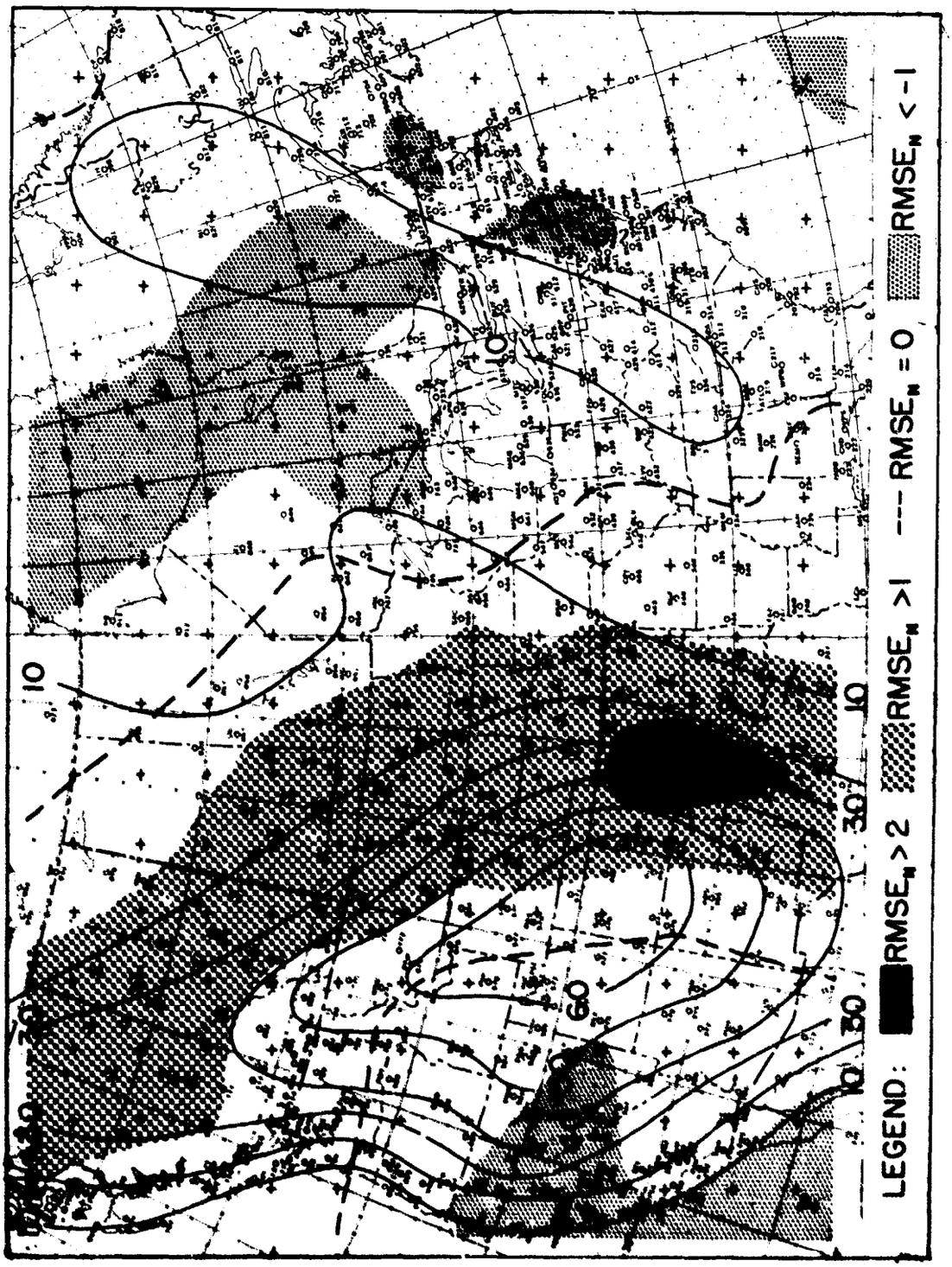

Fig. 3.31

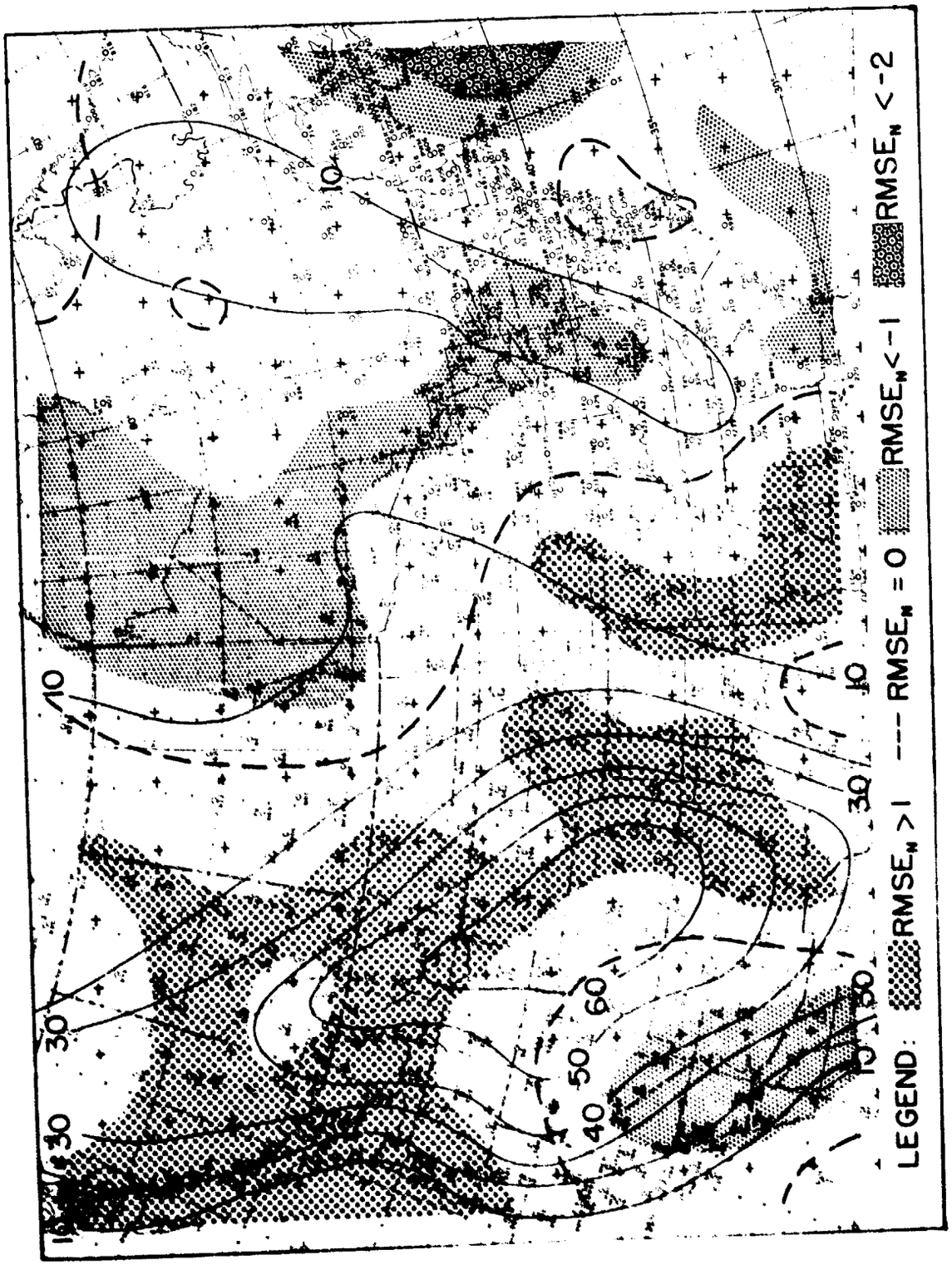

Fig. 3.32

of poorest forecast is in western Kansas south to the Texas panhandle. In the chart for 500 mb (Figure 3.32) the region of $RMSE_N > 1$ covers the northern half of the western boundary, probably due to errors introduced at the boundary, and continues southeastward in the lee of the Rocky Mountains. In both charts the forecasts are better in the eastern half of the region than in the western half, except for the area of $RMSE_N < -1$ in the southwestern corner. The chart for the 500 mb $RMSE_N$ has one small area of very good forecasts, ($RMSE_N < -2$) in the center of the eastern boundary. This region may be due to the favorable influence of the boundary conditions.

The values of the $RMSE_N$ in a particular column of grid points may be averaged to obtain a mean measure of the west-to-east variation of the forecast accuracy. The average values of $RMSE_N$ for each column are presented in Figure 3.33, where the mean height of the terrain is indicated by the shaded area. The mean $RMSE_N$ for both the 500 and 1000 mb forecasts show maxima in the lee of the Rockies. The 500 mb curve also has a secondary maximum in the lee of the lower Appalachian Range. The curves presented here support the deduction, made from the geographical distribution of the time correlations, that the forecasts are poorer in the western half of the region than in the eastern half. The geographical distribution of the normalized time root-mean-square errors indicate, much more clearly than any of the other data, that the region of poorest forecast is in the lee of the Rocky Mountains. This result may be due to some deficiency in the numerical prediction model. There are two classes of physical processes omitted from the prediction models that may be responsible. One may be termed a purely lee effect; the surface of the earth has been assumed perfectly flat in the derivation of the prediction equations. No consideration has been taken of the fact that air is forced to flow up over the mountains. The other effect is one due to the Rocky Mountains serving as a crude physical barrier, channeling the low-level outbreaks of polar air along their eastern slopes. The

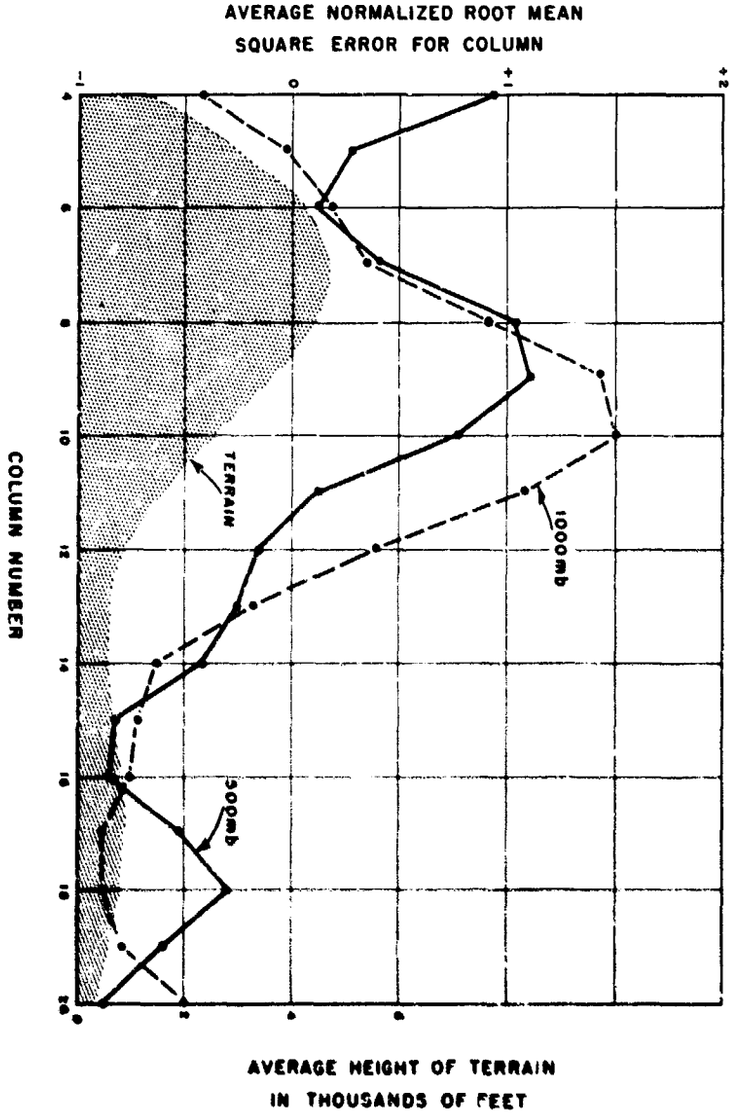
AVERAGE NORMALIZED ROOT MEAN
SQUARE ERROR FOR COLUMN
COLUMN NUMBER
TERRAIN
1000mb
500mb
AVERAGE HEIGHT OF TERRAIN
IN THOUSANDS OF FEET

Fig. 3.33

process of low-level advection is not included in the prediction model. It is therefore implied, by the analysis of the present results, that further generalizations of the numerical prediction models might well be directed toward the inclusion of topographical effects and low-level advection processes.

3.5 Comparison With No-Skill Forecasts

The results presented up to this point leave one question unanswered: "How do the correlation coefficients for the numerical predictions compare with correlation coefficients of forecasts obtained by some other technique?" In seeking such a comparison, it is desirable to use a "no-skill" forecast technique which utilizes the same given information as the numerical forecasting techniques. The significance of the comparison may be increased by the lack of sophistication of the no-skill forecast technique and the randomness of its selection. It is quite probable that, if enough different schemes are tried, we might eventually discover a simple scheme which would forecast "as well as" numerical prediction (say, in terms of the correlation coefficient).

In view of these considerations we shall now propose a simple forecast technique. The first step in preparing a 12-hour forecast is to shift the field of 500 mb height changes for the 12-hour period ending at the start of the forecast period two grid intervals to the east (an eastward velocity of approximately 7.5° longitude per 12 hours at 45° North). In the next step we make use of the heights at 12-hour verification time on the boundary (in order to make the technique comparable with the numerical forecasting technique described in Section 2) to compute the observed 12-hour 500 mb boundary height changes. The boundary changes are then used to improve the interior values obtained by straight extrapolation. An improved forecast 12-hour change for the first interior row is obtained by averaging the extrapolated height change, weighted one, and the observed height change at the neighboring boundary point, weighted three. The value for the second row is obtained by averaging the extrapolated and boundary changes, equally weighted. The third interior row of forecast changes is obtained by averaging the extrapolated change, weighted three, and the boundary change, weighted one. In each corner of the forecast region there are nine points for which the forecast changes are obtained by averaging the two values computed from each boundary. The scheme outlined provides a 12-hour 500 mb "forecast" in the same sense that the numerical predictions do. The interior data is based on information available up

U. S. WEATHER BUREAU
NWRC LIBRARY

to forecast time; boundary data is available at verification time.

For a 24-hour forecast no further boundary data are available; the forecast height change pattern for the first 12-hour period is shifted eastward two grid intervals as a forecast for the second 12-hour period. The forecasts for the first and second 12-hour periods are added to yield the 24-hour 500 mb height change prediction.

The "no-skill" 12- and 24-hour 500 mb forecasts were made for a sample of 30 randomly selected cases from among the 60 for which the numerical forecasts were made. The forecast 12- and 24-hour 500 mb height changes were correlated with the observed 12- and 24-hour 500 mb height changes, respectively, for each forecast. The root-mean-square error of the forecast height changes was also computed. Average values of these statistics are compared with the averages for the thermotropic forecasts for the same 30 cases in Table 3.3. On a daily basis the thermotropic 24-hour 500 mb forecasts were better than the no-skill forecasts at the one percent level in 14 cases, while the no-skill forecasts were better, at the same level, in only three cases. The frequency distributions of the 24-hour space correlations for the thirty 24-hour no-skill forecasts and the corresponding thermotropic forecasts are shown in Fig. 3.34. The no-skill forecasts did not do as well as the best thermotropic forecasts nor as poorly as the worst, i.e. in this sense it is a more

Table 3.3 -- Comparison of the 12- and 24-hour 500 mb forecasts obtained by the no-skill technique with those obtained by the numerical integration of the thermotropic equations.

	NO SKILL		THERMOTROPIC	
	Correlation Coefficient	RMSE in feet	Correlation Coefficient	RMSE in feet
12 Hour 500 mb	.710	139.3	.779	121.6
24 Hour 500 mb	.655	259.3	.710	242.0

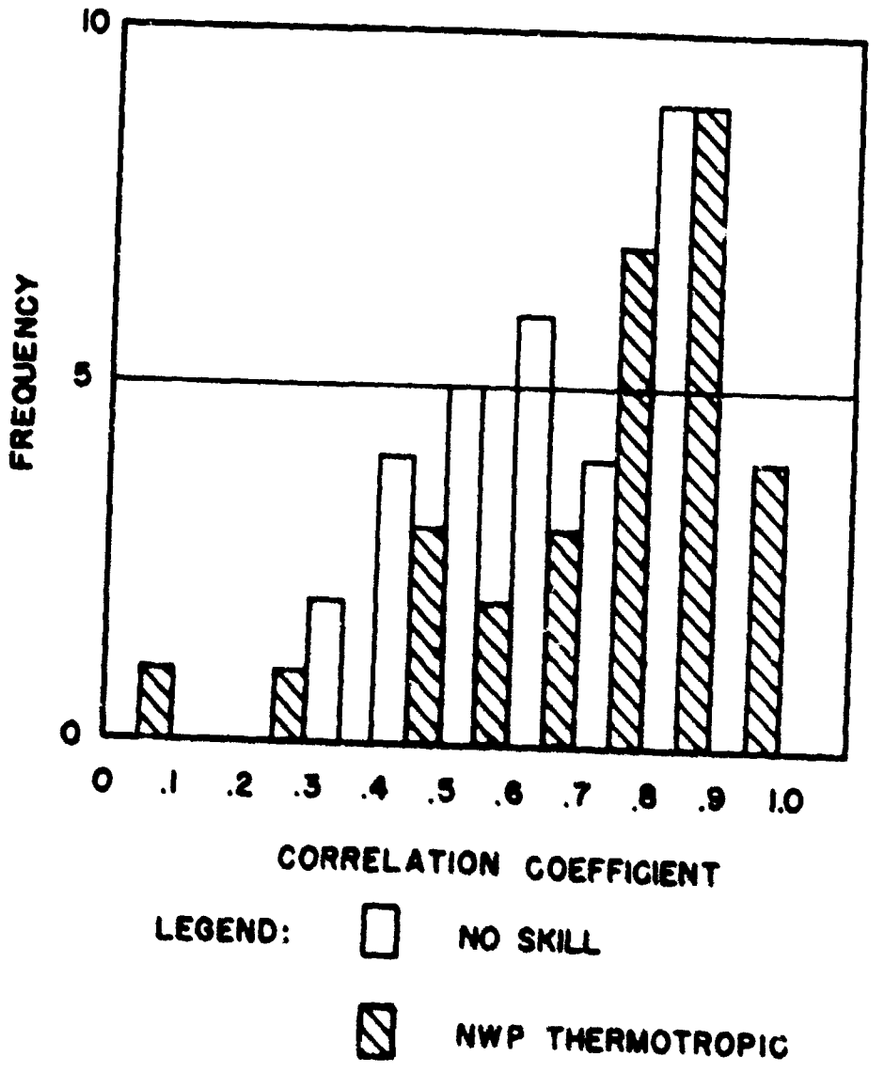
10
5
0
FREQUENCY
0 .1 .2 .3 .4 .5 .6 .7 .8 .9 1.0
CORRELATION COEFFICIENT
LEGEND:
NO SKILL
NWP THERMOTROPIC

conservative forecast scheme.

The time correlations of the forecast 24-hour 500 mb height changes with the observed height changes at each grid point were also computed and compared with the time correlations of the 24-hour 500 mb thermotropic forecasts. Figure 3.35 indicates the result of this comparison. In the shaded area, located to the east of the center of the forecast region, the thermotropic correlations are greater than the no-skill correlations by an amount that is significant at the one percent level. Near the boundary there is no pronounced superiority of one scheme over the other. In the interior of the region, where the no-skill technique does not take account of boundary effects, the integration of the equations is a much better technique than the straight extrapolation of the height change field. There are two possible explanations for this result. Either the equations "do something" in the interior, quite independently of boundary influences, that is more reliable meteorologically than an extrapolation of the past change pattern, or the equations furnish a mechanism for propagating the boundary information into the very center of the forecast region.

It is quite possible that the no-skill forecasts might be improved by using an interpolation scheme that brings the influence of the observed 12-hour changes further into the region. Results might also be improved if observed 500 mb heights at the 12-hour verification time were used along three boundary rows (as in the numerical forecasts) instead of along one (as in the no-skill forecasts). In this case a more elegant interpolation scheme, based on the gradient of the observed 12-hour change normal to the boundary, might be used to improve the interior values.

5.6 Summary

The correlations of the forecast 500 mb changes with observed changes are high enough to be quite encouraging; the correlation of the 1000 mb forecast changes with observed changes are not as high but are nevertheless felt to be significant in view of the relatively simple physical theory employed. More research is required to establish clearly the influence of the boundary conditions on the final forecast. The similarity of the behavior of the correlations of the 500 mb thermotropic forecasts and the correlations of the 500 mb barotropic forecasts remains the most striking feature of the results presented here. It is to be hoped that further, more subtle, analysis of the numerical forecasts may reveal the distinctions between the physical behavior of the two

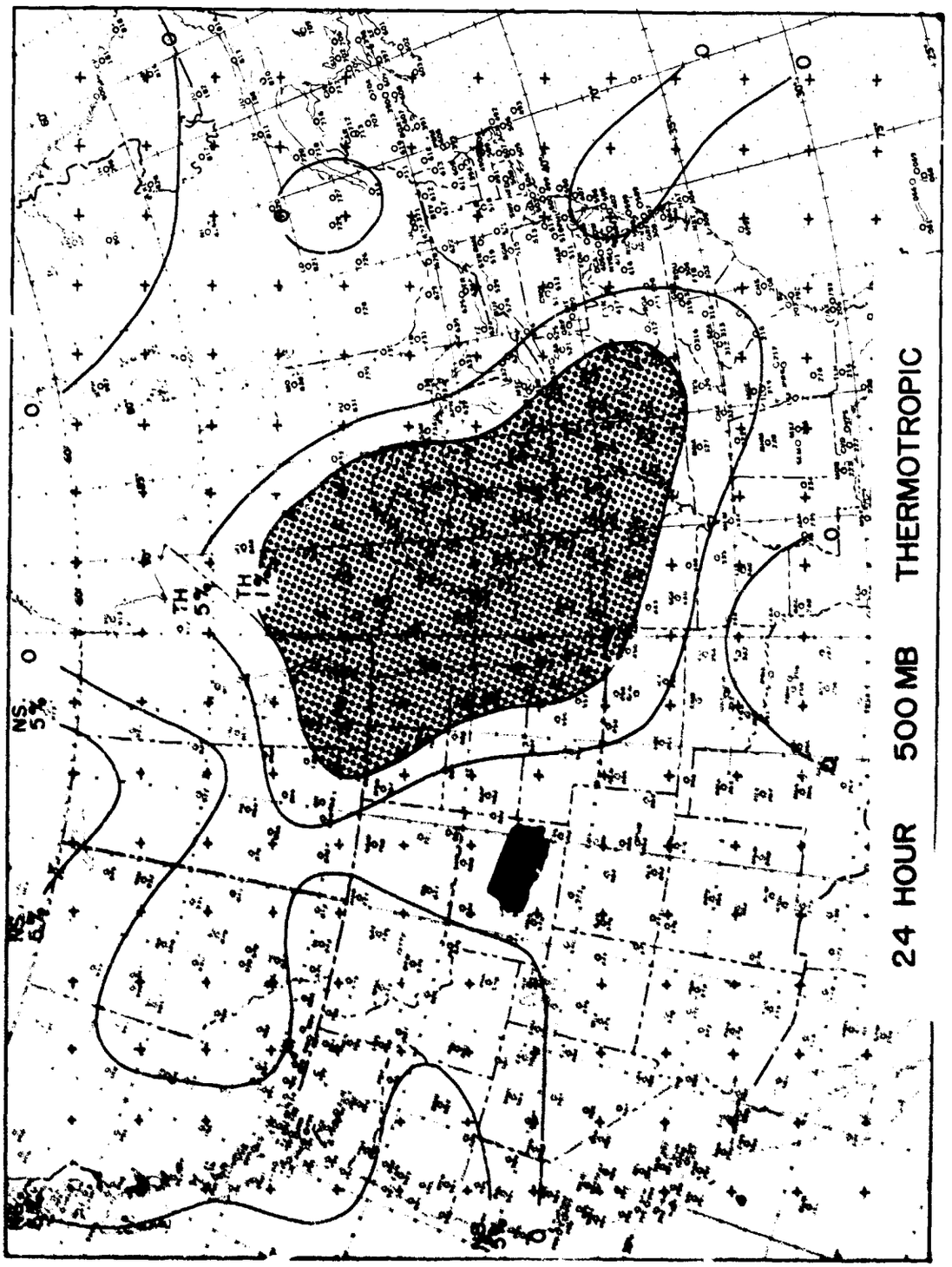

Fig. 3.35

models which have been indicated, for example, by stability studies.[4] The results of Section 3.4 indicate that further improvement in numerical forecasting may be gained within the framework of the present theory by including topographical effects.

4. The Synoptic Summary and Analysis of Forecasts

4.1 Introduction

To date, the interpretation of most numerical forecasts has been from the point of view of the dynamic meteorologist, i.e., the predictions are, in fact, solutions to a set of hydrodynamical equations and offer direct evidence of the accuracy of the theory and the suitability of the numerical procedures employed.

In addition to this interpretation, it was felt that in the present series of forecasts, a valuable summary of the results would be from the point of view of the synoptic meteorologist, i.e., the forecast behavior of typical synoptic systems and the forecasts' comparison with conventional technique. It is hoped that such a summary and analysis will permit an easier evaluation of numerical forecasting by meteorologists not directly engaged in this work; in particular, with the aid of the forecasts shown in the Appendix, it is hoped that a "feeling" for the performance of the relatively simple prediction models under a wide variety of synoptic conditions may be obtained.

The purpose of this section is accordingly to describe the data preparation and to present the synoptic study and summary of the forecasts made using the simple barotropic model and the thermotropic model.[1] The synoptic study of the forecast results includes an observation of the general level of performance of the numerical techniques and of the systematic errors which are in evidence. A discussion of the forecasts is included with consideration to initial flow patterns, types of systems, and geographical areas covered by the forecast. Case studies of interesting situations are used as illustrations of performance. The daily forecast and observed maps for the 500 mb and 1000 mb levels and 1000 - 500 mb computed vertical motion are included in the Appendix. The use of the thickness (1000 - 500 mb) for forecasting purposes is of particular interest to the synoptician, since there have been a number of studies made in the past to empirically relate the thickness patterns to the flow patterns at the surface and aloft for forecasting purposes. Some numerical thickness forecasts are presented here in detail to give an indication of the performance of this portion of the thermotropic model.

A discussion of the thermotropic model as a forecast technique is included and a comparison is made to other methods of prognosis.

4.2 Synoptic Data and Analyses

The decision was made to prepare one month of carefully analyzed maps at all the standard levels to serve as a test series for the numerical prediction techniques. This would provide maps for sixty sets of forecasts which, it was felt, would be a large enough sample to determine the level of performance of the forecast equations. A winter month was preferable since it provides the most difficult and extreme forecast cases, and a recent year was preferable from the viewpoint of data availability. Examination of maps of several winter months resulted in the choice of the month of January, 1953, as most suitable for testing purposes.

Data for the month of January, 1953, were obtained from the Daily Upper Air Bulletin published by the United States Navy, the data files of the Department of Meteorology, Massachusetts Institute of Technology, and from the data files of the Atmospheric Analysis Laboratory of the Geophysics Research Directorate. The data were entered on WBAN-1 maps, a Lambert conformal conic projection with a scale of 1:12,500,000, for the following eight levels for 0300 GMT and 1500 GMT of each day; surface, 1000, 850, 700, 500, 300, 200 and 100 mb. Figure 4.1 shows the areas of data coverage, analyses, data tabulation and forecast results.

The analyses of the map series were begun with the surface maps for each day, with time continuity established by tracing pressure centers, troughs and ridges from map to map. Data were sparse in the Pacific Ocean area, so the coded analysis of the San Francisco Weather Bureau office was used. The upper-air maps were analyzed on a light-table with the analyzed maps for the next lower level beneath them, which aided the maintainance of vertical continuity, although differential analysis would have been preferable if manpower and time had allowed. A smooth contour analysis depicting the major flow patterns was desirable for numerical prediction computations, and this was easily carried out on the lower-level maps while still fitting all radiosonde data. At the 200 and 100 mb levels, however, the accumulative temperature errors caused seemingly erratic station reports, which indicated very irregularly shaped systems and seemingly unrealistic flow patterns. The analyses at these levels were therefore in general tied to the lower layers to depict smooth

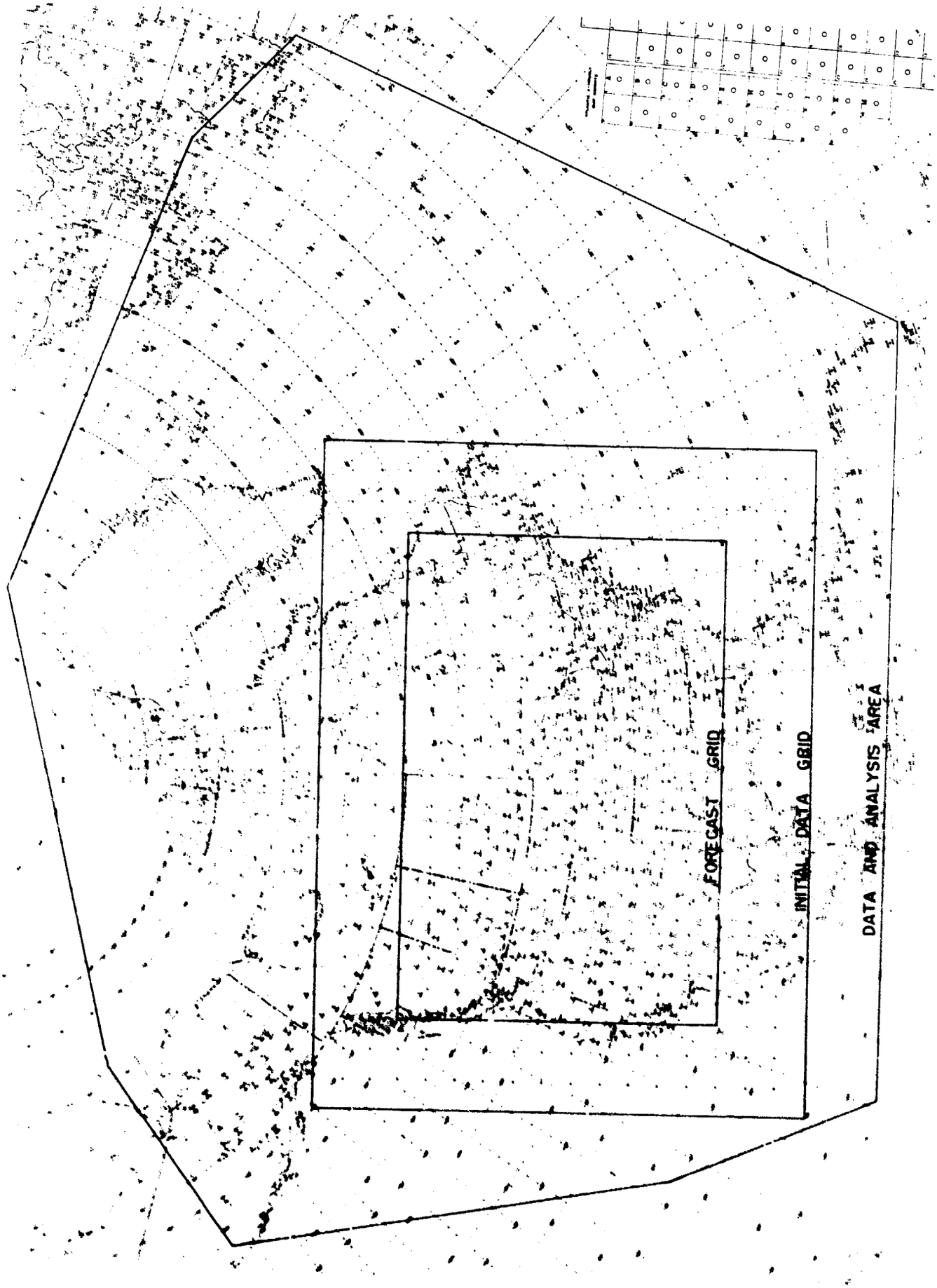

Fig. 4.1

large-scale flow patterns. Frequent errors in the radiosonde data received necessitated a close check on all map data. Reported heights, which did not appear to be consistent or were not in agreement with the general flow patterns, were re-computed from the ground level using the equivalent isothermal layer method. Some stations consistently reported either lower or higher heights than surrounding stations due to the use of different radiosonde equipment or calibration techniques, and this was taken into consideration in the final analysis. There were a total of 496 maps analyzed for the month of January 1953.

When the analyses were completed a square grid of 17 x 23 points was placed on each map (Fig. 4.1). At each grid point the height was interpolated to the nearest ten feet and entered on the map. The values were checked and transferred to tabulation sheets in preparation for the computations carried out on a high-speed electronic computer. Special attention was given to the data from the 1000 and 500 mb maps, as these were the levels used to test the performance of the thermotropic model and that of the barotropic model.

4.3 Characteristics of January 1953

Before undertaking the synoptic summary of the forecasts themselves, it is appropriate to discuss the general characteristics of the period for which these were performed. Records of the weather of January 1953 show that it was not a "typical" or "normal" month from the point of view of actual weather, in spite of the appearance of the usual number of large scale disturbances. It was a month of extremes in the Northern Hemisphere.[13] The United States experienced one of the warmest Januarys ever recorded; cold polar outbreaks were usually weak and of short duration, the most severe cold outbreak occurring on the 15th and 16th in the Great Plains and Mississippi Valley area. Precipitation was twice the normal in the Pacific northwest, southern Florida and New England, and generally above normal over the rest of the United States. The strongest development of the month occurred when a surface low formed in Texas on the 8th and moved to the southeastern United States, accompanied by heavy rain. This storm then moved northeastward and gave heavy snow and ice to New York and New England (see Appendix). On the 14th a cyclonic development on a cold front from the Pacific hit Salt Lake City with heavy snow.

The mean 500 mb map from the project's analyses, when compared with the normal January 500 mb map, shows above normal heights over the western United States and over the

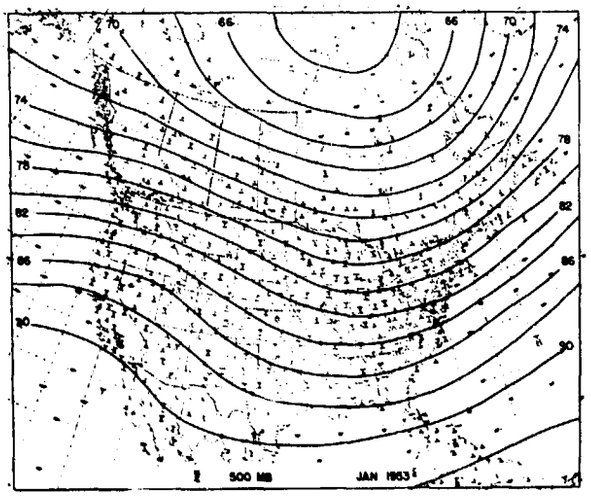

(a)

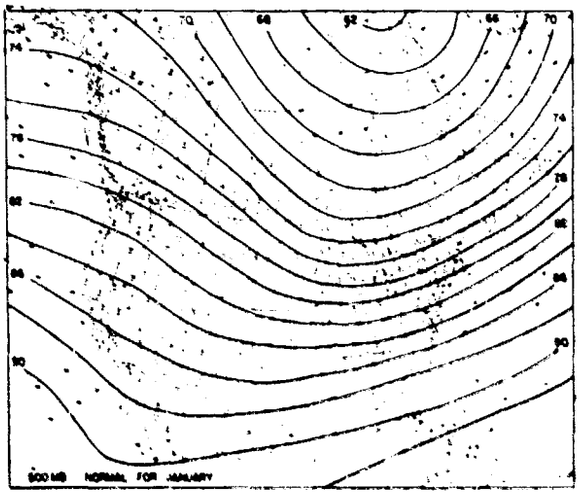

(b)

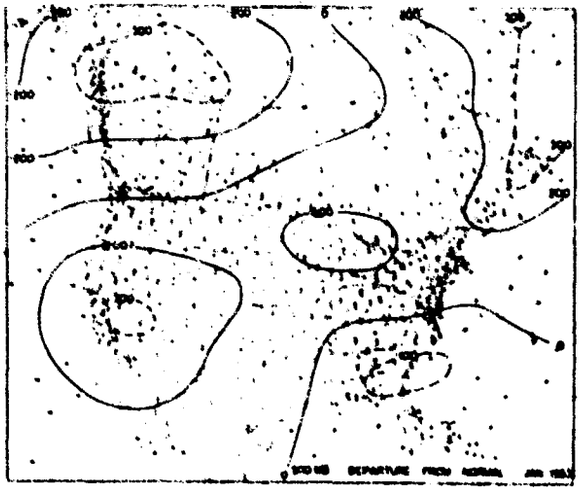

(c)

Fig. 4.2

north central and northeastern United States, with below normal heights over western Canada and the southeastern United States (Fig. 4.2). The major trough was located east of its normal position. The zonal flow near the west coast of the United States and Canada was considerably stronger than normal as indicated by the positioning of the centers of height anomaly. The mean jet stream location (200 mb) was along the northwestern United States border, then southeastward through the southeastern United States and then northeastward off the east coast of the United States, passing just east of Newfoundland. The favorite surface storm paths for the month were from the north Pacific along the northern United States border and from the southern Great Plains northeastward over the Great Lakes. Surface pressures were below normal over all of the United States, except the far southwest.

4.4 Synoptic Study of Numerical 500 and 1000 mb Forecasts

The verification of prognostic maps obtained using numerical methods or other techniques is a difficult problem. Statistical methods such as those employed in Section 3 can give an estimate of the accuracy of the forecasts but many questions remain unresolved. From a synoptician's viewpoint, the final analysis as to the value and usefulness of numerical methods depends on the accuracy in forecasting displacement of pressure centers, troughs and ridges, the accuracy of the wind forecast, and the usefulness of the forecast maps in predicting the actual weather.

A comparison of prognostic maps obtained using numerical methods with those obtained using the conventional field techniques is one way of estimating the general level of performance of the numerical methods.[10] Comparisons of this type have been made in the past. In 1951 a set of twenty-two consecutive 24-hour forecasts at 500 mb from the linearized barotropic theory were compared with synoptic forecasts at the Atmospheric Analysis Laboratory of the Geophysics Research Directorate. Correlation coefficients of the forecast versus observed changes and examination of the errors indicated that the two types of forecasts were of approximately equal accuracy; the average correlation for numerical methods was +0.73 and for synoptic methods was +0.74. Gates[14] showed a comparison of a numerical forecast and a synoptic forecast at 500 mb which indicated that the two methods were of comparable accuracy in the case examined. The sixty numerical forecasts of the present series were

compared with forecasts obtained using other techniques and, in addition, were studied to determine the reasons behind the distribution of various types of errors, in an attempt to discover weaknesses in the method.

4.4.1 Distribution of errors

Examination of the January 1953 forecasts revealed that there was a noticeable geographical distribution of the mean height-change errors. Figure 4.3 shows this error distribution for the 500 mb barotropic, 500 mb thermotropic, 1000 mb thermotropic, and the 1000 - 500 mb thermotropic thickness forecasts. These error maps were obtained by subtracting the actual 24-hour height change at each grid point from the forecast 24-hour height change for each of the sixty cases, and computing the algebraic mean error for each grid point for the month. The error distributions of the barotropic and [illegible] forecasts are very similar, with negative mean errors over the western United States and western Canada, and positive mean errors over the eastern United States and [illegible] Canada. The tendency to forecast lower [illegible] than observed over the western portion of [illegible] is striking. Mean negative errors [illegible] more than [illegible] are observed on both maps.

There were six [illegible] during the month when the 500 mb thermotropic [illegible] correlated 0.50 with the observed changes. [illegible] in all six of these cases was that [illegible] in the western portion of the [illegible], in varying degrees, in excess of [illegible] apparent that, among [illegible], [illegible] and a thermal [illegible], and [illegible] in the west and north have a considerable effect [illegible].

The [illegible] thickness error is quite different [illegible] maps. There is still a tendency [illegible] than observed over the [illegible] portion, [illegible] negative error is much smaller in size, both areally and quantitatively. There is a strong tendency [illegible] values greater than observed [illegible] over western Canada and the central [illegible]. [illegible] pattern of positive mean error suggests that [illegible] catch the full effect of cold [illegible], as the normal path of these outbreaks coincides quite well with the area of positive mean error in [illegible].

The distribution of the mean errors at 1000 mb shows the accumulative effects of the 500 mb and thickness

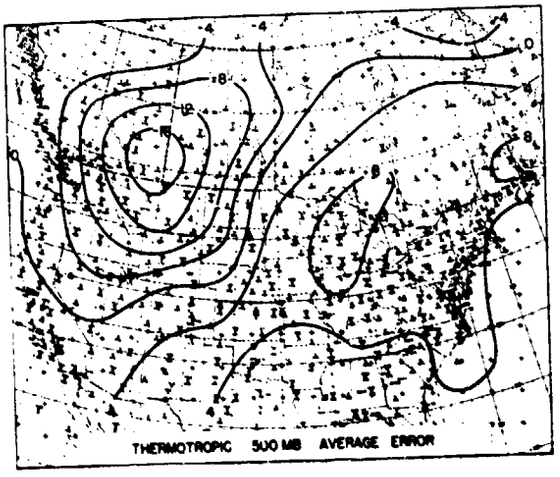

(a)

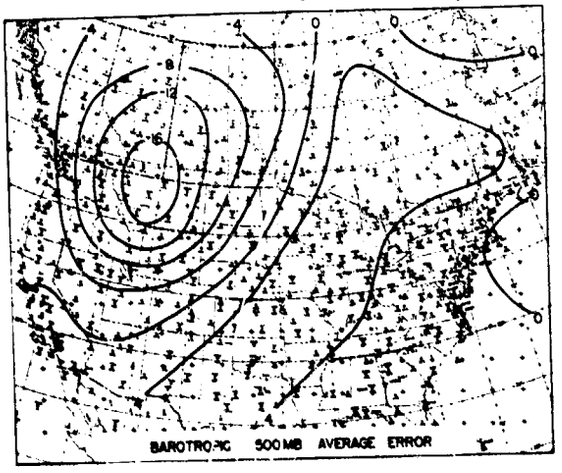

(b)

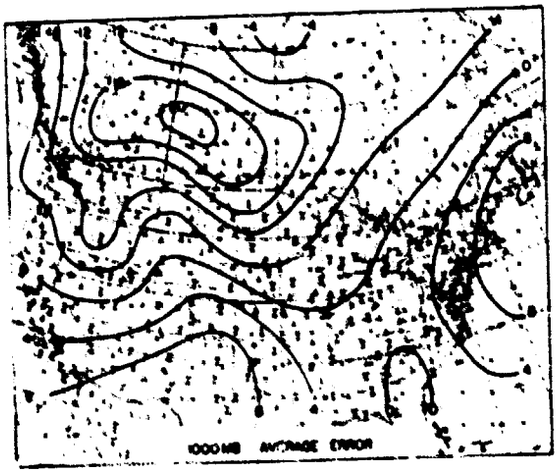

(c)

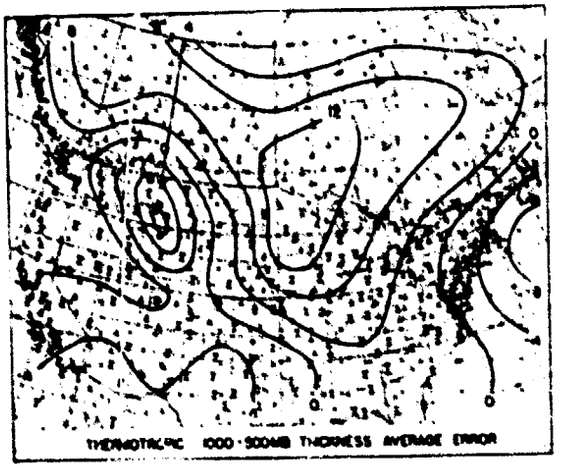

(d)

Fig. 4.3. Average forecast error charts 10's of feet.

errors. In western Canada the tendency to forecast 500 mb heights too low, and thickness values too high, resulted in 1000 mb height forecasts having a large negative mean error in that region. Deep 1000 mb lows were erroneously forecast to move into western Canada from the Pacific during the forecast series.

The forecast results were studied to determine whether there was any consistent relationship between the forecast error and the initial flow patterns at 500 mb. The errors were plotted at the grid points for each of the sixty cases and isoline analyses were made. The geographical locations of centers of error of more than 300 feet were noted relative to the trough and ridge pattern at 500 mb. Figure 4.4 shows that there is a tendency for positive height errors to be located ahead of the 500 mb troughs and the negative errors to be located to the rear of the 500 mb trough and ahead of the following ridge. This is evidence that the numerical methods generally forecast too slow a movement of the trough and ridge patterns. The same impression is obtained by merely looking through the series of forecasts. Error centers adjacent to the boundaries were not used in Fig. 4.

The numerical forecasts were more accurate over the eastern United States than elsewhere over the grid. This fact was shown by the average point correlations, root-mean-square errors and average errors (Section 3). The day-by-day observed height changes were as large over the eastern United States as over the rest of the grid. The size of the actual height changes, therefore, cannot be used to explain the difference in forecast accuracy over the grid area. Factors which may have contributed to the differences in accuracy are the high data density over the eastern United States, the distance of the eastern United States from western and northern computational boundary errors (which are the boundaries most affecting the forecasts), the inaccuracies in the data over the western portion of the grid due to the mountains and the flow barrier, and thermal block effects of the mountains in the west. The high level of accuracy of the forecasts over the eastern United States indicates that with an increase in the density and accuracy of upper air and surface data, a larger initial grid and inclusion of terms in the equations to take the mountain effects into account, we might be able to improve the numerical forecasts over a much larger area to a level of accuracy approaching that attained over the eastern United States.

The 500 mb forecast average error maps show negative

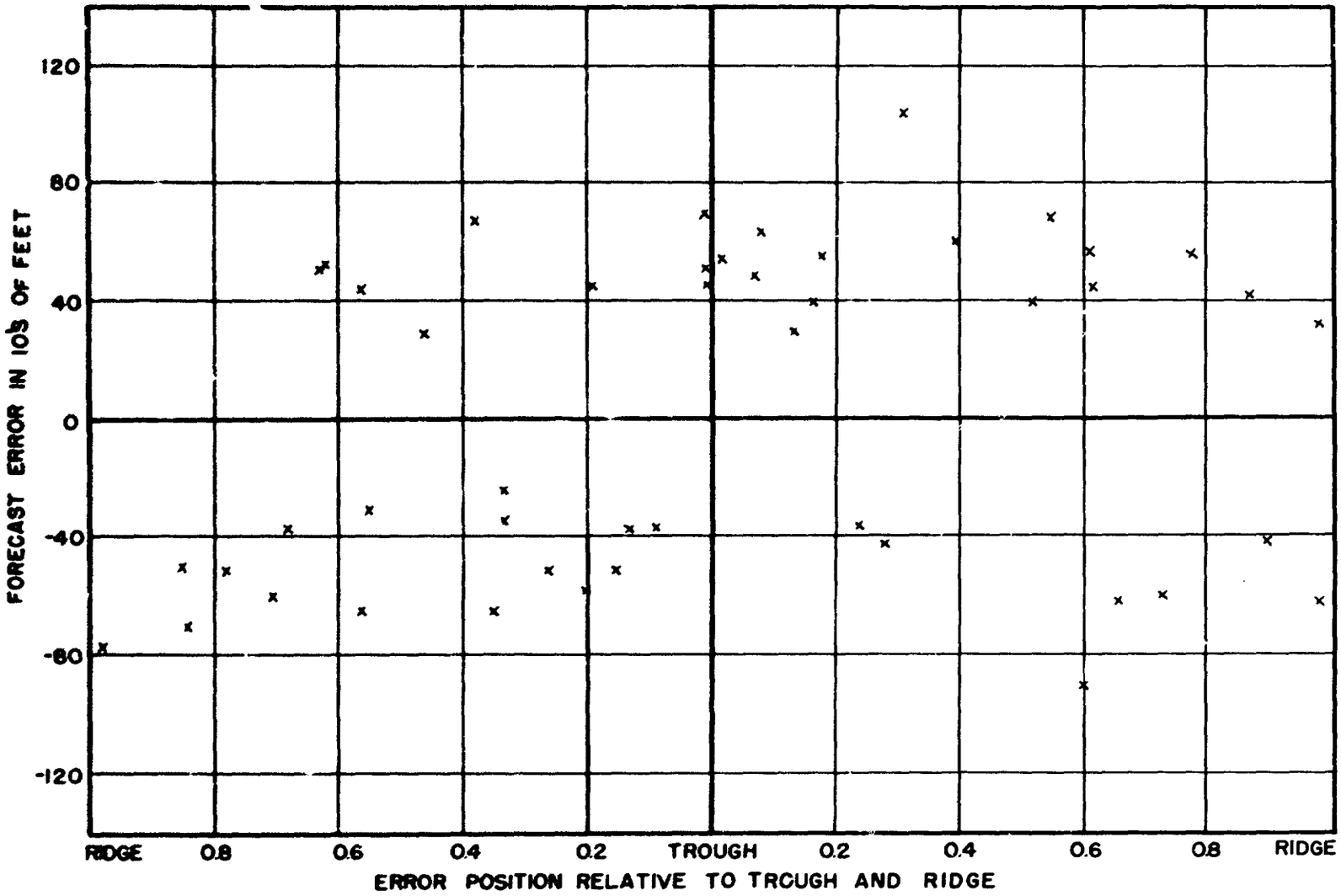
120
80
40
0
-40
-80
-120
FORECAST ERROR IN 10's OF FEET
RIDGE
0.8
0.6
0.4
0.2
TROUGH
0.2
0.4
0.6
0.8
RIDGE
ERROR POSITION RELATIVE TO TROUGH AND RIDGE

FIG. 4.4

errors in the northern portions of the grid area and positive errors in the southern portions. This indicates that both the barotropic and thermotropic models overforecast the zonal wind on the average during the month.

4.4.2 Forecasts at 500 mb

Messrs. Hering and Mount of the Synoptic Section of the Atmospheric Analysis Laboratory included a study of results of the numerical forecasts in their recent evaluation of forecast techniques. They measured the 500 mb gradients forecast over six stations in the United States using the 24-hour numerical forecasts on fifteen days with identifiable surface cyclonic centers. The average wind vector error of the forecasts was 26 knots. They note that the Air Weather Service forecast capabilities study found the average 500 mb wind vector error of a synoptic forecaster to be 25 knots. The distribution of numerical prediction errors is found in Fig. 4.5. The forecast area was divided into four sections, ten degrees of latitude by twenty degrees of longitude. The average zonal and meridional winds were obtained in each section by averaging the height differences on opposite sides of this 10 x 20 degree area. For comparative purposes the errors obtained using persistence, extrapolation of past 12- and 24-hour change, and the normal January map as a height gradient forecast are presented along with WBAN and numerical forecasts for each section in Tables 4.1 and 4.2. The wind component error of the numerical 24-hour 500 mb forecasts and of WBAN's 36-hour 700 mb forecasts is, on the average, about equal to the observed change. There is, on the average, a noticeable overforecast of the gradients by numerical methods for all the 10 x 20 sectors as well as for the single stations.

The displacement error of the 500 mb trough forecast by numerical methods was measured at the latitude of the surface low for the fifteen cases with identifiable surface lows. The average error of the 24-hour trough forecast was 1.6 degrees latitude (or about 160 nautical miles) for fourteen cases; the fifteenth case had no identifiable trough on the verification map. Vorticities in the 500 mb troughs for the fifteen cases with surface lows were computed using a 6° latitude grid. The 24-hour maximum vorticity change forecasts obtained using numerical methods were compared with the observed changes (Table 4.3). The numerical methods forecast the correct sign to the development in every case. On the average their forecast error of the vorticity change was about half of the observed change.

[illegible] -- Error in F[illegible] Meridional Wind Component
[illegible] 10° Latitude by 20° Longitude Area

[illegible]° lat.				
24 hr.	[illegible] mb [illegible]	± 1[illegible] kts	500 mb obs change	± 18 kts
	[illegible] mb NWP error	± 14 kts	500 mb NWP error	± 10 kts
[illegible] hr.	700 mb [illegible]	± 12 kts	700 mb obs change	± 14 kts
	700 mb WBAN error	± 12 kts	700 mb WBAN error	± 10 kts
	[illegible] mb 24 hr. trend error	± 2[illegible] kts	500 mb 24 hr.trend error	± 29 kts
	[illegible] mb 12 hr. trend error	± 2[illegible] kts	500 mb 12 hr.trend error	± 28 kts
	[illegible] mb normal map error	± 1[illegible] kts	500 mb normal map error	± 13 kts
	[illegible] mb normal map error	± 10 kts	700 mb normal map error	± 10 kts
[illegible]° lat.				
	[illegible] mb [illegible] change	± 16 kts	500 mb obs change	+ 21 kts
	[illegible] mb NWP error	± 11 kts	500 mb NWP error	[illegible] 8 kts
	[illegible] mb [illegible] change	± 12 kts	700 mb obs change	± 20 kts
	[illegible] WBAN error	± 1[illegible] kts	700 mb WBAN error	± 11 kts
	[illegible] mb 24 hr. trend error	± 2[illegible] kts	500 mb 24 hr.trend error	± 30 kts
	[illegible] mb 12 hr. trend error	± 2[illegible] kts	500 mb 12 hr.trend error	± 28 kts
	[illegible] mb normal map error	± 1[illegible] kts	500 mb normal map error	± 19 kts
	[illegible] mb normal map error	± 12 kts	700 mb normal map error	± 13 kts
[illegible]° lat.				

11[illegible]° [illegible] [illegible]° [illegible] long. 75° W long.

Table 4.2 -- Error in Forecasting the Zonal Wind Component over a 10° Latitude by 20° Longitude Area

55° N lat.				
24 hr.	500 mb obs change	± 8 kts	500 mb obs change	± 10 kts
	500 mb NWP error	± 10 kts	500 mb NWP error	± 9 kts
24 hr.	700 mb obs change	± 7 kts	700 mb obs change	± 9 kts
	700 mb WBAN error	± 7 kts	700 mb WBAN error	± 10 kts
	500 mb 24 hr. trend error	± 12 kts	500 mb 24 hr. trend error	± 15 kts
	500 mb 12 hr. trend error	± 15 kts	500 mb 12 hr. trend error	± 16 kts
	500 mb normal map error	± 15 kts	500 mb normal map error	± 14 kts
	700 mb normal map error	± 7 kts	700 mb normal map error	± 9 kts
45° N lat.				
	500 mb obs change	± 10 kts	500 mb obs change	± 10 kts
	500 mb NWP error	± 10 kts	500 mb NWP error	± 7 kts
	700 mb obs change	± 7 kts	700 mb obs change	± 10 kts
	700 mb WBAN error	± 7 kts	700 mb WBAN error	± 7 kts
	500 mb 24 hr. trend error	± 14 kts	500 mb 24 hr. trend error	± 15 kts
	500 mb 12 hr. trend error	± 17 kts	500 mb 12 hr. trend error	± 18 kts
	500 mb normal map error	± 9 kts	500 mb normal map error	± 14 kts
	700 mb normal map error	± 6 kts	700 mb normal map error	± 8 kts
35° N lat.				
	115° w. long.		95° w. long.	75° w. long.

Table 4.3 -- Maximum Vorticity Measured in 500 mb Troughs
Using a 6-Degree Latitude Grid

Run No.	Verifies	NWP 24-Hour Fcst.	Observed Initial	Observed 24-Hour Final	24-Hour Observed Change	24-Hour NWP Fcst. Change	NWP Change Error
1	2 Jan 53 15Z	42	55	30	-25	-13	12
2	3/03Z	28	35	25	-10	- 7	3
6	5/03Z	22	48	18	-30	-26	4
7	5/15Z	22	20	21	1	2	1
8	6/03Z	28	18	35	17	10	- 7
9	6/15Z	32	21	25	4	11	7
27	15/15Z	32	25	28	3	7	4
28	16/03Z	35	40	28	-12	- 5	7
45	24/15Z	30	48	38	-10	-18	- 8
46	25/03Z	38	30	50	20	8	-12
51	27/15Z	25	25	28	3	0	- 3
52	28/03Z	32	35	32	- 3	- 3	0
59	31/15Z	40	38	50	12	2	-10
60	1 Feb 53 03Z	48	35	50	15	13	- 2

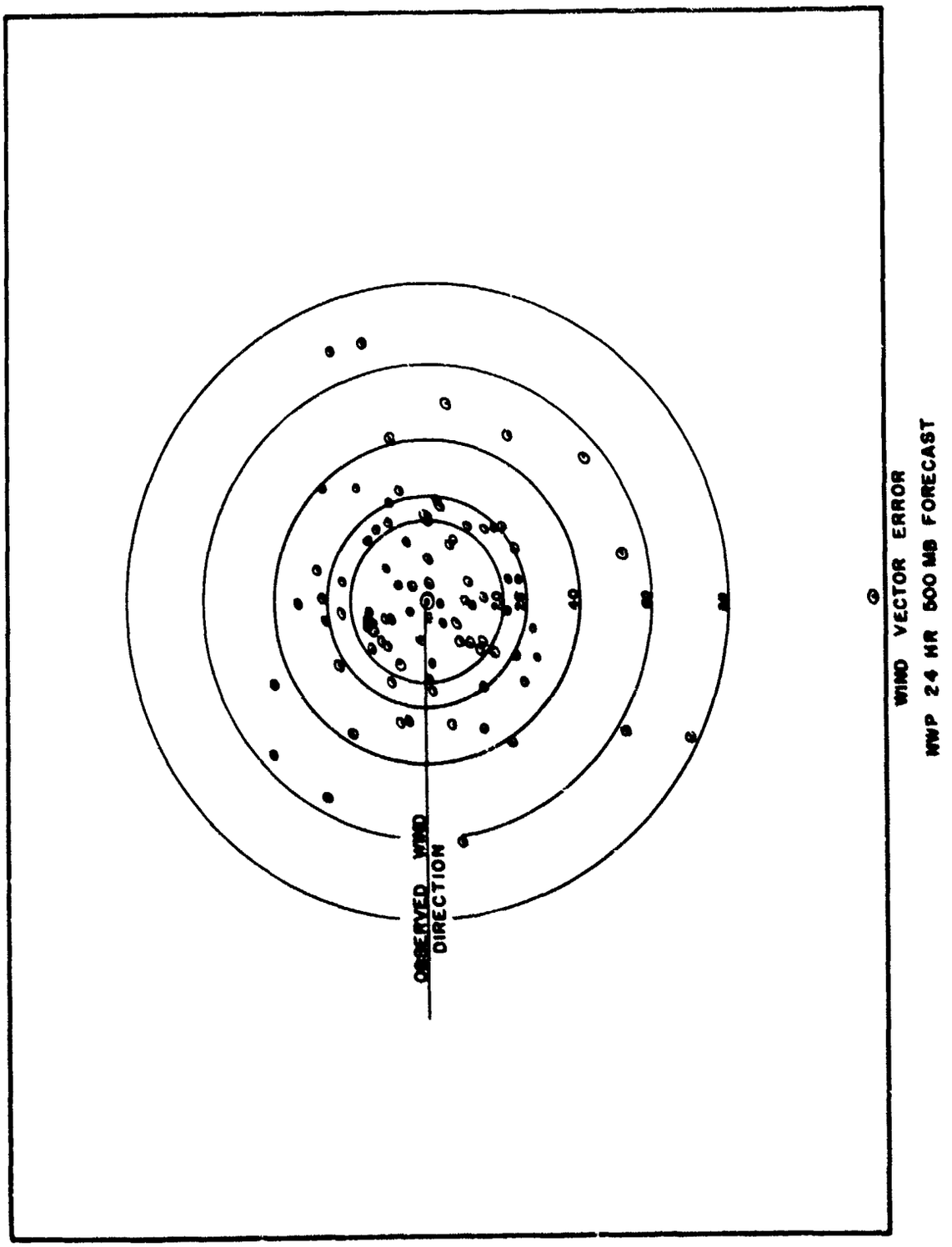
OBSERVED WIND DIRECTION
WIND VECTOR ERROR
NWP 24 HR 500 MB FORECAST

Fig. 4.5

This indicates that numerical forecasts generally underforecast both increases and decreases of the large-scale circulation intensity as measured in such a manner. The results of Hering and Mount's study of the 500 mb numerical forecasts give added indications that numerical methods are presently as accurate as other short-range forecast techniques at 500 mb.

4.4.3 Forecasts at 1000 mb

Hering and Mount in their forecast evaluation studies also compared the 1000 mbnumerical forecasts with forecasts made using conventional methods, as represented by WBAN's surface prognostic charts for the month of January 1953. Correlation coefficients were computed between the observed 30-hour surface pressure changes, and the changes predicted by WBAN for the January 1953 forecast series. A uniformly spaced grid of twenty stations covering the prediction area of the numerical forecasts was used to obtain such values for the WBAN prognostic charts. Correlation coefficients for the 30-hour surface forecasts are shown together with the coefficients obtained for the numerical 24-hour 1000 mb forecasts in Fig. 4.6.

These results show that the two methods are of comparable accuracy, with the coefficients for the conventional forecasts averaging slightly higher in spite of the longer forecast period. The root-mean-square coefficient of the series of fifty-eight WBAN prognostic charts was 0.75, as compared to 0.64 for the numerical forecasts. It is interesting to note that WBAN and NWP curves are in phase with their good and bad forecasts coinciding.

The 1000 mb forecasts were analyzed to determine the accuracy in predicting the displacement of low-pressure centers. Verification was initially intended to include all cyclonic centers with identifiable initial and subsequent 24-hour positions falling within the forecast grid. However, the boundary conditions produced a marked influence on the predicted position of those centers located near the outer limits of the grid area. This effect on the evaluation was reduced by eliminating all cases with final storm locations within two grid points of the boundaries. A total of fifteen cases were available from the January forecast series. The observed and predicted 12- and 24-hour positions are shown in Figure 4.7.

FIG. 4.6

CORRELATION COEFFICIENT

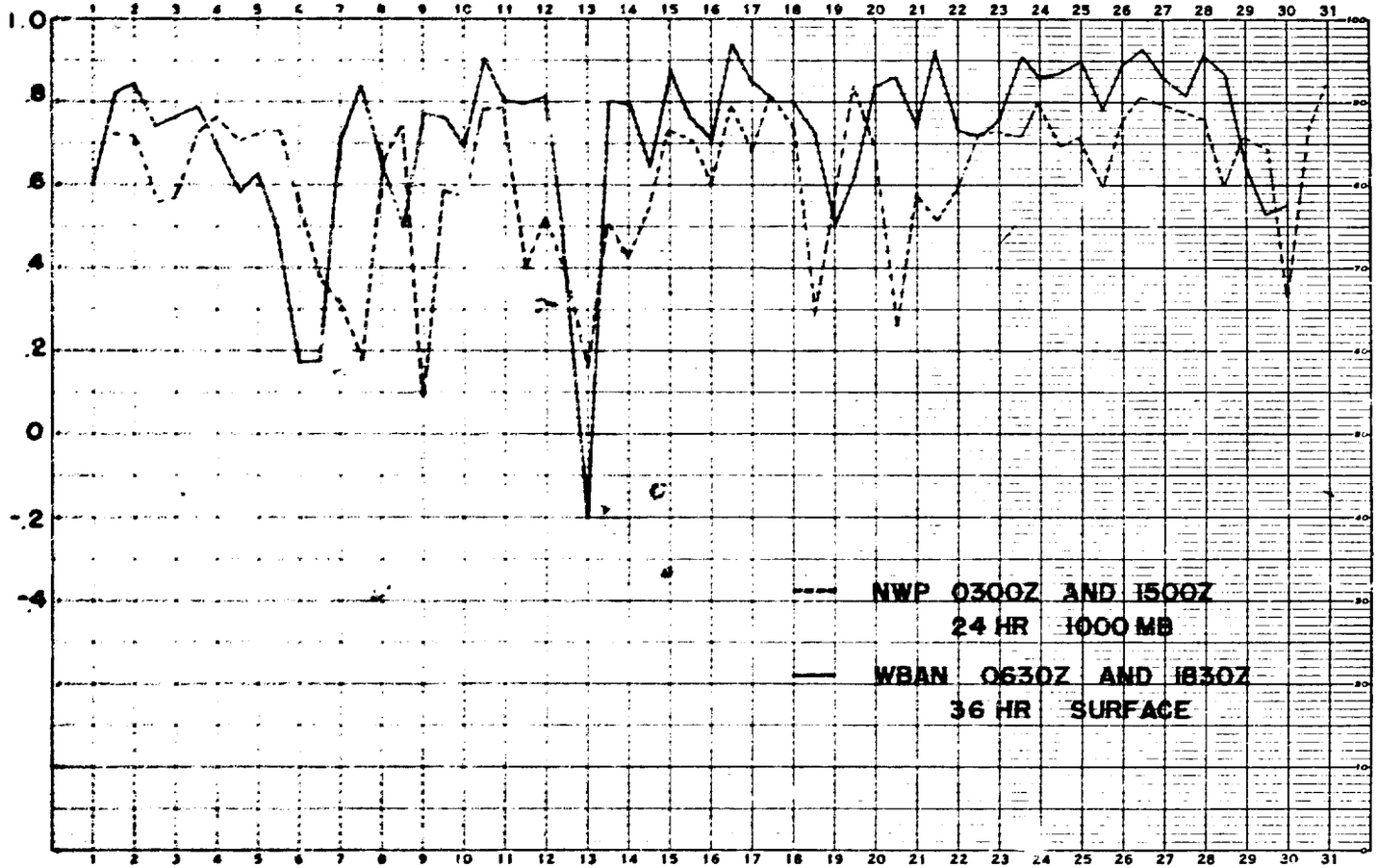

MONTH OF JANUARY 1955

For comparative purposes, a similar evaluation was made of the forecasts prepared by WBAN for this series of fifteen test cases. The surface prognostic charts transmitted on the facsimile network during January 1953 consisted of a 30-hour prediction of the pressure pattern, plus the forecasted 18-hour positions of pressure systems and frontal systems. The predicted 24-hour position of a low pressure center was obtained as a mid-point of a line connecting the 18- and 30-hour positions. These conventional forecasts cover a period which begins three hours later than that of the numerical forecasts.

Comparative results are shown in Table 4.4 and Figure 4.8. The observed final positions and tracks have been superimposed in Figure 4.8, such that the position error is given by the distance from the forecast point to the center point. The direction error is defined by the deviation from the horizontal line, and the speed error by the differences in line lengths connecting the initial positions with the center point and initial positions with the forecast positions. The overall accuracy for this test sample is essentially equal to that of the conventional methods of pressure pattern prognosis. The numerical displacement forecasts show a striking tendency to underestimate the speed of the 1000 mb cyclonic centers. The predicted 24-hour speed was too slow in each of the fifteen forecast situations, resulting in a mean algebraic speed error of about minus three degrees of latitude per day. A bias of an equal amount was noticed also in the 12-hour displacement forecasts. This systematic error appears to be primarily due to a tendency to overestimate the actual contour height at 500 mb in regions of anticyclonic curvature and underestimate, although to a lesser extent, the contour height in trough areas. Since cyclonic centers are commonly located between a ridge to the east and a trough to the west in the 500 mb pattern, the error tends to position the 1000 mb storm center too near the trough or cyclonic vorticity center at 500 mb.

A comparative evaluation was also made of forecasts of intensity changes for this sample of fifteen cases. The measure of intensity was arbitrarily chosen as the gradient of pressure over a six degree latitude distance averaged for the four cardinal directions from the center. Results of the test are summarized in Table 4.5. Figures in the table show the number of occurrences

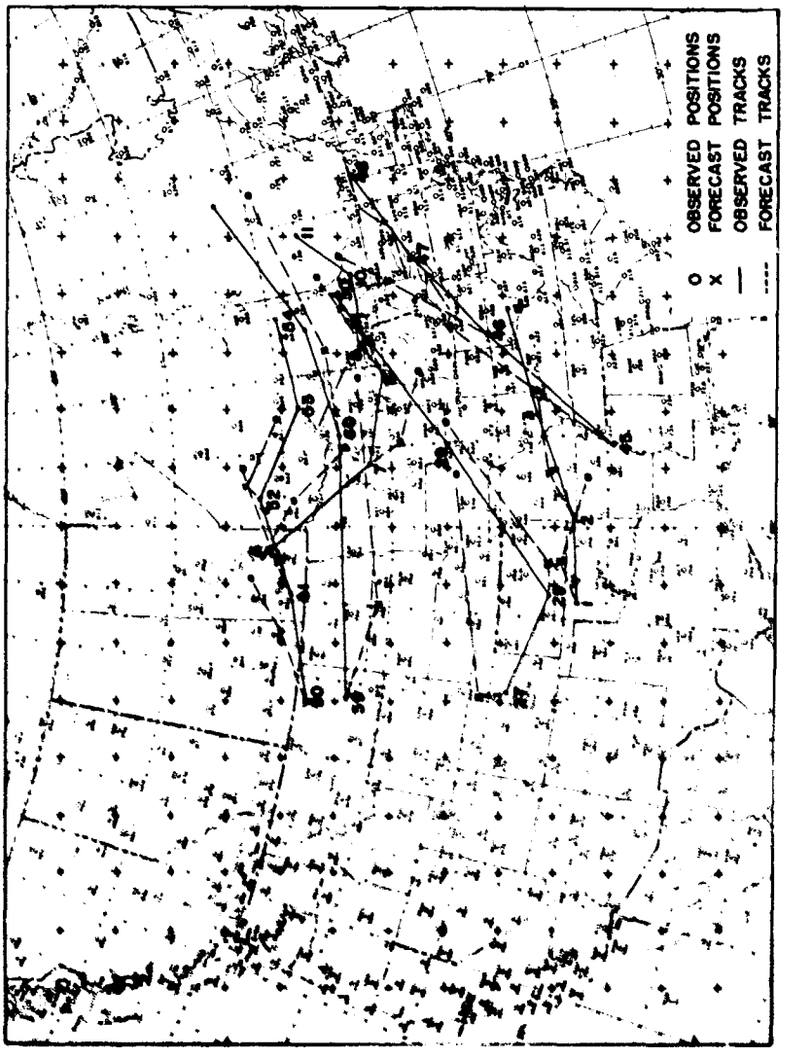

Fig. 4.7. Storm tracks (forecast and observed). Case numbers included

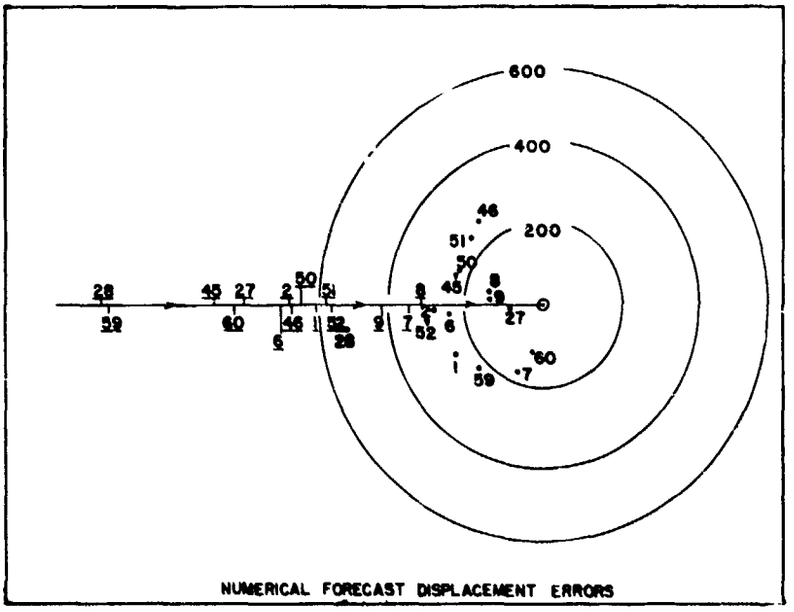

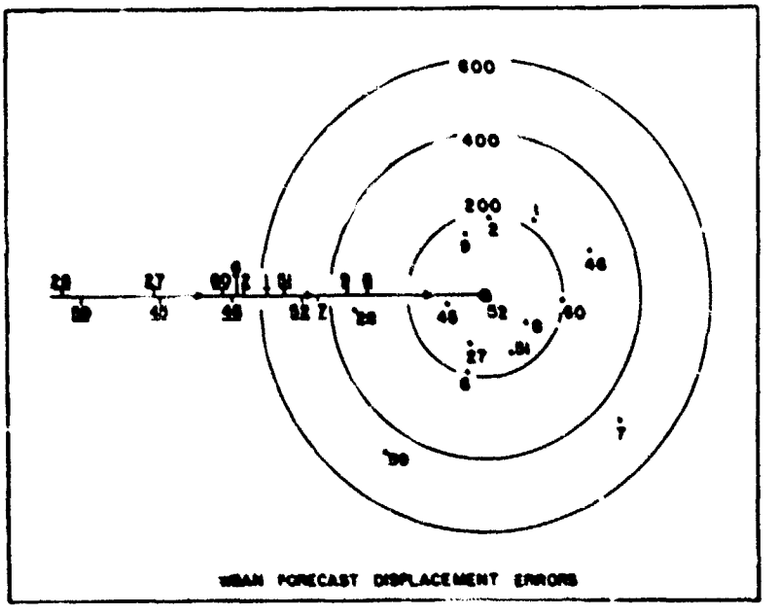

Fig. 4.8. Surface (1000 MB) Displacement Errors.

TABLE 4.5

FREQUENCY DISTRIBUTION OF INTENSITY CHANGES OF SELECTED CYCLONES

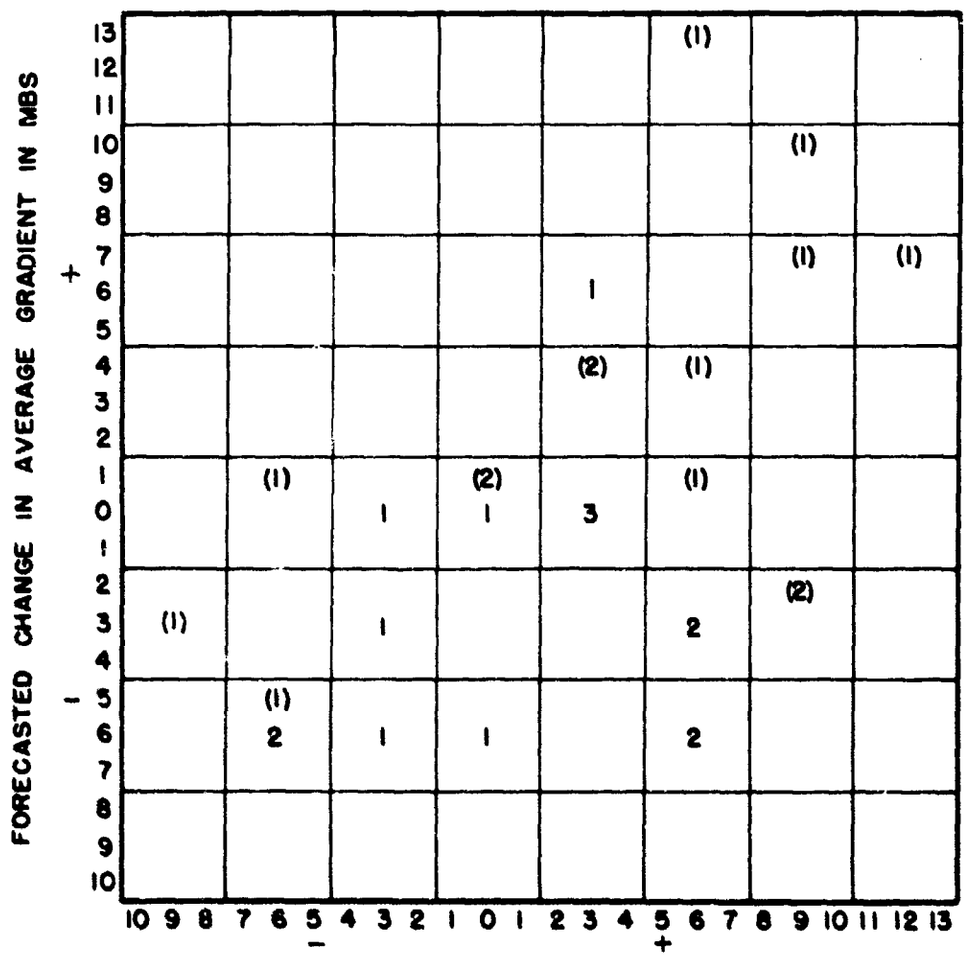

13														(1)								
12																						
11																						
10																		(1)				
9																						
8																						
7																		(1)		(1)		
6													1									
5																						
4													(2)		(1)							
3																						
2																						
1				(1)			1		(2)		1		3		(1)							
0																						
1																						
2																		(2)				
3		(1)					1								2							
4																						
5				(1)																		
6				2			1		1						2							
7																						
8																						
9																						
10																						

(N) WBAN 30 HR SURFACE FORECAST

N NWP 24 HR 1000 MB FORECAST

Table 4.4 -- Comparison of Numerical and Synoptic 24-hr Forecasts, 15 cases, January 1953.

	Direction Error in Deg.		Speed Error in MPH		Position Error in Deg. Lat.
	Ave.	Mean Algebraic	Ave.	Mean Algebraic	
Numerical Forecast	10.7	0	8.2	-8.2	3.4
WBAN Forecast	12.1	R3.2*	5.8	2.0	3.2

*R designates deviation to right when facing downstream.

of a particular combination. Numbers in parentheses are the results of the WBAN thirty-hour forecasts; other numbers show results of the 24-hour predictions by numerical methods. It is interesting to note that intensification of surface cyclonic circulation was predicted by the numerical method in only one case, whereas it was observed to occur in eight of the fifteen situations.

In addition to the study of the surface (1000 mb) forecasts an attempt was made to relate the accuracy (as indicated by correlations) of the numerical forecasts to the initial conditions on the surface map. No significant relationship was found. With initial conditions which appear to be similar, the accuracy of the numerical forecasts varies greatly.

It was noted that in the immediate area of low-level cold polar outbreaks, the 1000 mb height rises were not forecast very accurately by the numerical methods. This may be due to the fact that this low-level cold air advection is generally an ageostrophic advection and, therefore, cannot be detected by the equations. The overall correlations do not reflect this error as the area wherein this advection takes place is generally small compared with the total grid area.

During the major cold polar outbreak of the month on the 15th and 16th, the averaged correlations of forecast versus observed height changes for the four cases were above the monthly average at both 500 mb and 1000 mb. The four 500 mb cases averaged + 0.79, as compared with the monthly average of + 0.74, and the 1000 mb cases averaged + 0.70, as compared with a monthly average of + 0.6[illegible]. The movement of the major storm of the 8th and 9th was forecast well, but the height rises connected with the cold air advection to the northwest of the storm were not well forecast. The case of 14 January, when Salt Lake City had a heavy snowfall, was a case where the numerical method produced a poor forecast of the movement of the low center. The center was forecast to move too far north and the height values of the center were forecast considerably lower than were observed.

4.4.4 Location of jets and fronts

How well one can forecast the location and strength of the jet stream (or zone of maximum winds) at 500 mb using the numerical prognostic maps, is undoubtedly of interest to the synoptician. A case-by-case examination of the 500 mb forecast and observed maps (see Appendix) revealed that the maximum gradient at 500 mb is usually well placed by the numerical forecasts but, on the average, a tighter gradient is forecast than is observed.

The ability to locate the surface frontal systems on the numerical 1000 mb prognostic maps is another point of interest. Examination of the 1000 mb forecast and observed maps leads to the conclusion that the surface frontal systems generally cannot be successfully located on the prognostic charts. Attempts to locate the frontal systems by placing them in the 1000 mb trough lines results in gross errors in a high percentage of the cases.

4.4.5 Vertical motions

The series of numerical computations has provided computed instantaneous vertical motions in the 1000 - 500 mb layer for the initial time for each of the sixty forecast cases. These are the mean vertical motions through the whole layer. The maps showing the geographical distribution of these vertical motions are included in the Appendix. It is interesting to note, in general, the computations result in mean ascending motion in the quadrant to the northeast of surface low centers, where forecasters normally expect major precipitation, and descending motion to the southwest of surface low centers, where rapid clearing is to be expected. This places the centers of ascending motion to the east of the 500 mb trough and the center of descending motion immediately to the rear of the 500 mb trough, as might be expected. The normal rate of speed of the vertical motions at the centers is about 4 cm/sec, with maximum ascending motion speeds of 12 cm/sec during the month, and maximum descending motion speeds of 8 cm/sec.

The map of vertical motions for 1500 GMT of 16 January (Figure 4.9) shows a typical distribution of values. Ascending motion was occurring northeast of the low center in eastern Canada with maximum values of 6 cm/sec. General cloudiness and steady precipitation was occurring in this area. A large area of descending motion lay

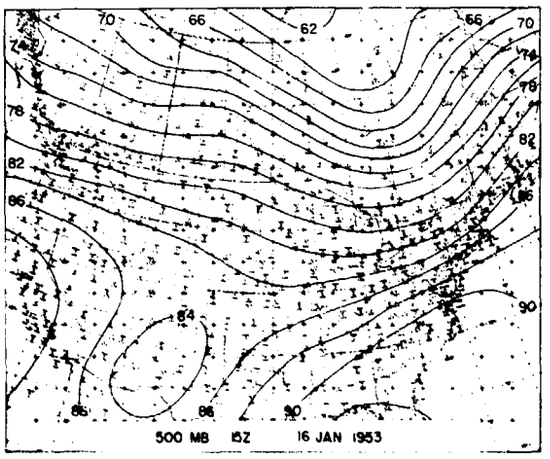
70
66
62
66
70
74
78
82
86
90
84
86
86
90
500 MB 15Z 16 JAN 1953

(a)

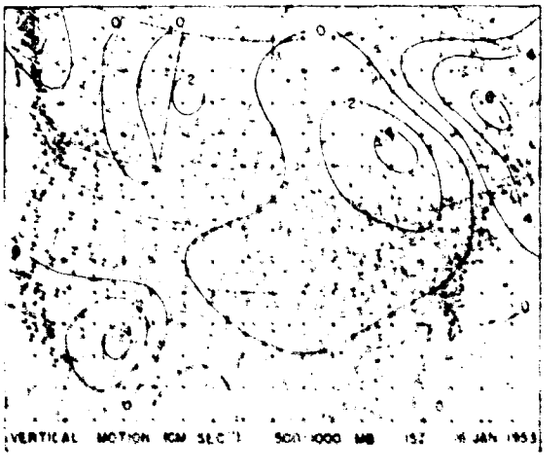
0
0
2
2
4
4
0
0
VERTICAL MOTION (CM SEC⁻¹) 500-1000 MB 15Z 16 JAN 1953

(b)

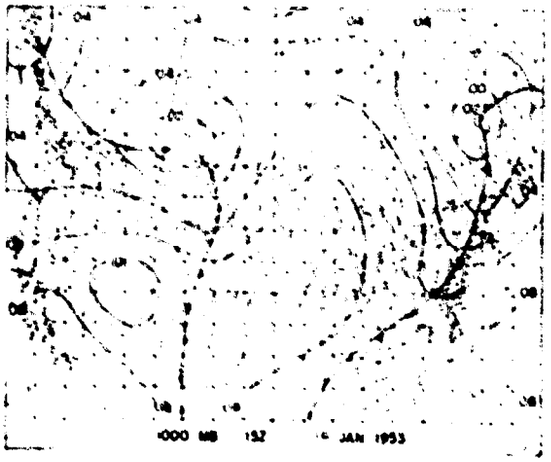
04
04
04
04
08
08
08
08
12
12
1000 MB 15Z 16 JAN 1953

(c)

Fig. 4.9

southwest of the surface low center with maximum values of 4 cm/sec, and generally fair weather was present over the whole area of descending motion. An area of ascending motion was associated with a surface low center in western Canada, but the maximum strength of the motion was confined to a smaller closed area of 2 cm/sec. Variable cloudiness and scattered precipitation was the condition in the northwestern United States and southwestern Canada. In the southwestern United States there was an area of descending motion connected with a surface high pressure call in that locality with generally clear skies. The maximum vertical speed was 4 cm/sec.

4.5 Case Studies of the 500-1000 mb Thickness Forecasts

The thermotropic model employs the 1000 - 500 mb thickness value as one of its parameters in forecasting for the 500 mb and 1000 mb levels. The 1000 mb forecasts, by the nature of the thermotropic model, have errors in them which are introduced by both the 500 mb equation and the 1000 - 500 mb thickness equations. Thus, with a perfect thickness forecast, the 1000 mb prognostic map would still have the errors which were present in the 500 mb forecast. Since the 1000 mb verifications do not indicate the degree of accuracy of the thickness forecasts, for the above reason, and in consideration of the interest of the field forecaster in the use of thickness maps, a few cases were chosen in order to make a closer study of the performance of the thickness equation and to attempt to discover possible sources of error.

Three cases were chosen for study where the correlations were relatively high for the 500 mb forecasts and quite low for the 1000 mb forecasts, indicating that there was a major error in the thickness forecasts. A fourth case was chosen because it was unique in the series. In this case the 500 mb correlation was low and the 1000 mb correlation was relatively high. The thickness boundary errors were averaged for each of the thirty-one points and plotted on a map covering the verification area (Figure 4.10). The largest average errors appear in the northeast corner of the grid area. The values on the north boundary averaged 1.5 to 2 times the values on the south boundary. This probably accounts in part for the relatively large errors which occurred in general in the northern portion of the grid area.

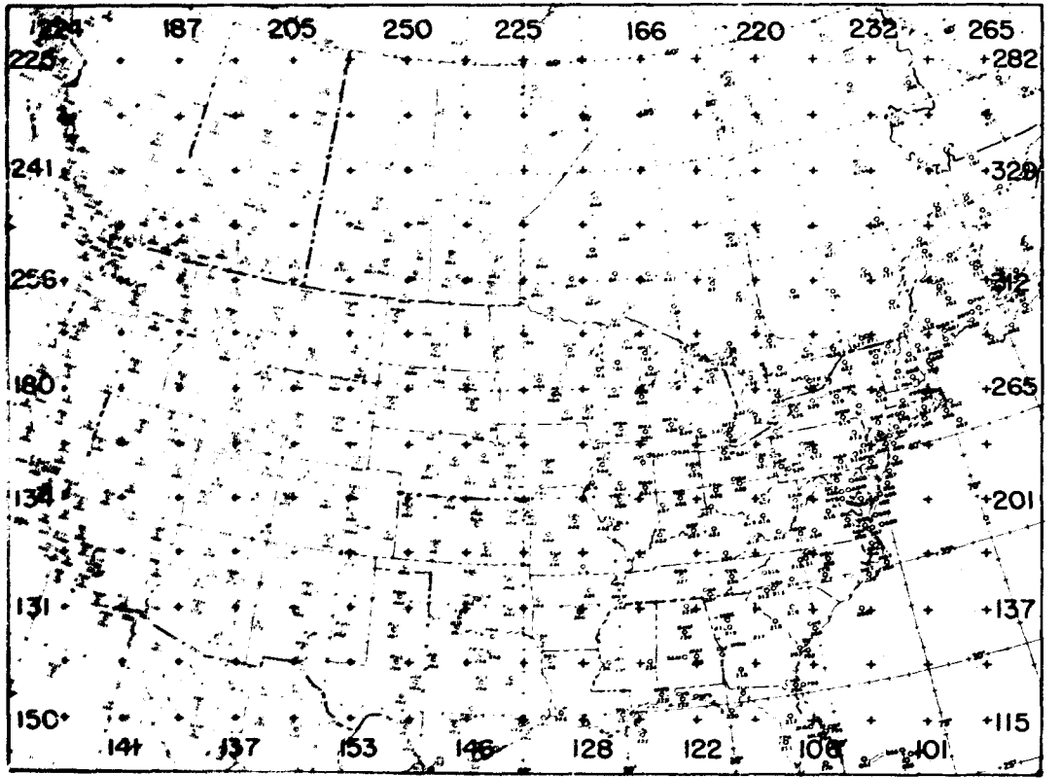

AVERAGED THICKNESS BOUNDARY ERRORS

Fig. 4.10.

The dates and correlations of the four selected cases are listed below:

	Initial Time	R_{500}	R_{1000}
Case 1	9 January 0300 GMT	0.62	0.08
Case 2	7 January 0300	0.80	0.32
Case 3	13 January 0300	0.76	0.17
Case 4	19 January 1500	0.28	0.84

Case 1

This case is of greatest interest in the northwestern portion of the grid where very large errors occurred in the thickness forecast. The initial 500 mb map (Figure 4.11) shows a moderately strong trough over the central United States which developed during the forecast period into a deep low center over Alabama with generally straight west-east flow over the rest of the grid. The 1000 mb maps showed a low center moving from the Mississippi - Alabama border to Georgia during the period. The initial map had a deep low off the northwestern coast of the United States and the final map had a low center just north of North Dakota.

The predicted 1000 mb map agreed with the observed map over the eastern United States but was very much in error in the northwest, where a deep low was forecast in the region into which a ridge of high pressure was observed to move. The 500 mb predicted map had a contour pattern similar to that of the observed map but the gradient was forecast too strong in the northwest.

The 500 mb forecast error map shows that the overly strong gradient predicted in the northwest was a result of forecasting 600 foot excessive height rises in the north central portion of grid, and 600 foot excessive falls in the northwest corner of the grid. The latter error may well be a boundary effect, but the error in overforecasting the anticyclonic buildup in the north central is a feature

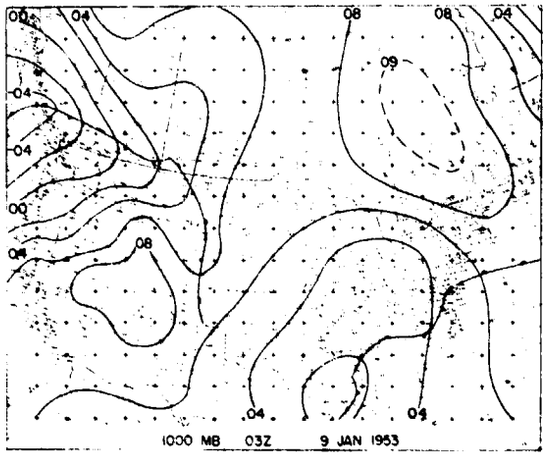

(a)

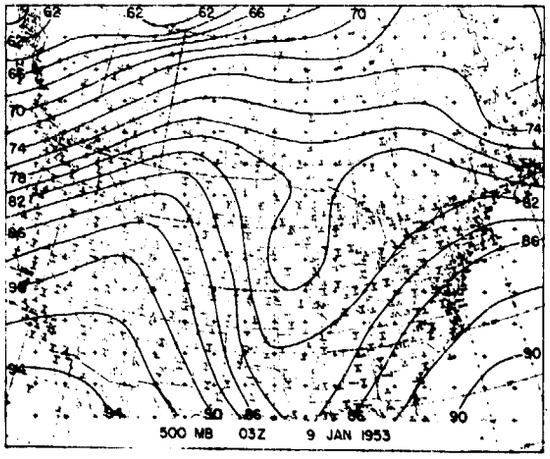

(b)

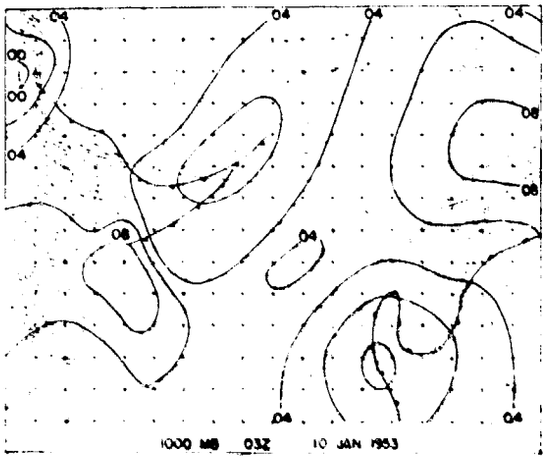

(c)

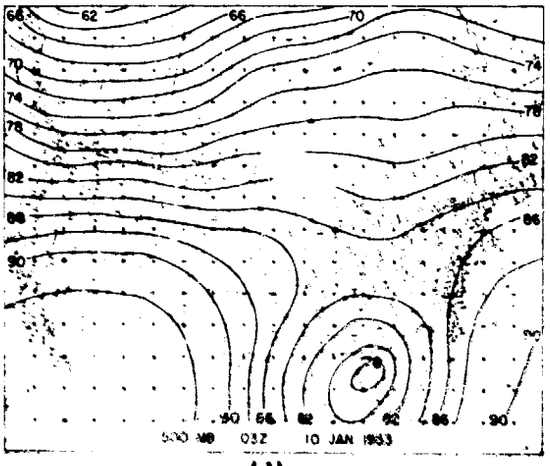

(d)

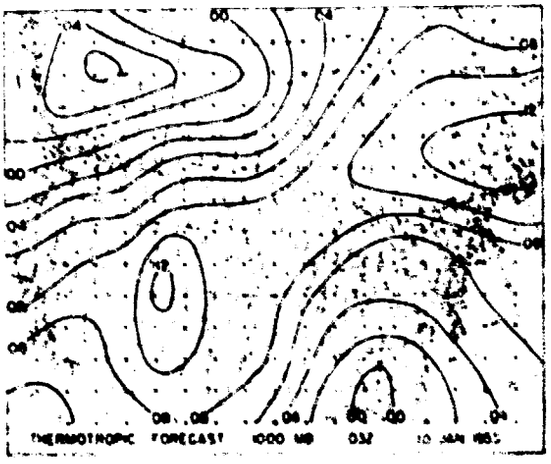

(e)

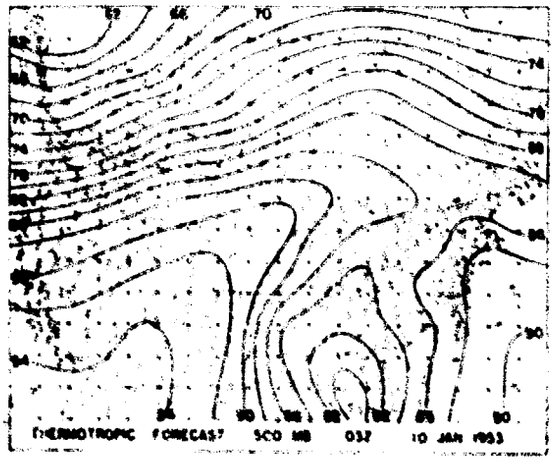

(f)

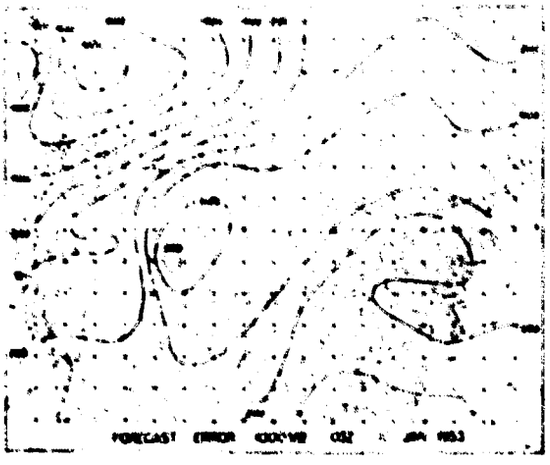

(h)

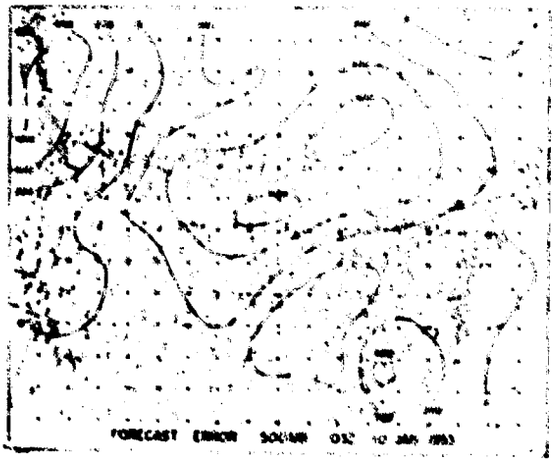

(i)

Fig. 4.11 a-n. Case 1. 9 January - 10 January 1953. 0300 GMT

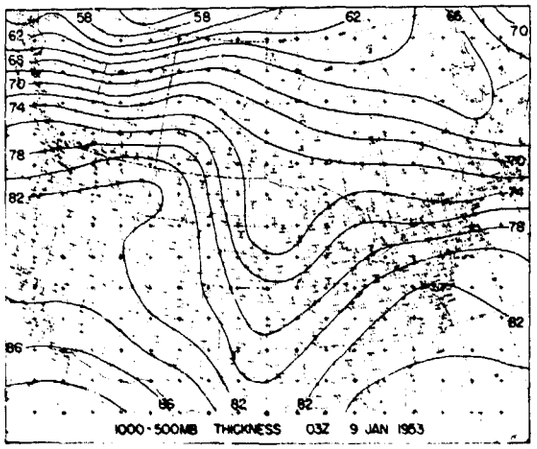
1000-500MB THICKNESS 03Z 9 JAN 1963

(i)

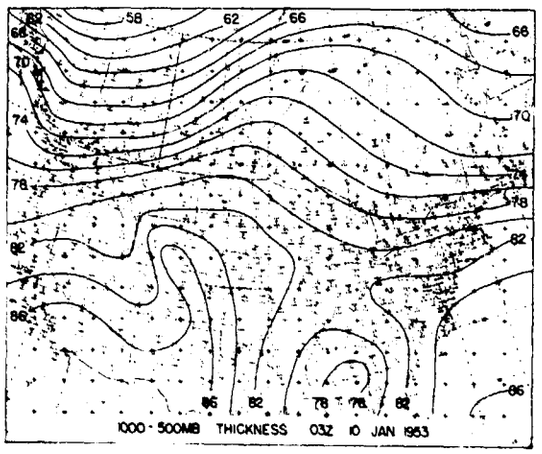
1000-500MB THICKNESS 03Z 10 JAN 1963

(j)

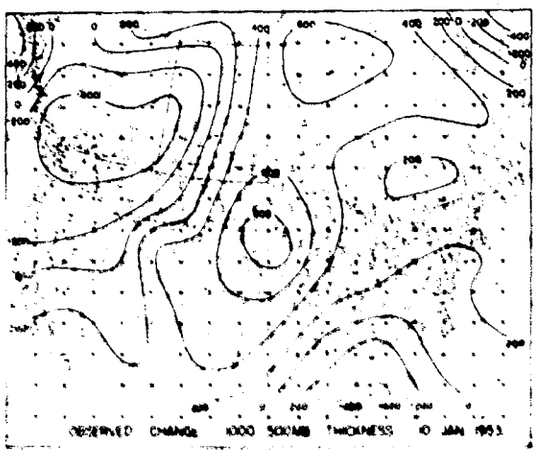

(k)

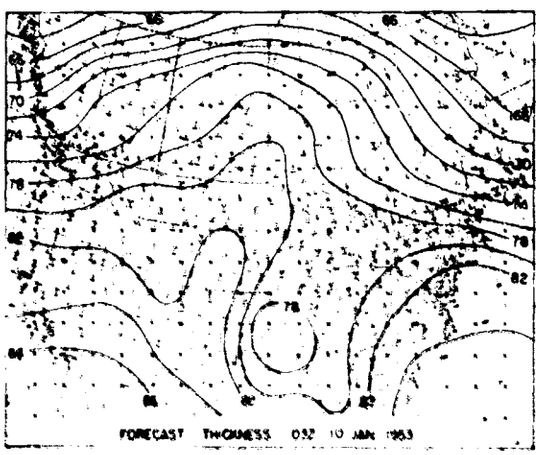
FORECAST THICKNESS 03Z 10 JAN 1963

(l)

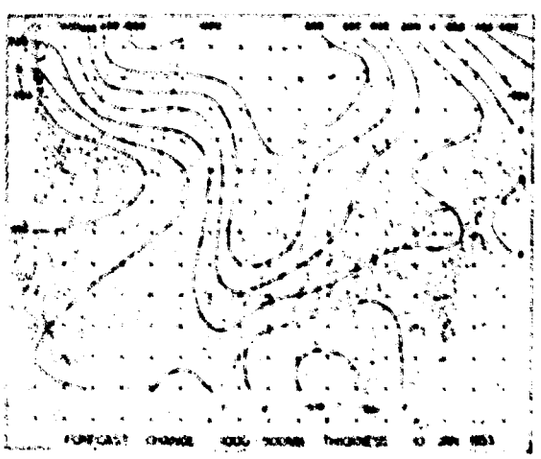

(m)

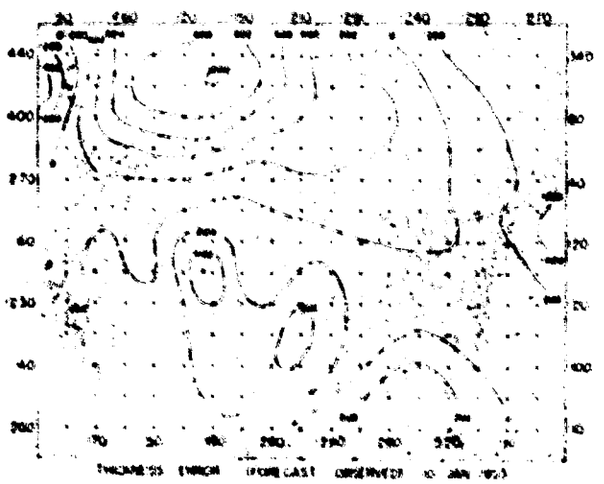

(n)

which appears in many of the forecasts, and is apparently inherent in the equations or methods of solution.

The 1000 mb error map shows heights predicted 1000 feet too low in western Canada and 800 feet too high over the eastern Rockies. The thickness error map shows the amount of error contributed to the 1000 mb map by the thickness forecast. There is an area of 1000 foot thickness error in the region of the large 1000 mb error. A 400 foot error near the northwestern corner of the grid is of the same size as the boundary error and is likely a direct result of the boundary error. The boundary error values north of the major thickness error of 1000 feet are smaller than the monthly average values of boundary error, and cannot very well be considered important in producing the large error. Examination of the 1000 mb and 850 mb charts revealed an ageostrophic flow across the packed thickness lines producing cold air advection in the region of large error whereas the contour lines did not indicate this advection.

The initial thickness map shows a pattern very similar to the initial 500 mb map. From these two maps there is no reason immediately apparent for expecting warming in western Canada. Anticyclonic thermal vorticity values along the southwestern Canadian coastline due to slight anticyclonic curvature and wind shear may have contributed largely to the forecast, as these values of vorticity would have been advected by the equations into the region of large error. The forecast thickness map shows how the ridge of thickness values was built up in central Canada and the gradient was decreased in western Canada. The observed thickness map shows that there was actually a decrease in thickness across the western half of Canada and a maintenance of the strong west-east gradient.

Speculating on the possible reasons for the large thickness errors in this case, it appears that the following factors are the most probable reasons for the errors:

(1) The nongeostrophic flow in the low levels may be an important contribution to the thickness decreases over the period by advection of cold air at these levels.

(2) The forecast equation may not give proper weighting to its individual terms, since the coefficients of the thermal advection terms in both equations were empirically determined. Theoretical work done since the tests were carried out indicates that the coefficients were probably too small.

(3) The mountain barrier effects may be important in this case, with a very strong west-east component to the wind.

Case 2

This case is of major interest in the area just south of Hudson Bay where there was a 600 foot error in the thickness forecasts. The initial 500 mb map (Figure 4.12) shows a very flat trough over southern Hudson Bay, weak to moderate west-east flow over the United States and a low center in western Canada. During the period there was little change in the pattern, with small height rises over southern Hudson Bay. The 1000 mb maps were much the same at the beginning and end of the period, with a deep low off the northwestern United States coast, and a weak low over the south central United States; there was an increase in the 1000 mb heights over Hudson Bay.

The predicted 500 mb map has a strong ridge built up through the central United States and Canada and a strong gradient across the northern United States and southern Canada. The correlation coefficient is misleading in this case, since the forecast and observed changes are pretty well in phase as to sign, thus giving a good correlation, whereas the equations overforecast the size of the changes by a considerable amount. This tendency to overforecast height rises in the vicinity of ridges is illustrated again by this case.

The predicted 1000 mb map has a low off the northwest coast of the United States much deeper than observed and strong high centers southwest of Hudson Bay and over Lake Michigan. The 1000 mb error map shows the extent of the overforecast of high pressure southwest of Hudson Bay in the same region of maximum 500 mb error.

The thickness error map shows that sizable thickness decreases were forecast in the Hudson Bay region resulting in errors in excess of 600 feet. Boundary errors

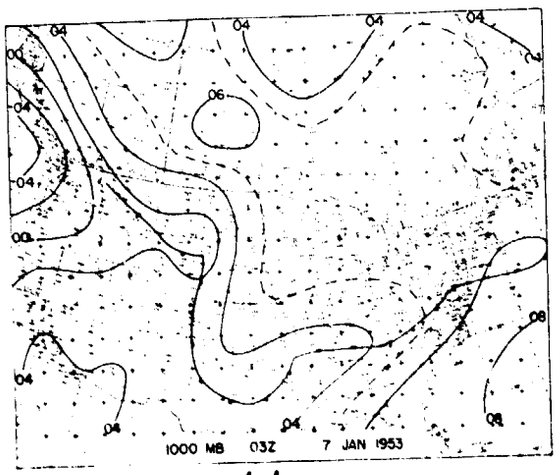
1000 MB 03Z 7 JAN 1953

(a(

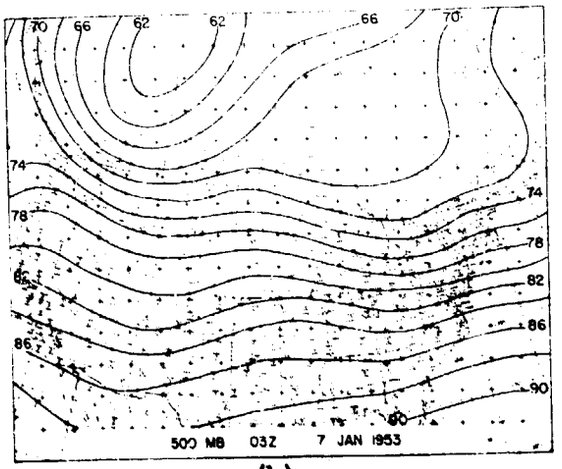
500 MB 03Z 7 JAN 1953

(b)

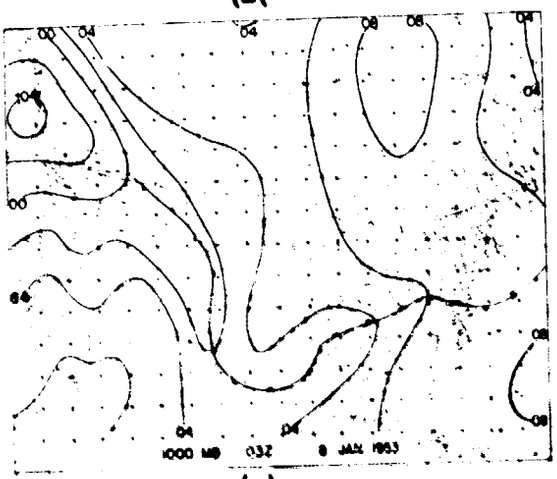
1000 MB 03Z 8 JAN 1953

(c)

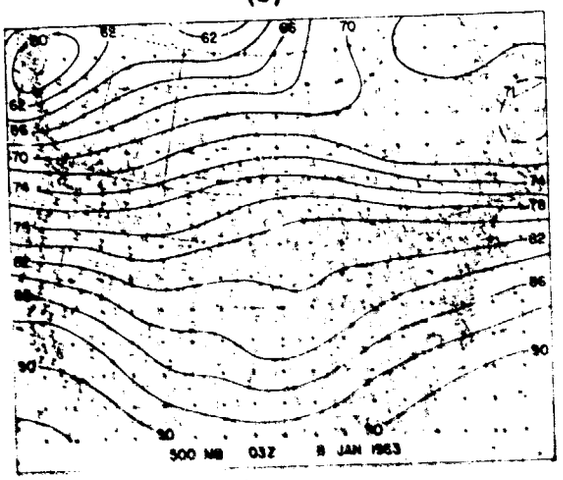
500 MB 03Z 8 JAN 1953

(d)

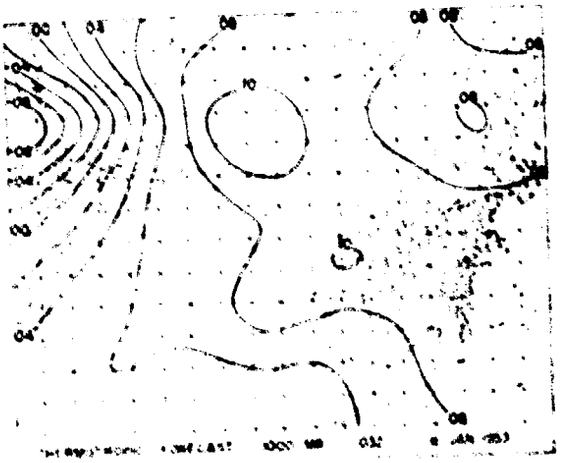

(e)

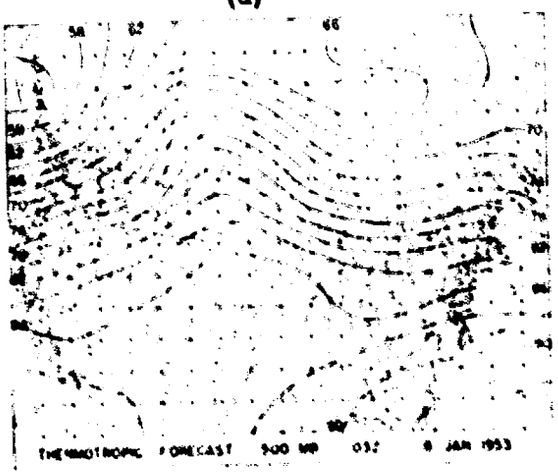
500 MB 03Z 8 JAN 1953

(f)

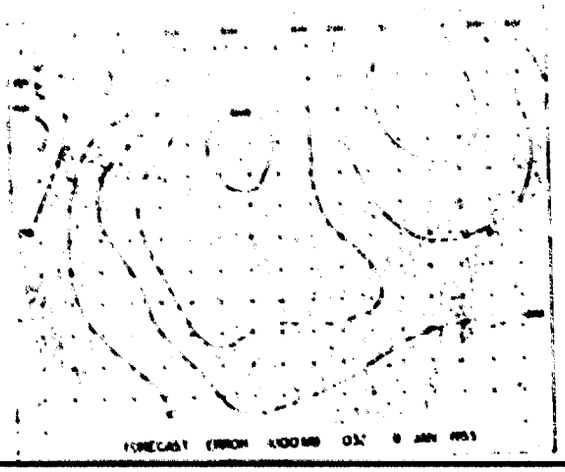

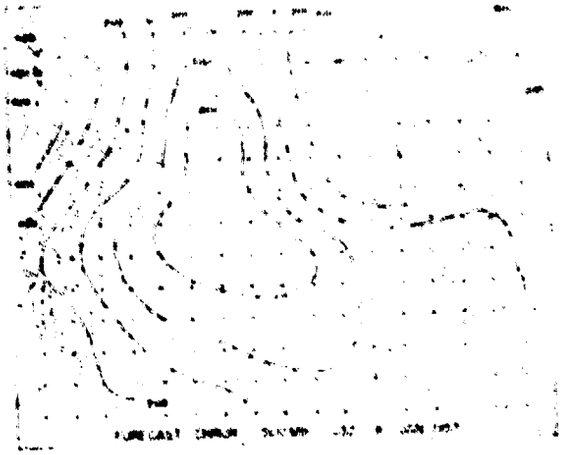

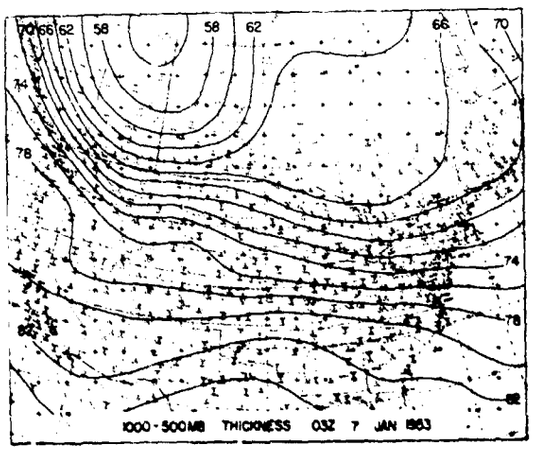

(h)

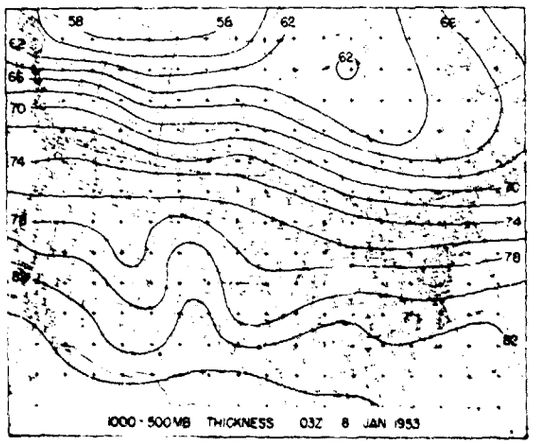

(i)

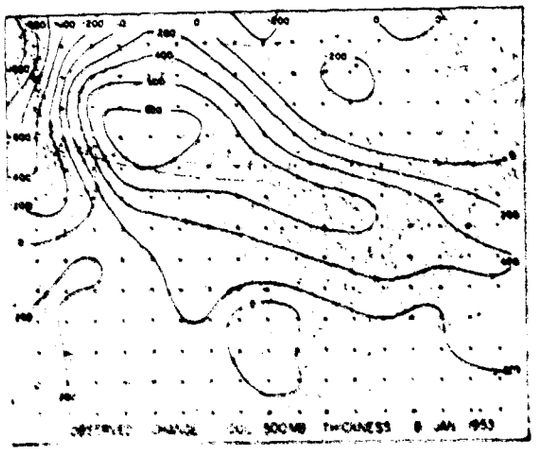

(j)

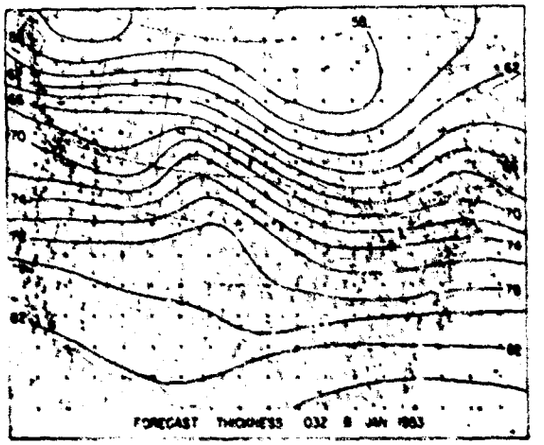

(k)

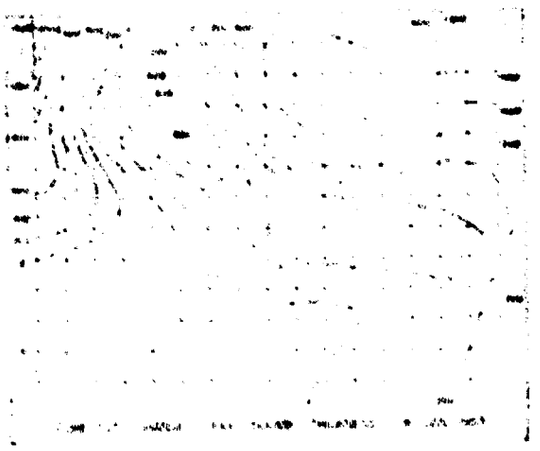

(l)

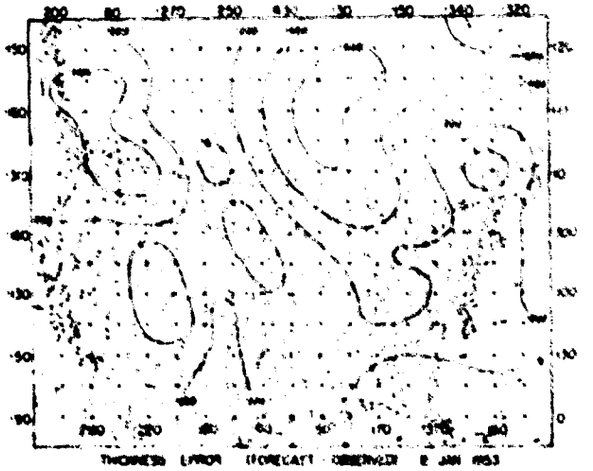

(m)

Fig. 4.12 a-n. Case 2. 7 January 1953 - 8 January 1953. 0300Z

were very small to the north of this major error and cannot account for the errors. The predicted and observed thickness change maps indicate that the strong warming which occurred in southwestern Canada was forecast, but show that very little cooling occurred over Hudson Bay where strong cooling was predicted. The predicted and observed thickness maps show how the forecast of strong cooling over Hudson Bay resulted in a poor thickness forecast. The thermal gradient along the United States - Canada border was forecast much too strong, and a trough over Hudson Bay was forecast to be much too deep.

The initial thickness and 500 mb maps indicate that the forecast of lower thickness values over Hudson Bay was probably caused by the advection of increased cyclonic vorticity values into that region, and not from advection of cooler air in the layer. The initial maps indicated some slight warm air advection south of Hudson Bay using the 500 mb flow and the thickness lines as the temperature field. It appears that the advection of vorticity was weighted too strongly by the equations in this case.

Case 5

In this case there is a sizable thickness forecast error in the region near the western United States - Canada border. The initial and observed 500 mb maps (Figure 4.13) show a relatively unchanged zonal flow through the period, while the surface maps show a buildup of a polar high in western Canada. The predicted 500 mb map shows good agreement with the observed map, while the predicted 1000 mb map shows a deepening trough extending along the western United States - Canada border.

The forecast error maps emphasize the accuracy of the 500 mb forecast except near border points, while showing a 600 foot error in the 1000 mb forecast along the United States - Canada border. The thickness error map shows that thicknesses were forecast more than 400 feet too large in the area of maximum 1000 mb error. Other large thickness errors are located near regions of large boundary errors. The observed thickness change map shows that there was cooling in the layer over a large area in northwestern United States and Canada, whereas there were thickness increases forecast in some portions of this region.

The initial and observed thickness maps show that the thermal jet moved southward from western Canada into the north central United States, whereas the forecast did not move the thermal jet southward. The 500 mb flow, as well as the low-level flow, had a component across the thermal gradient so as to cause colder air to be advected southward into the north central United States. It appears that the equation weighted the advection of anticyclonic thermal vorticity into the north central United States to the point of forecasting thickness increases rather than decreases. Results of the verification studies carried out on the month's data indicate that the forecast equations tend to consistently overweight the vorticity advection effects, and underweight the effects of thermal advection.

Case 4

This case will not be discussed in detail. This was the case of a poor 500 mb forecast and a good 1000 mb forecast (Figure 4.14). The 500 mb errors were small and scattered. The low correlation indicates that the forecast and observed changes patterns were out of phase, and the major error apparently was one of not moving the systems fast enough from west to east. The initial thickness pattern was almost identical with the 500 mb pattern as the surface flow was weak. The thickness forecast was similar to the 500 mb forecast with errors of similar size and location. When the thickness forecast was subtracted from the 500 mb forecast the errors cancelled and the result was a 1000 mb prognostic map with practically no errors. The similarity of the two forecast equations is shown here by the similarity of the thickness and 500 mb forecasts and the error distributions starting with similar patterns.

4.6 The Thermotropic Model as a Forecast Technique

The thermotropic model can be regarded as a practical operational forecasting technique considering both accuracy and time involved. There are several advantages in numerical methods over the conventional field techniques. Numerical weather prediction is an objective technique, not subject to errors of oversight or the physical or mental conditions of a forecaster. The assumptions made in developing the equations are at least internally consistent. While their solution requires no

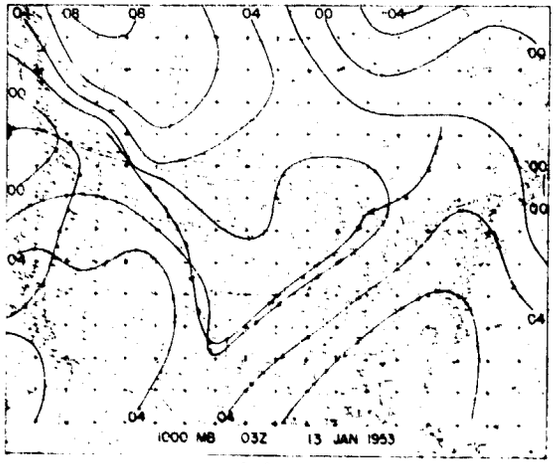
1000 MB 03Z 13 JAN 1953

(a)

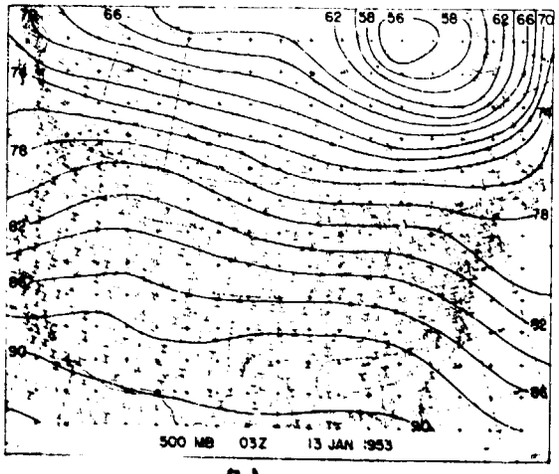
500 MB 03Z 13 JAN 1953

(b)

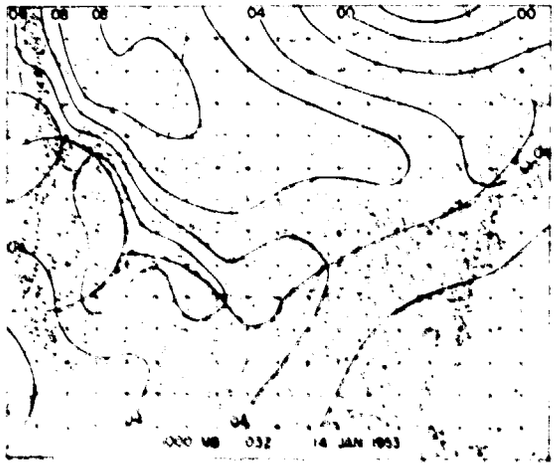

(c)

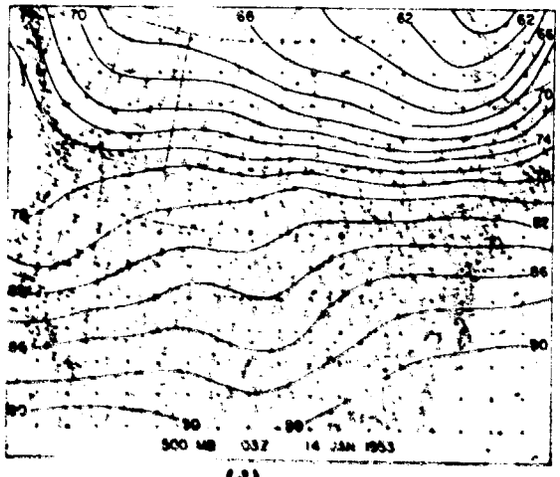
500 MB 03Z 14 JAN 1953

(d)

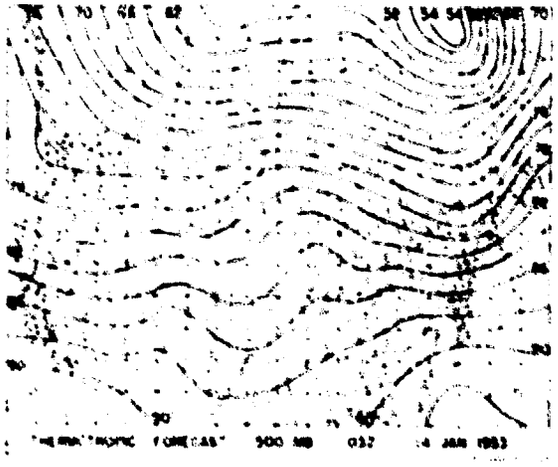

(e)

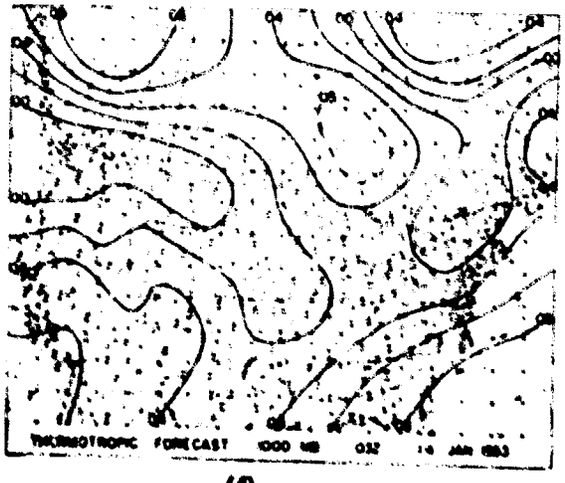
THERMOTROPIC FORECAST 1000 MB 03Z 14 JAN 1953

(f)

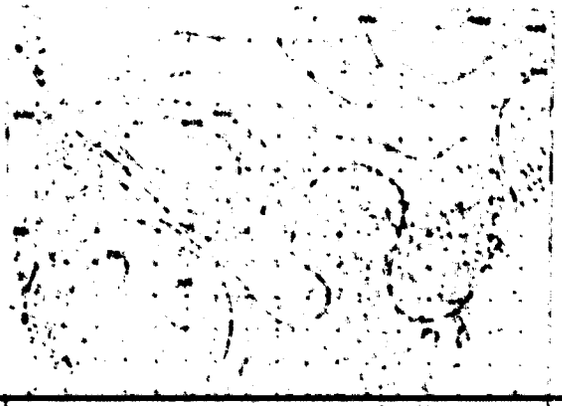

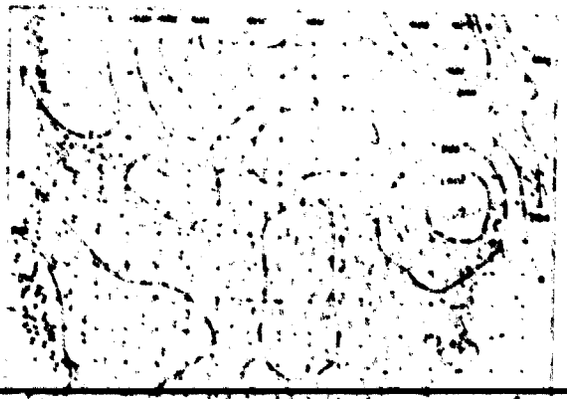

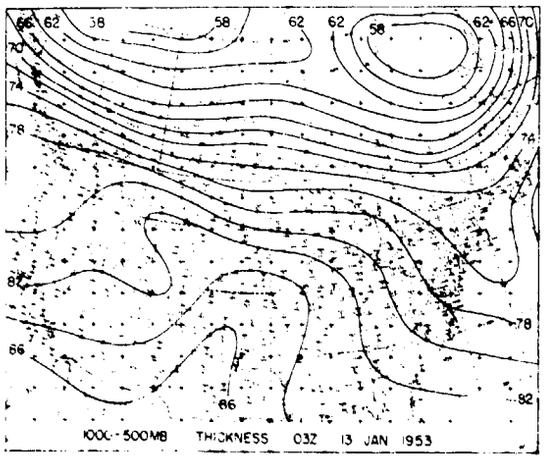

(i)

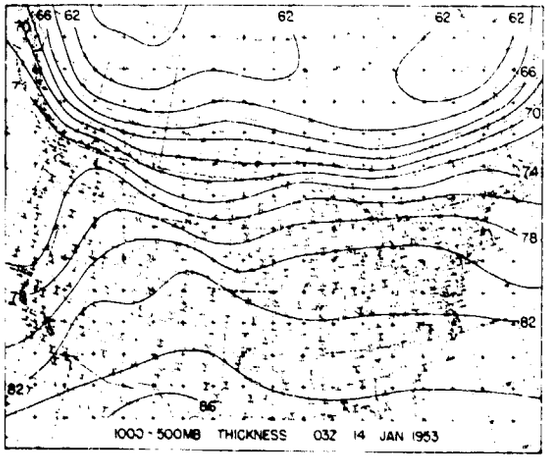

(j)

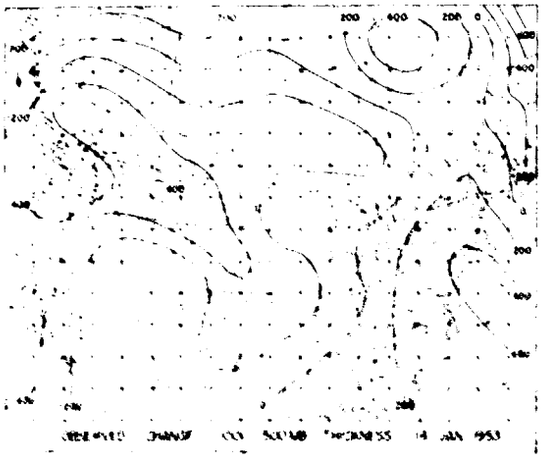

(k)

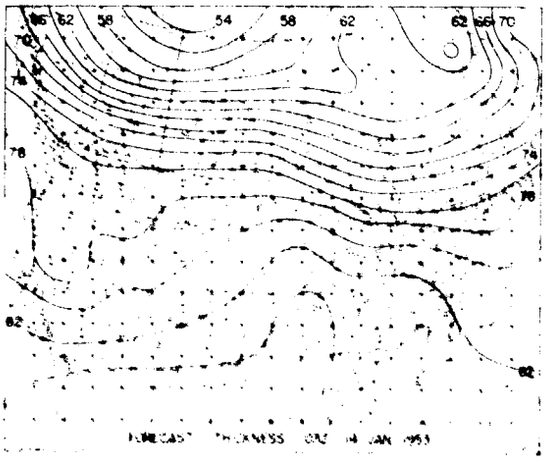

(l)

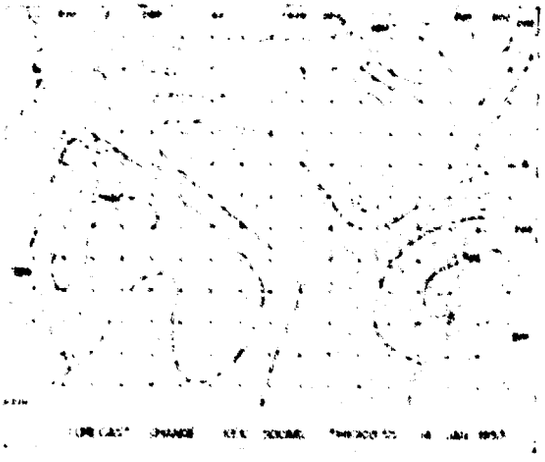

(m)

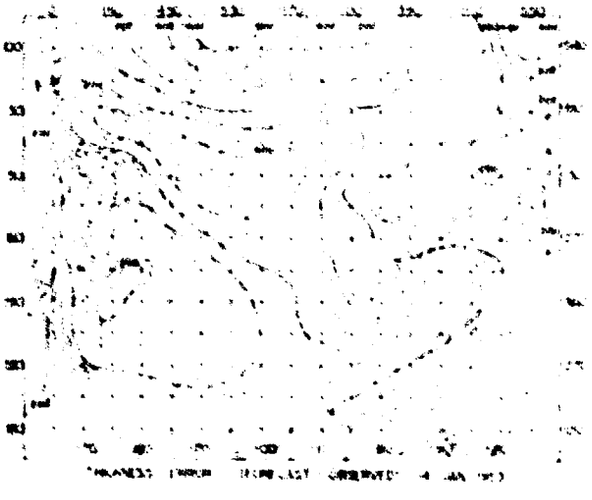

(n)

Fig. 4.13 a-n. Case 3. 13 January - 14 January 1953.

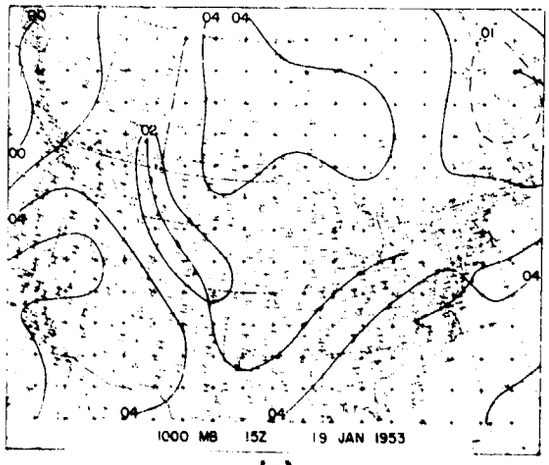
1000 MB 15Z 19 JAN 1953

(a)

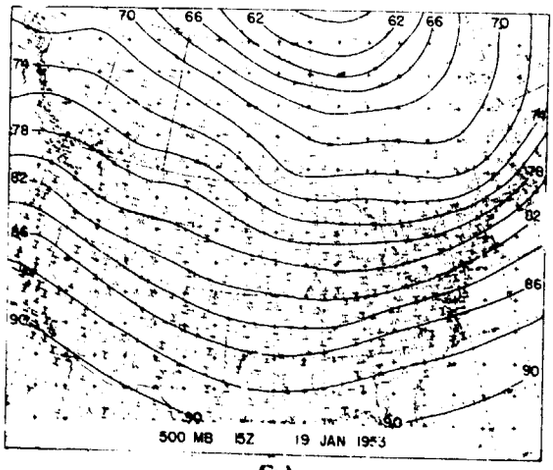
500 MB 15Z 19 JAN 1953

(b)

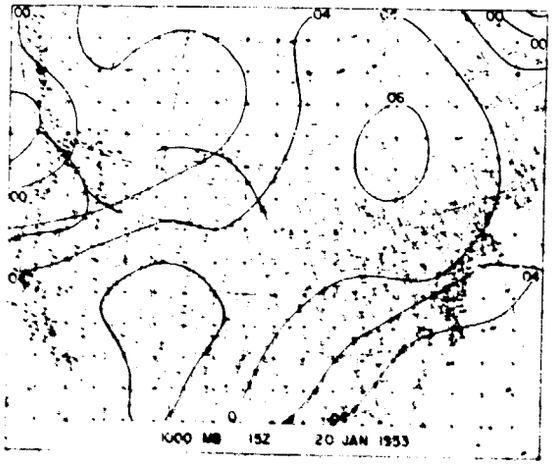
1000 MB 15Z 20 JAN 1953

(c)

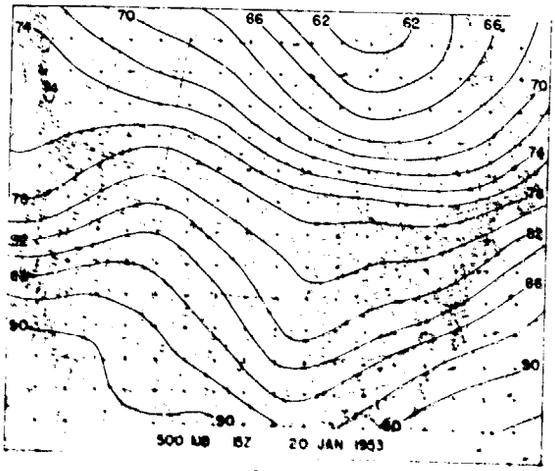
500 MB 15Z 20 JAN 1953

(d)

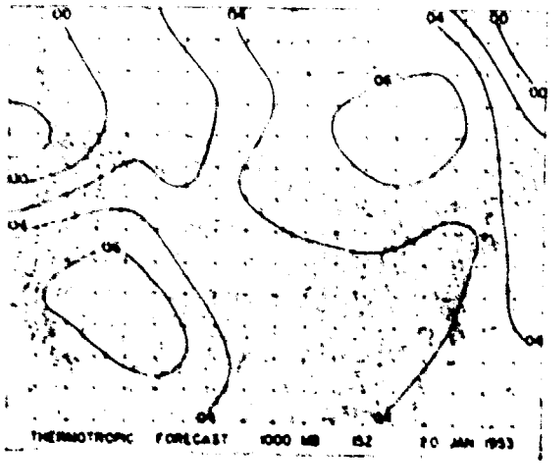
THERMOTROPIC FORECAST 1000 MB 15Z 20 JAN 1953

(e)

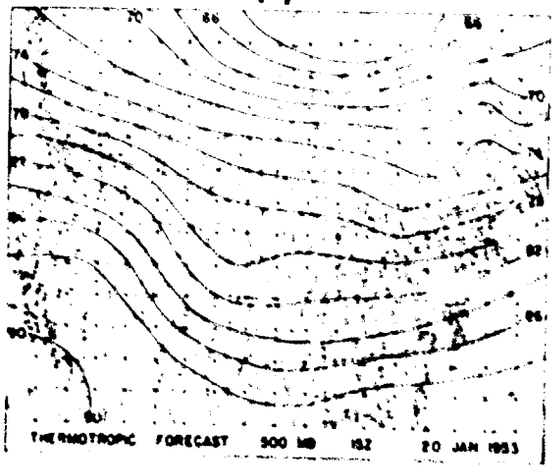
THERMOTROPIC FORECAST 500 MB 15Z 20 JAN 1953

(f)

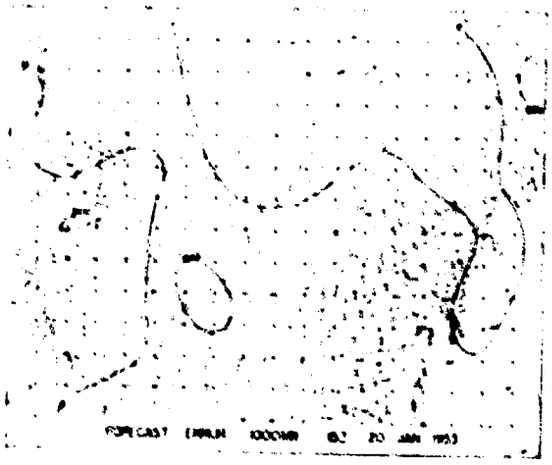

(g)

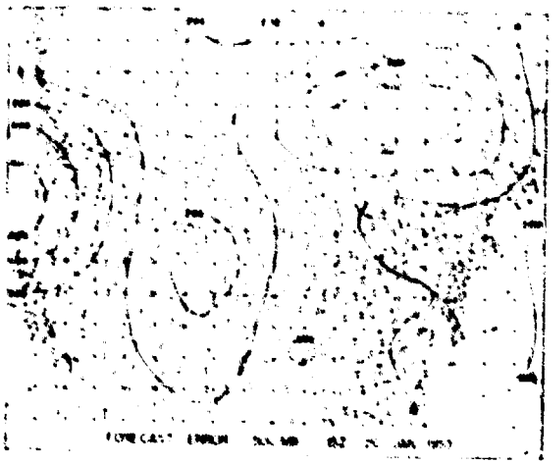

(h)

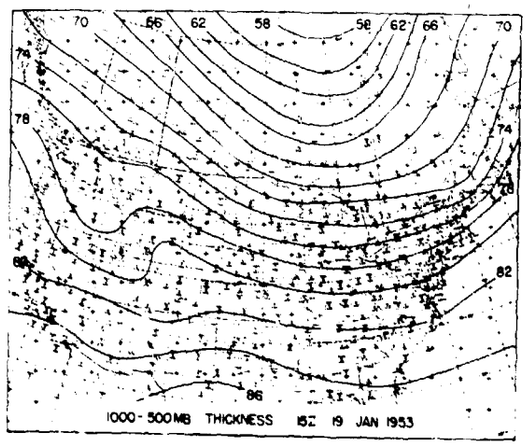

(i)

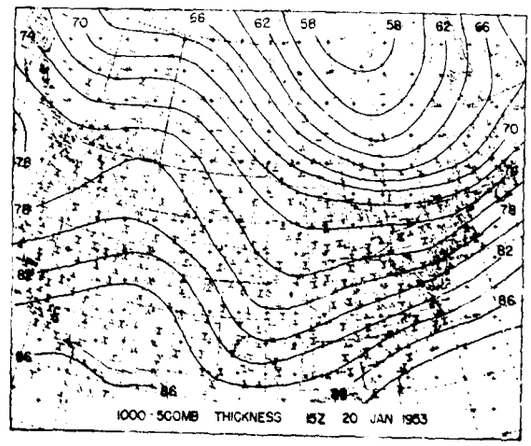

(j)

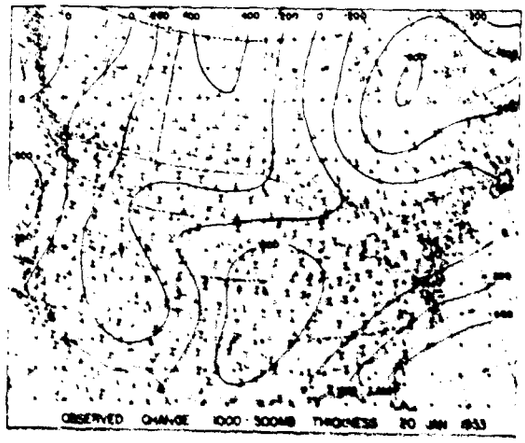

(k)

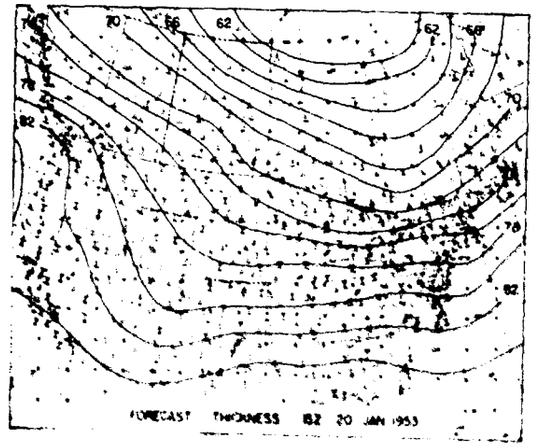

(l)

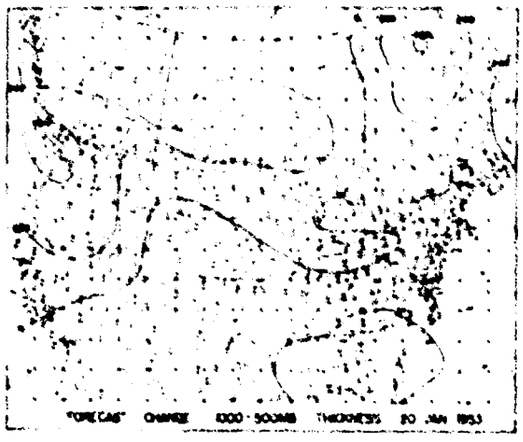

(m)

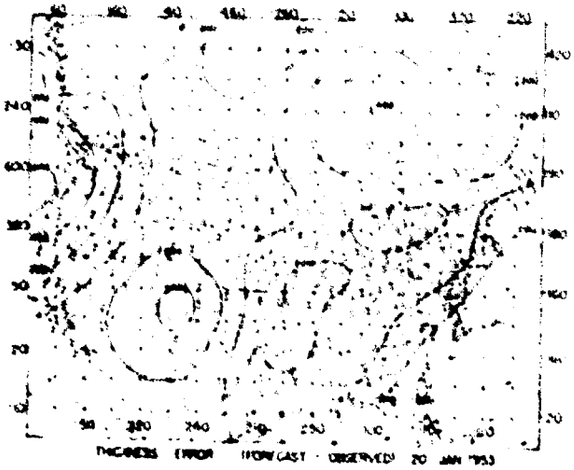

(n)

Fig. 4.14 a-n. Case 4. 19 January 1953 - 20 January 1953. 1500Z

knowledge of preceding weather in forecasting for a limited area, boundary conditions are required which may include information of past weather. Numerical methods are consistent in that they will always give the same forecast with the same initial and boundary conditions, and offer the mean vertical motions in the 1000 - 500 mb layer as a by-product of the forecasts. Finally, a number of factors contributing to pressure changes can be more exactly weighted individually and collectively by numerical methods than by subjective techniques; vorticity advection effects, for example, are objectively determined. An important aspect of numerical methods is that they are still in the development stage and can be expected to show continued improvement with time.

Some disadvantages are also evident in this and other numerical models. First, one may mention that numerical methods are sensitive to errors in analysis; the analyses of initial data must be smooth and accurate to obtain best forecast results. Sparse data over a region are more of a handicap when using numerical methods than when using the conventional field techniques; data are generally required over a much larger area than the area of forecast results. Second, arbitrarily assumed boundary values produce errors, and errors are introduced by finite-difference methods of solution and other mathematical approximations. Most models now in use do not yet have provisions for taking the terrain effects and thermal source effects into account. Therefore, additional errors are introduced into the forecasts from these sources. As far as the equations are concerned, pressur systems act the same over oceans and continents, over warm sources and cold sources. Strong cold polar outbreaks into the United States in winter normally occur with a strong ageostrophic component to the winds in the levels below 500 mb; quasi-geostrophic models, such as the thermotropic model, cannot predict the changes occurring due to this cold air advection. There are some cases in the January 1953 series where the numerical forecasts missed strong surface pressure buildups which occurred with strong low-level cold air advection. The area of the grid which was most affected by this type of error was just east of the Rocky Mountains along the United States - Canada border.

4.7 Summary

The tests carried out on the thermotropic and barotropic models indicate that numerical prediction has developed to a point where usable forecasts can be made on a routine daily basis at upper levels and near the earth's surface. Comparisons between numerical methods and conventional field techniques using the same data show that the numerical methods are consistently as accurate a forecasting technique as other available methods. The thickness equation in the thermotropic model apparently forecasts as accurately as the 500 mb equation, but the overall accuracy of the 1000 mb forecasts is somewhat lower than the 500 mb forecasts due to the accumulation of errors from both the 500 mb and thickness forecasts.

The barotropic and thermotropic 500 mb forecasts were so similar, as shown by the statistical study of Section 3, it must be assumed that (1) the equations themselves are, in effect, nearly identical, (2) the methods of computation influenced the results to such an extent that the results were forced to be similar, or (3) that January 1953 was a month in which the atmosphere was equivalently barotropic throughout. Cases such as those of 8 and 9 January make the third assumption appear unlikely. Sections of the maps on these dates showed very strong thermal advection and yet the barotropic and thermotropic forecasts were similar in these regions.

There are a number of causes for errors in the numerical methods which must be eliminated in order to improve further the technique.

(1) The mountains in the western United States and Canada are important as a flow barrier and as a thermal barrier between the cold polar source in Canada and the relatively warm Pacific Ocean. The effects of the terrain should be included in numerical methods to improve the forecasts near mountainous areas.

(2) The method of boundary specification should be improved in order to reduce the errors introduced by the computations involving incorrect boundaries. The results of these tests have shown that the boundary errors are occasionally an important influence in the forecast even at interior grid points.

(3) The quasigeostrophic character of the equations should be altered in order to account for the effects of strong thermal advection due to a nongeostrophic wind component. There were several cases of polar outbreaks occurring during the month which were misforecast by the model.

(4) The method of computing and advecting vorticities apparently produces errors under certain conditions. With strong shear conditions, for example, there is a tendency to produce too great a height change downstream, which is particularly noticeable in several cases where strong anticyclogenesis was predicted in a region downstream from a region of strong anticyclonic shear. This anticyclogenesis was not observed. In some cases, when the vorticity advection and thermal advection were working to produce height changes of opposite sign, the vorticity advection was emphasized by the equations with the result that height changes of the wrong sign were predicted.

(5) A predicted 1000 mb chart may not best be obtained by combining thickness forecasts and 500 mb forecasts. Errors are accumulative in most cases, resulting in a decrease in the accuracy of the 1000 mb forecasts, as compared with the individual 500 mb and thickness forecasts.

The fact that the thermotropic model employs thickness forecasts is synoptically interesting. Thickness patterns relative to storm tracks and the development of systems have been the subject of many synoptic studies, including a comprehensive study by Sutcliffe and Forsdyke,[15] and interesting applications by George[16] and Owens.[17] The numerical prediction project has used the thickness forecast only as a means to obtain a 1000 mb forecast, and the verification program was concentrated on the 500 mb and 1000 mb forecasts. The only thickness forecasts evaluated thus far are included in the present study. Considering the general interest of meteorologists, particularly synopticians, in the thickness map, a more complete study of the numerical thickness forecast is in order.

The continued development of numerical methods promises to produce better forecasts in the future. The mountain effects can and should be incorporated into the equations. The boundaries can be moved far from the region of forecast interest to reduce their effects or other methods of solution can be employed. Continued research should provide answers as to the best methods of vorticity computation and advection, the inclusion of nongeostrophic wind components, and the best levels at which to employ the numerical methods. It is hoped that numerical methods will eventually be able to supply the synoptic meteorologist with an accurate, objective prognosis of the flow patterns from which he can predict the precipitation and cloud condition by associated studies, and by consideration of local influences on the overall weather pattern.

5. General Summary and Conclusion

The series of numerical forecasts described in this report constitutes perhaps the first extensive study of the barotropic and simple baroclinic nonlinear atmospheric models over a wide range of synoptic conditions, and lay the groundwork for the further systematic study of the behavior of numerical prediction models. The further research suggested by this work, which has been discussed in sections 3.6 and 4.7 in connection with the statistical and synoptic forecast evaluations, stems from a number of general characteristics of the results and which may be summarized as follows.

(1) Perhaps the most striking characteristic of the numerical forecasts is the high degree of similarity between the barotropic and thermotropic predictions for the 500 mb level. In each case of the series of 60 forecasts, made from the initial data observed every 12 hours at 03Z and 15Z during the entire month of January, 1953, the barotropic solutions have been found to account for the position and orientation of the large-scale disturbances. In some cases important differences in the forecast amplitude changes of the disturbances were found between the two models, but were on the average small and not significantly different on the statistical basis of the correlation between predicted and observed changes. This evidence reflects the quasi-barotropy of the atmosphere on an average basis, and strongly suggests that the

baroclinic component of the flow introduced by the thermotropic model at 500 mb is in general relatively small, and that for 24-hour forecasts, at least, the atmosphere may be considered either equivalent-barotropic or thermotropic for the purpose of predicting the flow in the middle troposphere.

(2) A second important characteristic of the numerical forecasts is the marked influence of the lateral boundary conditions imposed during the relaxation process. These conditions not only seriously altered the computed changes in the immediate vicinity of the boundaries, an effect which was, of course, anticipated, but in addition frequently extended their effect well into the interior of the forecast area. For those cases in which there was a large change in contour height imposed on the boundary, the predictions are in general noticeably poor; this circumstance frequently occurred over the northwestern U. S. and southwestern Canada. These boundary effects in general appear to have affected the barotropic and thermotropic forecasts in much the same manner, and in the regions near the boundaries probably account for the similarity of the forecasts.

(3) A third important feature of the numerical forecasts is the high level of both statistical and synoptic performance over the eastern half of the United States. In this area, the 24-hour forecasts for both the 500 and 1000 mb levels correlate with the observed changes at 0.8 - 0.9, and consistently display the correct position and orientation of the large-scale disturbances, as may be seen from an inspection of the maps in the Appendix. The fields of computed vertical motion also bear out many familiar synoptic relations between the vertical velocity and the synoptic pattern. A tendency is evident, however, for the models to slightly underforecast the observed intensity changes and the speed of propagation of well developed disturbances. On an average basis the models appear to produce better forecasts in the eastern and southwestern U. S., with poorer average performance in the central plains States. This average behavior is suggestive of an important effect of the Rocky Mountains upon the flow, and in several specific cases the terrain-free equations were unable to predict adequately cyclogenesis in the lee of the western mountains.

In studying the errors of numerical forecasts, not only must the physical approximations introduced in the models be kept in mind, but the errors introduced by the numerical methods of representation and solution themselves must be considered. Through the use of a specially prepared set of synoptic charts embodying all available data, it is felt that the purely observational and analysis errors have not seriously affected the overall character of the present series of forecasts. In the regions most likely free of the destructive effects of erroneous boundary conditions and of the effects of mountainous terrain, namely the eastern United States, the forecasts' errors in many cases suggest an important effect of the relative vorticity in comparison to the coriolis parameter. This effect, it will be recalled, was omitted from the thermotropic equations and may partially explain the observed tendency of the equations to over-develop anticyclonic disturbances and to underdevelop cyclonic disturbances; in the atmosphere, there is observed, of course, an asymetrical development of these disturbances, whereby the cyclone experiences the greater amplitude change. This effect, together with the systematic truncation errors introduced by the use of spatial finite-differences, may account for the underforecasts of the speed of many disturbances. In some cases there appears to be an appreciable error, especially in the 1000 mb forecasts, due to an inadequate representation of low-level temperature gradients by the 500-1000 mb thickness pattern; these errors may also be due to the neglect of the so-called "twisting" terms and to the neglect of the effects of the vertical advection of vorticity, which will be most serious in regions of strong vertical motion.

From the present tests of the barotropic and thermotropic models, one cannot, of course, expect a complete documentation of all of the vorticity generation and transport effects operating in the atmosphere. It is felt that the present tests have shown, however, that even these relatively simple models are capable of accounting for a large portion of the observed behavior of the large-scale atmospheric disturbances, and that in areas free of the more obvious sources of error, perform at a level comparable with if not slightly in excess of that achieved by the conventional synoptic forecast techniques.

Much further research remains to be performed in order to gain a clearer understanding of the behavior of large-scale atmospheric disturbances; research is in progress at the present time to investigate more fully the effects of the imposed boundary conditions, the effects of mountainous terrain, and the effects of the use of finite-differences, as the first stages of a program to isolate and study the specific effects of the various physical processes themselves. At their present stage of development, however, the present techniques of numerical prediction are felt to be suitable for operational application from the standpoints of feasibility, economy, and overall reliability.

REFERENCES

1. Thompson, P. D. and Gates, W. L., " A test of numerical prediction methods based on the barotropic and two-parameter baroclinic models." To be published in Journal of Meteorology (1956).

2. Eliassen, A., "Simplified models of the atmosphere, designed for the purpose of numerical weather prediction." Tellus 4, 145-157 (1952).

3. Eady, E. T., "Note on weather computing and the so-called 2 1/2 - dimensional model." Tellus 4, 157-168 (1952).

4. Thompson, P. D., "On the theory of large-scale disturbances in a two-dimensional baroclinic equivalent of the atmosphere," Quarterly Journal of the Royal Meteorological Society 79, 51-69 (1953).

5. Charney, J. G. and Phillips, N. A., "Numerical integration of the quasi-geostrophic equations for barotropic and simple baroclinic flows." Journal of Meteorology 10, 71-99 (1953).

6. Sawyer, J. S. and Bushby, F. H., "A baroclinic model atmosphere suitable for numerical integration." Journal of Meteorology 10, 54-59 (1953).

7. Frankel, S. P., "Convergence rates of iterative treatments of partial differential equations." Mathematical Tables and other Aids to Computation 4, 65-75 (1950).

8. Charney, J. G., Fjörtoft, R. and von Neumann, J., "Numerical integration of the barotropic vorticity equation." Tellus 2, 237-254 (1950).

9. Charney, J. G., "Numerical prediction of cyclogenesis." Proceedings of the National Academy of Sciences 40, 99-110 (1954).

10. Lonnqvist, O., "The comparison between numerical methods and methods now in use for forecasting meteorological charts." Tellus 4, 195-200 (1952).

11. Staff members, Institute of Meteorology, University of Stockholm, "Results of forecasting with the barotropic model on an electronic computer (BESK)." Tellus 6, 139-149 (1954).

12. Bushby, F. H. and Hinds, M. K., "The computation of forecast charts by application of the Sawyer-Bushby two-parameter model." Quarterly Journal of the Royal Meteorological Society 80, 165-173 (1954).

13. Smith, K. E., "The weather and circulation of January, 1953." Monthly Weather Review 81, 16-19 (1953).

14. Gates, W. L., "A method of numerical forecasting by juxtaposition of one-dimensional solutions and its application to the equivalent barotropic model." Journal of Meteorology 10, 149-159 (1953).

15. Sutcliffe, R. C. and Forsdyke, A. G., "The theory and use of upper-air thickness patterns in forecasting." Quarterly Journal of the Royal Meteorological Society 76, 189-217 (1950).

16. George, C. A., "Thermal thickness patterns and tropical storms." Indian Journal of Meteorology and Physics 4, 279-290 (1953).

17. Owens, J. C., "Discussion on 'progging' the surface and 500-mb levels in the United States." U. S. Weather Bureau, Cleveland, Ohio (1953).

APPENDIX

On the following pages are presented the 24-hour numerical forecasts prepared from the thermotropic and barotropic models from each 1500 G.C.T. synoptic chart for 1 January through 31 January 1953, a total of 30 cases. Each day's forecasts are presented in a series of eight maps on two pages arranged as follows.

On the first page of each forecast:

upper left - the observed initial 500 mb map (initial conditions).

upper right - the observed final 500 mb map (verification).

lower left - the 24-hour barotropic 500 mb forecast.

lower right - the 24-hour thermotropic 500 mb forecast.

On the second page of each forecast:

upper left - the observed initial 1000 mb map (initial conditions).

upper right - the observed final 1000 mb map (verification).

lower left - the vertical velocity computed from the thermotropic model at the time of the initial map.

lower right - the 24-hour thermotropic 1000 mb forecast.

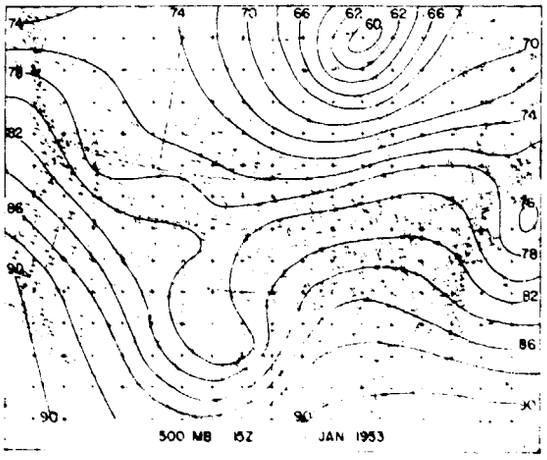
500 MB 15Z JAN 1953

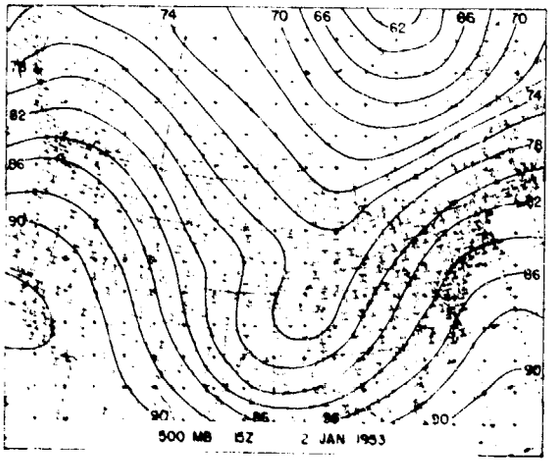
500 MB 15Z 2 JAN 1953

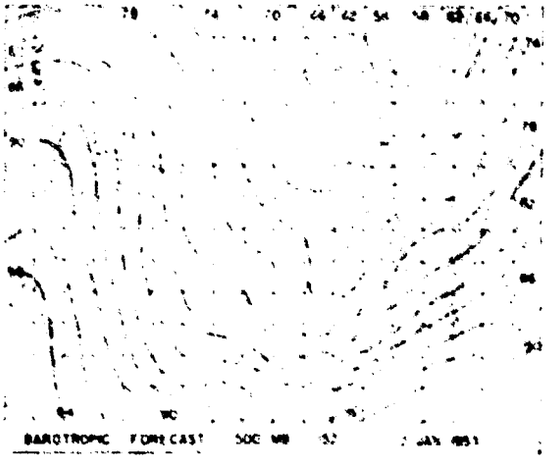
BAROTROPIC FORECAST

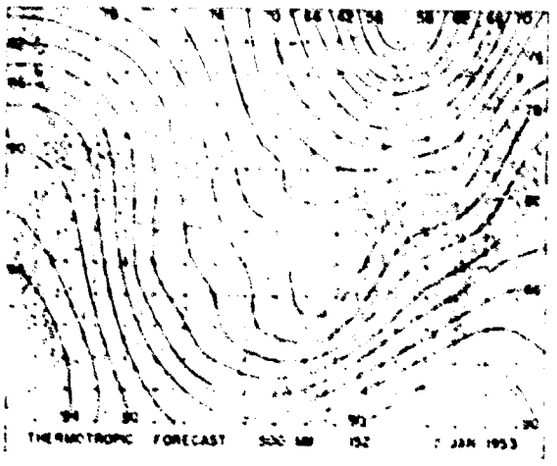
THERMOTROPIC FORECAST

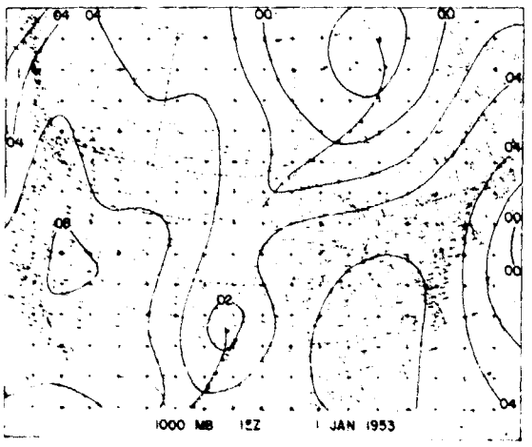
1000 MB 12Z 1 JAN 1953

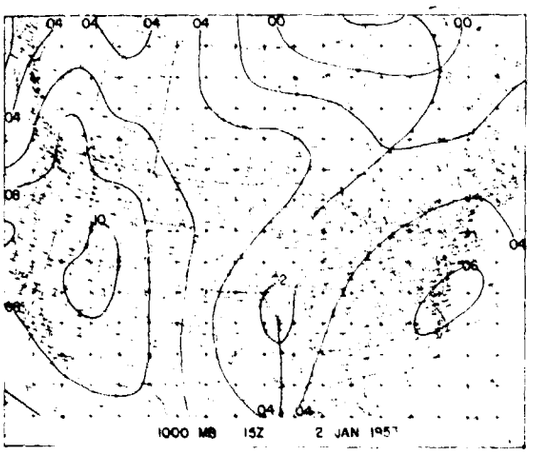
1000 MB 15Z 2 JAN 1953

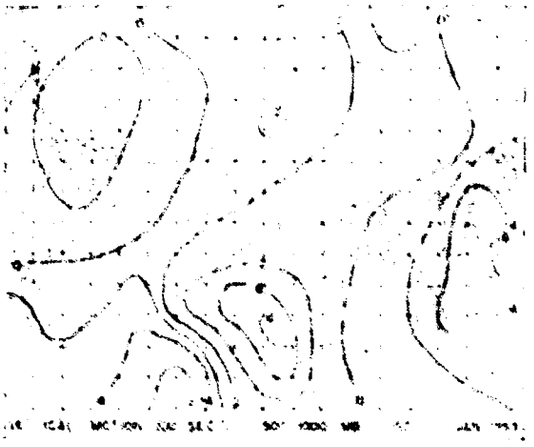

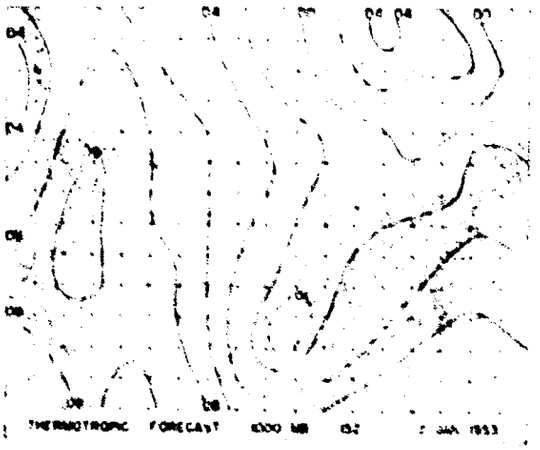
THERMOTROPIC FORECAST 1000 MB 00Z 2 JAN 1953

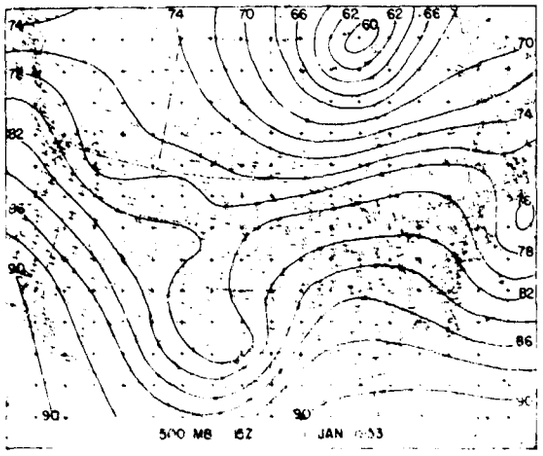
74
70
66
62
60
62
66
70
74
78
82
86
90
500 MB 15Z JAN 1953

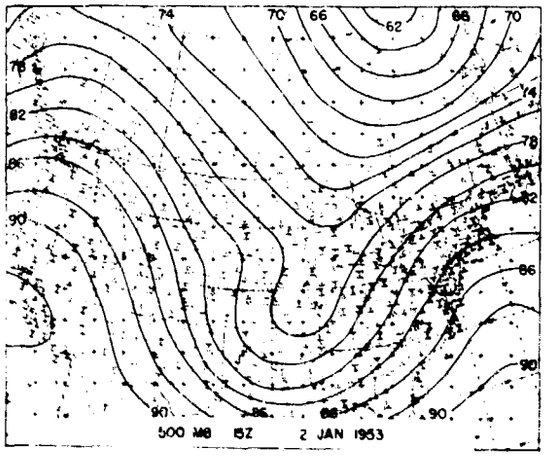
74
70
66
62
66
70
74
78
82
86
90
500 MB 15Z 2 JAN 1953

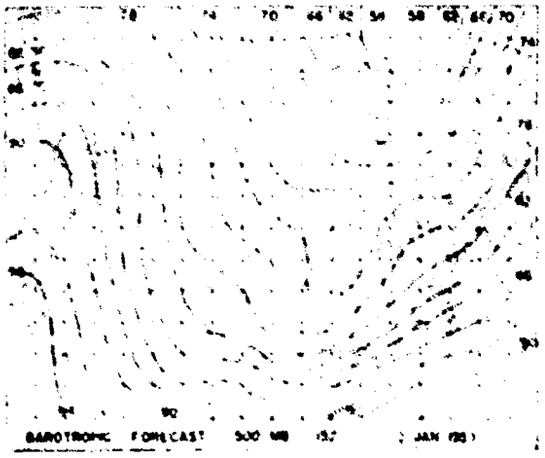
BAROTROPIC FORECAST 500 MB 15Z JAN 1953

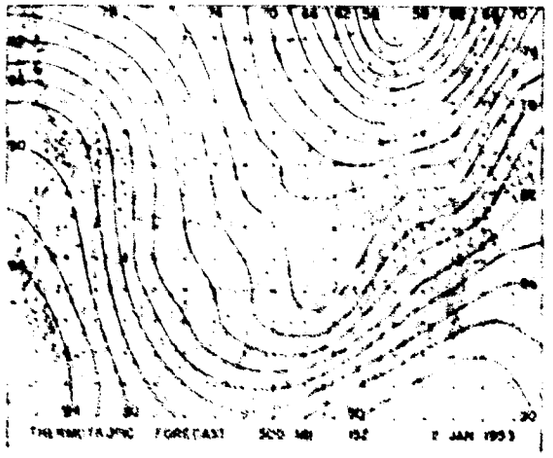
THERMOTROPIC FORECAST 500 MB 15Z 2 JAN 1953

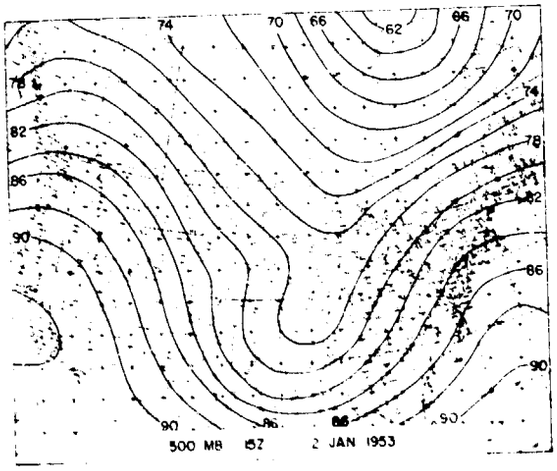
500 MB 15Z 2 JAN 1953

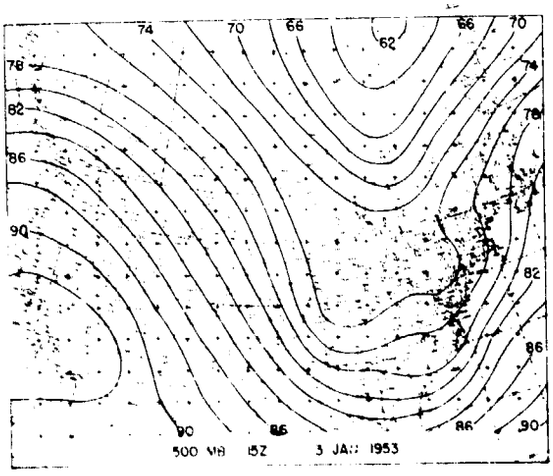
500 MB 15Z 3 JAN 1953

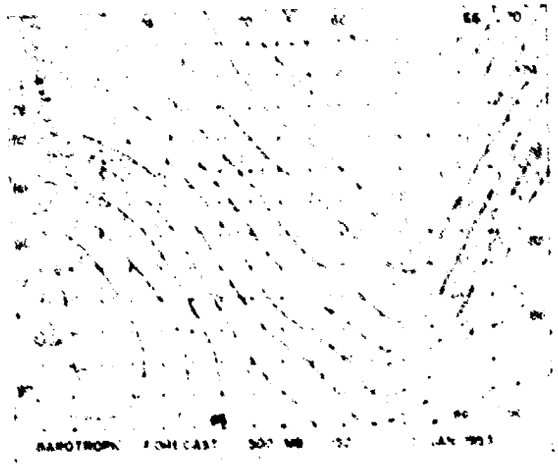

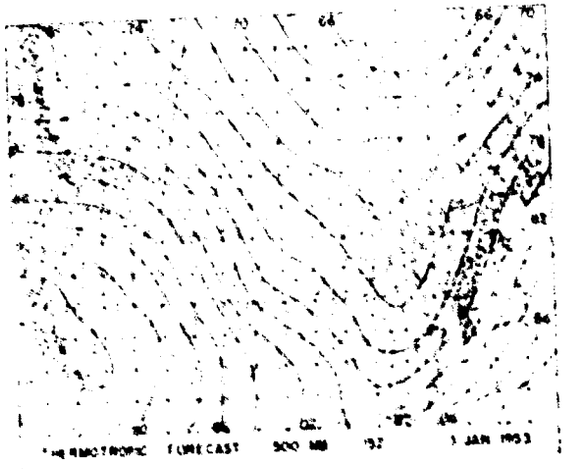

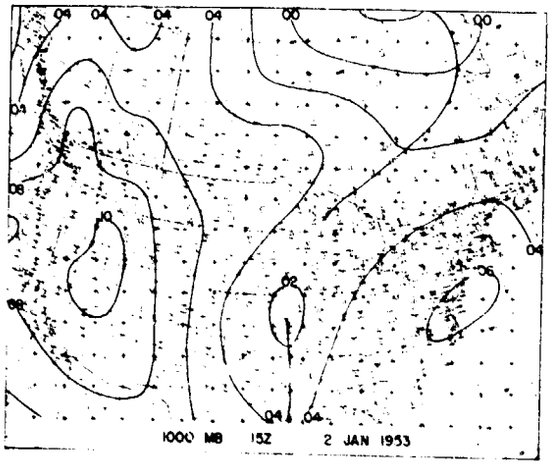
1000 MB 15Z 2 JAN 1953

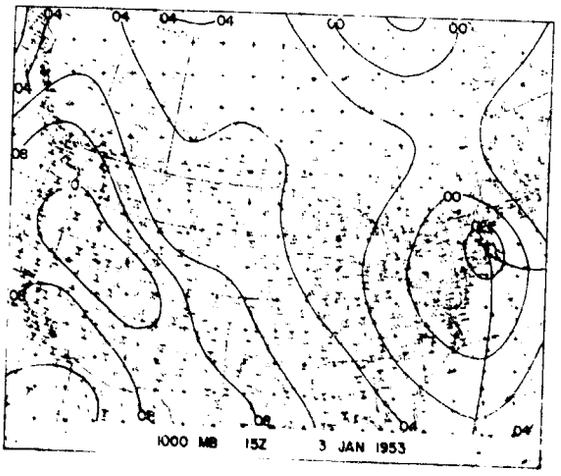
1000 MB 15Z 3 JAN 1953

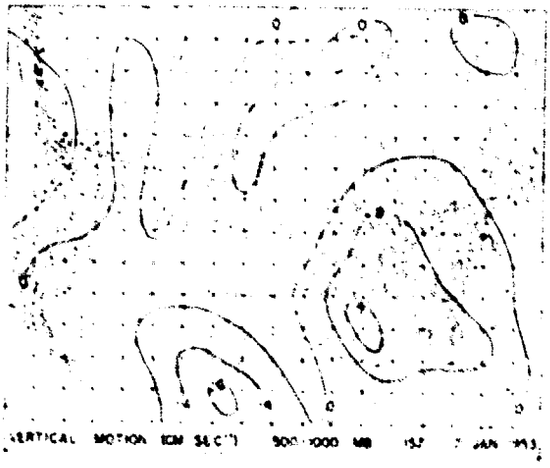

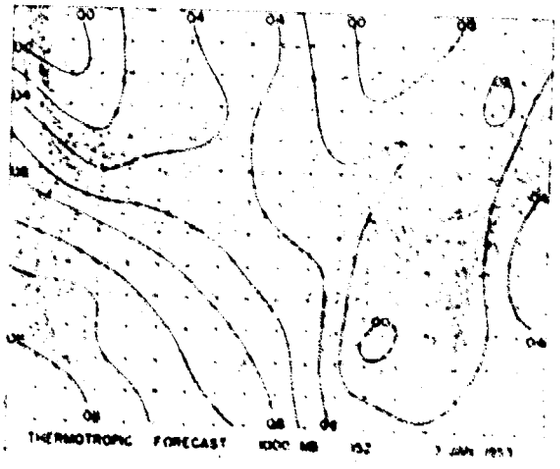
THERMOTROPIC FORECAST

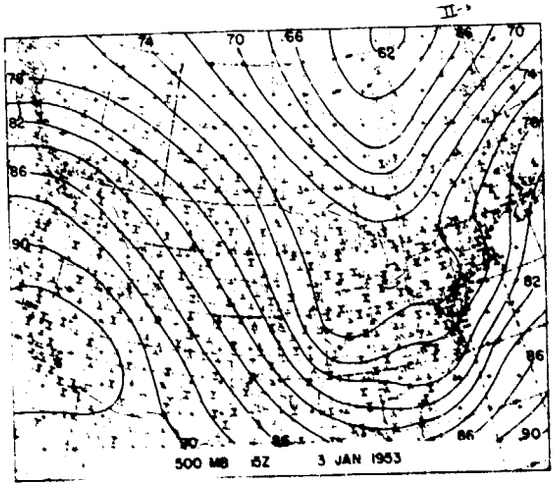
500 MB 15Z 3 JAN 1953

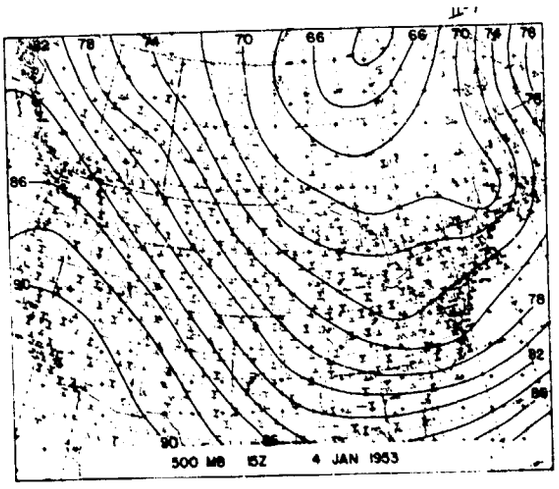
500 MB 15Z 4 JAN 1953

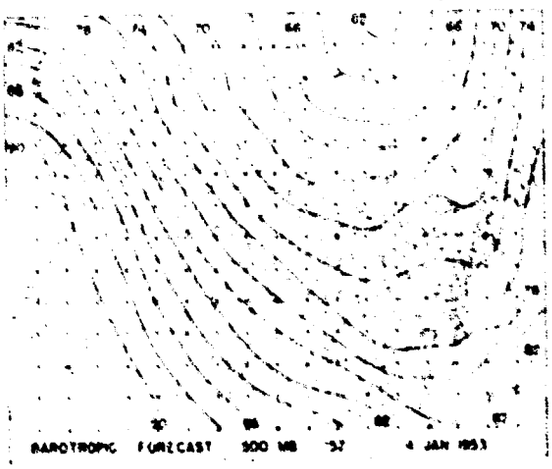
BAROTROPIC FORECAST 500 MB 4 JAN 1953

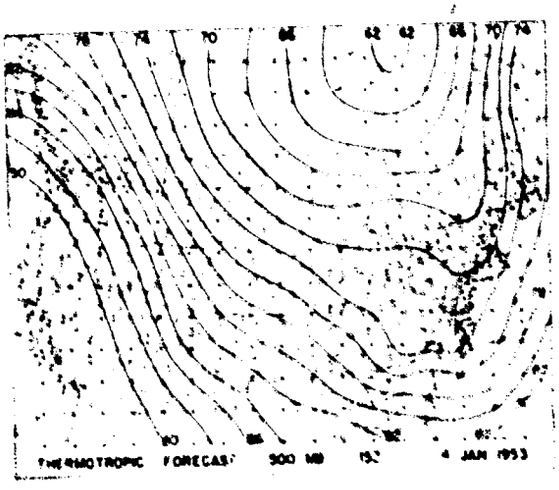
THERMOTROPIC FORECAST 500 MB 4 JAN 1953

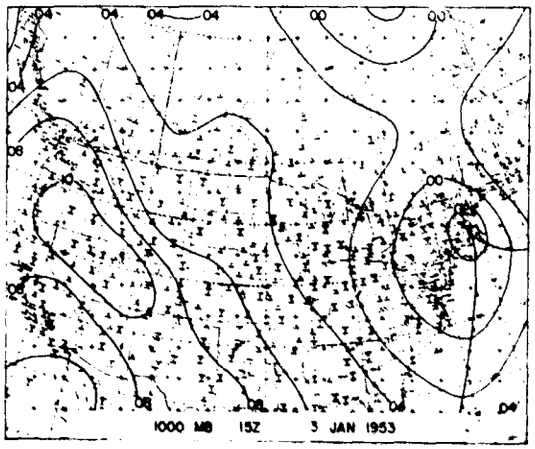
1000 MB 15Z 3 JAN 1953

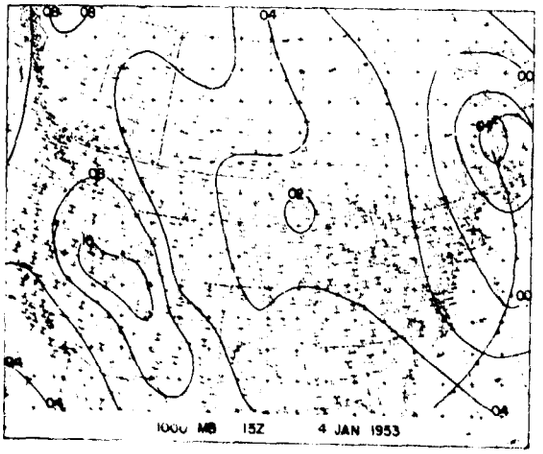
1000 MB 15Z 4 JAN 1953

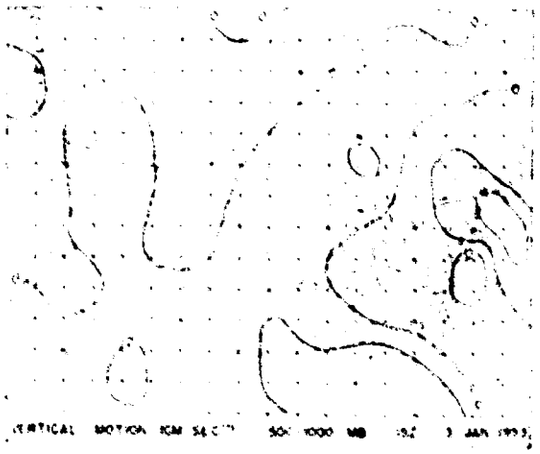

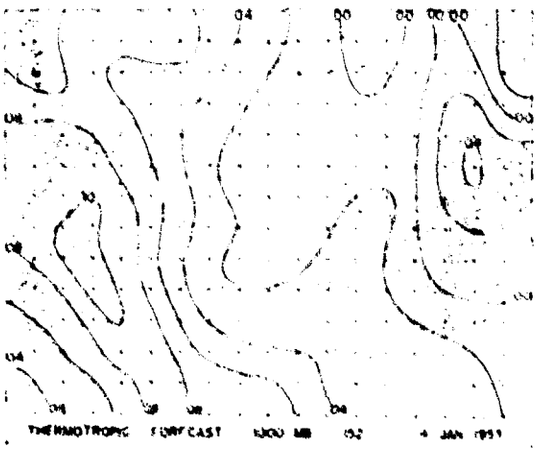

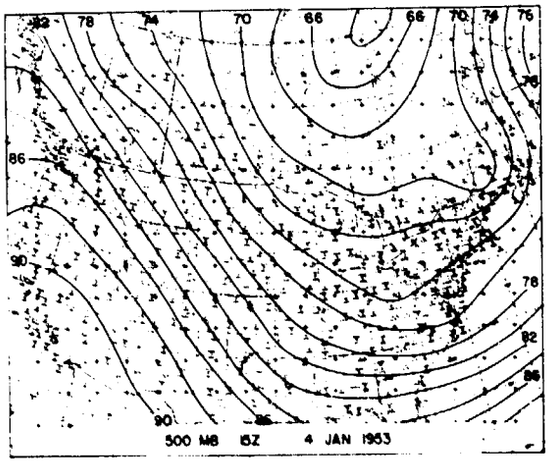
500 MB 15Z 4 JAN 1953

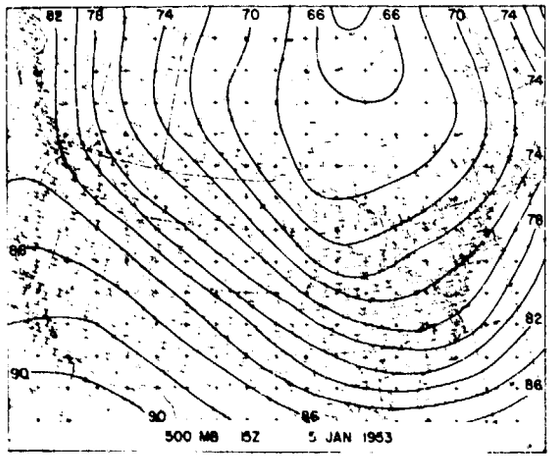
500 MB 15Z 5 JAN 1953

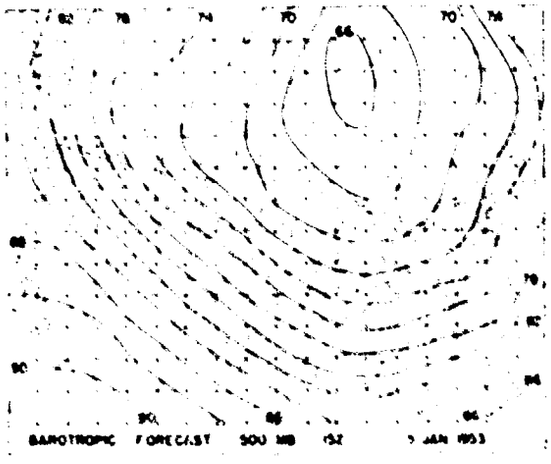
BAROTROPIC FORECAST 500 MB 15Z 5 JAN 1953

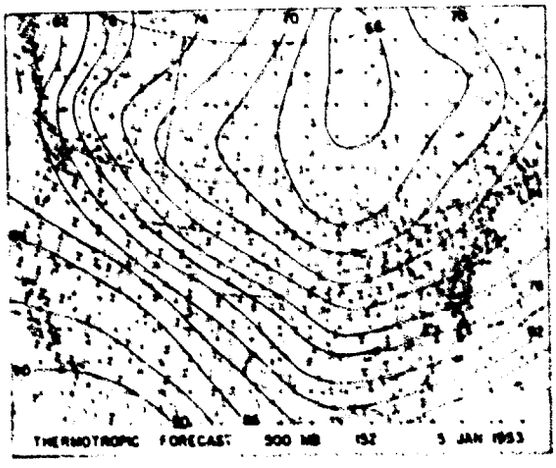
THERMOTROPIC FORECAST 500 MB 15Z 5 JAN 1953

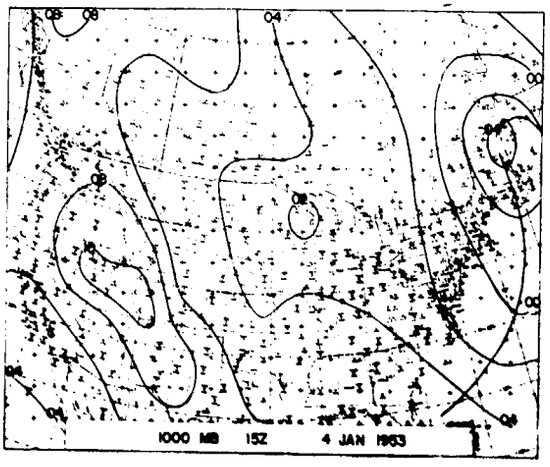
1000 MB 15Z 4 JAN 1953

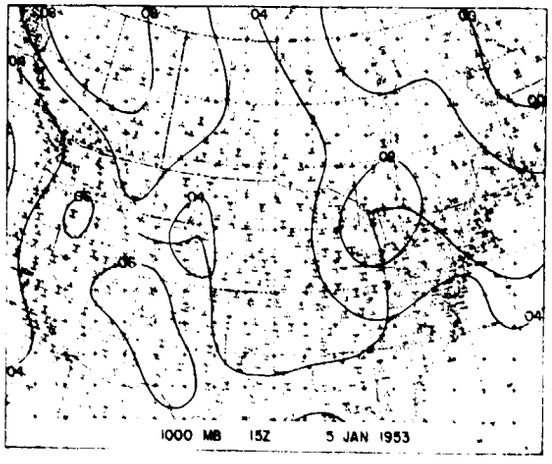
1000 MB 15Z 5 JAN 1953

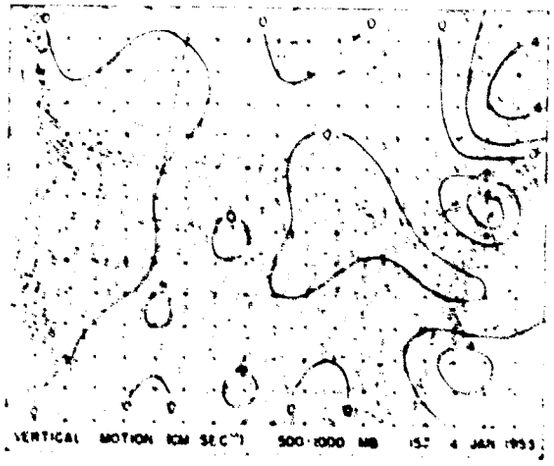
VERTICAL MOTION (CM SEC⁻¹) 500-1000 MB 15Z 4 JAN 1953

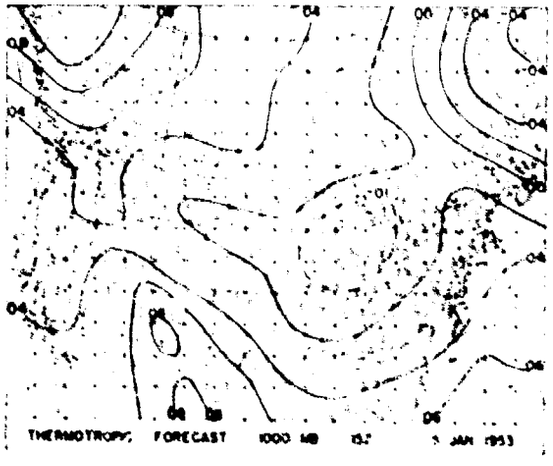
THERMOTROPY; FORECAST 1000 MB 15Z 5 JAN 1953

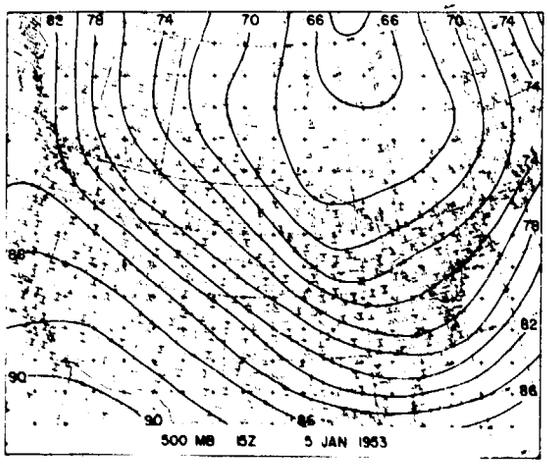
500 MB 15Z 5 JAN 1953

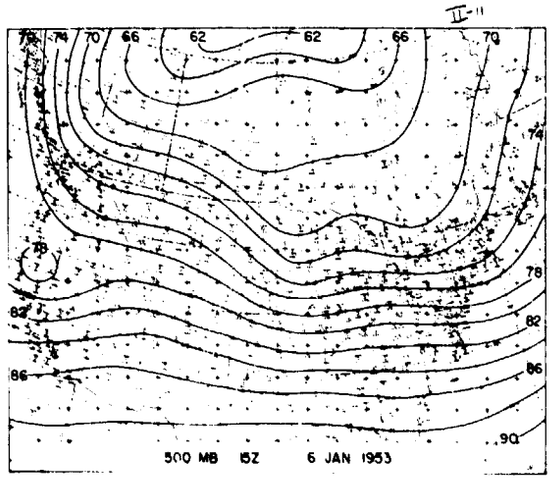
500 MB 15Z 6 JAN 1953

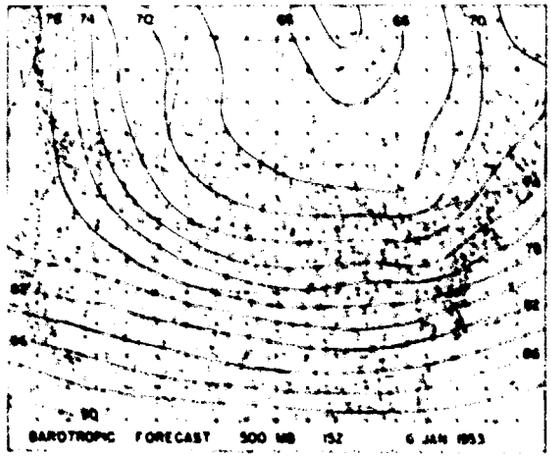
BAROTROPIC FORECAST 500 MB 15Z 6 JAN 1953

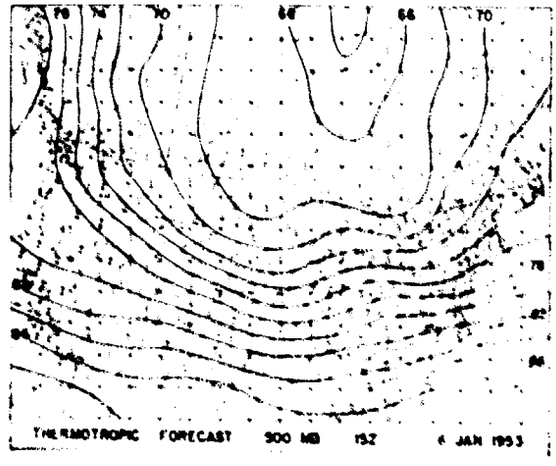
THERMOTROPIC FORECAST 500 MB 15Z 6 JAN 1953

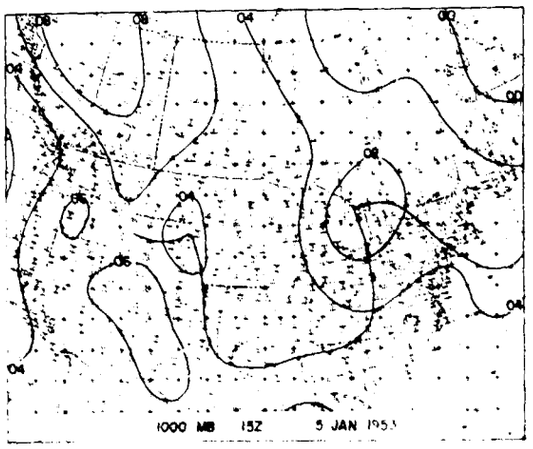
1000 MB 15Z 5 JAN 1953

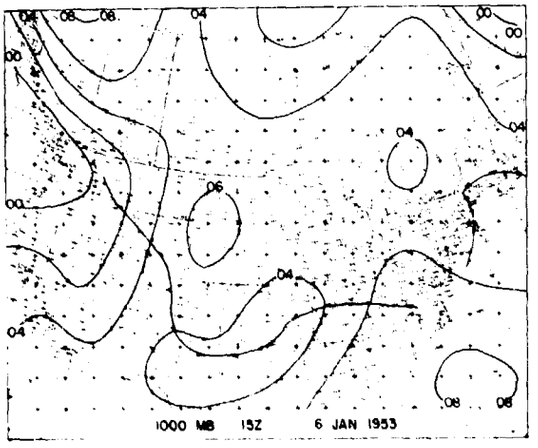
1000 MB 15Z 6 JAN 1953

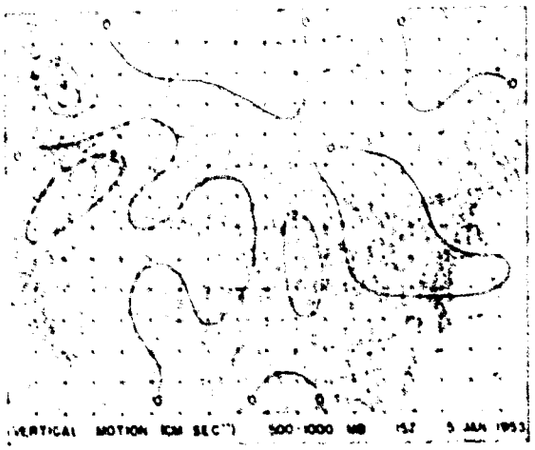
VERTICAL MOTION (CM SEC⁻¹) 500-1000 MB 15Z 5 JAN 1953

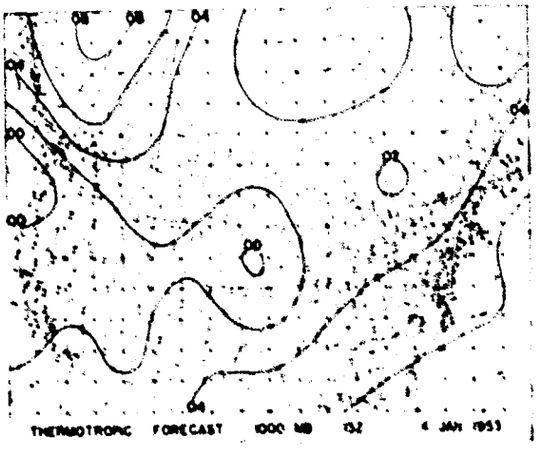
THERMOTROPIC FORECAST 1000 MB 15Z 6 JAN 1953

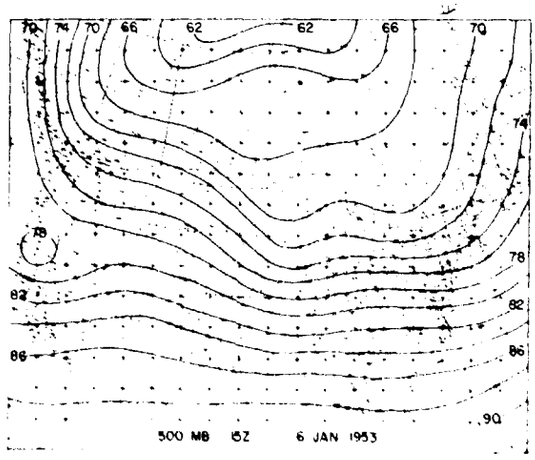
500 MB 15Z 6 JAN 1953

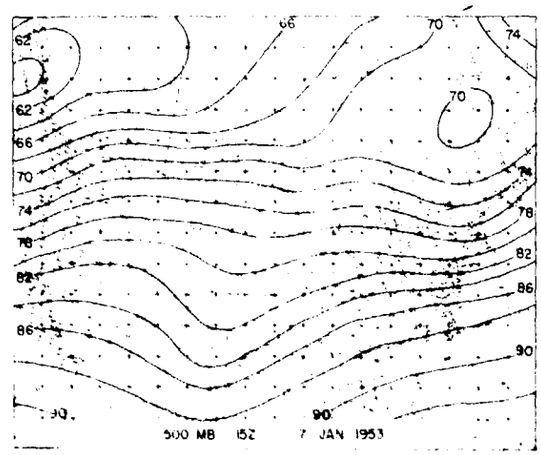
500 MB 15Z 7 JAN 1953

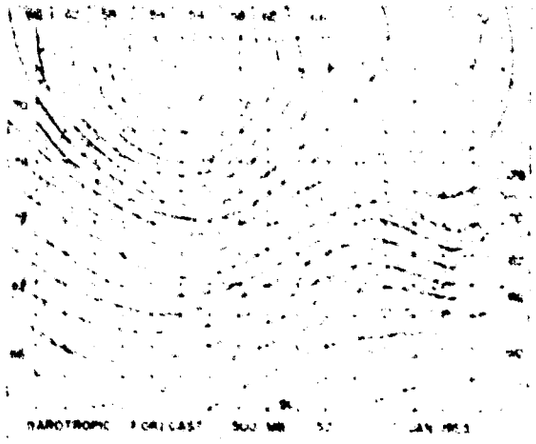

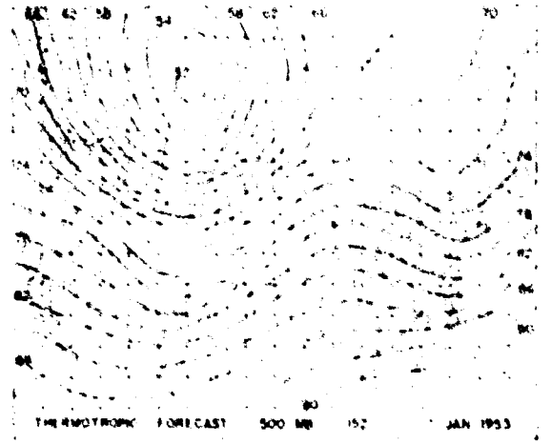

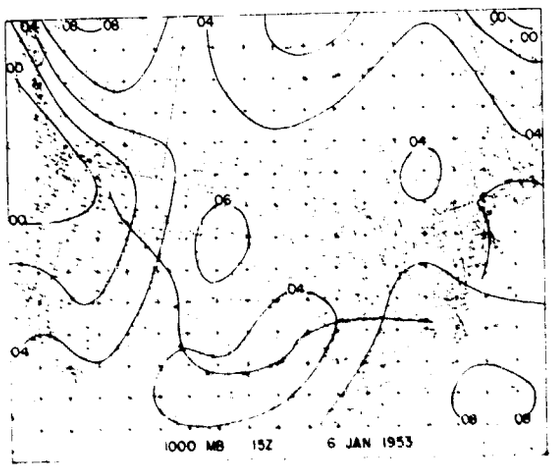
1000 MB 15Z 6 JAN 1953

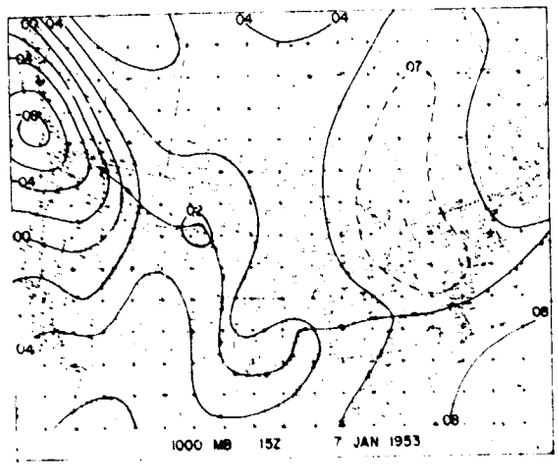
1000 MB 15Z 7 JAN 1953

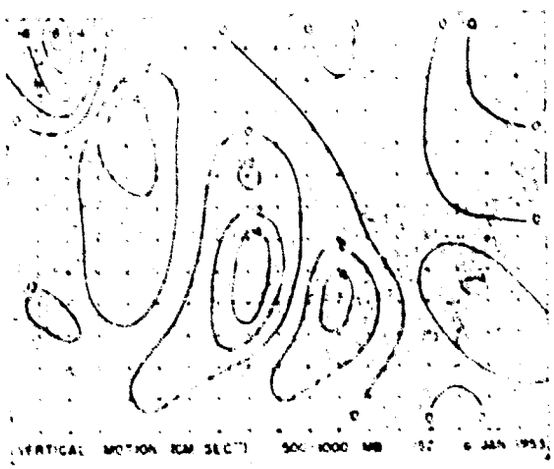

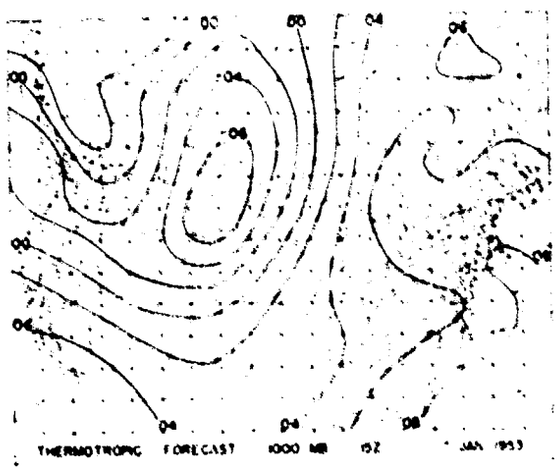
THERMOTROPIC FORECAST 1000 MB 15Z

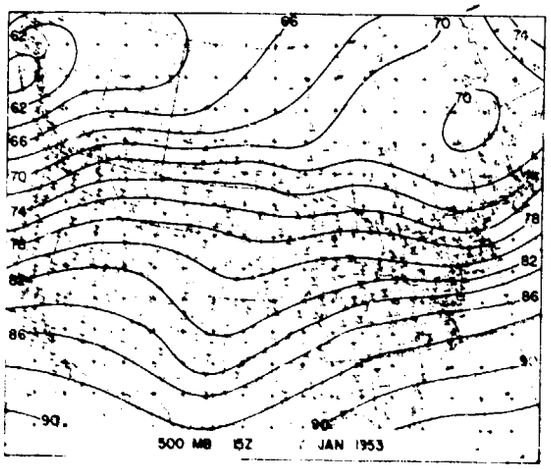
500 MB 15Z JAN 1953

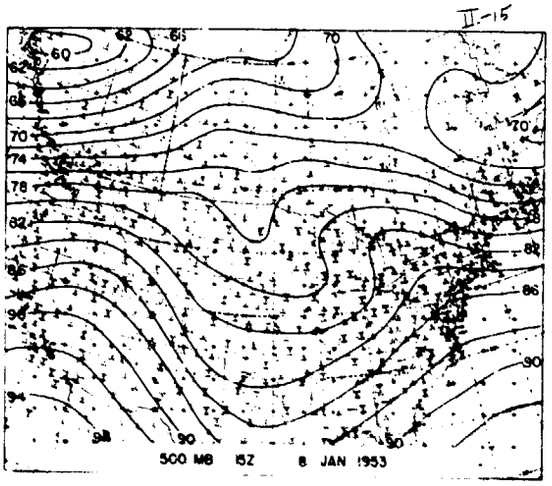
500 MB 15Z 8 JAN 1953

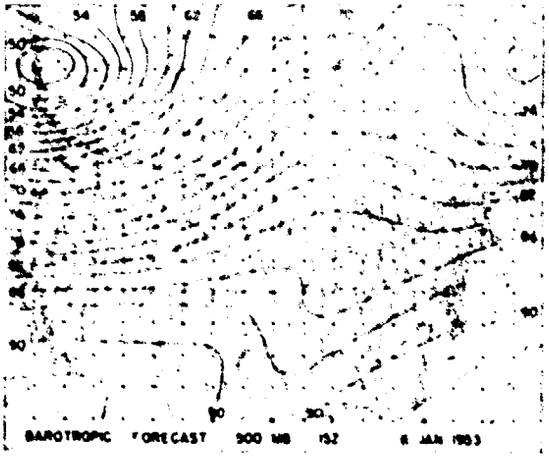
BAROTROPIC FORECAST 500 MB 15Z 8 JAN 1953

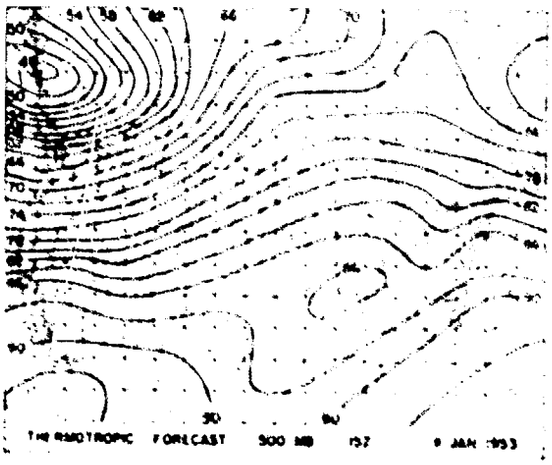
BAROTROPIC FORECAST 500 MB 15Z 8 JAN 1953

II-17

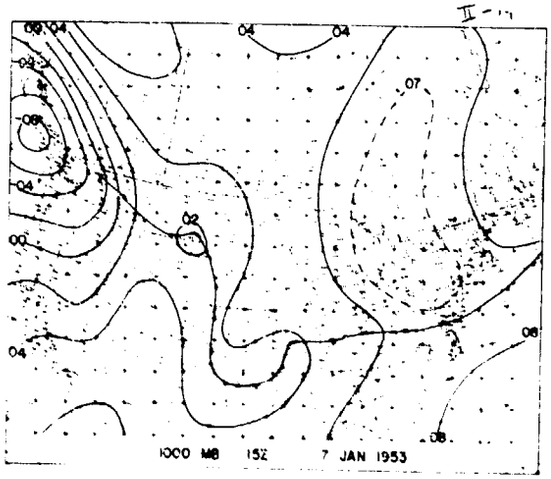
1000 MB 15Z 7 JAN 1953

II-16

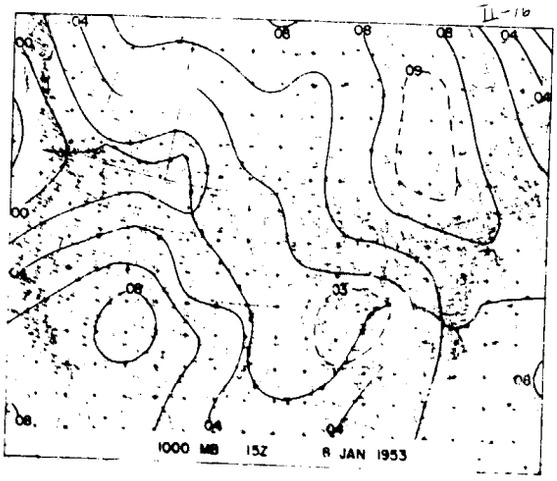
1000 MB 15Z 8 JAN 1953

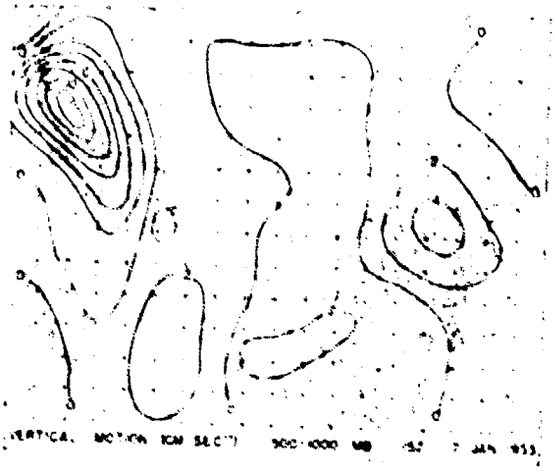

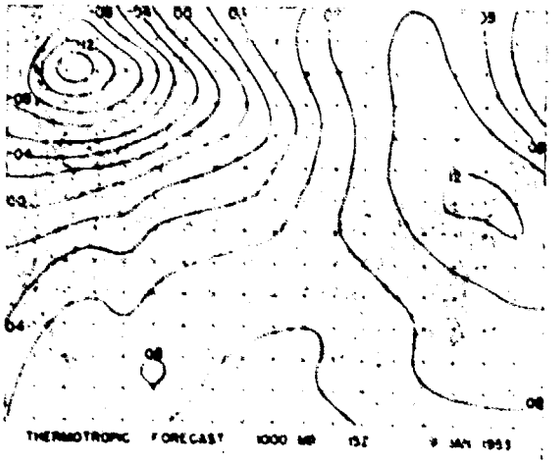
THERMOTROPIC FORECAST 1000 MB 15Z

II-15

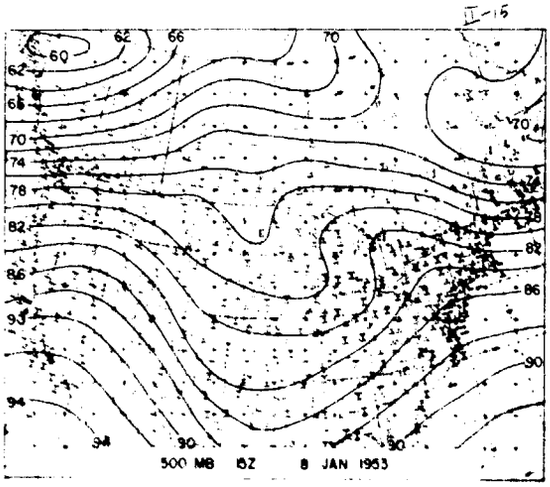

II-17

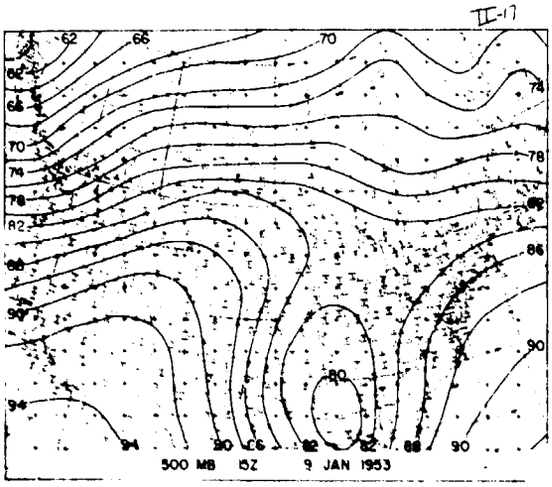

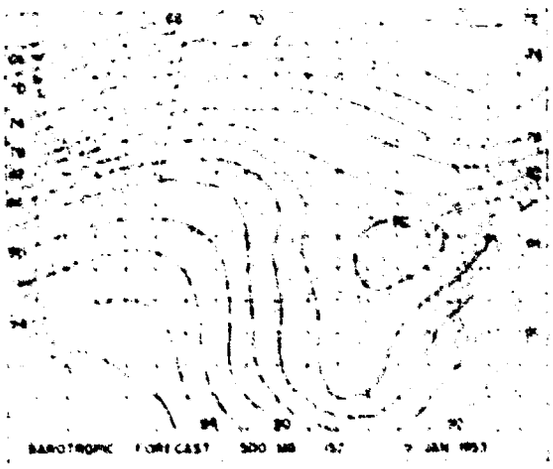

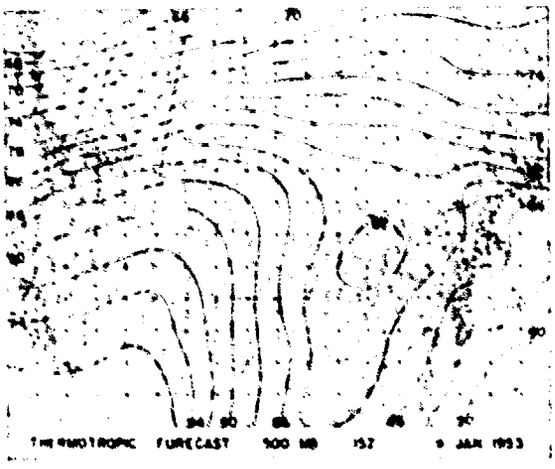

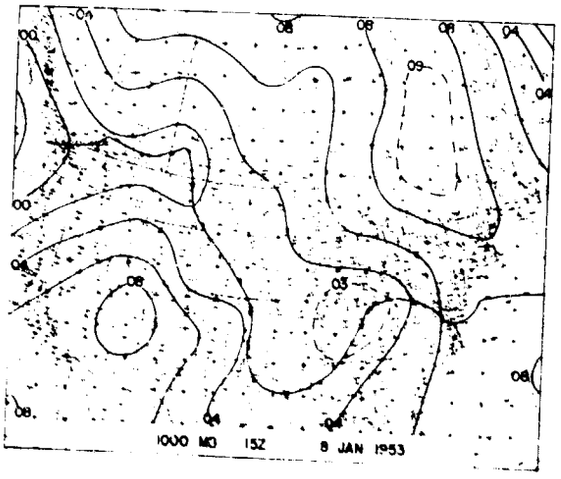
1000 MB 15Z 8 JAN 1953

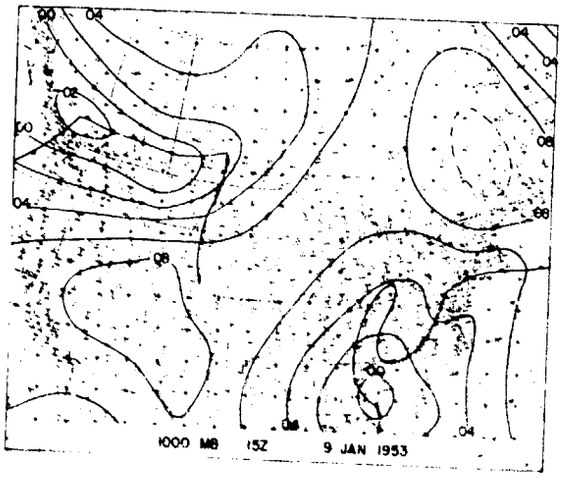
1000 MB 15Z 9 JAN 1953

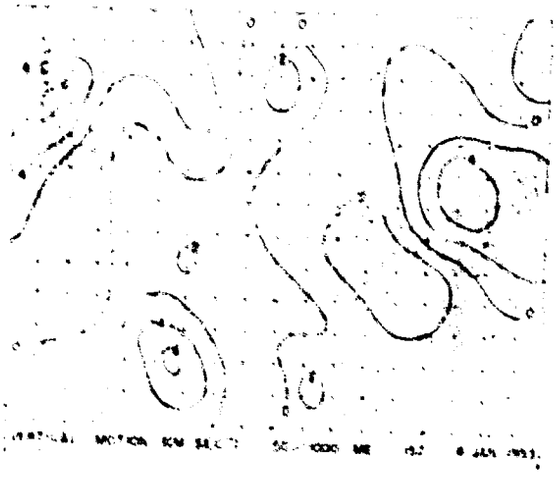

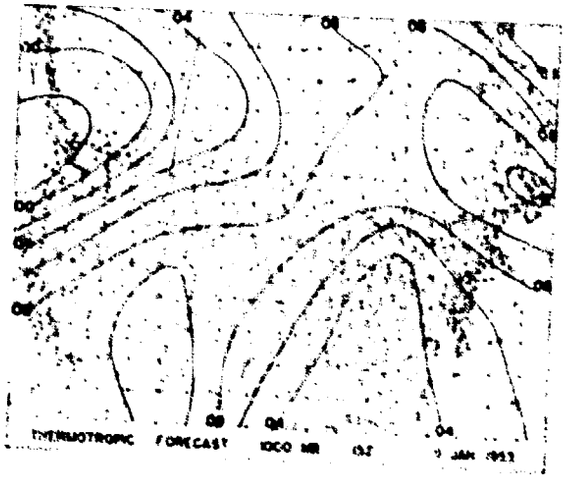
BAROTROPIC FORECAST 1000 MB 15Z

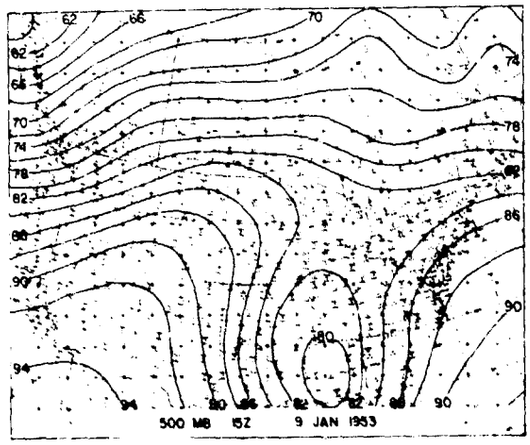
500 MB 15Z 9 JAN 1953

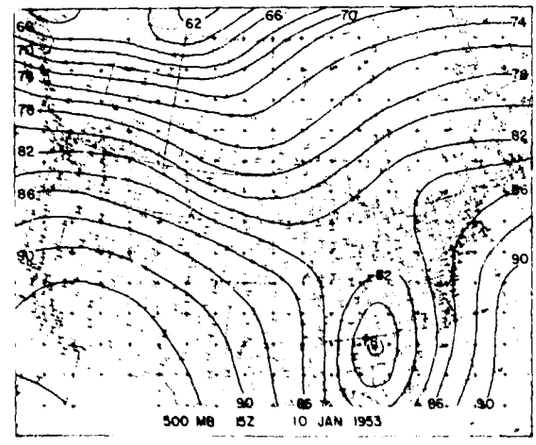
500 MB 15Z 10 JAN 1953

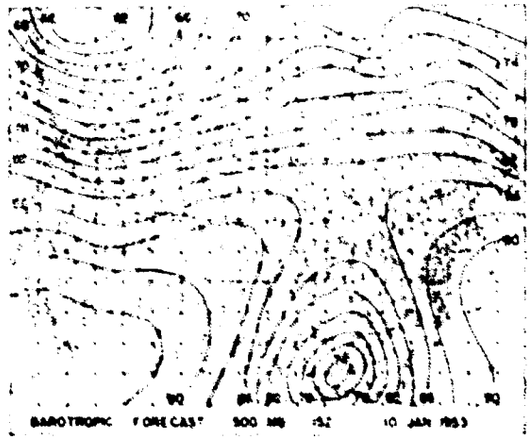
BAROTROPIC FORECAST 500 MB 15Z 10 JAN 1953

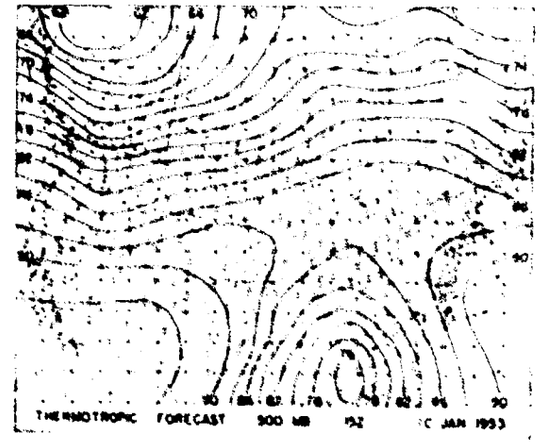
THERMOTROPIC FORECAST 500 MB 15Z

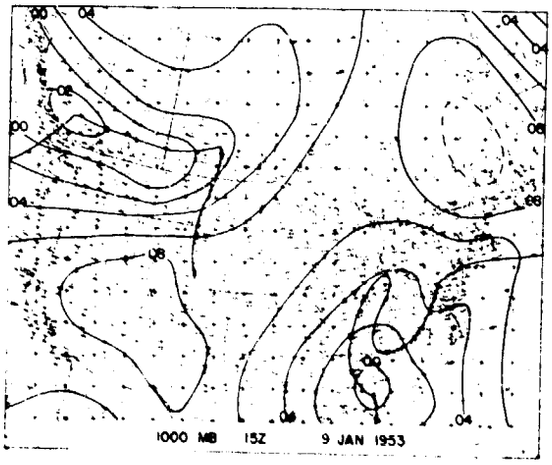
1000 MB 15Z 9 JAN 1953

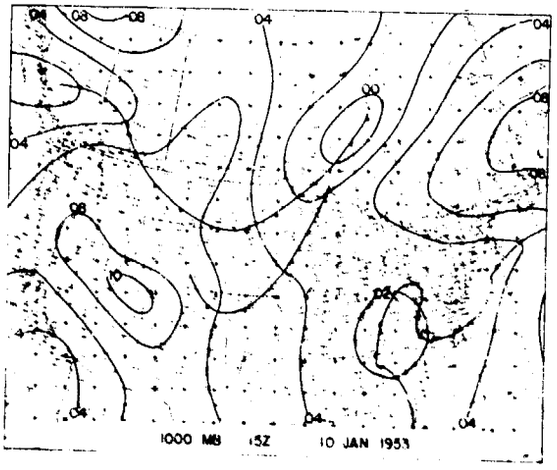
1000 MB 15Z 10 JAN 1953

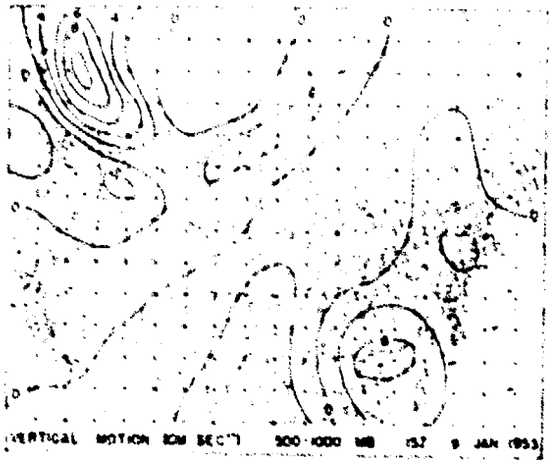
VERTICAL MOTION (CM SEC⁻¹) 500-1000 MB 15Z 9 JAN 1953

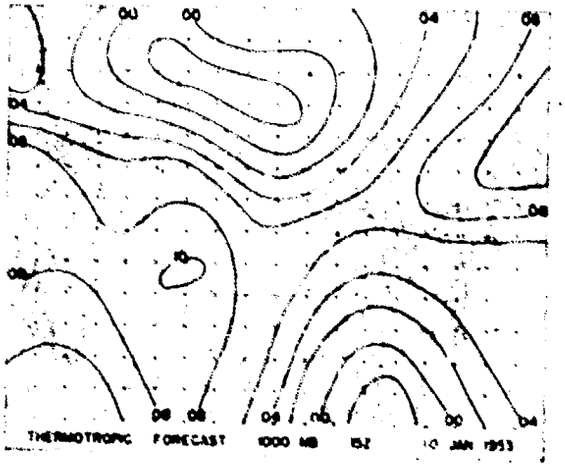
THERMOTROPIC FORECAST 1000 MB 15Z 10 JAN 1953

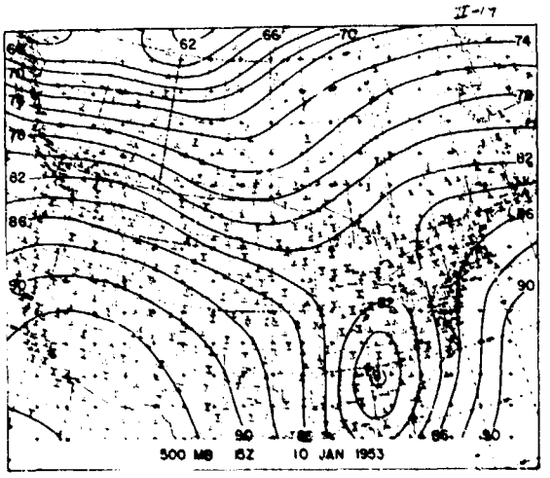
500 MB 15Z 10 JAN 1953

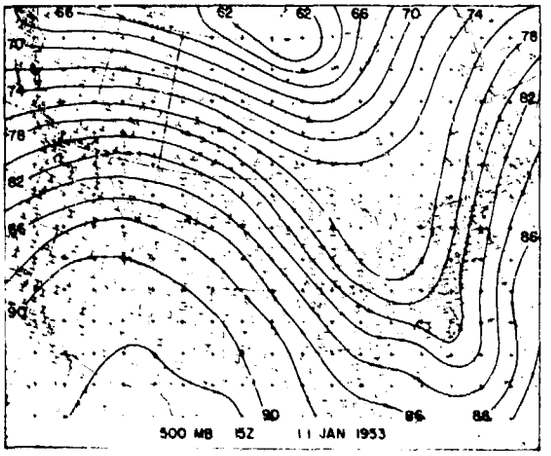
500 MB 15Z 11 JAN 1953

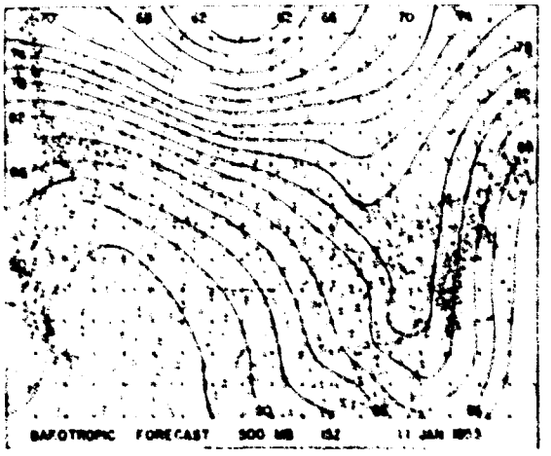
BAROTROPIC FORECAST 500 MB 15Z 11 JAN 1953

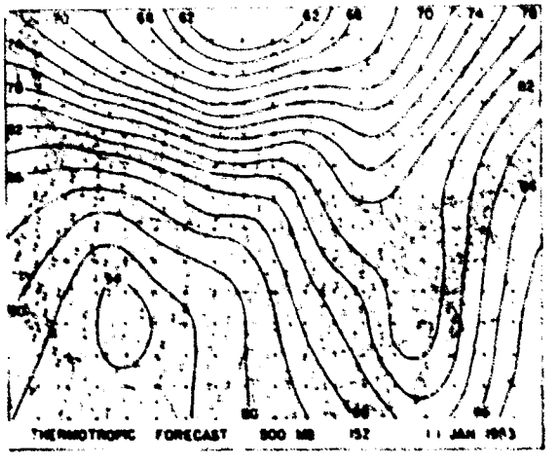
THERMOTROPIC FORECAST 500 MB 15Z 11 JAN 1953

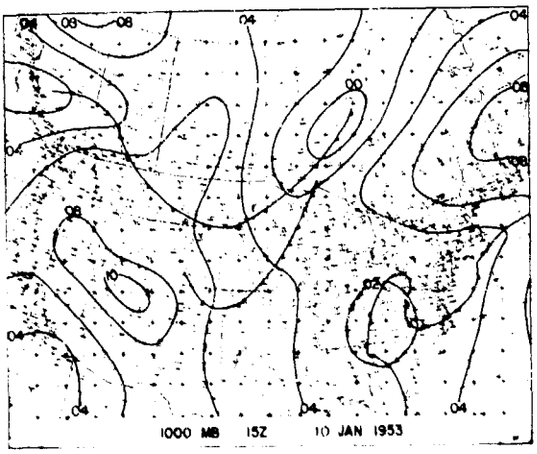
1000 MB 15Z 10 JAN 1953

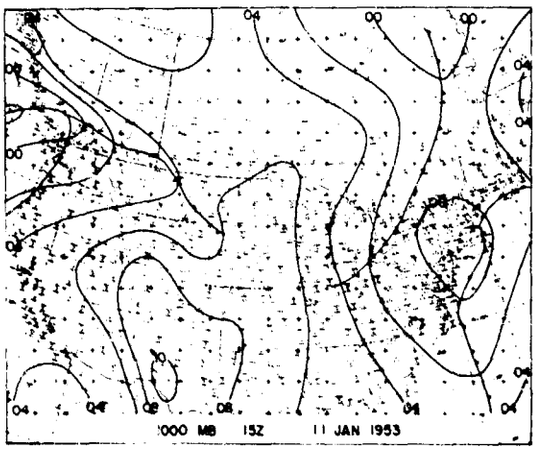
1000 MB 15Z 11 JAN 1953

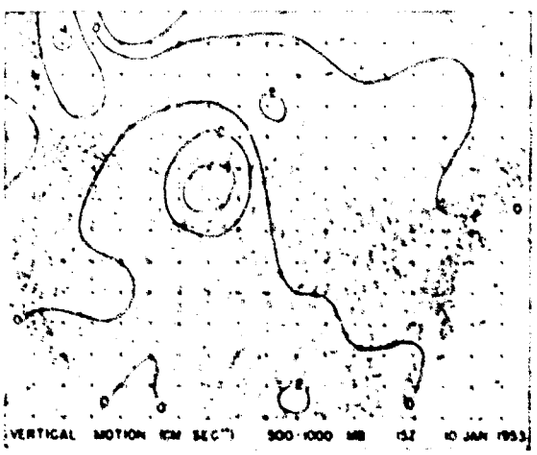
VERTICAL MOTION (CM SEC⁻¹) 500-1000 MB 15Z 10 JAN 1953

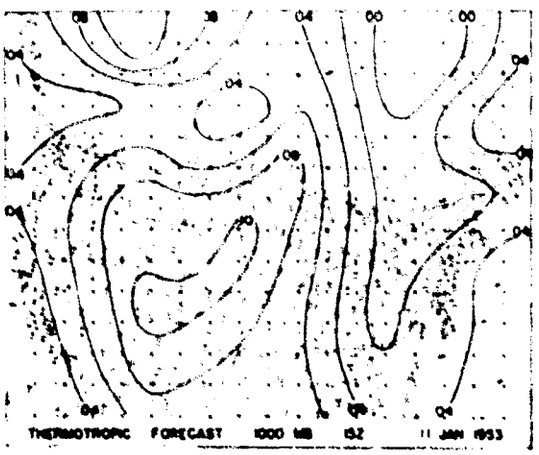
THERMOTROPIC FORECAST 1000 MB 15Z 11 JAN 1953

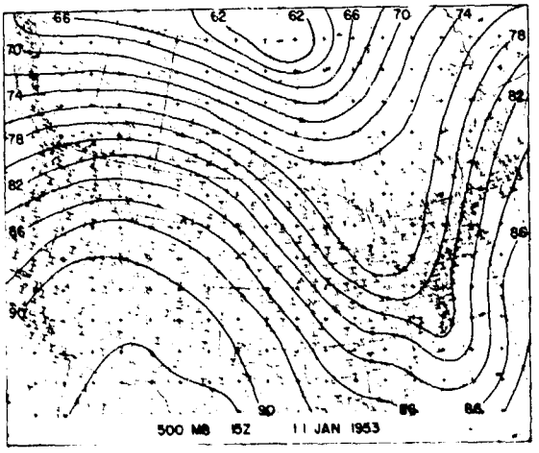
500 MB 15Z 11 JAN 1953

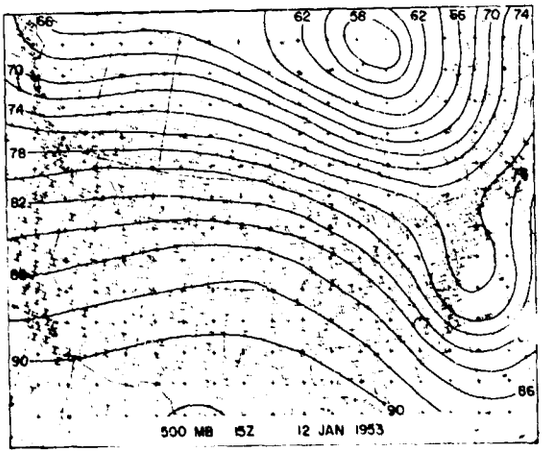
500 MB 15Z 12 JAN 1953

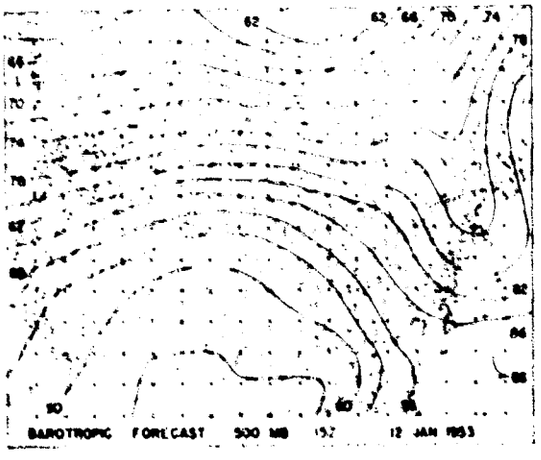
BAROTROPIC FORECAST 500 MB 15Z 12 JAN 1953

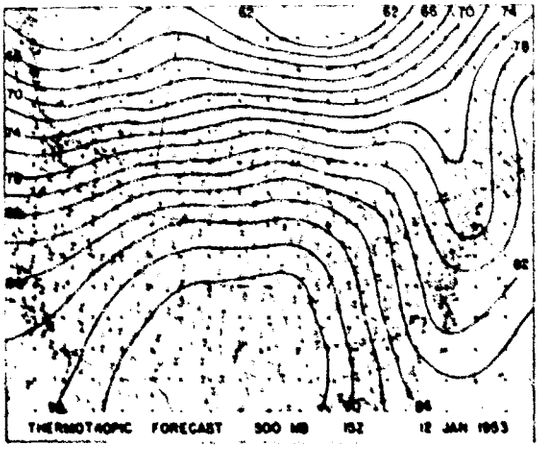
THERMOTROPIC FORECAST 500 MB 15Z 12 JAN 1953

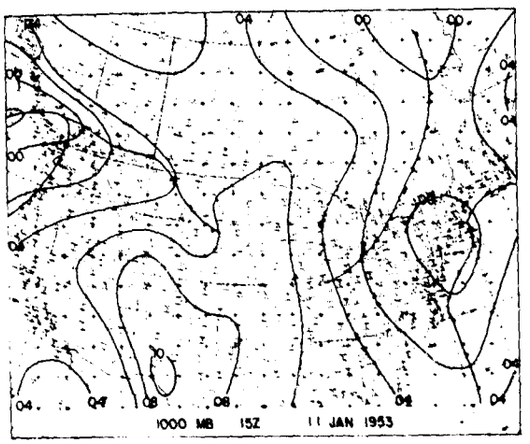
1000 MB 15Z 11 JAN 1953

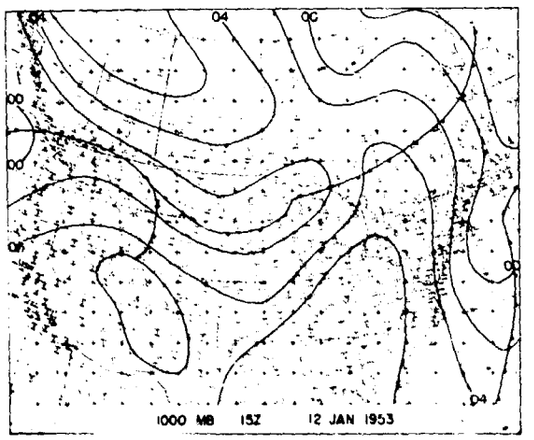
1000 MB 15Z 12 JAN 1953

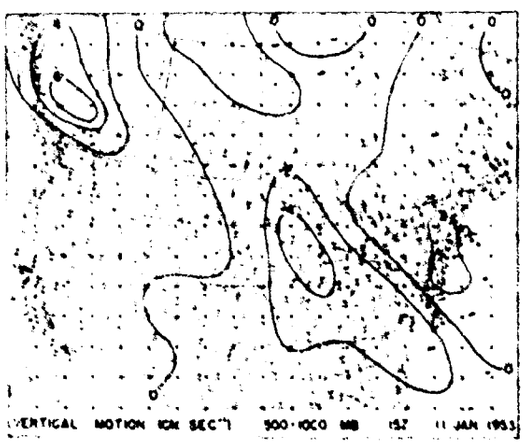
VERTICAL MOTION (CM SEC⁻¹) 500-1000 MB 15Z 11 JAN 1953

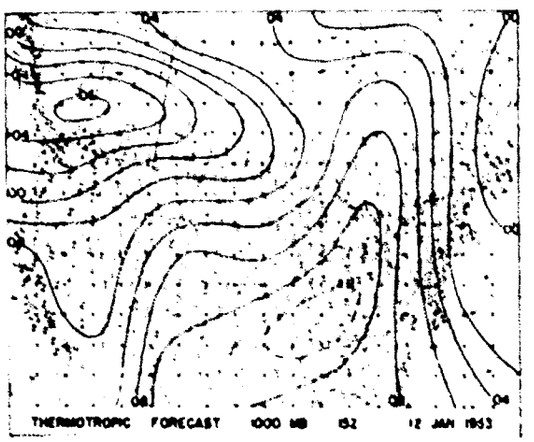
THERMOTROPIC FORECAST 1000 MB 15Z 12 JAN 1953

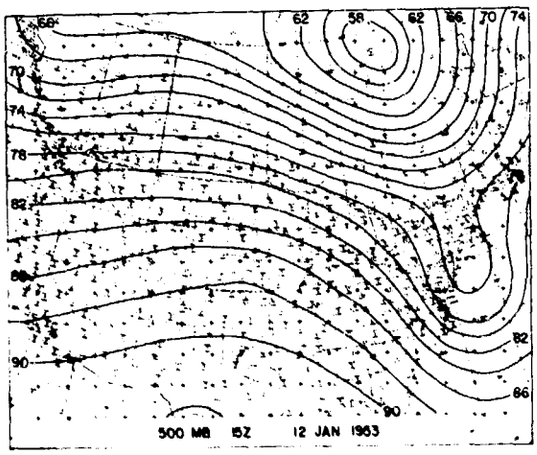
500 MB 15Z 12 JAN 1953

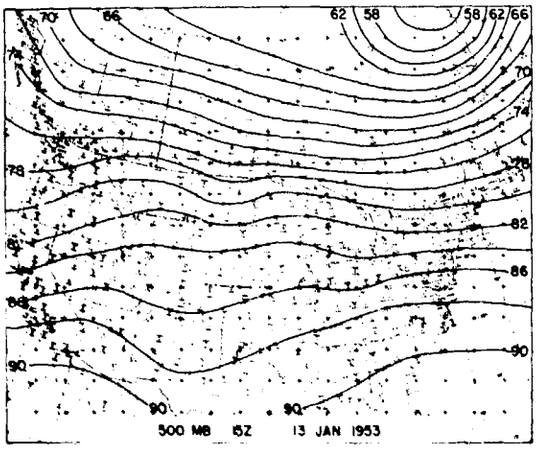
500 MB 15Z 13 JAN 1953

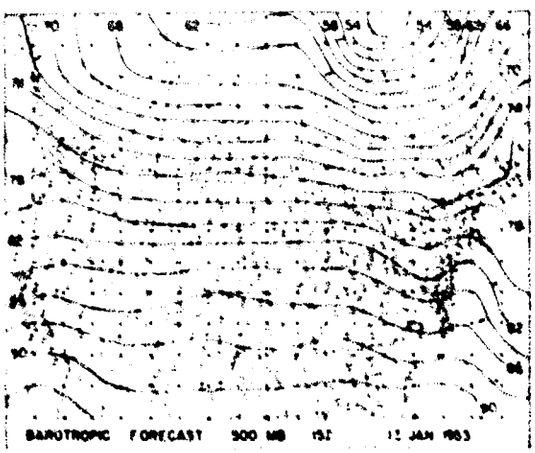
BAROTROPIC FORECAST 500 MB 15Z 13 JAN 1953

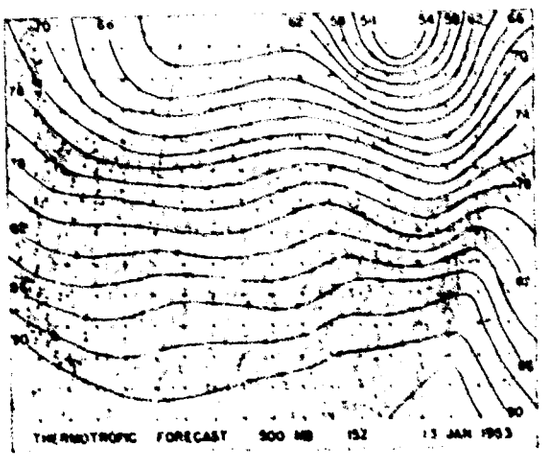
THERMOTROPIC FORECAST 500 MB 15Z 13 JAN 1953

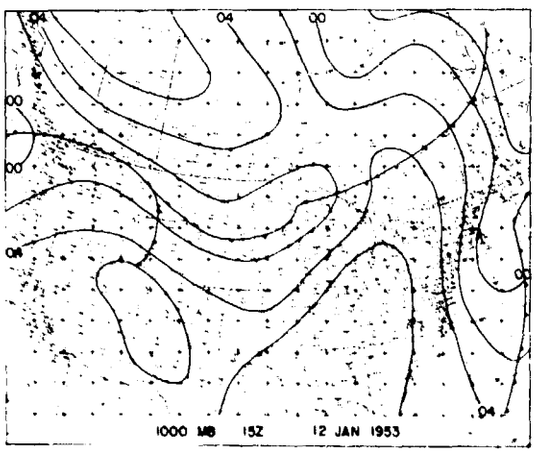
1000 MB 15Z 12 JAN 1953

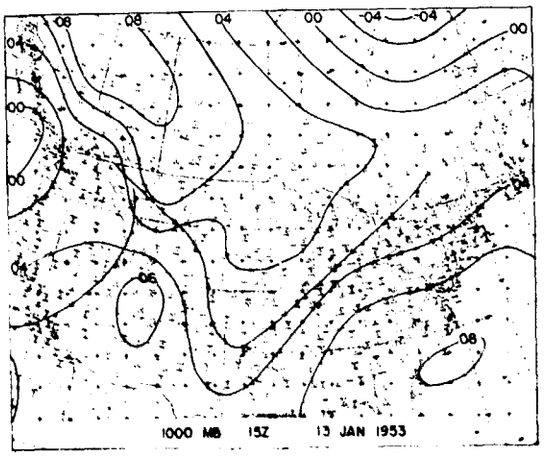
1000 MB 15Z 13 JAN 1953

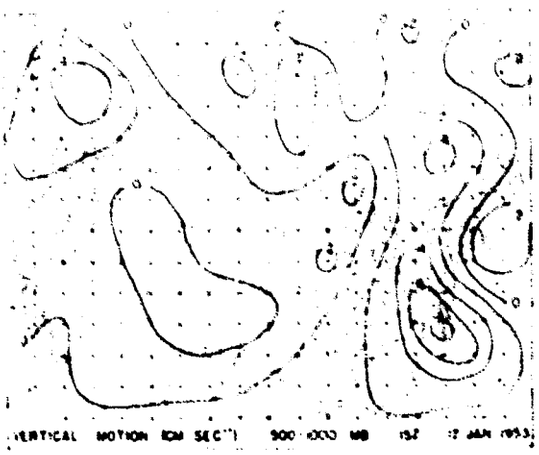
VERTICAL MOTION (CM SEC⁻¹) 500-1000 MB 15Z 12 JAN 1953

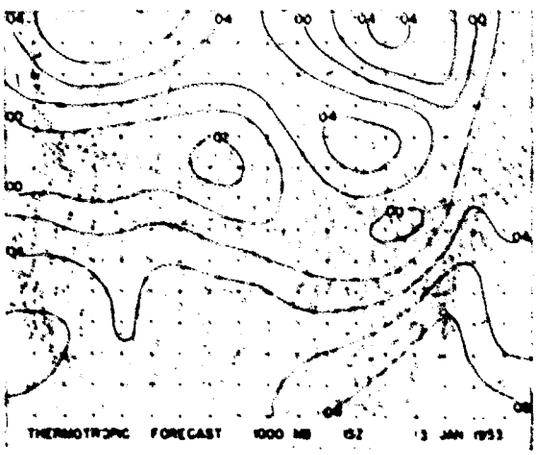
THERMOTROPIC FORECAST 1000 MB 15Z 13 JAN 1953

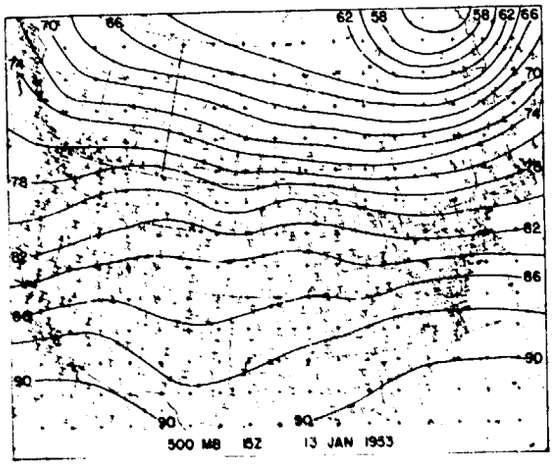
500 MB 15Z 13 JAN 1953

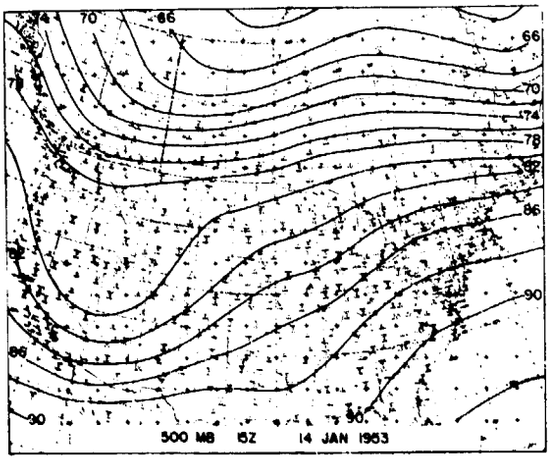
500 MB 15Z 14 JAN 1953

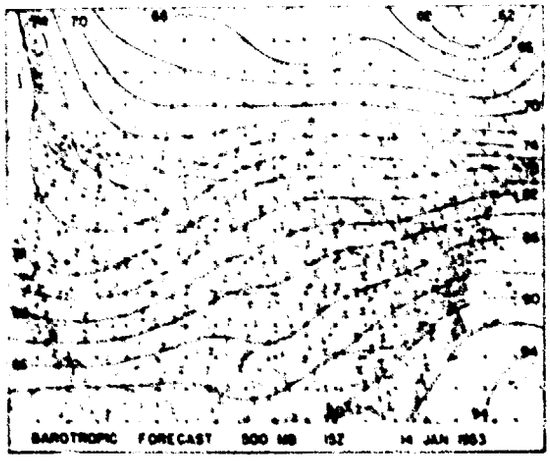
BAROTROPIC FORECAST 500 MB 15Z 14 JAN 1953

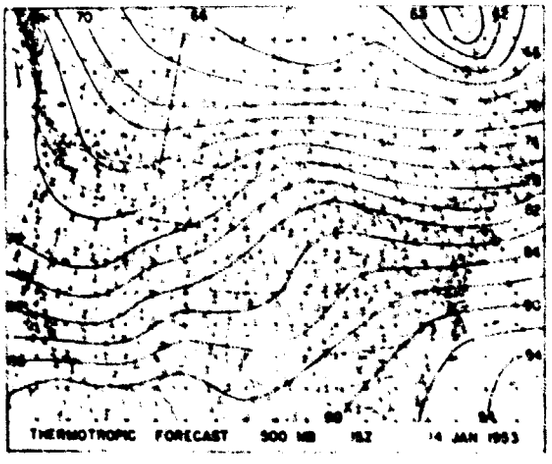
THERMOTROPIC FORECAST 500 MB 15Z 14 JAN 1953

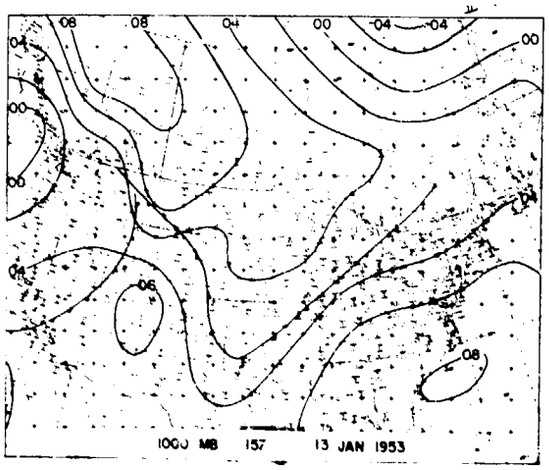
1000 MB 157 13 JAN 1953

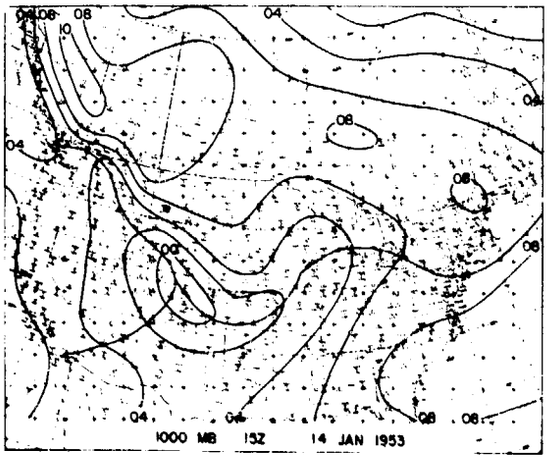
1000 MB 152 14 JAN 1953

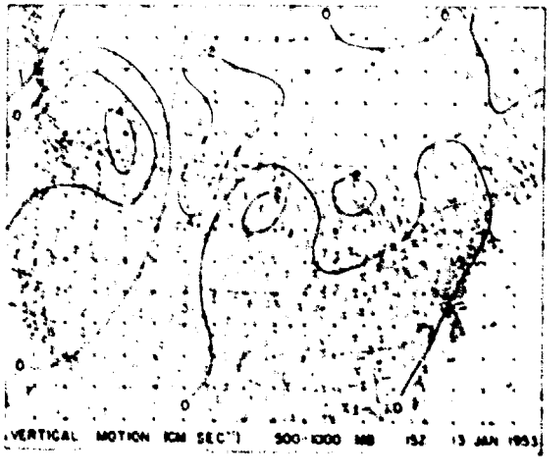
VERTICAL MOTION (CM SEC⁻¹) 500-1000 MB 152 13 JAN 1953

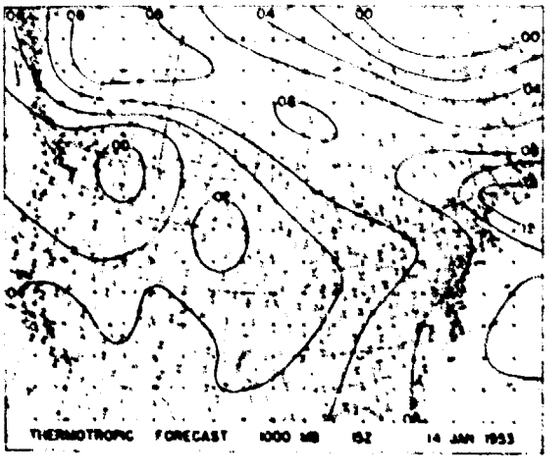
THERMOTROPIC FORECAST 1000 MB 152 14 JAN 1953

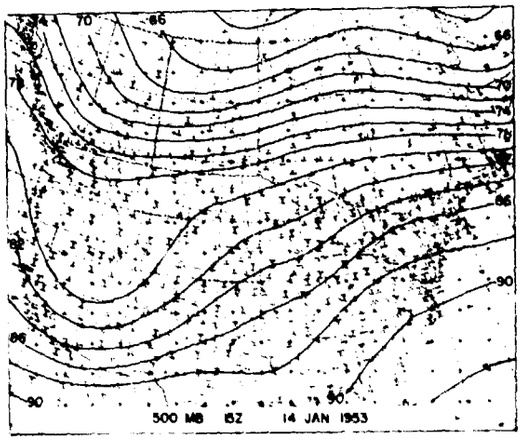
500 MB 15Z 14 JAN 1953

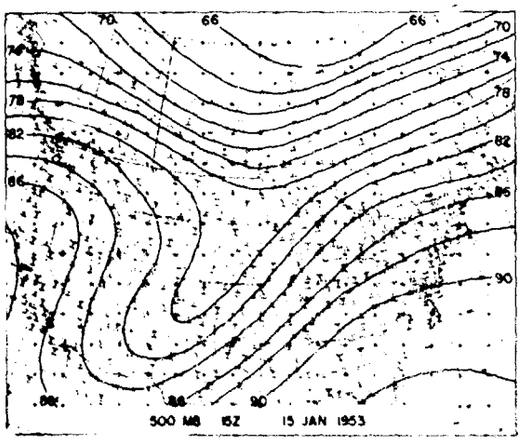
500 MB 15Z 15 JAN 1953

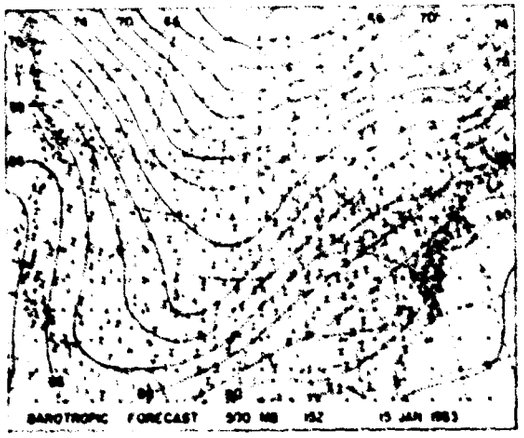
BAROTROPIC FORECAST 500 MB 15Z 15 JAN 1953

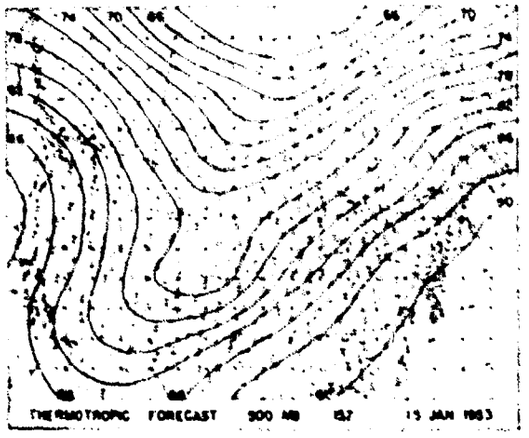
THERMOTROPIC FORECAST 500 MB 15Z 15 JAN 1953

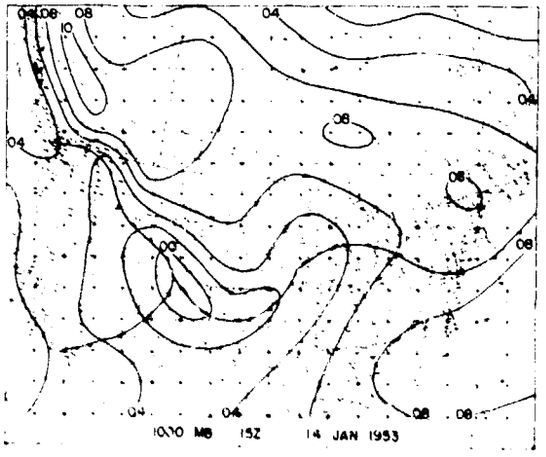
1000 MB 15Z 14 JAN 1953

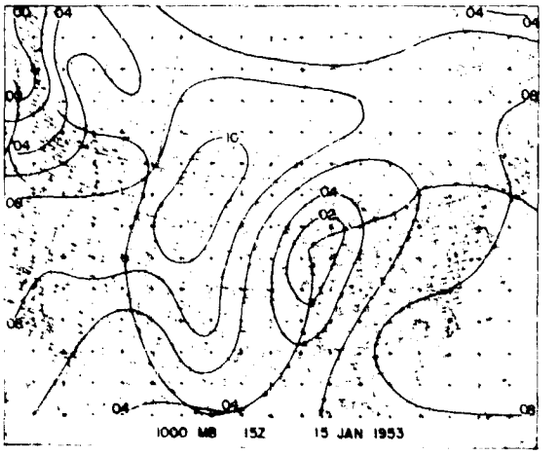
1000 MB 15Z 15 JAN 1953

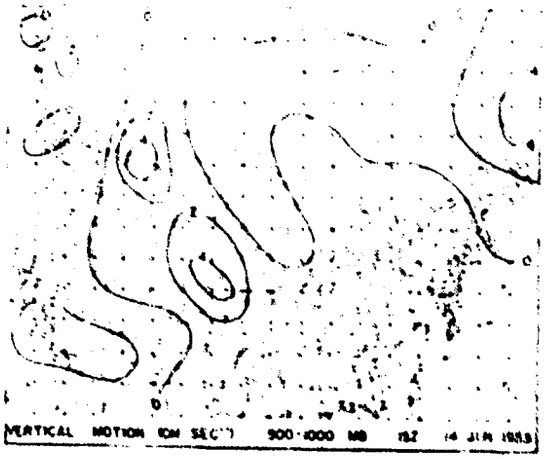
VERTICAL MOTION (DM SEC⁻¹) 500-1000 MB 15Z 14 JAN 1953

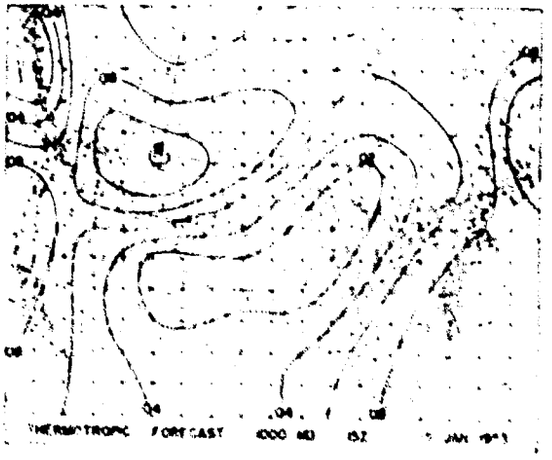
THERMOTROPIC FORECAST 1000 MB 15Z

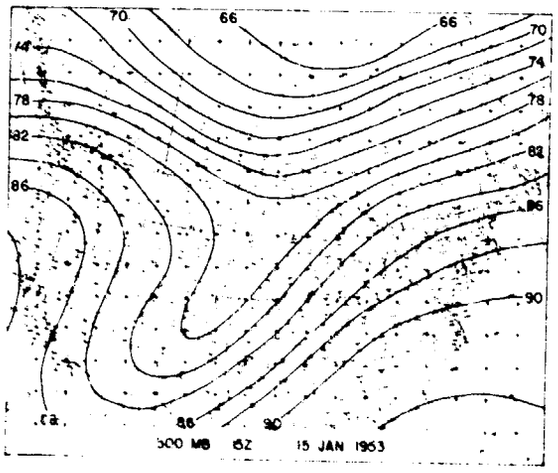
70
66
66
70
74
78
82
86
90
86
90
500 MB 15 JAN 1953

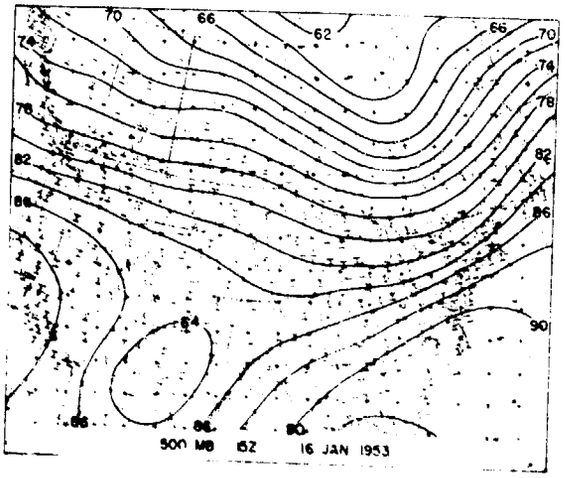
70
66
62
66
70
74
78
82
86
84
90
86
80
500 MB 16 JAN 1953

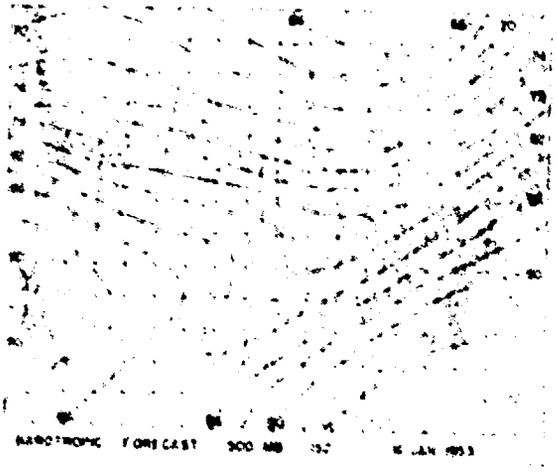

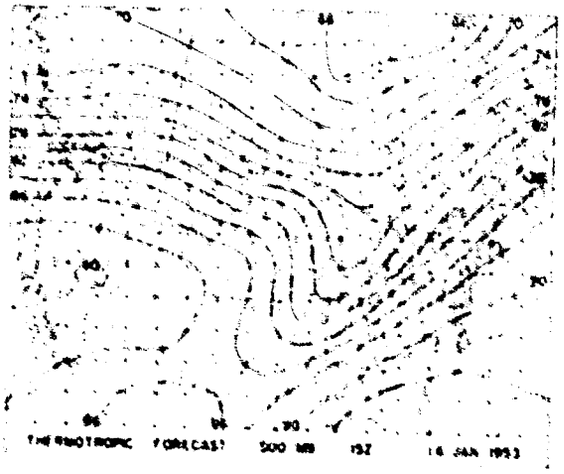

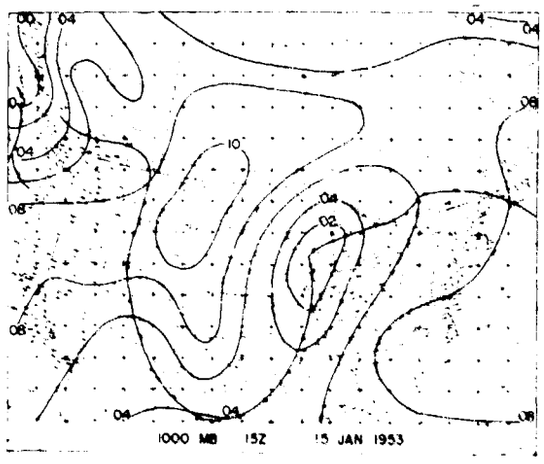
1000 MB 15Z 15 JAN 1953

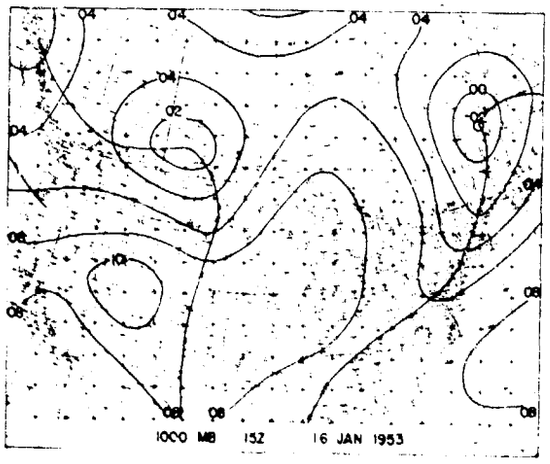
1000 MB 15Z 16 JAN 1953

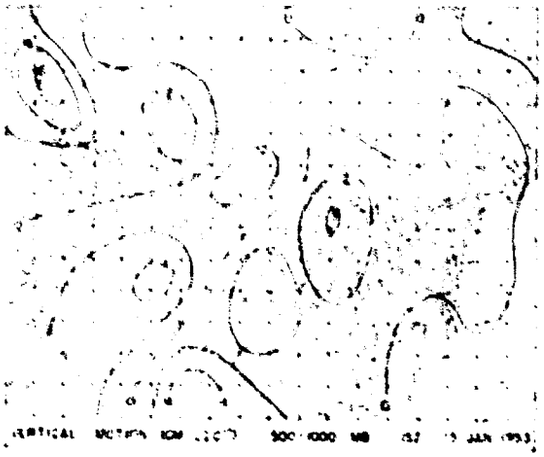

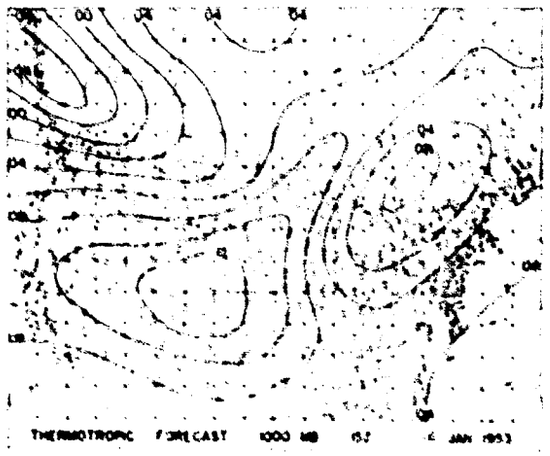
THERMOTROPIC FORECAST 1000 MB

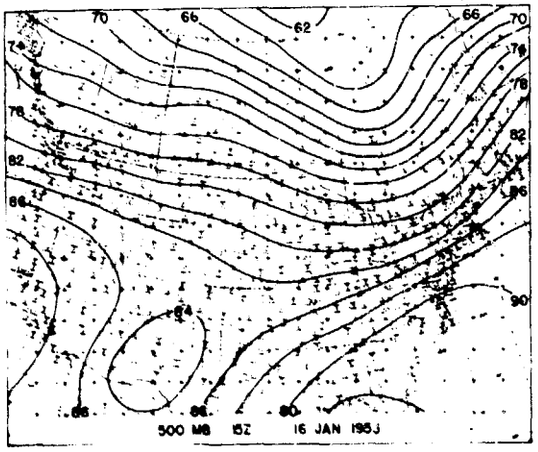
500 MB 15Z 16 JAN 1953

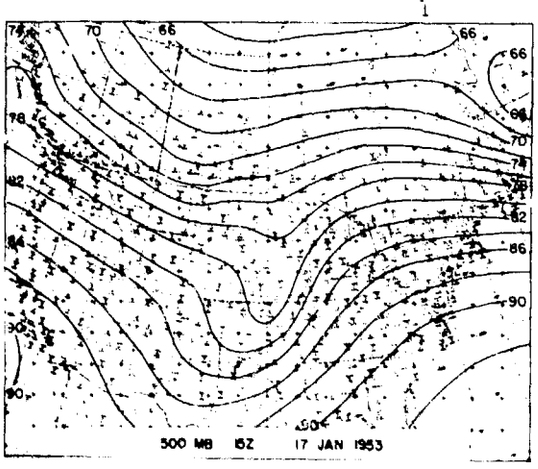
500 MB 15Z 17 JAN 1953

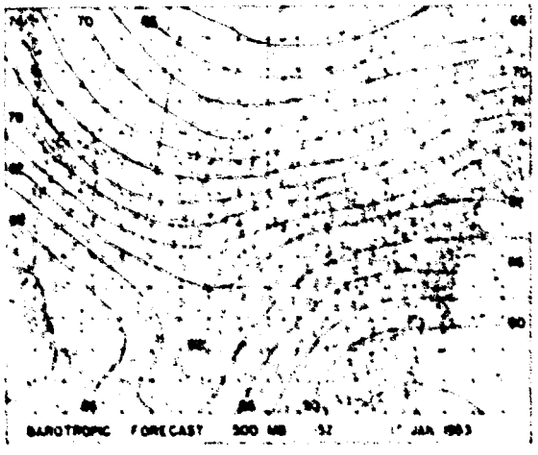
BAROTROPIC FORECAST 500 MB

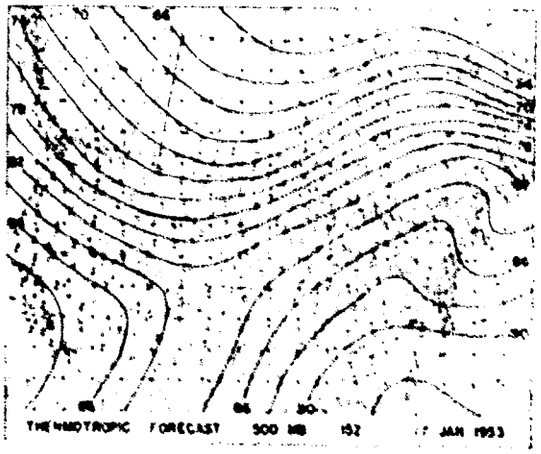
THERMOTROPIC FORECAST 500 MB 15Z

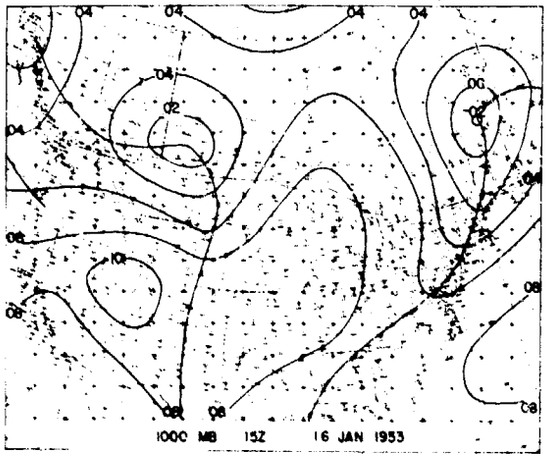
1000 MB 15Z 16 JAN 1953

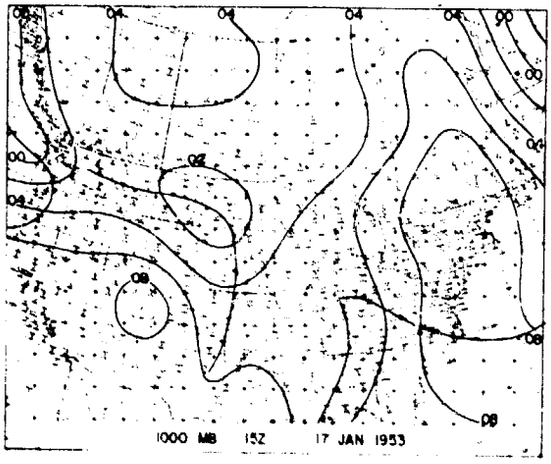
1000 MB 15Z 17 JAN 1953

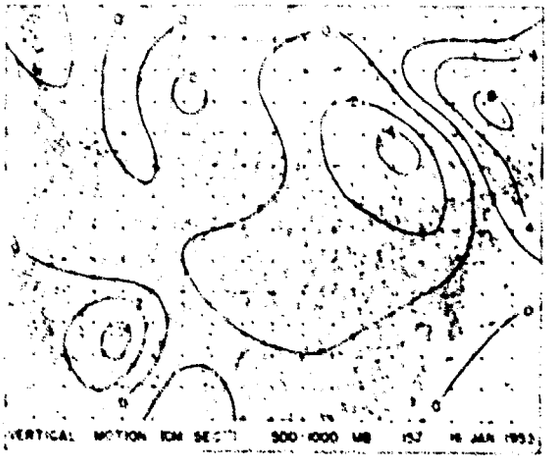
VERTICAL MOTION (CM SEC⁻¹) 500-1000 MB 15Z 16 JAN 1953

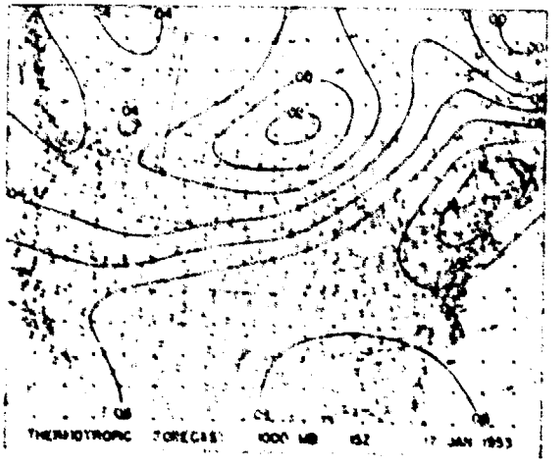
THERMOTROPIC FORECAST 1000 MB 15Z 17 JAN 1953

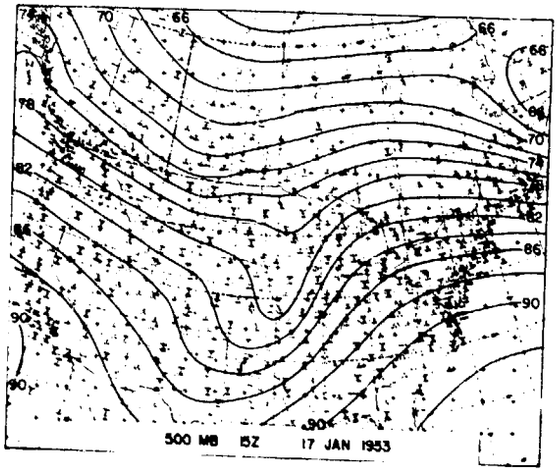
500 MB 15Z 17 JAN 1953

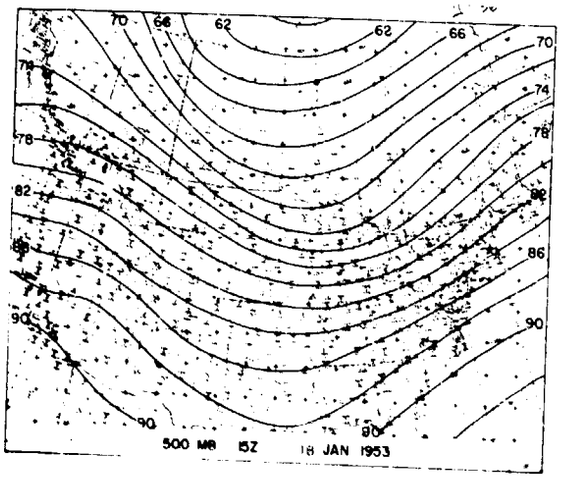
500 MB 15Z 18 JAN 1953

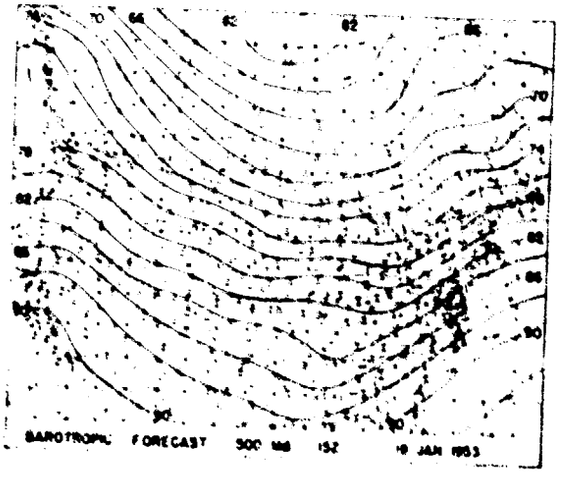
BAROTROPIC FORECAST 500 MB 15Z 18 JAN 1953

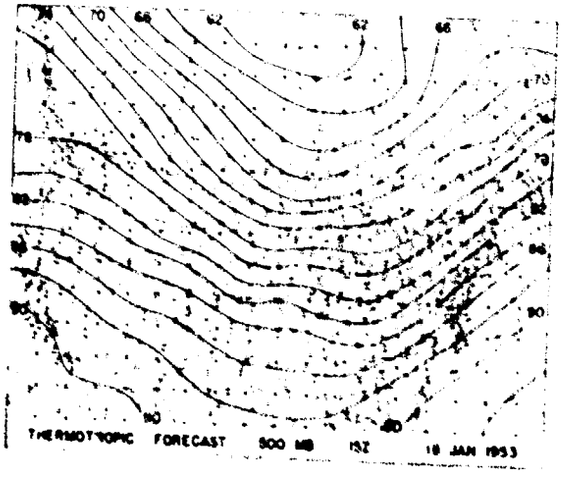
THERMOTROPIC FORECAST 500 MB 15Z 18 JAN 1953

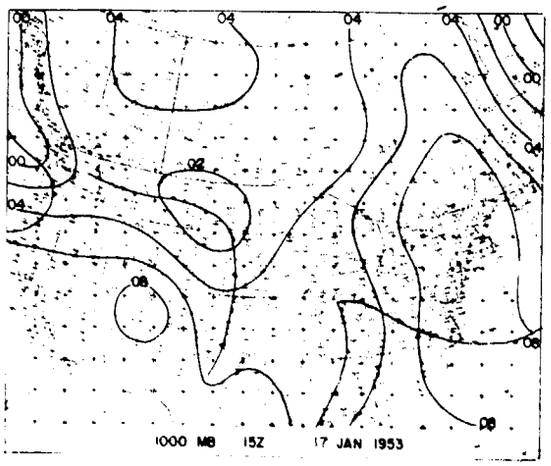
1000 MB 15Z 17 JAN 1953

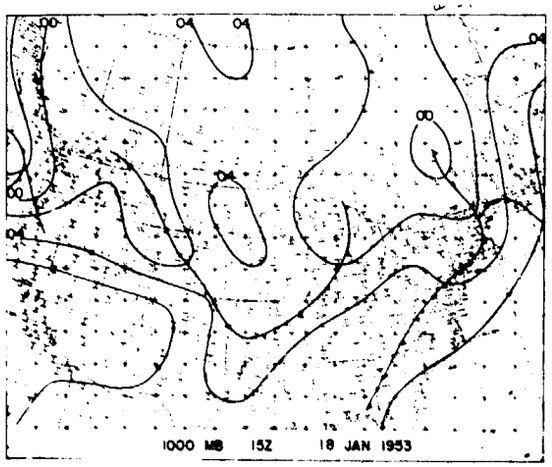
1000 MB 15Z 18 JAN 1953

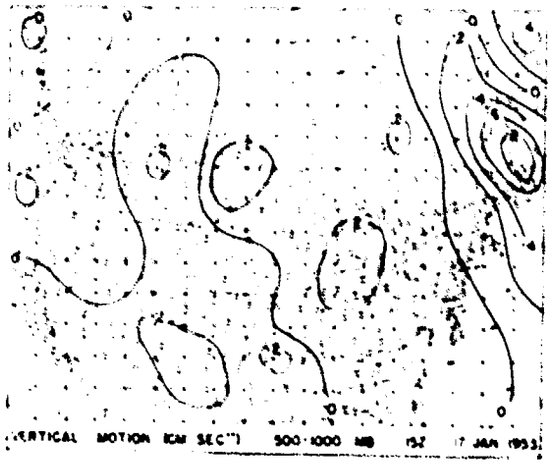
VERTICAL MOTION (CM SEC⁻¹) 500-1000 MB 15Z 17 JAN 1953

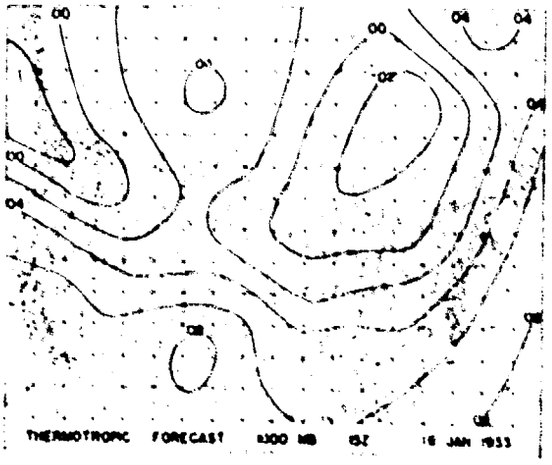
THERMOTROPIC FORECAST 1000 MB 15Z 18 JAN 1953

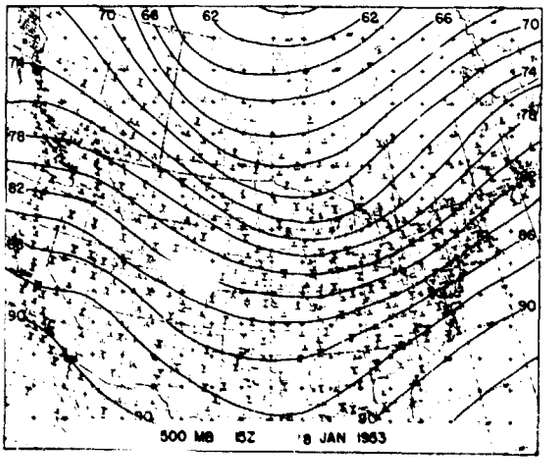
500 MB 15Z 18 JAN 1953

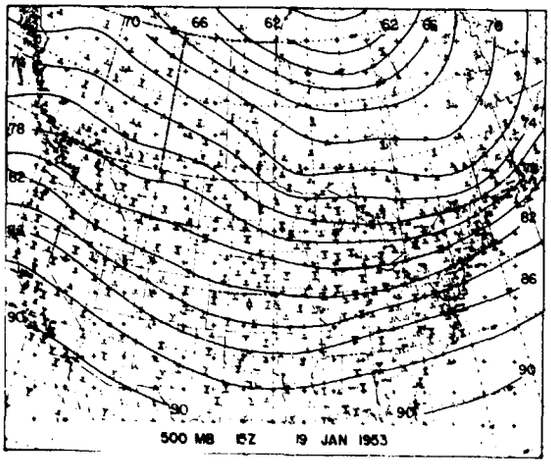
500 MB 15Z 19 JAN 1953

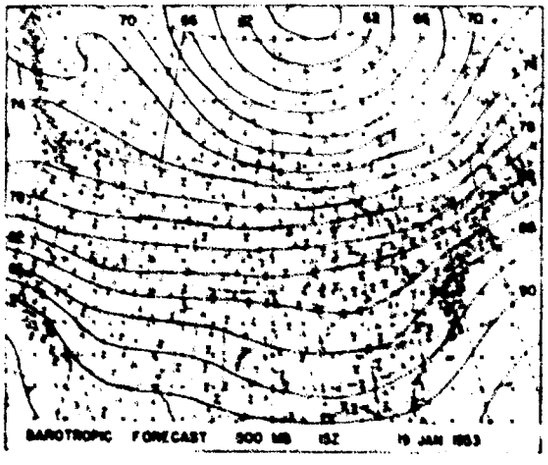
BAROTROPIC FORECAST 500 MB 15Z 19 JAN 1953

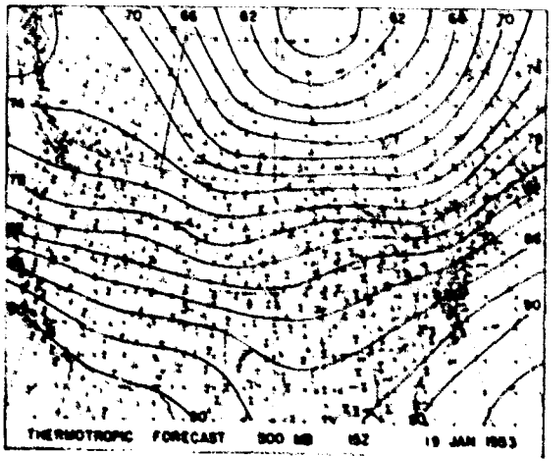
THERMOTROPIC FORECAST 500 MB 15Z 19 JAN 1953

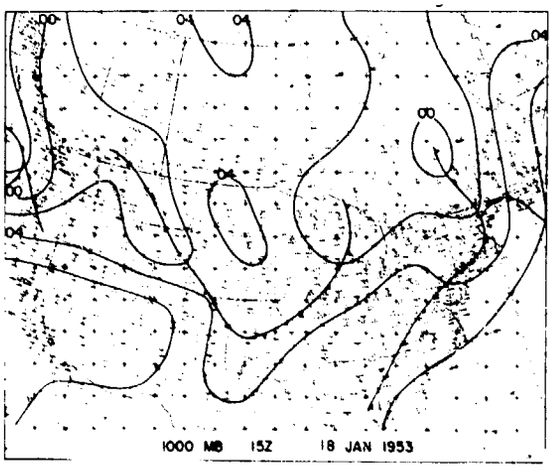
1000 MB 15Z 18 JAN 1953

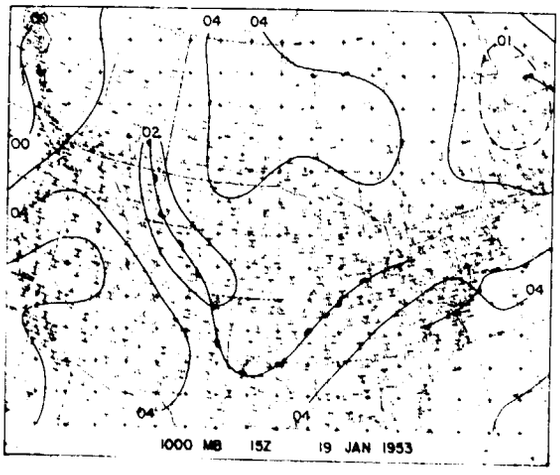
1000 MB 15Z 19 JAN 1953

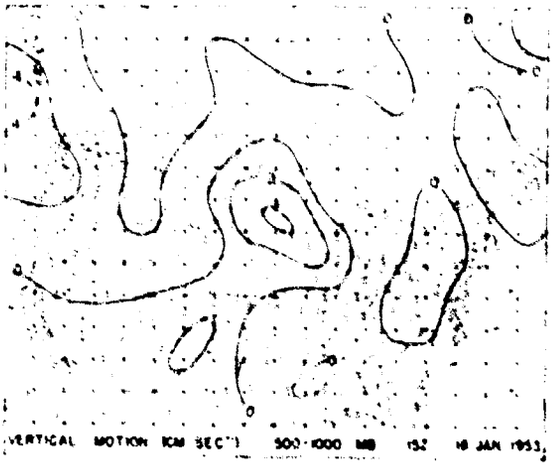
VERTICAL MOTION (CM SEC⁻¹) 500-1000 MB 15Z 18 JAN 1953

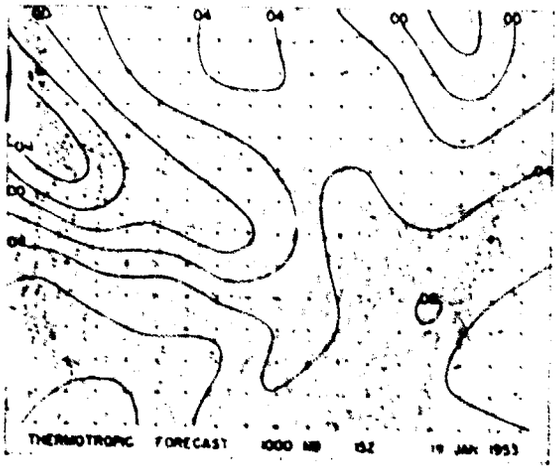
THERMOTROPIC FORECAST 1000 MB 15Z 19 JAN 1953

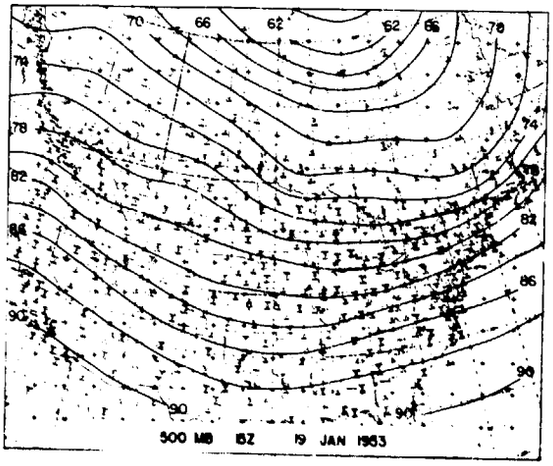
500 MB 15Z 19 JAN 1953

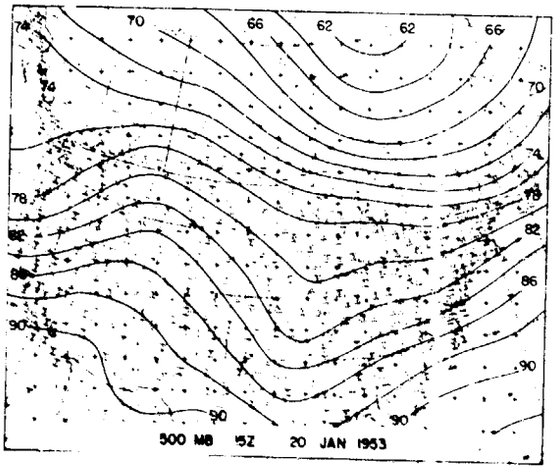
500 MB 15Z 20 JAN 1953

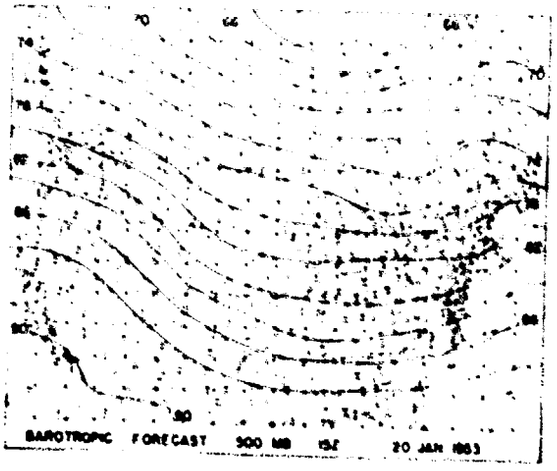
BAROTROPIC FORECAST 500 MB 15Z 20 JAN 1953

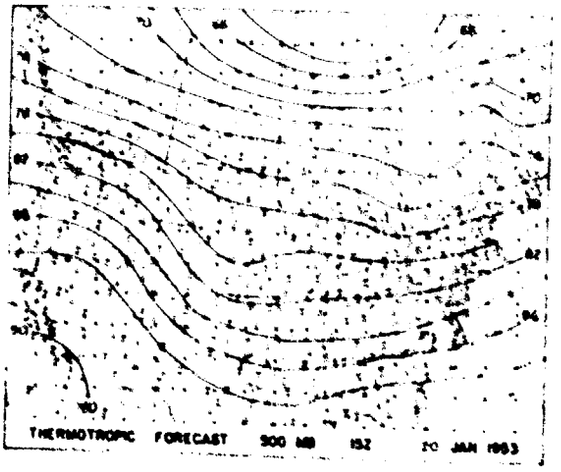
THERMOTROPIC FORECAST 500 MB 15Z 20 JAN 1953

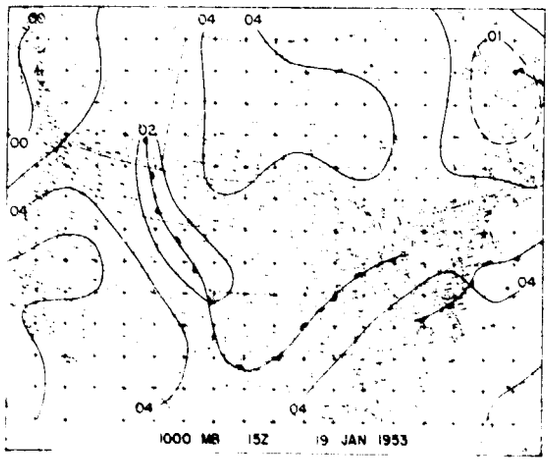
1000 MB 15Z 19 JAN 1953

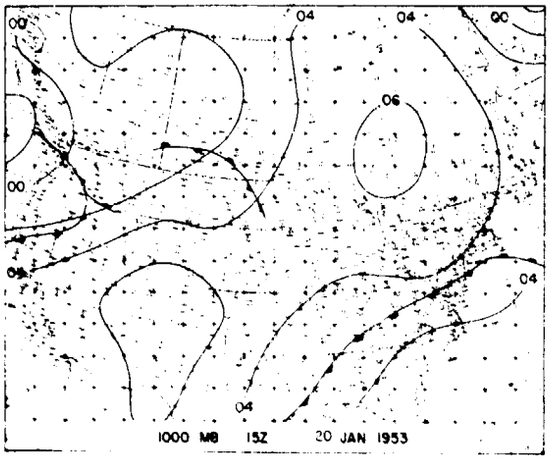
1000 MB 15Z 20 JAN 1953

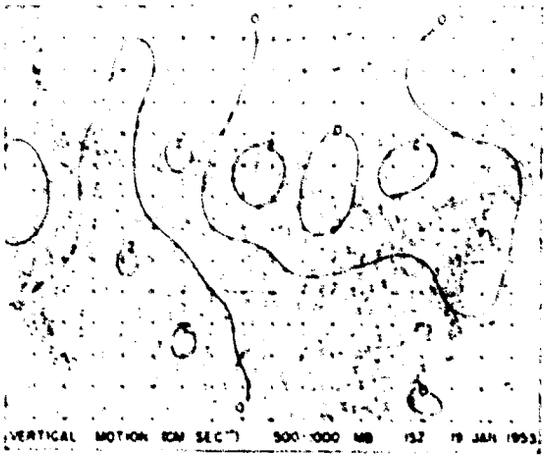
VERTICAL MOTION (CM SEC⁻¹) 500-1000 MB 15Z 19 JAN 1953

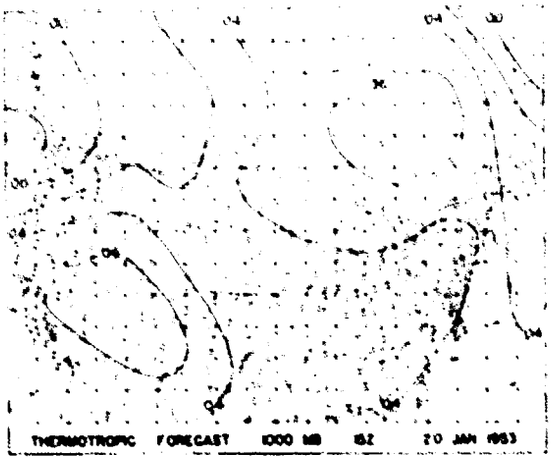
THERMOTROPIC FORECAST 1000 MB 15Z 20 JAN 1953

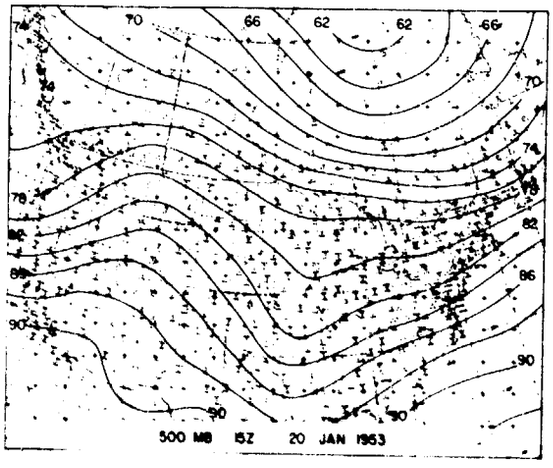
500 MB 15Z 20 JAN 1953

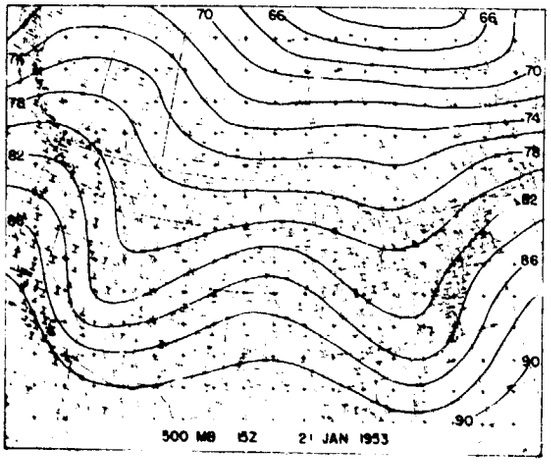
500 MB 15Z 21 JAN 1953

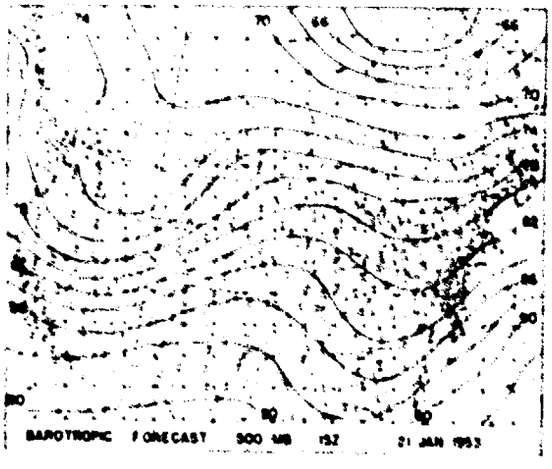
BAROTROPIC FORECAST 500 MB 15Z 21 JAN 1953

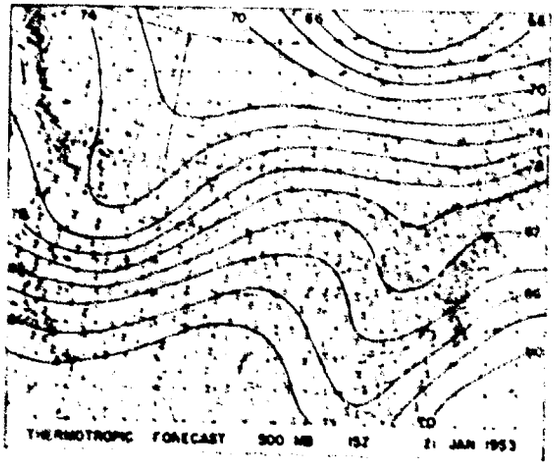
THERMOTROPIC FORECAST 500 MB 15Z 21 JAN 1953

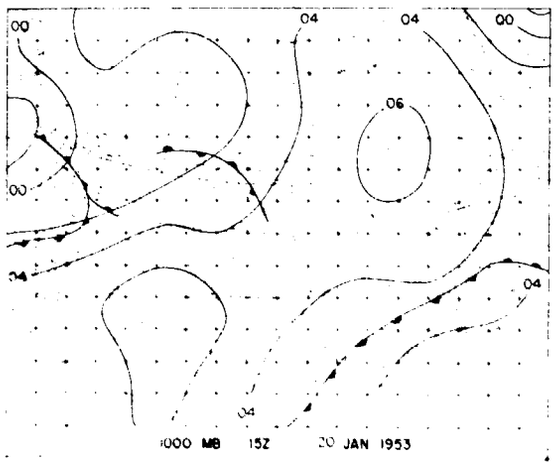
1000 MB 15Z 20 JAN 1953

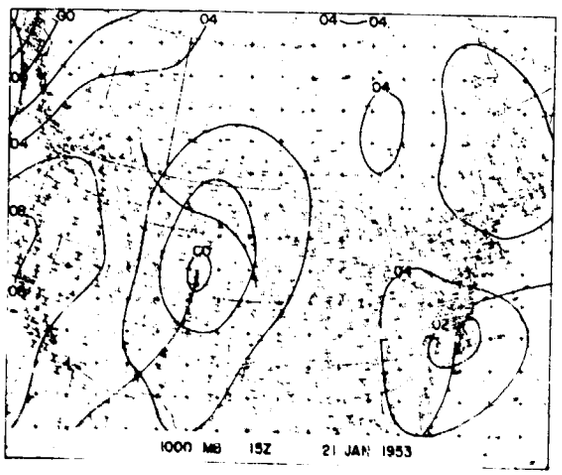
1000 MB 15Z 21 JAN 1953

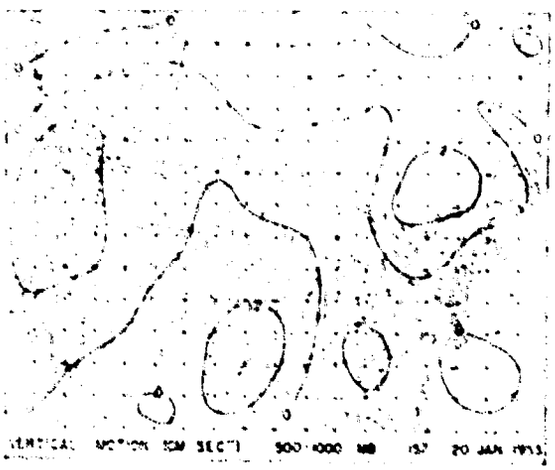

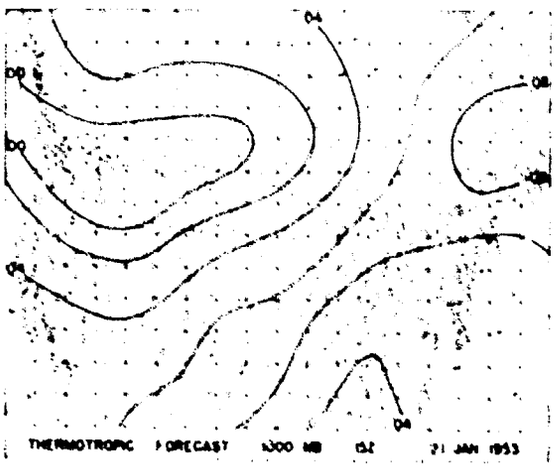
THERMOTROPIC FORECAST 1000 MB 15Z 21 JAN 1953

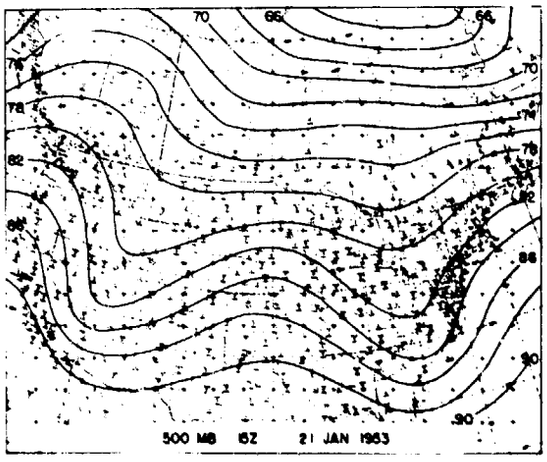
500 MB 15Z 21 JAN 1963

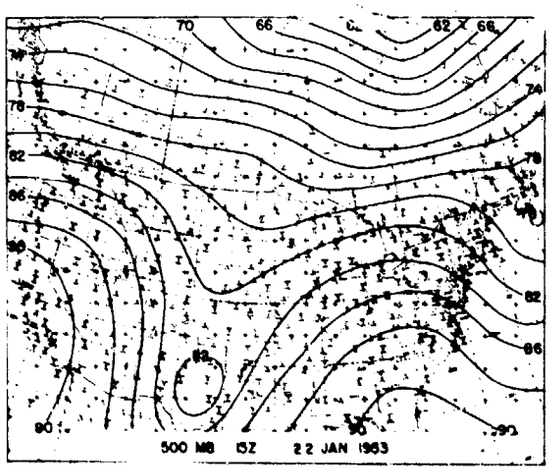
500 MB 15Z 22 JAN 1963

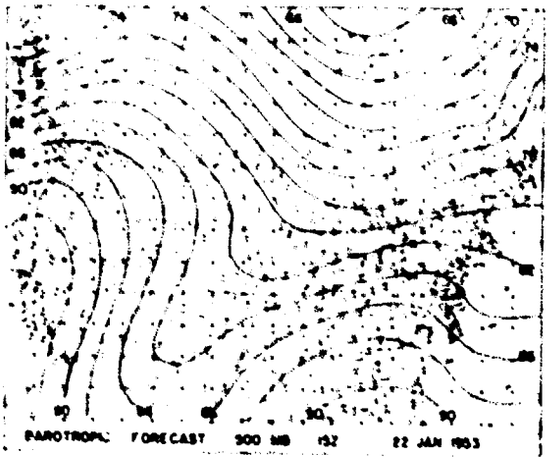
BAROTROPIC FORECAST 500 MB 15Z 22 JAN 1963

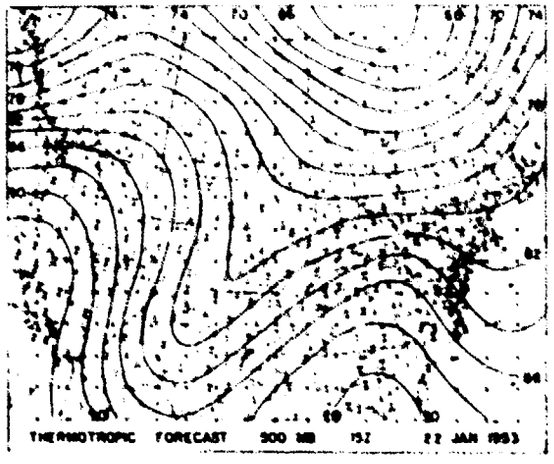
THERMOTROPIC FORECAST 500 MB 15Z 22 JAN 1963

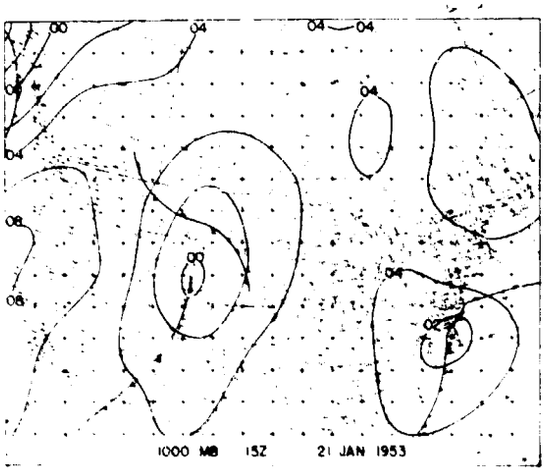
1000 MB 15Z 21 JAN 1953

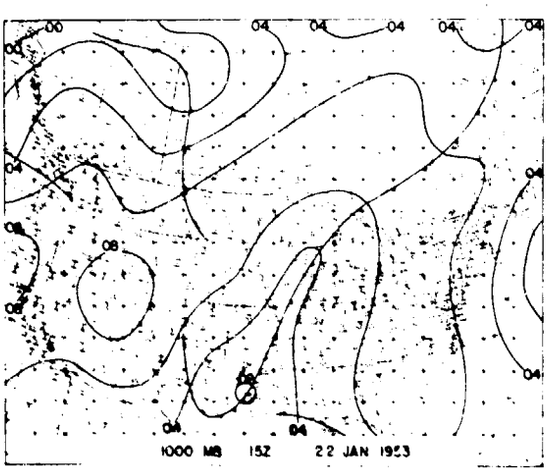
1000 MB 15Z 22 JAN 1953

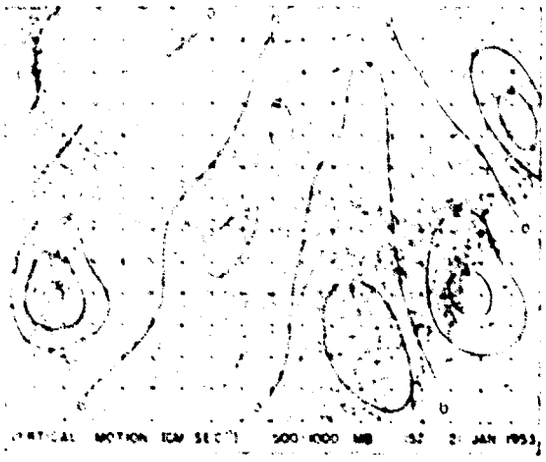

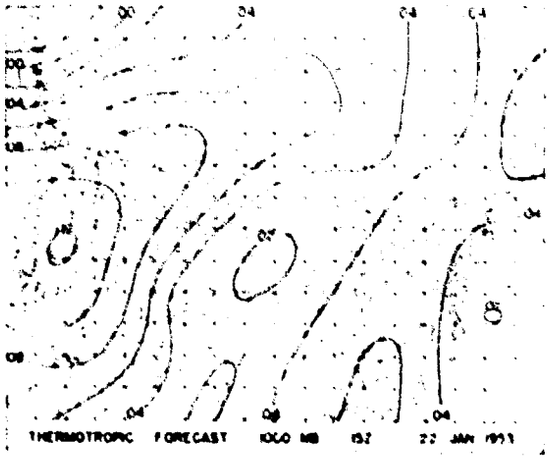
THERMOTROPIC FORECAST 1000 MB 15Z 22 JAN 1953

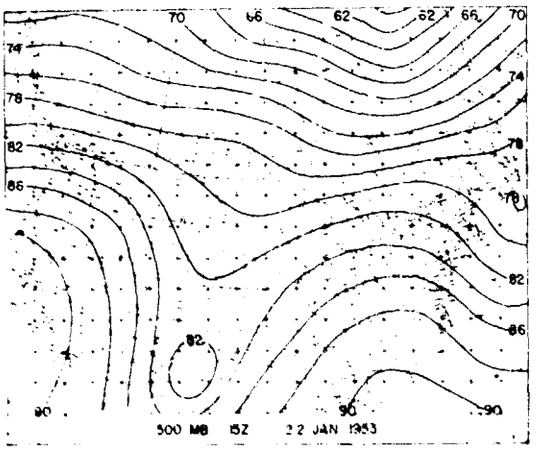
500 MB 15Z 22 JAN 1953

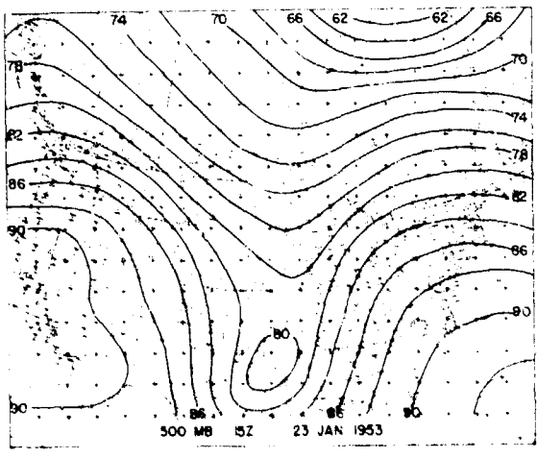
500 MB 15Z 23 JAN 1953

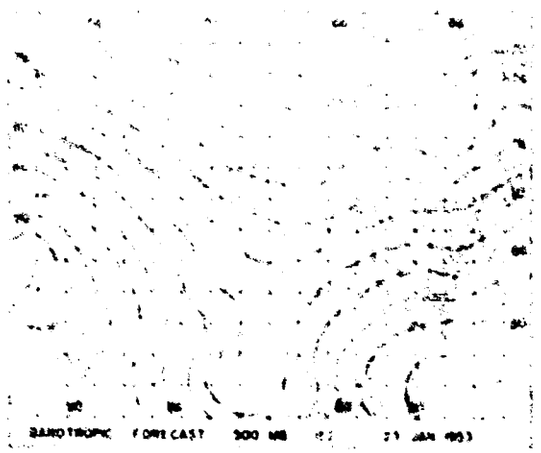

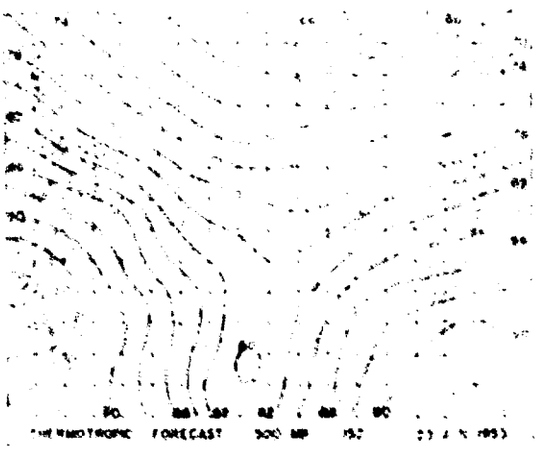

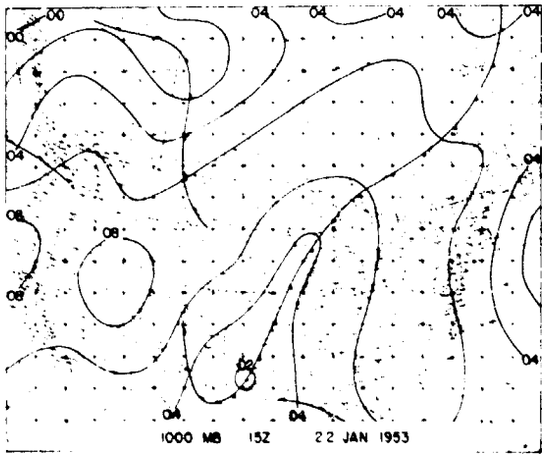
1000 MB 152 22 JAN 1953

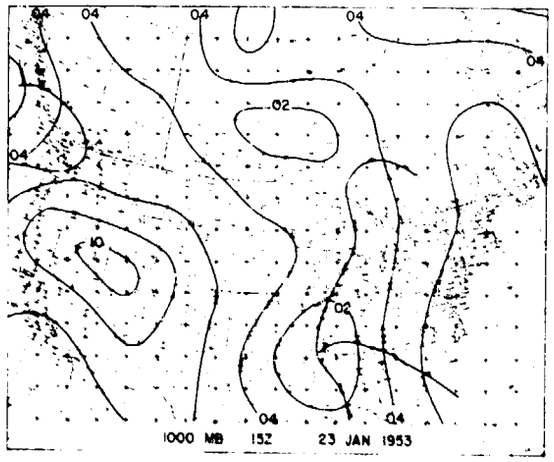
1000 MB 152 23 JAN 1953

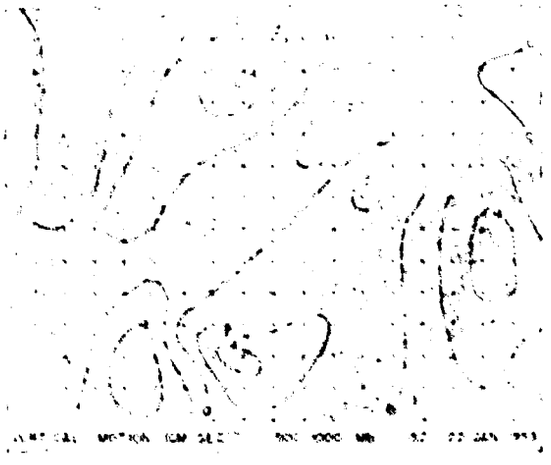

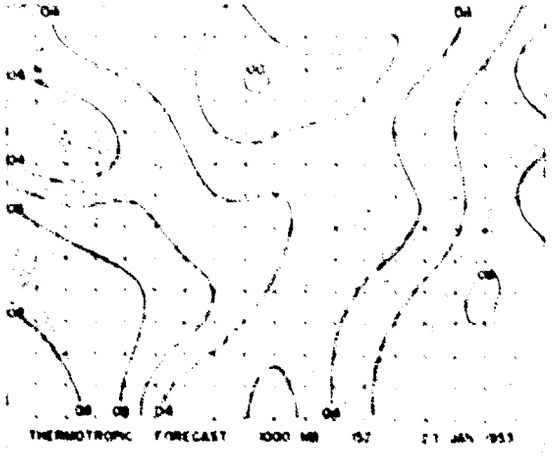
THERMOTROPIC FORECAST 1000 MB 152

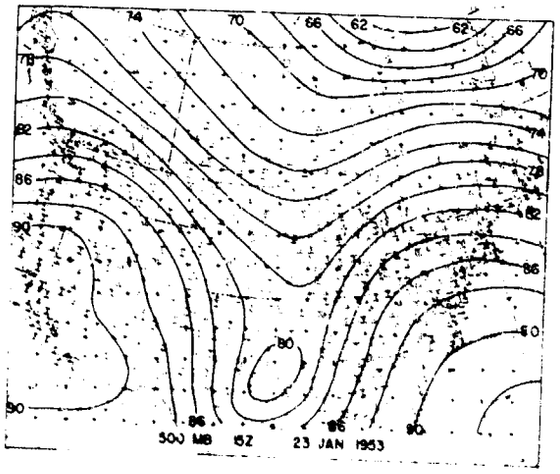
500 MB 15Z 23 JAN 1953

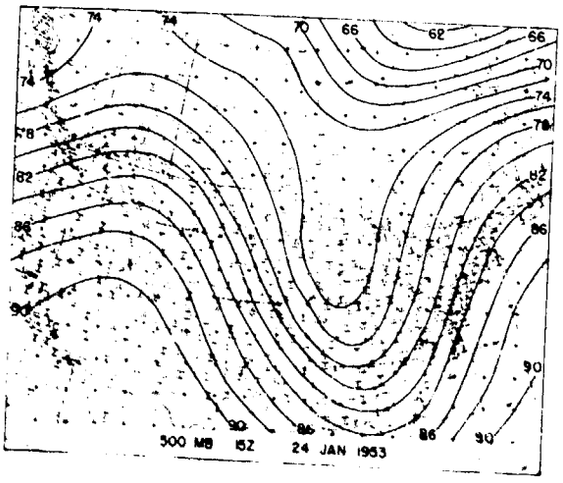
500 MB 15Z 24 JAN 1953

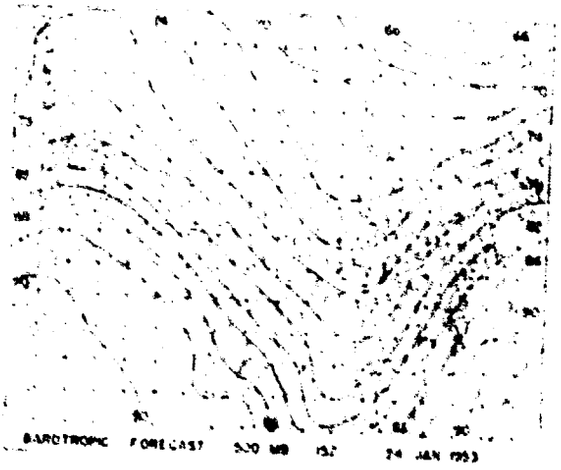
BAROTROPIC FORECAST 500 MB 15Z 24 JAN 1953

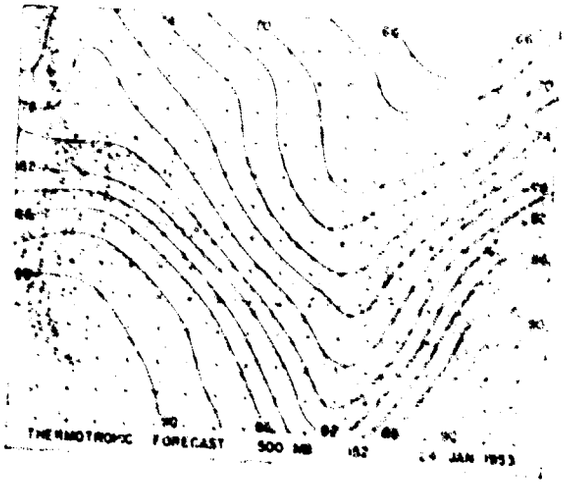
THERMOTROPIC FORECAST 500 MB 15Z JAN 1953

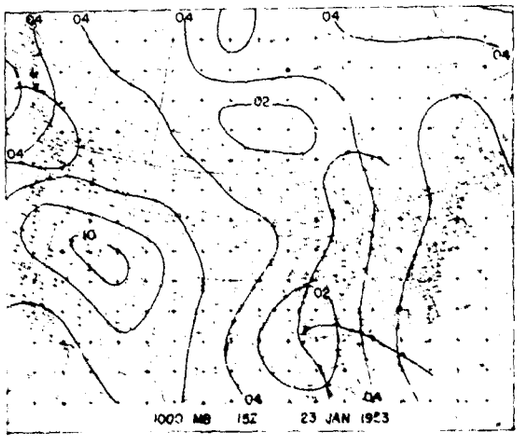
1000 MB 15Z 23 JAN 1953

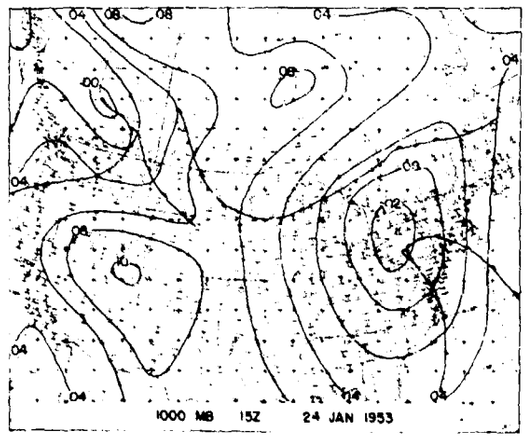
1000 MB 15Z 24 JAN 1953

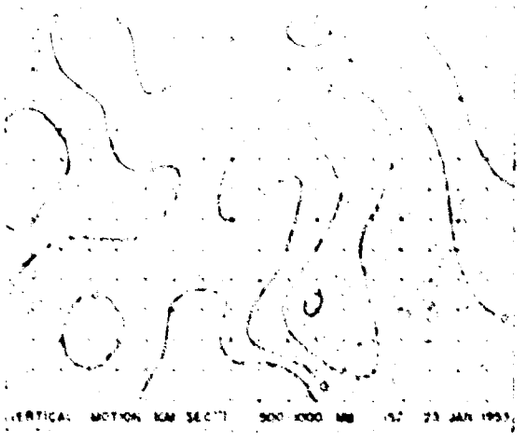
VERTICAL MOTION (CM SEC⁻¹) 500 1000 MB 15Z 23 JAN 1953

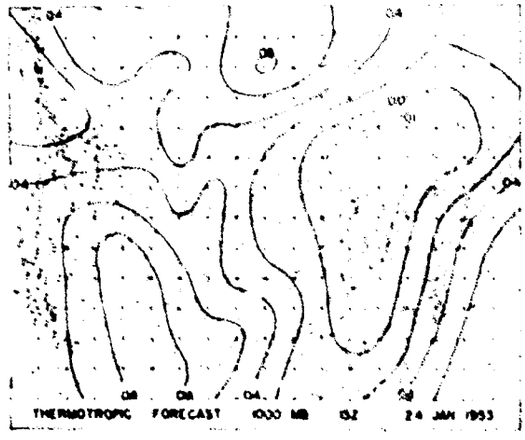
THERMOTROPIC FORECAST 1000 MB 15Z 24 JAN 1953

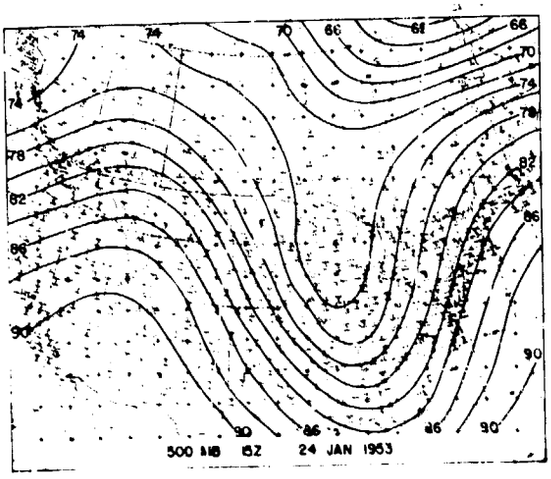
500 MB 15Z 24 JAN 1953

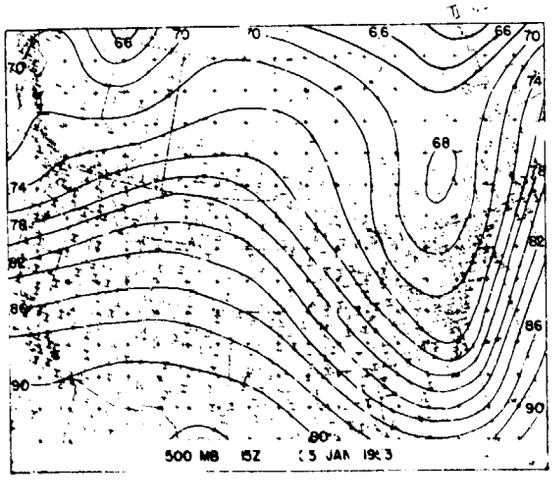
500 MB 15Z 25 JAN 1953

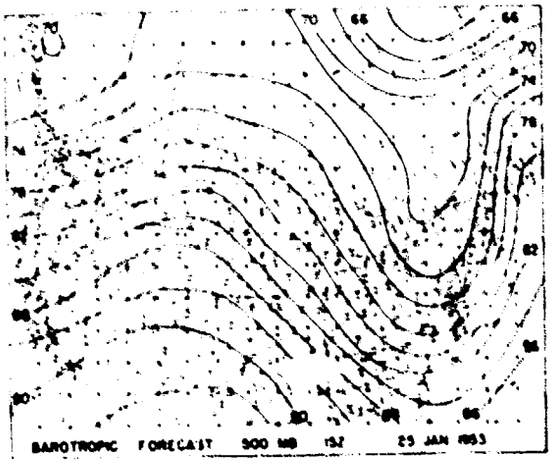
BAROTROPIC FORECAST 500 MB 15Z 25 JAN 1953

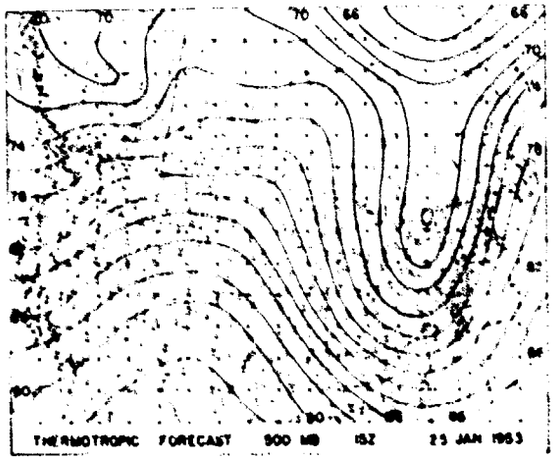
THERMOTROPIC FORECAST 500 MB 15Z 25 JAN 1953

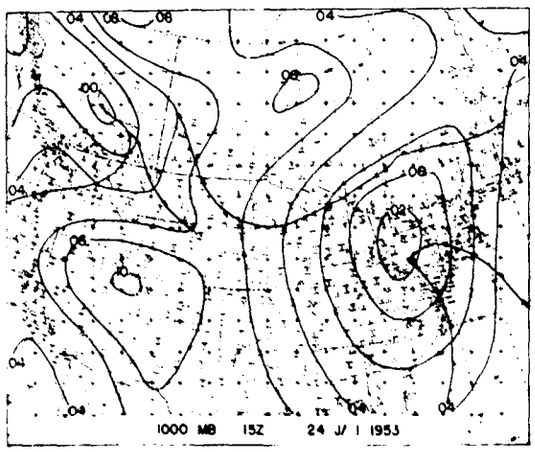
1000 MB 15Z 24 JAN 1953

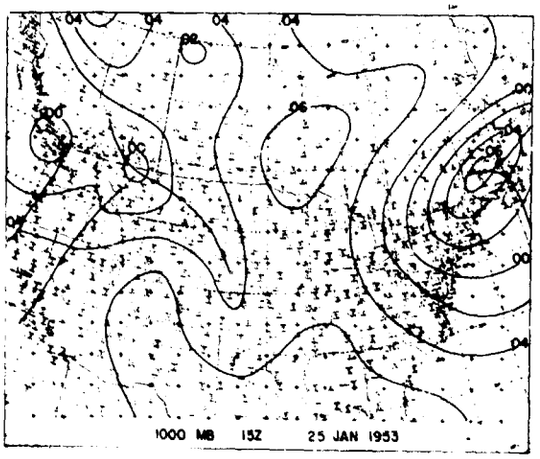
1000 MB 15Z 25 JAN 1953

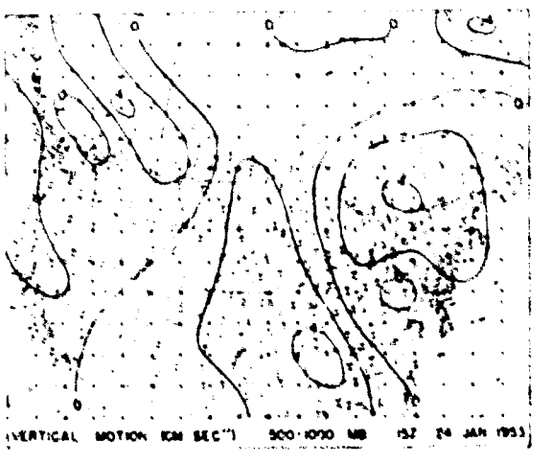
VERTICAL MOTION (CM SEC⁻¹) 500-1000 MB 15Z 24 JAN 1953

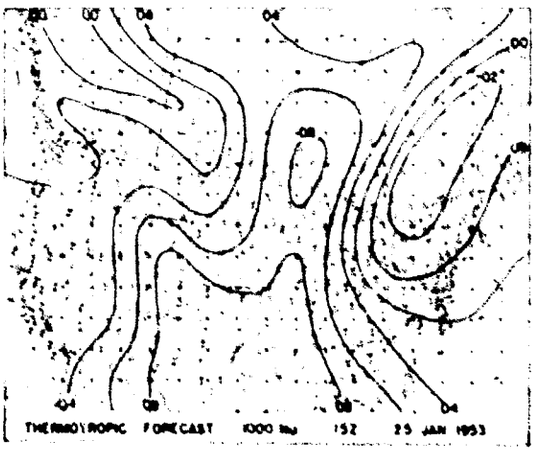
THERMOTROPIC FORECAST 1000 mb 15Z 25 JAN 1953

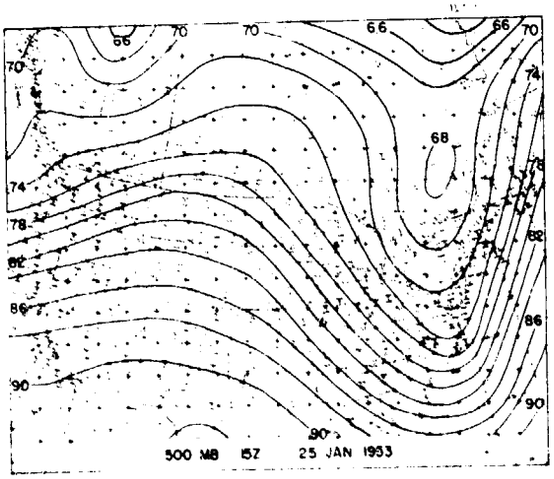
500 MB 15Z 25 JAN 1953

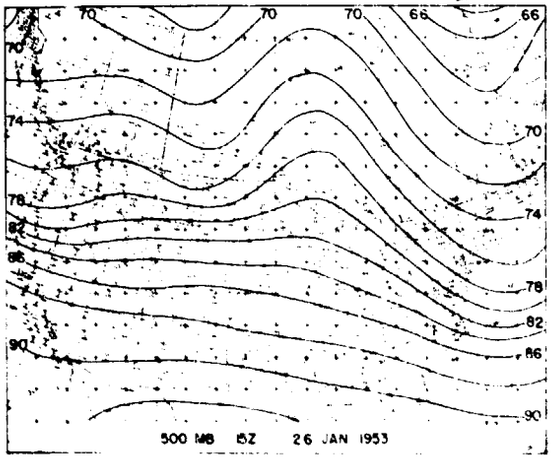
500 MB 15Z 26 JAN 1953

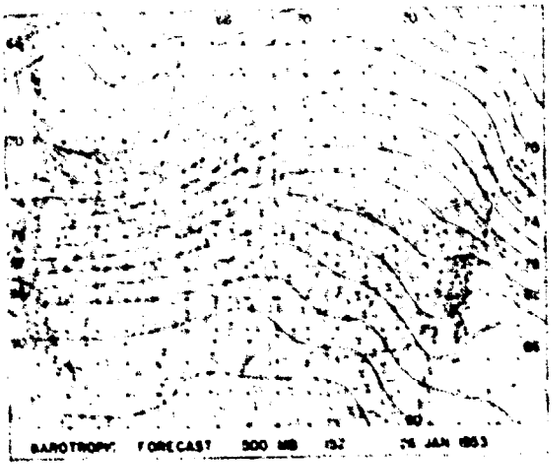
BAROTROPY FORECAST 500 MB 15Z

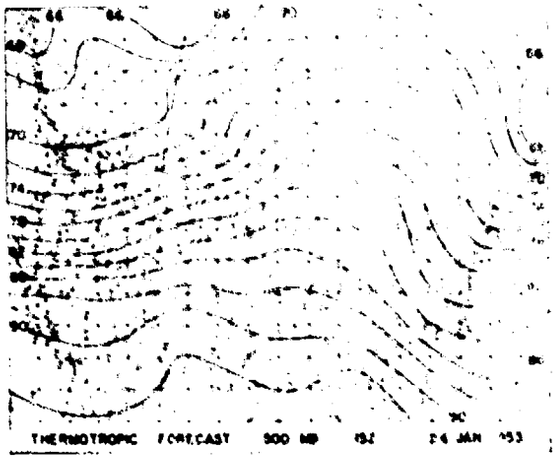
THERMOTROPIC FORECAST 500 MB 15Z

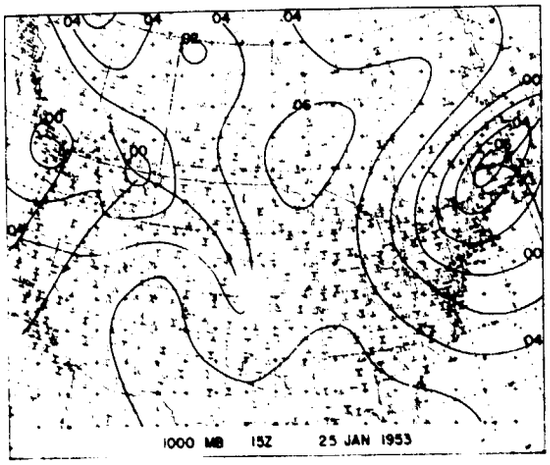
1000 MB 15Z 25 JAN 1953

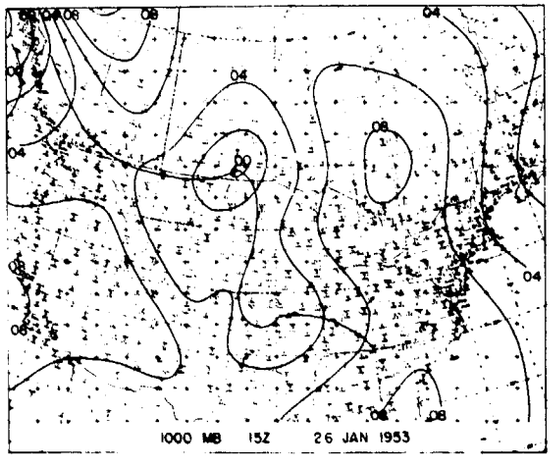
1000 MB 15Z 26 JAN 1953

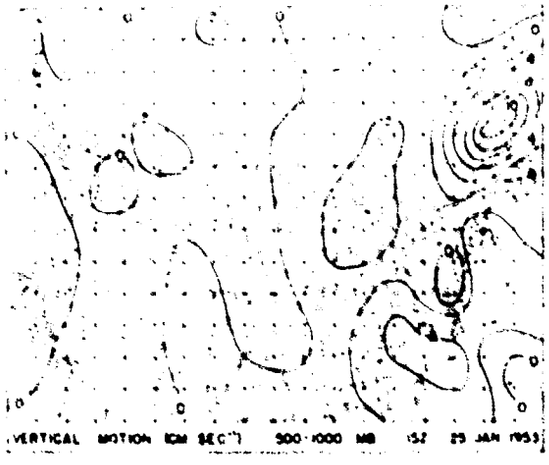
VERTICAL MOTION (CM SEC⁻¹) 500-1000 MB 15Z 25 JAN 1953

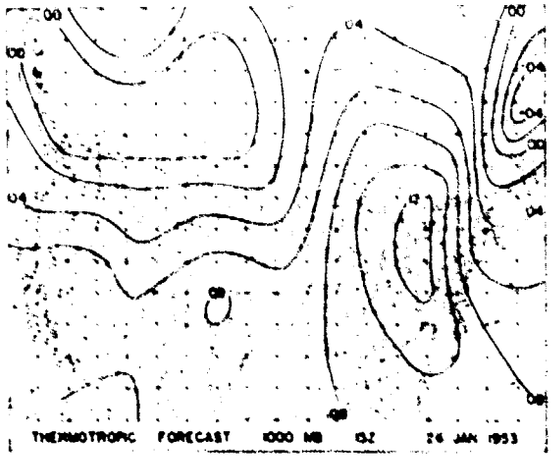
THERMOTROPIC FORECAST 1000 MB 15Z 26 JAN 1953

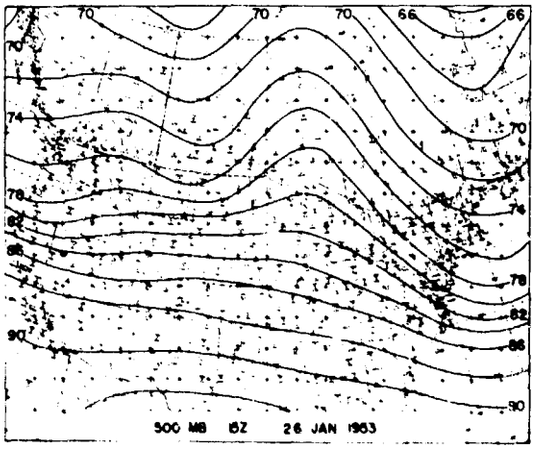
500 MB 15Z 26 JAN 1953

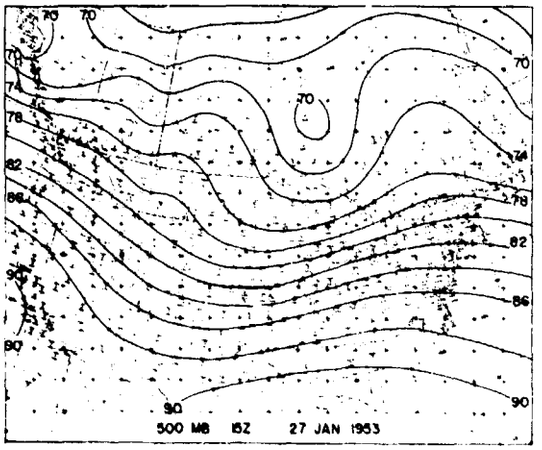
500 MB 15Z 27 JAN 1953

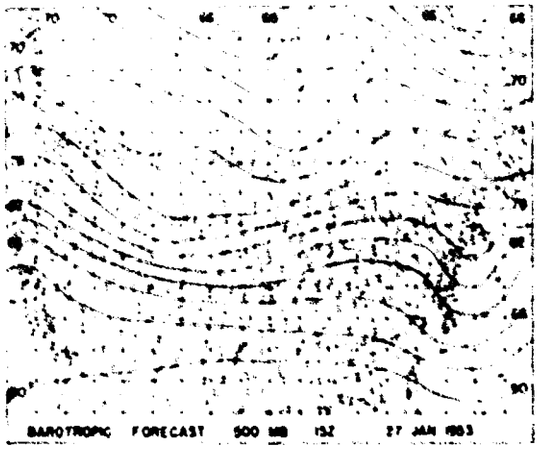
BAROTROPIC FORECAST 500 MB 15Z 27 JAN 1953

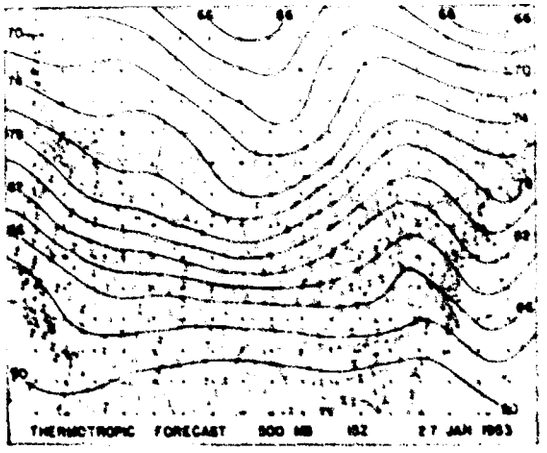
THERMOTROPIC FORECAST 500 MB 15Z 27 JAN 1953

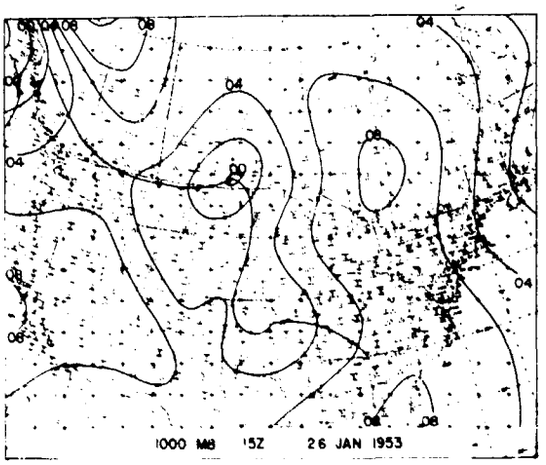
1000 MB 15Z 26 JAN 1953

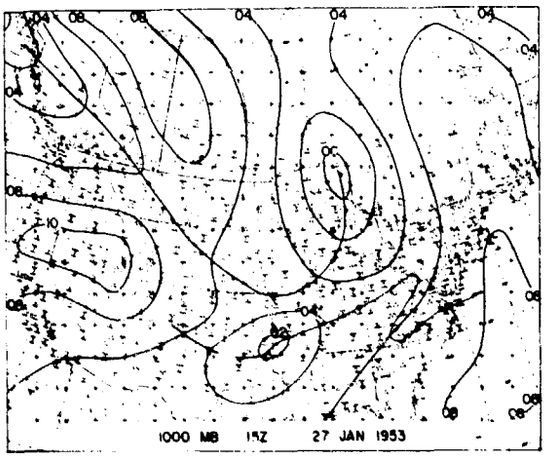
1000 MB 15Z 27 JAN 1953

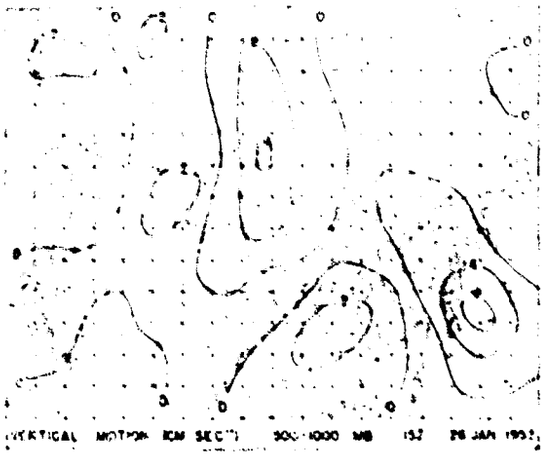
VERTICAL MOTION (CM SEC⁻¹) 500-1000 MB 15Z 26 JAN 1953

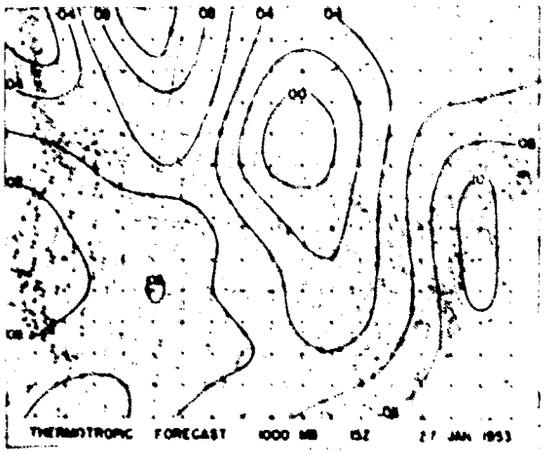
THERMOTROPIC FORECAST 1000 MB 15Z 27 JAN 1953

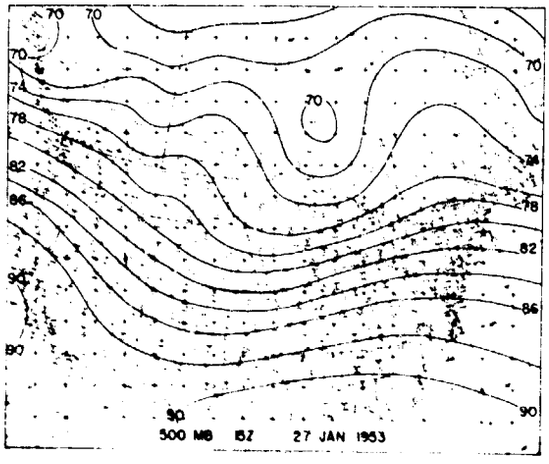
500 MB 15Z 27 JAN 1953

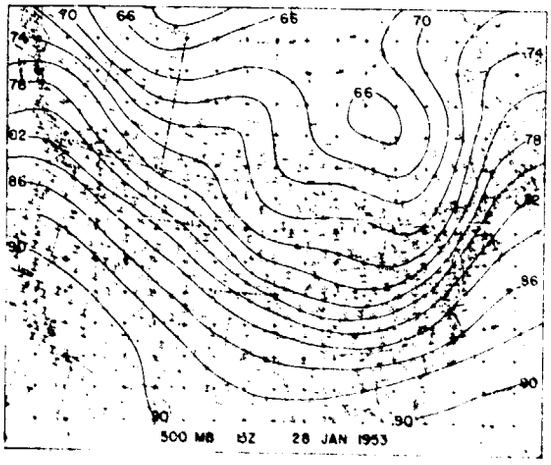
500 MB 15Z 28 JAN 1953

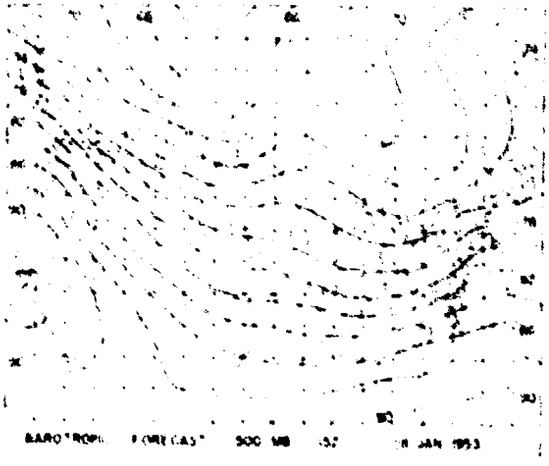

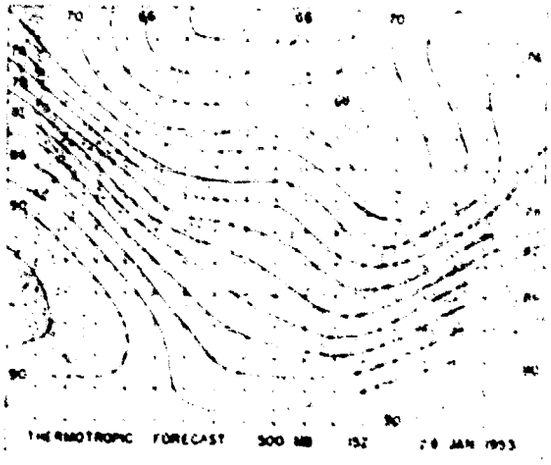

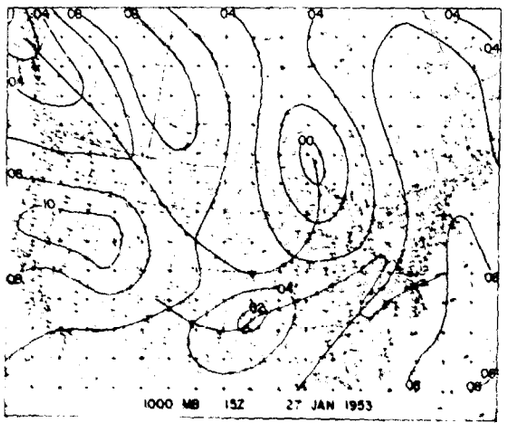
1000 MB 15Z 27 JAN 1953

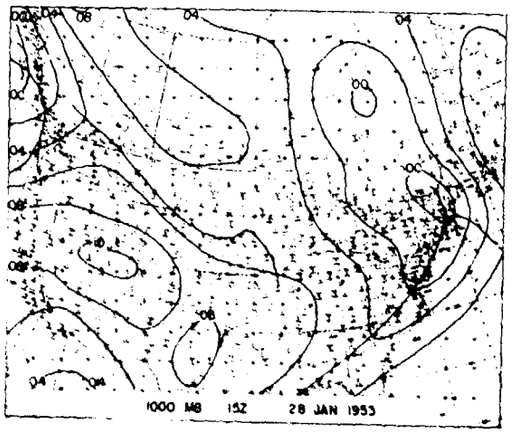
1000 MB 15Z 28 JAN 1953

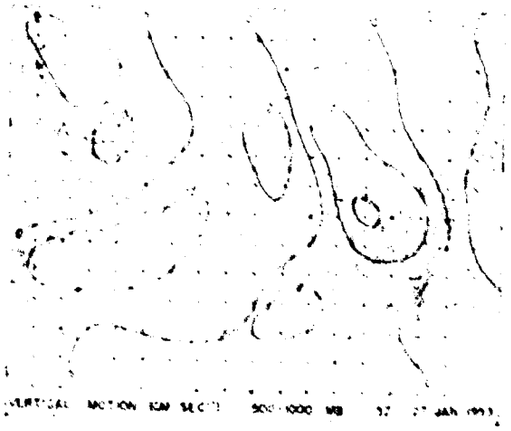

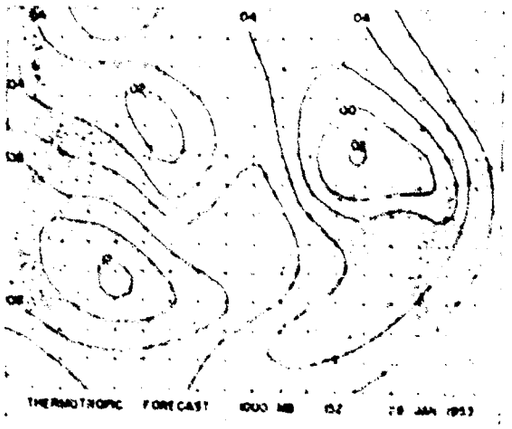
THERMOTROPIC FORECAST 1000 MB 15Z 28 JAN 1953

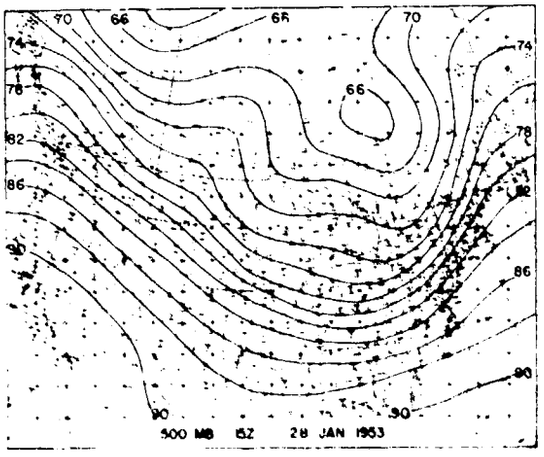
500 MB 15Z 28 JAN 1953

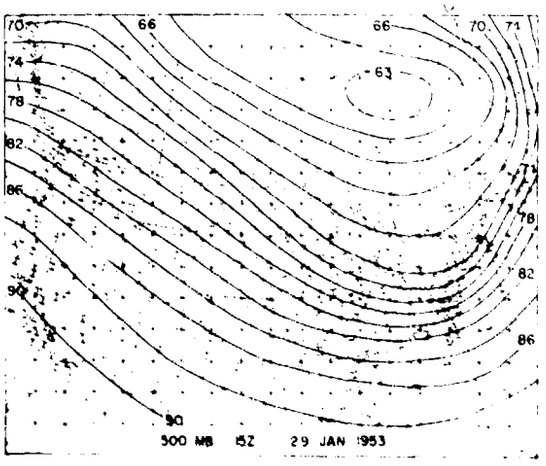
500 MB 15Z 29 JAN 1953

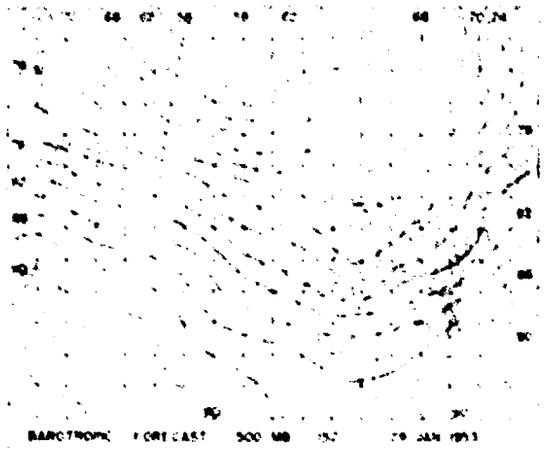

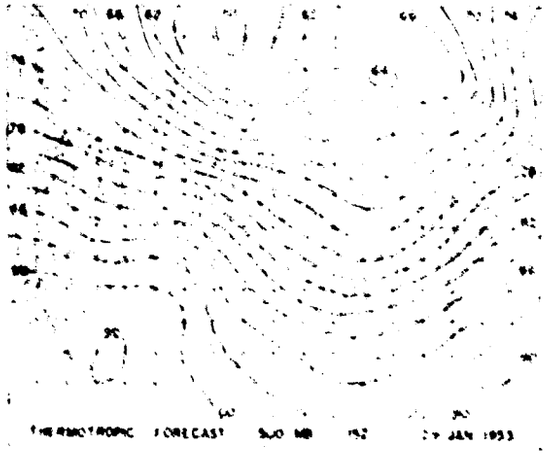

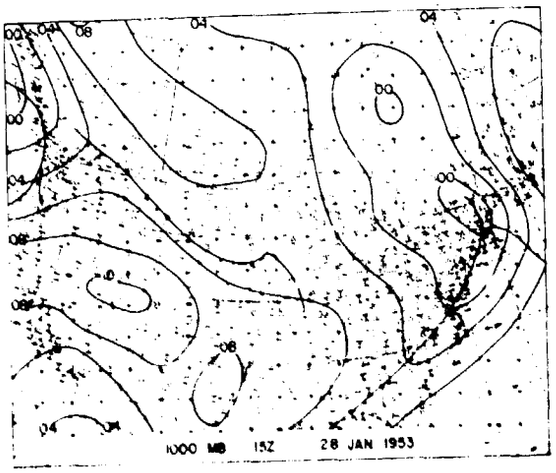
1000 MB 15Z 28 JAN 1953

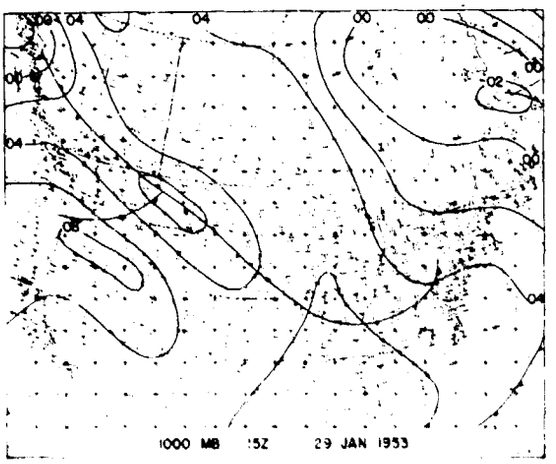
1000 MB 15Z 29 JAN 1953

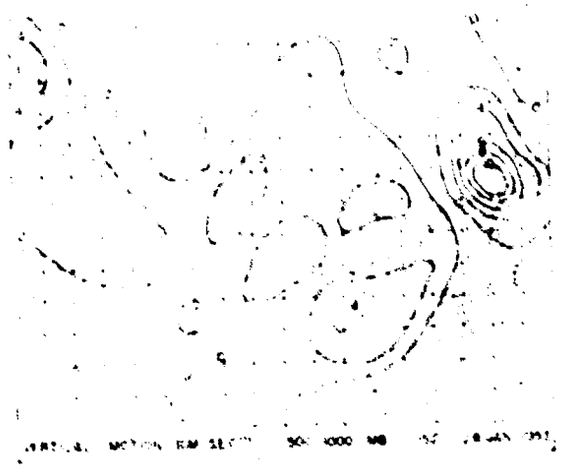

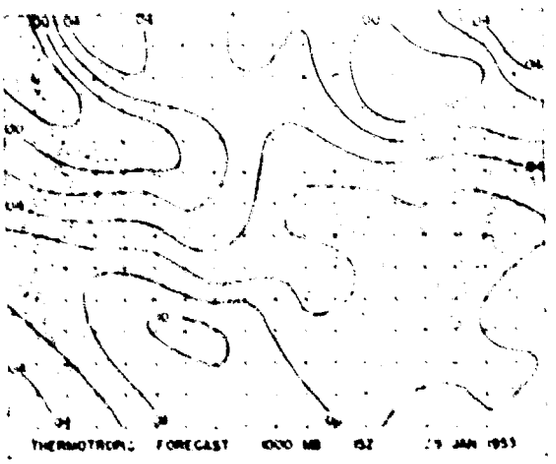
THERMOTROPIC FORECAST 1000 MB 15Z 29 JAN 1953

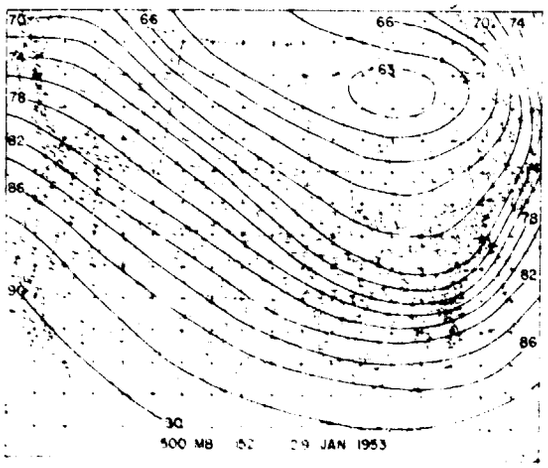
70
66
66
70
74
78
82
86
90
78
82
86
30
500 MB
JAN 1953

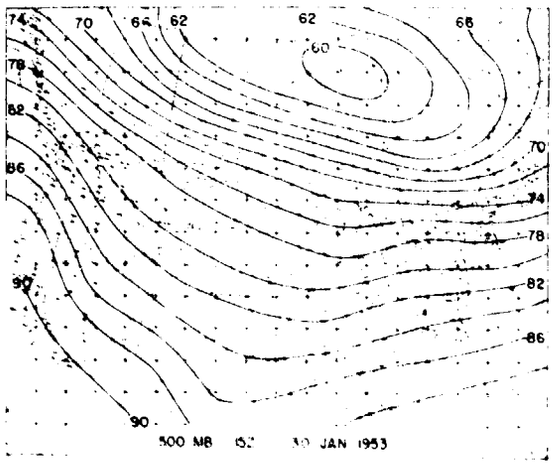
74
70
66
62
62
66
60
78
82
86
70
74
78
82
86
90
500 MB
JAN 1953

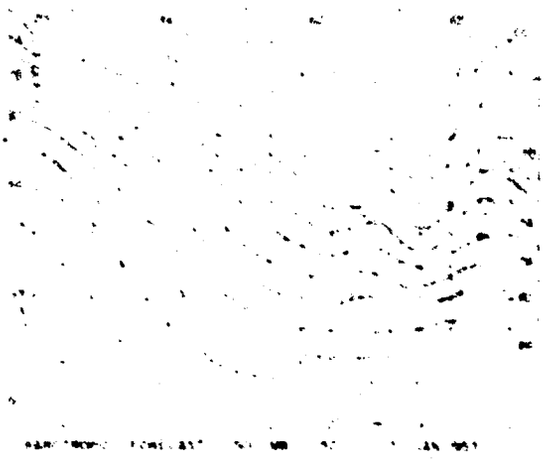

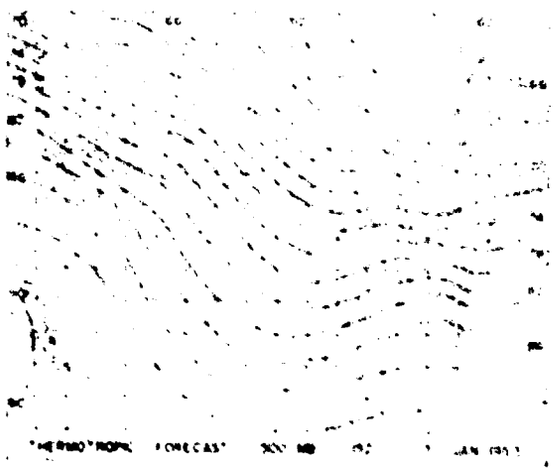

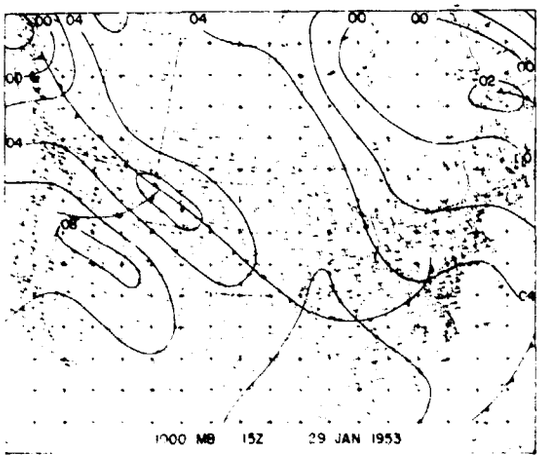
1000 MB 15Z 29 JAN 1953

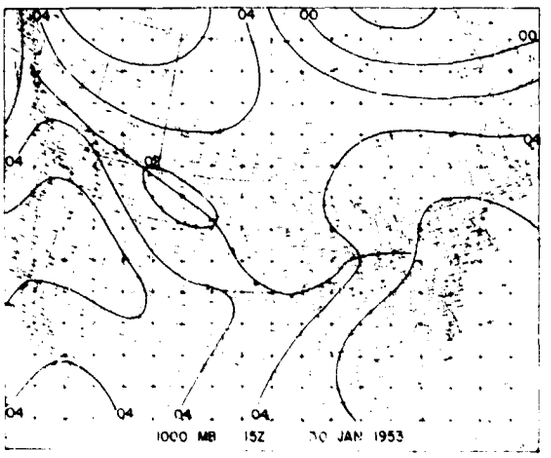
1000 MB 15Z 30 JAN 1953

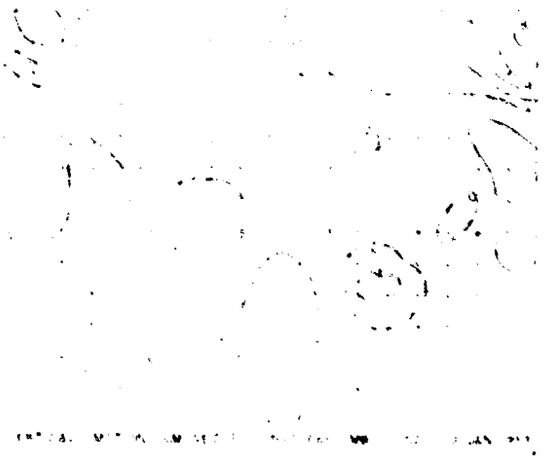

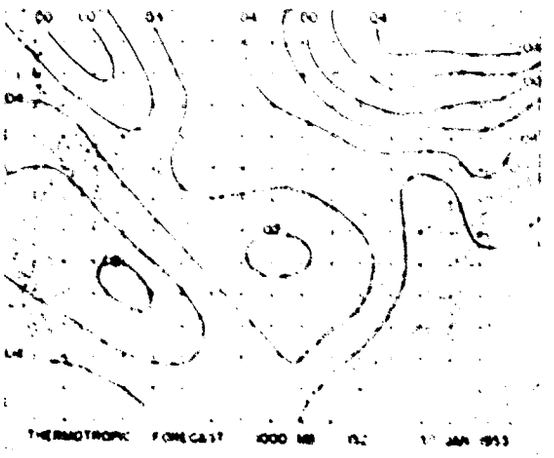

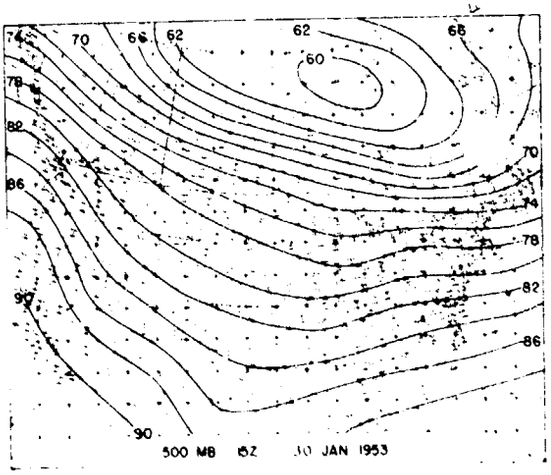
500 MB 15Z 30 JAN 1953

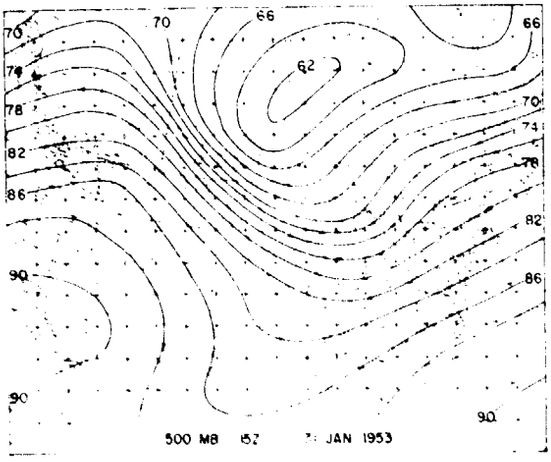
500 MB 15Z JAN 1953

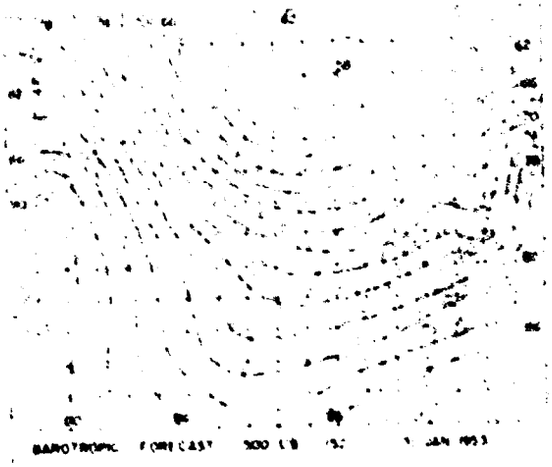
BAROTROPIC FORECAST

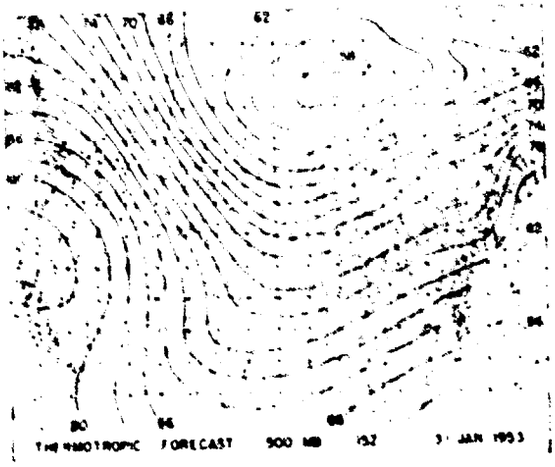
THERMOTROPIC FORECAST 500 MB 15Z JAN 1953

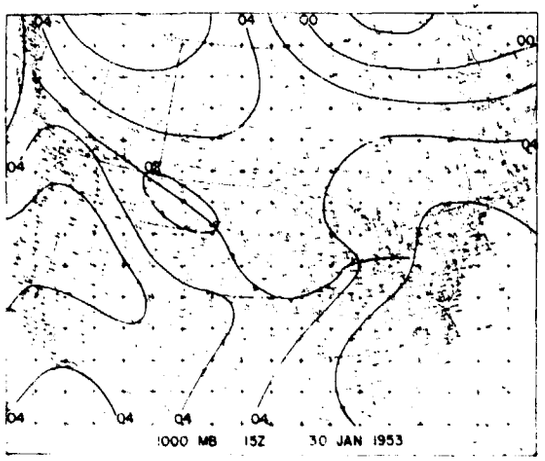
1000 MB 15Z 30 JAN 1953

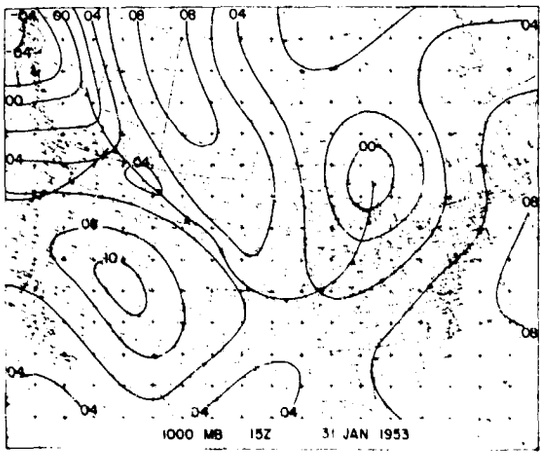
1000 MB 15Z 31 JAN 1953

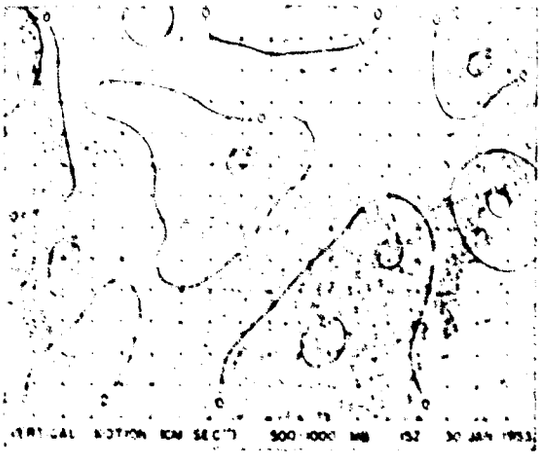

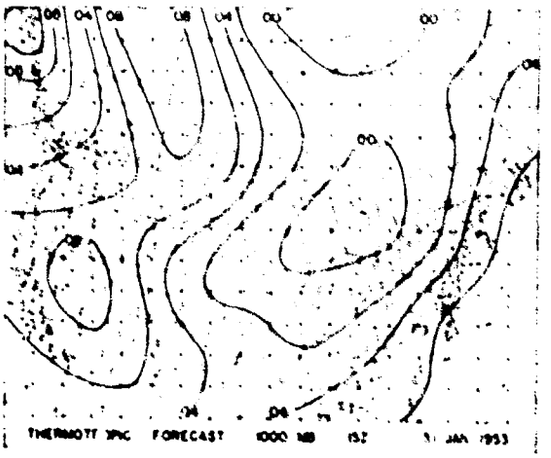
FORECAST 1000 MB 15Z

GEOPHYSICAL RESEARCH PAPERS

No. 1. Isotropic and Non-Isotropic Turbulence in the Atmospheric Surface Layer, Heinz Lettau, Geophysics Research Directorate, December 1949.

No. 2. Effective Radiation Temperatures of the Ozonosphere over New Mexico, Adel, Geophysics R-D, December 1949.

No. 3. Diffraction Effects in the Propagation of Compressional Waves in the Atmosphere, Norman A. Haskell, Geophysics Research Directorate, March 1950.

No. 4. Evaluation of Results of Joint Air Force-Weather Bureau Cloud Seeding Trials Conducted During Winter and Spring 1949, Charles E. Anderson, Geophysics Research Directorate, May 1950.

No. 5. Investigation of Stratosphere Winds and Temperatures From Acoustical Propagation Studies, Albert P. Crary, Geophysics Research Directorate, June 1950.

No. 6. Air-Coupled Flexural Waves in Floating Ice, F. Press, M. Ewing, A. P. Crary, S. Katz, and J. Oliver, Geophysics Research Directorate, November 1950.

No. 7. Proceedings of the Conference on Ionospheric Research (June 1949), edited by Bradford B. Underhill and Ralph J. Donaldson, Jr., Geophysics Research Directorate, December 1950.

No. 8. Proceedings of the Colloquium on Mesospheric Physics, edited by N. C. Gerson, Geophysics Research Directorate, July 1951.

No. 9. The Dispersion of Surface Waves on Multi-Layered Media, Norman A. Haskell, Geophysics Research Directorate, August 1951.

No. 10. The Measurement of Stratospheric Density Distribution with the Searchlight Technique, L. Elterman, Geophysics Research Directorate, December 1951.

No. 11. Proceedings of the Conference on Ionospheric Physics (July 1950) Part A, edited by N. C. Gerson and Ralph J. Donaldson, Jr., Geophysics Research Directorate, April 1952.

No. 12. Proceedings of the Conference on Ionospheric Physics (July 1950) Part B, edited by Ludwig Katz and N. C. Gerson, Geophysics Research Directorate, April 1952.

No. 13. Proceedings of the Colloquium on Microwave Meteorology, Aerosols and Cloud Physics, edited by Ralph J. Donaldson, Jr., Geophysics Research Directorate, May 1952.

No. 14. Atmospheric Flow Patterns and Their Representation by Spherical-Surface Harmonics, B. Haurwitz and Richard A. Craig, Geophysics Research Directorate, July 1952.

No. 15. Back-Scattering of Electromagnetic Waves From Spheres and Spherical Shells, A. L. Aden, Geophysics Research Directorate, July 1952.

No. 16. Notes on the Theory of Large-Scale Disturbances in Atmospheric Flow With Applications to Numerical Weather Prediction, Philip Duncan Thompson, Major, U. S. Air Force, Geophysics Research Directorate, July 1952.

GEOPHYSICAL RESEARCH PAPERS (Continued)

No. 17. The Observed Mean Field of Motion of the Atmosphere, Yale Mintz and Gordon Dean, Geophysics Research Directorate, August 1952.

No. 18. The Distribution of Radiational Temperature Change in the Northern Hemisphere During March, Julius London, Geophysics Research Directorate, December 1952.

No. 19. International Symposium on Atmospheric Turbulence in the Boundary Layer, Massachusetts Institute of Technology, 4-8 June 1951, edited by E. W. Hewson, Geophysics Research Directorate, December 1952.

No. 20. On the Phenomenon of the Colored Sun, Especially the "Blue" Sun of September 1950, Rudolf Penndorf, Geophysics Research Directorate, April 1953.

No. 21. Absorption Coefficients of Several Atmospheric Gases, K. Watanabe, Murray Zelikoff and Edward C. Y. Inn, Geophysics Research Directorate, June 1953.

No. 22. Asymptotic Approximation for the Elastic Normal Modes in a Stratified Solid Medium, Norman A. Haskell, Geophysics Research Directorate, August 1953.

No. 23. Forecasting Relationships Between Upper Level Flow and Surface Meteorological Processes, J. J. George, R. O. Roche, H. B. Visscher, R. J. Shafer, P. W. Funke, W. R. Biggers and R. M. Whiting, Geophysics Research Directorate, August 195..

No. 24. Contributions to the Study of Planetary Atmospheric Circulations, edited by Robert M. White, Geophysics Research Directorate, November 1953.

No. 25. The Vertical Distribution of Mie Particles in the Troposphere, R. Penndorf, Geophysics Research Directorate, March 1954.

No. 26. Study of Atmospheric Ions in a Nonequilibrium System, C. G. Stergis, Geophysics Research Directorate, April 1954.

No. 27. Investigation of Microbarometric Oscillations in Eastern Massachusetts, E. A. Flauraud, A. H. Meara, F. A. Crowley, Jr., and A. P. Crary, Geophysics Research Directorate, May 1954.

No. 28. The Rotation-Vibration Spectra of Ammonia in the 6- and 10-Micron Regions, R. G. Breene, Jr., Capt., USAF, Geophysics Research Directorate, June 1954.

No. 29. Seasonal Trends of Temperature, Density, and Pressure in the Stratosphere Obtained With the Searchlight Probing Technique, Louis Elterman, July 1954.

No. 30. Proceedings of the Conference on Auroral Physics, edited by N. C. Gerson, Geophysics Research Directorate, July 1954.

No. 31. Fog Modification by Cold-Water Seeding, Vernon G. Plank, Geophysics Research Directorate, August 1954.

GEOPHYSICAL RESEARCH PAPERS (Continued)

No. 32. Adsorption Studies of Heterogeneous Phase Transitions, S. J. Birstein, Geophysics Research Directorate, December 1954.

No. 33. The Latitudinal and Seasonal Variations of the Absorption of Solar Radiation by Ozone, J. Pressman, Geophysics Research Directorate, December 1954.

No. 34. Synoptic Analysis of Convection in a Rotating Cylinder, D. Fultz and J. Corn, Geophysics Research Directorate, January 1955.

No. 35. Balance Requirements of the General Circulation, V. P. Starr and R. M. White, Geophysics Research Directorate, December 1954.

No. 36. The Mean Molecular Weight of the Upper Atmosphere, Warren E. Thompson Geophysics Research Directorate, May 1955.

No. 37. Proceedings on the Conference on Interfacial Phenomena and Nucleation.
I. Conference on Nucleation.
II. Conference on Nucleation and Surface Tension.
III. Conference on Adsorption.
Edited by H. Reiss, Geophysics Research Directorate, July 1955.

No. 38. The Stability of a Simple Baroclinic Flow With Horizontal Shear, Leon S. Pocinki, Geophysics Research Directorate, July 1955.

No. 39. The Chemistry and Vertical Distribution of the Oxides of Nitrogen in the Atmosphere, L. Miller, Geophysics Research Directorate, April 1955.

No. 40. Near Infrared Transmission Through Synthetic Atmospheres, J. N. Howard, Geophysics Research Directorate, November 1955.

No. 41. The Shift and Shape of Spectral Lines, R. G. Breene, Geophysics Research Directorate, October 1955.

No. 42. Proceedings on the Conference on Atmospheric Electricity, R. Holzer, W. Smith, Geophysics Research Directorate, December 1955.

No. 43. Methods and Results of Upper Atmospheric Research, J. Kaplan, G. Schilling, H. Kallman, Geophysics Research Directorate, November 1955.

No. 44. Luminous and Spectral Reflectance as Well as Colors of Natural Objects, R. Penndorf, Geophysics Research Directorate, February 1956.

No. 45. New Tables of Mie Scattering Functions for Spherical Particles, R. Penndorf, B. Goldberg, Geophysics Research Directorate, March 1956.